GEOLOGICA ULTRAIECTINA

Mededelingen van de
Faculteit Aardwetenschappen
Universiteit Utrecht

No. 141

MIOCENE MAGNETOSTRATIGRAPHY AND CYCLOSTRATIGRAPHY IN THE MEDITERRANEAN: EXTENSION OF THE ASTRONOMICAL POLARITY TIME SCALE

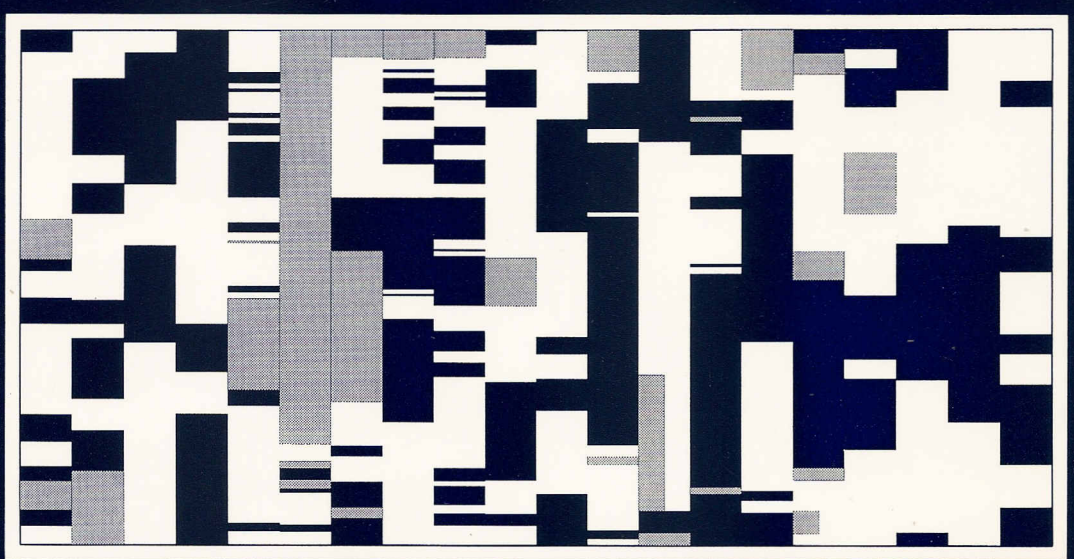

WOUT KRIJGSMAN

GEOLOGICA ULTRAIECTINA

Mededelingen van de
Faculteit Aardwetenschappen
Universiteit Utrecht

No. 141

MIOCENE MAGNETOSTRATIGRAPHY AND CYCLOSTRATIGRAPHY IN THE MEDITERRANEAN: EXTENSION OF THE ASTRONOMICAL POLARITY TIME SCALE

CIP-GEGEVENS KONINKLIJKE BIBLIOTHEEK, DEN HAAG

Krijgsman, Wout

Miocene magnetostratigraphy and cyclostratigraphy in the Mediterranean: extension of the astronomical polarity time scale / Wout Krijgsman, - Utrecht: Faculteit Aardwetenschappen, Universiteit Utrecht. - (Geologica Ultraiectina, ISSN 0072-1026 ; no. 141)
Proefschrift Universiteit Utrecht. - Met lit. opg. - Met samenvatting in het Nederlands.
ISBN 90-71577-95-3
Trefw.: paleomagnetisme / stratigrafie

MIOCENE MAGNETOSTRATIGRAPHY AND CYCLOSTRATIGRAPHY IN THE MEDITERRANEAN: EXTENSION OF THE ASTRONOMICAL POLARITY TIME SCALE

MIOCENE MAGNETOSTRATIGRAFIE EN CYCLOSTRATIGRAFIE IN HET MIDDELLANDSE ZEEGEBIED: UITBREIDING VAN DE ASTRONOMISCHE POLARITEITSTIJDSCHAAL

(met een samenvatting in het Nederlands)

PROEFSCHRIFT

TER VERKRIJGING VAN DE GRAAD VAN DOCTOR
AAN DE UNIVERSITEIT UTRECHT
OP GEZAG VAN DE RECTOR MAGNIFICUS PROF. DR. J.A. VAN GINKEL
INGEVOLGE HET BESLUIT VAN HET COLLEGE VAN DEKANEN
IN HET OPENBAAR TE VERDEDIGEN
OP MAANDAG 13 MEI 1996 DES NAMIDDAGS TE 14.30 UUR

DOOR

WOUT KRIJGSMAN

geboren op 25 december 1966,
te Rotterdam

1996

PROMOTOR: PROF. DR. J.D.A. ZIJDERVELD

CO-PROMOTORES: DR. C.G. LANGEREIS
DR. F.J. HILGEN

I know that we can never
live those times again
so I let my dreams
take me back to where we've been

Green on Red, 1991

Voor Joop en Nel

This study was supported by The Netherlands Geosciences Foundation (GOA) with financial aid from the Netherlands Organisation of Scientific Research (NWO).

Research was carried out at:

Paleomagnetic laboratory "Fort Hoofddijk"
Faculty of Earth Sciences
Utrecht University
Budapestlaan 17
3584 CD Utrecht
The Netherlands

Universiteit Utrecht

The author can be reached through E-mail at: krijgsma@geof.ruu.nl

CONTENTS

BIBLIOGRAPHY

Chapter 1:

Krijgsman, W., F.J. Hilgen, C.G. Langereis and W.J. Zachariasse, The age of the Tortonian-Messinian boundary. *Earth Planet Sci. Lett.*, **121**, 533-547, 1994.

Chapter 2:

Krijgsman, W., F.J. Hilgen, C.G. Langereis, A. Santarelli and W.J. Zachariasse, Late Miocene magnetostratigraphy, biostratigraphy and cyclostratigraphy in the Mediterranean, *Earth Planet Sci. Lett.*, **136**, 475-494, 1995.

Chapter 3:

Hilgen, F.J., W. Krijgsman, C.G. Langereis, L.J. Lourens, A. Santarelli and W.J. Zachariasse, Extending the astronomical (polarity) time scale into the Miocene, *Earth. Planet. Sci. Lett.*, **136**, 495-510, 1995.

Chapter 4:

Krijgsman, W., F.J. Hilgen, A. Negri, J.R. Wijbrans and W.J. Zachariasse, The Monte del Casino section: A potential Tortonian-Messinian boundary stratotype, *Palaeogeogr. Palaeoclimatol. Palaeoecol.* **submitted.**

Chapter 5:

Hilgen, F.J., W. Krijgsman and J.R. Wijbrans, Age determination of the FCT-sanidine by comparing Ar/Ar and astronomical ages of late Miocene ash beds in the Mediterranean, *Geoph. Res. Lett.*, **(to be) submitted.**

Chapter 6:

Krijgsman, W., C.G. Langereis, R. Daams and A.J. van der Meulen, Magnetostratigraphic dating of the middle Miocene climate change in the continental deposits of the Aragonian type area in the Calatayud-Teruel basin (Central Spain). *Earth Planet. Sci. Lett.*, **128**, 1994.

Chapter 7:

Krijgsman, W., M. Garcés, C.G. Langereis, R. Daams, J. van Dam, A.J. van der Meulen, A.J. Agustí and L. Cabrera, A new chronology for the middle to late Miocene continental record in Spain *Earth Planet. Sci. Lett.*, **accepted.**

Chapter 8:

Krijgsman, W., W. Delahaije, C.G. Langereis and P.L. de Boer, Cyclicity and NRM acquisition in a continental red bed sequence: potential for an astronomical polarity time scale, *J. Geoph. Res.*, **submitted.**

Chapter 9:

Krijgsman, W., C.E. Duermeijer, C.G. Langereis, H. de Bruijn, G. Saraç and P.A.M. Andriessen, Magnetic polarity stratigraphy of late Oligocene to middle Miocene mammal-bearing localities in Central Anatolia (Turkey), *Newslett. Stratigr.*, **in press.**

Samenvatting (Summary in Dutch)

In de begin jaren 60 werd aangetoond dat het aardmagneetveld op onregelmatige perioden van de geologische geschiedenis van polariteit is veranderd en sindsdien zijn er verscheidene tijdschalen geconstrueerd op basis van deze polariteits omkeringen. Het correleren van karakteristieke polariteits-patronen in stratigrafische opeenvolgingen naar deze geomagnetische polariteits-tijdschalen (GPTS) wordt magnetostratigrafie genoemd. Magnetostratigrafie heeft momenteel een belangrijk tijdskader verschaft en is nu, tesamen met biostratigrafie en radiometrische dateringen een van de standaard methoden in de stratigrafie. Het is een betrouwbare methode om absolute ouderdommen van sedimentaire opeenvolgingen te bepalen en kan ook toegepast worden op secties waar radio-metrisch dateren onmogelijk is door de afwezigheid van vulkanisch materiaal.

Een grote doorbraak in ouderdomsbepalingen is, sinds kort, astronomisch dateren. Hierbij worden cyclische variaties in de geologische geschiedenis gecalibreerd naar berekende astronomische tijdseries van periodieke bewegingen van de baan van de aarde en van de rotatie-as. Deze cycli kunnen gebruikt worden om de hoeveelheid aanwezige tijd in sedimentaire afzettingen te schatten. Vooral het Middellandse Zee gebied heeft het voordeel door zijn latitudinale positie in combinatie met zijn semi-gesloten configuratie dat haar sedimenten bijzonder gevoelig zijn om astronomisch beinvloedde veranderingen te registreren. Een astronomische polariteits tijdschaal (APTS) is reeds geconstrueerd voor het Pleistoceen en Plioceen, gebaseerd op cyclische variaties in mariene afzettingen. Deze APTS heeft bewezen nauwkeuriger en betrouwbaarder

te zijn dan de conventionele tijdschalen en is daarom in zijn geheel ingebed in de meest recente standaard GPTS.

Het belangrijkste doel van dit proefschrift is het uitbreiden van de astronomische polariteits tijdschaal naar het Mioceen. Tegelijkertijd zal een geïntegreerd magnetostratigrafisch en cyclostratigrafisch raamwerk ontwikkeld worden voor het mariene Midden tot Laat Mioceen. Een tweede doelstelling is, om met behulp van een betrouwbare magnetostratigrafie, een nauwkeurige chronologie te construeren voor de continentale tijdschaal. De basis voor dit proefschrift ligt, zowel voor het mariene gedeelte als het continentale gedeelte, in de uitgebreide veldstudies. Gedurende dit proefschrift zijn er 53 weken in het veld doorgebracht wat ongeveer een kwart van de totale promotietijd besloeg.

Mariene secties

Het eerste probleem dat zich voordeed bij de ontwikkeling van een geïntegreerd stratigrafisch raamwerk voor mariene afzettingen was de ouderdom van de Tortoniën/Messiniën (T/M) grens. Bij de aanvang van dit proefschrift was er nog totaal geen overeenstemming over de posititie van de T/M grens in de GPTS, en ouderdommen varieerden van 5.6 tot 6.4 Ma. Hoofdstuk 1 behandelt de resultaten van de (her)bemonstering van secties op Kreta, nu aangevuld met cyclostratigrafische data. Het was de bedoeling om de duur van individuele polariteitszones te bepalen door het aantal precessie gerelateerde sedimentaire cycli per polariteitszone te tellen. Deze astronomische duur kan vervolgens vergeleken worden met de duur van de opeenvolgende (sub)chrons in de GPTS. Een re-evaluatie van de secties op Kreta werd nog relevanter toen een nieuwe GPTS gepubliceerd werd waarin twee niet eerder geregistreerde normale subchrons in het omgekeerde interval van Chron 6 (C3Br.1n, C3Br.2n) waren herkend. Het blijkt dat nu een overduidelijke correlatie gemaakt kan worden tussen de polariteits opeenvolgingen op Kreta en de nieuwe GPTS. Het eerste voorkomen (first occurrence, FO) van de G. conomiozea groep (planktonische foraminiferen), wat per definitie de basis van het Messiniën vormt, wordt aangetroffen in het omgekeerde interval van anomalie C3Br.1r. Dit leidt tot een ouderdomsbepaling van 6.92 miljoen jaar (volgens de GPTS van CK92) voor de T/M grens en een duur van 1.76 miljoen jaar voor het Messiniën. De astronomische duur voor de polariteits zones zijn in goede overeenstemming met die van de GPTS, maar blijken gemiddeld ongeveer 10% korter te zijn.

De secties op Kreta kunnen helaas niet uitgebreid worden naar oudere niveau's, wat wel mogelijk blijkt te zijn op Gavdos (Metochia sectie) en Sicilië (Gibliscemi sectie). In **Hoofdstuk 2** wordt een nieuwe chronologie gepresenteerd voor het Laat Mioceen in het Middellandse Zee gebied door het combineren van magnetostratigrafische, biostratigrafische (planktonische foraminiferen en dinoflagellaten) en cyclostratigrafische gegevens. Een gedetailleerde biostratigrafische analyse resulteerde in de identificatie van 13 planktonische foraminiferen en 9 dinoflagellaten bio-events, die alle nauwkeurig gedateerd zijn. De T/M grens, nu

gedefinieerd door het eerste veelvuldige voorkomen (FRO) van de *G. conomiozea* group, heeft een ouderdom van 7.12 miljoen jaar volgens de (vernieuwde) GPTS van CK95.

In **Hoofdstuk 3** wordt vervolgens een astronomische polariteits tijdschaal gepresenteerd voor het Laat Mioceen (6.7-9.7 Ma), gebaseerd op de correlatie van karakteristieke sedimentaire patronen in de Metochia en Gibliscemi secties naar de 65°N zomer instralingscurve van La90. Deze correlatie levert ouderdommen voor alle sedimentaire cycli en vervolgens ook voor de geregistreerde polariteits-omkeringen en bio-events. De T/M grens is astronomisch gedateerd op 7.24 miljoen jaar, de duur van het Messiniën is 1.91 miljoen jaar.

De Monte del Casino sectie in de noordelijke Apennijnen (Italie) wordt beschouwd in **Hoofdstuk 4** als een potentieel geschikte kandidaat om de T/M grens stratotype te definieren. Deze sectie heeft een goede cyclostratigrafie, tephrastratigrafie en biostratigrafie (planktonische foraminiferen en nanno-fossielen). Een correlatie, in detail, kan gemaakt worden naar Metochia, Gibliscemi en de secties op Kreta met het gebruik van cyclostratigrafie in combinatie met planktonische foraminiferen biostratigrafie. Een betrouwbare magnetostratigrafie, voor het T/M grens interval, is helaas niet verkregen doordat een secondaire component het magnetische signaal verstoort. Vergelijking van radiometrische ($^{40}Ar/^{39}Ar$) ouderdommen van ingeschakelde vulkanische as-lagen met hun astronomische ouderdom geeft een redelijke schatting van de ouderdom van de sectie maar deze $^{40}Ar/^{39}Ar$ ouderdommen blijken niet gebruikt te kunnen worden voor zeer nauwkeurige dateringen.

Ook de astronomisch gedateerde secties van Kreta, Gavdos en Koufonisi bevatten vulkanische as-lagen. In **Hoofdstuk 5** vergelijken we de astronomische ouderdommen van deze assen met hun $^{40}Ar/^{39}Ar$ ouderdommen van biotiet en veldspaat. Microprobe analyses laten zien dat deze assen van elkaar onderscheiden kunnen worden op basis van hun samenstelling. De beste resultaten worden verkregen uit de Faneromeni sectie Hiervan is in de veldspaatfractie de sanidien van de plagioklaas gescheiden. De eerste resultaten laten zien dat het gebruik van een ouderdom van 27.92 Ma voor de standaard sanidien (TCR) een ouderdom geeft die goed overeenstemt met de astronomische ouderdom.

Continentale secties

In de continentale biostratigrafische tijdschaal voor het Europese Mioceen ontbrak nog altijd een betrouwbare chronologie. Correlatie van Neogene Mammal (MN) Zones en de corresponderende fauna assemblages naar de absolute tijdschaal vond voornamelijk plaats op basis van correlatie naar de mariene biostratigrafie en regionale zones (e.g. Paratethys Stages). Magneto-stratigrafie aan continentale afzettingen wordt vaak moeilijk geacht wegens de vermeende aanwezigheid van hiaten en (onbekende) veranderingen van de sedimentatiesnelheid en de schaarste and lange continue secties. De vergelijking

van continentale fossielen en hun regionale zones met de mariene tijdschaal was altijd tamelijk onbetrouwbaar omdat er geen nauwkeurige dateringen waren.

In **Hoofdstuk 6** wordt een belangrijke klimaat omslag in de zoogdier biostratigrafie (naar een kouder en natter klimaat) magnetostratigrafisch gedateerd en blijkt plaats te hebben gevonden op 14.1 Ma. Deze ouderdom komt exact overeen met de ouderdoms bepaling van 14.1-14.05 Ma voor de belangrijkste toename in $\delta^{18}O$ (duidend op ijskapvorming) in mariene afzettingen. Deze twee onafhankelijke waarnemingen van een tijds-equivalente koude periode in zowel continentale als mariene afzettingen bevestigen en dateren een belangrijke mondiale koude periode in het Midden Mioceen. Een belangrijk resultaat is dat drie MN zone grenzen magnetostratigrafisch gedateerd worden. Deze blijken opvallend jonger te zijn (tot 3 Ma) dan tot dusver in de bestaande tijdschalen was aangenomen.

In **Hoofdstuk 7** wordt de chronologie van Miocene zoogdier (MN) zones sterk uitgebreid, gebaseerd op biostratigrafische gegevens en een magnetostratigrafie, met een hoog oplossend vermogen, van zoogdier-fossielen bevattende secties in Spanje. Deze spaanse secties vertegenwoordigen een bijna complete magnetostratigrafische opeenvolging van het Onder Aragoniën (MN 4; 18 Ma) tot het Midden Turoliën (MN 12; 7 Ma). Zeven opeenvolgende MN zone grenzen zijn direct gedateerd in secties die vaak meerdere fauna's boven elkaar bevatten.

Een van deze spaanse secties, de Armantes sectie in het Calatayud-Daroca bekken, is een "red bed" afzetting die opgebouwd is uit een regelmatige afwisseling (10 meter schaal) van rode silten en roze/witte kalken. Tussen deze kalkbanken is op kleinere schaal een gelaagdheid (2-3 m schaal) te zien welke gekenmerkt wordt door verschillen in carbonaatgehalte en de daarvan afhankelijke weerstand tegen verwering. De correlatie van de magnetostratigrafie met de GPTS resulteert in een periodiciteit van 111 kyr voor de (grotere schaal) cycliciteit hetgeen een duidelijke relatie suggereert met de periode voor eccentriciteit van de baan van de aarde. In **Hoofdstuk 8** worden de resultaten van een gedetailleerde bemonstering van een interval in de Armantes sectie, bestaande uit drie kalkbanken, gepresenteerd. Het kan worden aangetoond dat de geobserveerde cycliciteit is gerelateerd aan astronomische klimaatsveranderingen. De paleomagnetische resultaten tonen verder aan dat dit type afzettingen zeer geschikt is voor de constructie van een APTS in deze continentale afzettingen.

Tenslotte worden in **Hoofdstuk 9** de resultaten van zes Laat Oligocene tot Midden Miocene zoogdierfossiel bevattende secties in centraal Turkije gepresenteerd, en waar mogelijk gecorreleerd naar de GPTS. De correlatie van turkse faunas met europese is van vitaal belang voor het begrijpen van de geologische and klimatologische gebeurtenissen die zoogdieren hebben aangezet tot een migratie van Azië naar Europa.

Prologue

Magnetostratigraphy

Ever since it was demonstrated in the early 1960s that the Earth has reversed the polarity of its magnetic field at irregular intervals throughout geological history, time scales have been constructed based on these polarity reversals. The magnetostratigraphic dating technique concerns the correlation of magnetic polarity patterns of stratigraphic intervals to this geomagnetic polarity time scale (GPTS). Magnetostratigraphy has now provided an important global time framework and has taken its place alongside biostratigraphy and radiometric dating as one of the standard branches of stratigraphy. It is an accurate method to assign absolute ages to sedimentary sequences and can also be applied to sections were radiometric dating is impossible because of the absence of volcanic material.

The discovery of polarity reversals is attributed to Brunhes (1906) whose systematic investigations of the directions of remanent magnetism in rocks led to the observation that certain lava flows were magnetised in a direction approximately antiparallel to the present geomagnetic field. The first true magnetostratigraphic investigation of determinations of paleomagnetic directions in known stratigraphic sequences were reported by Matuyama (1929). He demonstrated that young Quaternary rocks were magnetised in the same direction as the present day field, whereas older Quaternary rocks were magnetised in the opposite direction. The development of radiometric dating techniques enabled Cox et al. (1963) to propose the first GPTS, based on direct paleomagnetic measurements and K/Ar datings of volcanic rocks.

Marine magnetic anomalies potentially provide the richest source of information on the pattern of geomagnetic field reversals from the late Jurassic to the present. The hypothesis of sea-floor spreading (Hess, 1960) and the existence

of polarity reversals where combined by Vine and Mattews (1963) into one single theory, in which they suggested that sea-floor magnetic anomalies might be related to geomagnetic polarity reversals. The reversal pattern for the past 165 Myr is accurately known from the marine magnetic anomaly profiles of the ocean floor. On the assumption of a constant spreading rate, Heirtzler et al. (1968) used a long magnetic profile in the south Atlantic to extend the GPTS into the Mesozoic. Combined magnetostratigraphic, biostratigraphic and radiometric results of deep-sea sediments from the Deep Sea Drilling Project (DSDP), have confirmed the general validity and accuracy of the GPTS.

Numerous additions and revisions have been made since (e.g. LaBrecque et al., 1977) and the increase of more reliable calibration points have resulted in several refinements (Lowrie and Alvarez, 1981; Berggren et al., 1985). A major improvement came recently when Cande and Kent (1992) published their GPTS, based on a synthetic anomaly profile sequence from the South Atlantic with additions from fast spreading plates, which made it possible to recognise also shorter subchrons.

In the last decades, magnetic polarity stratigraphy of land-based sections has become an important tool for stratigraphic correlations and for relative and absolute dating of sedimentary sequences. The global and essentially synchronous nature of polarity reversals can be used to obtain information on the synchrony or diachrony of various geological and biostratigraphical events and to correlate marine and continental sequences.

Cyclostratigraphy

It has long been realised that sedimentary cycles may reflect climatic oscillations that are ultimately controlled by the Earth's orbital cycles, hence, can be used to estimate the amount of time represented (Gilbert, 1895; Bradley, 1929; Milankovitch, 1941; see also Fisher 1980; Berger, 1989). At the end of the last century, Gilbert, (1895) proposed that the deposition of late Cretaceous carbonate-marl cycles had been the result of astronomical forcing. Based on this assumption he calculated the length of part of the late Cretaceous, and his estimate is in good agreement with modern geological time scales (Fisher, 1980). Later, Bradley (1929) recognised precessional cycles in shale-dolomite sequences using varves as precise measure of sedimentation rates. While these works were largely unnoticed, Milankovitch revived the debate about the possible influence of astronomical parameters upon the Earth's climate when he published his "landmark paper" on the causal relationship between astronomical parameters and the ice ages (Milankovitch, 1941). Today, the idea of astronomical variables leaving traces in the sedimentary record is widely accepted.

Astronomical forcing of climate and thus of sedimentary facies depends upon the changing position of the Earth's axis in its varying path around the Sun (Berger, 1977). Such variations depend on the interaction of gravitational forces in

the rotating Sun-Earth-Moon system, and on the influences of the other planets in our solar system. The resulting orbital perturbations give rise to variations in eccentricity (with main periods of 400 and 100 kyr), obliquity (41 kyr) and precession (23 and 19 kyr) (Berger, 1977). Eccentricity is a measure of the degree of elongation of the Earth's orbit around the Sun and varies between nearly zero (circular orbit) and 0.06 (elliptical orbit). Obliquity describes the angle between the Earth's axis of rotation and the orbital plane and varies between 22° and 25°. Precession describes the spinning of the Earth's rotational axis around a circular path, caused the combined effects of solar and lunar attraction on the Earth. Caused by the opposite movement of the eccentricity orbit, the precession of the equinoxes, also called climatic precession, completes one full cycle on average every 21.7 kyr. These astronomical parameters are climatically important because they cause variations in the spatial distribution of solar energy reaching the Earth's surface, and thus influence the distribution of climatic zones and the variation of the receipt of solar energy with latitude over the year (Berger and Loutre, 1991).

In marine sediments of the oceans, these orbital influences are clearly recorded in oxygen isotope records of planktonic and benthic foraminifera and reflect primarily changes in global ice volume (Emiliani, 1955; Shackleton and Opdyke 1973). Orbital influences are clearly expressed in all types of sedimentary cycles deposited throughout the Earth's history. The Mediterranean has the clear advantage that its latitudinal position in combination with its semi-enclosed, land-locked basin configuration makes its sediments particularly sensitive to record astronomically induced oscillations in climate. Sedimentary cycles consist usually of alternations of homogeneous marls and brownish coloured, organic rich, laminated beds termed sapropels. These sapropels have been related to enhanced fluvial run-off, which pronouncedly affected the Mediterranean water budget and led to a diminished vertical water exchange, anoxic or dysoxic bottom water conditions and the deposition of a sapropel. The enhanced run-off has been connected to the intensification of the monsoonal system which in turn may result from orbitally forced variations in low latitude summer insolation (Rossignol-Strick, 1983; Rohling and Hilgen, 1991).

Astronomical Polarity Time Scale

During the last decade, a major breakthrough in age determination has been astronomical dating: the calibration or tuning of cyclic variations in the geological past to computed astronomical time series of orbital variations. An astronomical polarity time scale (APTS) has been constructed for the Pleistocene and Pliocene (i.e. the past 5.32 Myr), based on cyclic variations in the marine record (Shackleton et al., 1990; Hilgen, 1991a,b). This APTS proved to be more accurate and have much higher resolution than conventional time scales and it has therefore entirely been incorporated in the most recent standard GPTS which is

CK95 (Cande and Kent, 1995). Furthermore, the APTS has been succesfully applied to paleoclimate studies (Lourens et al., 1992) and in studies of seafloor spreading history (Wilson, 1993; Langereis et al., 1994). The accuracy of this APTS has been confirmed by $^{40}Ar/^{39}Ar$ dating (see Renne et al., 1994).

For studies directed at paleoclimatic and paleoenvironmental reconstructions, the application of the APTS is fundamental. Until now, the construction of the APTS is entirely based on open marine sequences. The inclusion of the continental record, however, would be helpful since a more comprehensive understanding of paleoclimate and paleoclimatic change is only achieved by accurate and high-resolution time-stratigraphic correlations between the continental and marine record. In fact, the terrestrial sedimentary record seems to be the logical place to look for Milankovitch cycles because, in the absence of oceanographic processes with their intrinsic and complicated non-linear (feed-back) mechanisms, a more direct registration of orbitally induced changes in climate may be expected.

Background of this research

It was in the mid 1970's when Prof. Zijderveld together with Prof. Drooger initiated a detailed stratigraphic study to investigate the usefulness, potential and restrictions of magnetostratigraphy, in particular to determine whether biostratigraphic datum planes were synchronous or diachronous. This was the first step towards a strong and forwarding integration of two different but closely connected disciplines at Faculty of Earth Sciences of the Utrecht University. The selected time slice concerned the latest Miocene, a biostratigraphically well-known interval straddling the Tortonian/Messinian boundary which is defined by the first occurrence of the planktonic foraminifera species *Globorotalia conomiozea*. In the subsequent thesis of Langereis (1984), excellent magneto-stratigraphic results were obtained from selected sections on Crete, less favourable results were derived from sections in Italy. The sections from Crete showed that the FO of the *G. conomiozea* group occurs in a reversed polarity zone - interpreted to represent the reversed subchron of Chron 5 (now termed C3An) - and consequently had an age of 5.6 Ma (Langereis et al., 1984), according to the GPTS of Lowrie and Alvarez (1981). However, Berggren et al. (1985) rejected this age estimate and suggested that the Cretan results were incorrectly interpreted. Their arguments were essentially based on the duration of the Messinian - and hence on the age of the Miocene/Pliocene boundary - and on assumed global synchronism of biostratigraphic datum levels.

In view of this ongoing controversy, the logical next step of the Utrecht group was to study the upper boundary of the Messinian in detail This resulted in the first accurate age estimates for the M/P boundary of 4.83-4.84 Ma on the basis of a detailed magnetostratigraphy (Zijderveld et al., 1986). In the last decade, the early Pliocene and early late Pliocene sediments of the Mediterranean have been

the subject of intensive magnetostratigraphic (Hilgen and Langereis, 1988; Langereis and Hilgen, 1991; Zijderveld et al., 1991), cyclostratigraphic (Hilgen 1987, 1990; Hilgen and Langereis, 1989) and biostratigraphic (Zachariasse et al., 1987) research. The resulting integrated stratigraphic framework was subsequently used to construct an APTS - for the entire Mediterranean Pliocene and lower Pleistocene - by correlating characteristic sedimentary cycle patterns to astronomical target curves (Hilgen et al., 1991a,b). Furthermore, the Pliocene formed an interesting study object for various disciplines and resulted in dissertations on cyclostratigraphy (Hilgen, 1991), paleomagnetic reversals (Linssen, 1991; Van Hoof, 1993), magnetic minerals (Van Velzen, 1994), tectonic rotations (Scheepers, 1994), paleoclimatology (Lourens, 1994), geochemistry (Van Os, 1993), and palynology (Versteegh, 1995).

Now that the Pliocene timeframe had been reliably established it was time to restudy the Tortonian and Messinian with the same research strategy: first to establish an accurate magnetostatigraphic and cyclostratigraphic framework for this time span. It was from this point that this PhD thesis started.

Summary of this research

The first aim of this thesis was to extend the astronomical polarity time scale into the Miocene and to develop an integrated magnetostratigraphy and cyclostratigraphy for the middle to late Miocene marine record. The second aim was to establish an accurate chronology for the Miocene continental record on the basis of high-resolution magnetostratigraphic calibrations and hence to allow marine-continental correlations. The basis of all studies in this thesis lies without any doubt in extensive fieldwork. It is crucial that sections are sampled in sufficient detail; they need to be long, continuous, and must not show signs of hiatuses or drastically changing sedimentation rates.

Marine sections

To establish an integrated stratigraphic framework for the marine late Miocene the first problem to deal with was the still existing controversy over the age of the Tortonian/Messinian boundary. When this research started, there was no general consensus concerning the position of the T/M boundary in the GPTS, and age estimates ranged from 5.6 Ma (Langereis et al., 1984) to 6.4 Ma (Berggren et al., 1985). **Chapter 1** presents the results from resampling of the Cretan sections of Langereis et al. (1984) supplemented by cyclostratigraphic data. We aimed to estimate the duration of the successive individual polarity zones, based on the number of presumably precession-related sedimentary cycles per polarity zone. These estimates can then be compared with the duration of the successive (sub)chrons in the GPTS. A re-evaluation of the Cretan sections had become

especially relevant, since Cande and Kent (1992) had constructed a new GPTS in which they recognise two additional normal subchrons in the reversed interval of Chron 6 (C3Br.1n, C3Br.2n). We show that the polarity sequences on Crete can now be unambiguously correlated to CK92. The FOD of *G. conomiozea* occurs in the reversed interval of anomaly C3Br.1r. This correlation leads to an age determination of 6.92 Ma (according to CK92) for the T/M boundary and a duration of 1.76 Myr for the Messinian. The astronomically derived durations of the Cretan polarity zones are in good agreement with CK92, but appear to be approximately 10% shorter.

Unfortunately, the sections of Crete cannot be extended downwards to older levels, but longer and continuous upper Miocene sections are found on Gavdos (Metochia section) and Sicily (Giblisciemi section). In **Chapter 2,** a new chronology for the late Miocene of the Mediterranean is presented by combining magnetostratigraphic, biostratigraphic (planktonic foraminifera and dinoflegellates) and cyclostratigraphic data. Detailed biostratigraphic analysis resulted in the identification of 13 planktonic foraminiferal and 9 dinoflagellate bioevents, which are all accurately dated. The T/M boundary, now defined by the first regular occurrence (FRO) of the *G. conomiozea* group, is determined in chron C3Br.1r with an age of 7.12 Ma, according to the revised GPTS (CK95) of Cande and Kent (1995).

In **Chapter 3,** an astronomical polarity time scale is presented for the late Miocene (6.7-9.7 Ma) based on the correlation of characteristic sedimentary cycle patterns in the Metochia and Giblisciemi sections to the 65°N summer insolation curve La90 of Laskar (1990). This correlation yields ages for all sedimentary cycles hence also for the recorded polarity reversals and planktonic foraminiferal and dinoflagellate events. The T/M boundary is astronomically dated at 7.24 Ma, the duration of the Messinian is estimated at 1.91 Myr.

In **Chapter 4** the Monte del Casino section of the Northern Apennines (Italy) is considered as a potentially suitable candidate to define the T/M boundary stratotype. The section yields a good cyclostratigraphy, tephrastratigraphy and biostratigraphy (planktonic foraminifera and nannofossils) and can be correlated in detail to Metochia, Gibliscemi and the Cretan sections using cyclostratigraphic patterns in combination with the high-resolution planktonic foraminiferal biostratigraphy. Unfortunately, a reliable magnetostratigraphy could not be established in the T/M boundary interval because of a secondary magnetisation carried by iron sulphides. Comparison of Ar/Ar ages of intercalated volcanic ash layers with their astronomical ages, shows that biotites give a good approximation of the age of the section, but are not suitable for accurate dating.

The astronomically dated sections on Crete, Gavdos and Koufonisi contain volcanic ash layers. In **Chapter 5** we compare the astronomical ages of the ashes with their $^{40}Ar/^{39}Ar$ ages on biotites and feldspars. Microprobe analyses show that the ashes can be distinguished on the basis of their composition of the biotite and feldspars. It shows that the most reliable $^{40}Ar/^{39}Ar$ dating comes from the Faneromeni section, where the sanidine is separated from the plagioclase.

Preliminary results suggest that the use of a fluent monitor standard age of 27.92 Ma for the TCR sanidine shows a good agreement with the astronomical ages.

Continental sections

A reliable chronological framework was still lacking for (most of) the continental biostratigraphic time scale for the European Miocene. Correlation of Neogene Mammal (MN) zones and corresponding fauna assemblages to the absolute time scale was mainly based on correlation with marine biostratigraphy and regional zonations (e.g. Paratethys Stages). Radiometric datings on intercalated volcanic sediments are rare and nearly always require extrapolation over a large stratigraphic distance towards the position of the fossil locality. Magnetostratigraphic studies in continental deposits are often thought to be hampered by hiatuses, (unknown) changes of sedimentation rates and the scarcity of long continuous outcrops. The comparison of continental fossil localities or regional zonations and the marine time scale remained ambiguous, in absence of reliable age determinations.

In **Chapter 6** three MN (Mammal Neogene) zone boundaries are accurately dated. They appear to be significantly younger (up to 3 Myr) than previously assumed in continental time scales. Furthermore, an important climate change in the continental biostratigraphic record to a cooler and more humid climate is magnetostratigraphically dated to occur at 14.1 Ma. This age is consistent with the age estimate of 14.1-14.05 Ma for the main increase in $\delta^{18}O$ in the marine record. These independent observations of time-equivalent cooling in both the continental and marine records confirm and accurately date a global cooling event in the middle Miocene.

In **Chapter 7** a detailed chronology for the middle to late Miocene continental record is presented, based on high-resolution biostratigraphic and magneto-stratigraphic data of mammal-bearing sections in Spain. Our results indicate that these sections compose an almost complete magnetostratigraphic succession from the lower Aragonian (MN 4; 18 Ma) to the middle Turolian (MN 12; 7 Ma). Seven successive MN zone boundaries are directly dated in sections which often contain faunas of two successive regional zones.

One of the spanish sections, that of Armantes in the Calatayud-Daroca basin, is a red bed sequence consisting of a regular alternation (10 m scale) of reddish silts and pink/white limestones. In between these limestones, a smaller-scale bedding (2-3 m scale) is intercalated, characterised by varying carbonate content and related erosional resistance. Correlation of the magnetic polarity sequence to the GPTS results in a periodicity of 111 kyr for the large-scale cyclicity, suggesting a relation with the eccentricity cycle of the Earth's orbit. In **Chapter 8,** the results of a detailed sampling - of an interval which includes three limestone beds - suggests that the observed cyclicity in the Armantes section is indeed related to astronomically induced climate changes and that the paleomagnetic

properties of these type of sediments are suitable for constructing of a astronomical polarity time scale (APTS) for the continental realm.

Finally, in **Chapter 9**, the magnetostratigraphic results of six late Oligocene to middle Miocene mammal-bearing sections in central Turkey are presented and - where possible - correlated to the geomagnetic polarity time scale (GPTS). Correlation of the Turkish faunas to the European faunas is of crucial importance to understand what geologic or climatic events have triggered the migration of mammals from Anatolia to Europe during the middle and late Miocene.

Chapter 1

The age of the Tortonian/Messinian boundary

Abstract

The Tortonian/Messinian boundary is marked by the first occurrence datum (FOD) of *Globorotalia conomiozea* which is found all over Crete in open-marine marls with good paleomagnetic properties. Within the framework of the MIOMAR project, the previously studied sections of Langereis et al. (1984) have been extended and (partly) resampled. Here, we present new magneto-stratigraphic and biostratigraphic results from sections on eastern Crete (Faneromeni), central Crete (Kastelli) and western Crete (Potamida and Skouloudhiana) supplemented by cyclostratigraphic data.

The recently developed geomagnetic polarity time scale (CK92) of Cande and Kent (1992) allows an unambiguous correlation of the polarity sequences on Crete. The FOD of *G. conomiozea* occurs in the reversed interval of anomaly C3Bn.1r. This leads to a new age determination of 6.92 Ma for the Tortonian/Messinian boundary and a duration of 1.76 Myr for the Messinian. A slightly modified version of CK92 - if we use more recent age estimates - provides an age of 7.10 Ma and a duration of 1.78 Myr, respectively.

Bipartite sedimentary cycles are distinctly present in the studied Cretan sections. Assuming that these cycles are precession-induced and using an average periodicity of 21.7 kyr enables us to independently estimate the duration of the successive individual polarity zones. The astronomically derived durations of the Cretan polarity zones are in good agreement with CK92, but are approximately 10% shorter.

This chapter has been published as: W. Krijgsman, F.J. Hilgen, C.G. Langereis, W.J. Zachariasse, The age of the Tortonian/Messinian boundary, *Earth Planet. Sci. Lett.*, 121, 533-547, 1994.

Introduction

The Tortonian/Messinian (T/M) boundary is defined in section Falconara on southern Sicily at the level which corresponds with the first occurrence of the *Globorotalia conomiozea* group (d'Onofrio et al., 1975; Colalongo et al., 1979). Most attempts to date the T/M boundary were based on correlating magneto-stratigraphic records of Mediterranean T/M boundary sections with the Geomagnetic Polarity Time Scale (GPTS). Direct magnetostratigraphic control of the boundary stratotype at Falconara itself is not possible because the entire section is subrecently remagnetised (Langereis and Dekkers, 1992). Upper Miocene sections on Crete, however, proved to be of excellent paleomagnetic quality and resulted in a first reliable magnetostratigraphy for the T/M boundary in the Mediterranean (Langereis et al., 1984). On Crete, *G. conomiozea* invariably first occurs in a short interval of reversed polarity, which was correlated with the reversed subchron of Chron 5 (anomaly 3An.1r) in the then available GPTS (Lowrie and Alvarez, 1981). This correlation resulted in an age of 5.6 Ma for the FOD of *G. conomiozea* and, consequently, also for the T/M boundary. Mainly on the basis of biostratigraphic arguments, this calibration was questioned by Berggren et al. (1985). They correlated the same Cretan polarity sequence differently to the geomagnetic polarity time scale - correlating the reversed T/M boundary interval with the upper reversed interval of chron 6 - and obtained an age of 6.1 Ma. Channell et al. (1990), however, found the FOD of *G. conomiozea* in a normal polarity interval at ODP Site 654 in the Tyrrhenian Sea. They derived an age of 6.44 Ma or 5.40 Ma, pending two different interpretations of the nannofossil record (Kastens, 1992). Magnetostratigraphic studies from outside the Mediterranean yielded similar ambiguous results with ages ranging between 5.6 and 6.44 Ma for the FOD of *G. conomiozea* (Loutit and Kennett, 1979; Moreau et al., 1985; Hodell and Kennett, 1986; Edwards, 1987; Turner et. al., 1989). For the actual dating of the T/M boundary these studies are considered less critical because it is questionable whether the FOD of *G. conomiozea*, which represents a migratory event in the Mediterranean (Zachariasse, 1975, 1979), is globally synchronous (Scott, 1980).

An accurate age for the FOD of *G. conomiozea* and hence the T/M boundary will also provide the exact duration of the Messinian, the termination of which is now accurately dated (see Hilgen and Langereis, 1993; and references therein). The age of the T/M boundary is thus an essential parameter for understanding the processes that took place during the Messinian, a period marked by evaporite formation in the Mediterranean (Messinian "salinity crisis"). To provide an unambiguous magnetostratigraphic correlation of the boundary to the GPTS, we decided to restudy the Cretan sections of Langereis (1984). These sections contain distinct sedimentary cycles of various types ($CaCO_3$ cycles, sapropels). These sedimentary cycles are similar to the cycles which have been found in the Mediterranean Plio-Pleistocene and which were correlated to the astronomical cycle of precession (Hilgen, 1991a,b). We initially aimed to estimate the duration

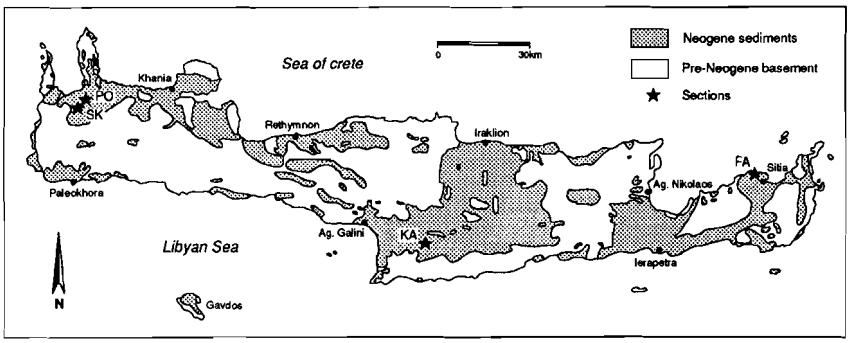

Figure 1. Location of the Cretan sections (FA=Faneromeni; KA=Kastelli; SK=Skouloudhiana; PO = Potamida).

of the successive individual polarity zones on Crete, based on the number of presumably precession-related sedimentary cycles per polarity zone. These estimates can then be compared with the duration of successive (sub)chrons in the GPTS. A re-evaluation of the Cretan sections has become especially relevant, since Cande and Kent (1992) have constructed a new geomagnetic polarity time scale (CK92) in which they recognise two additional normal subchrons in the reversed interval of Chron 6 (C3Br.1n, C3Br.2n). This resulted in an essentially different polarity pattern for the late Miocene.

The present study is part of the MIOMAR (MIOcene Marine Archives Reading) project. Major aims are to extend the astronomical polarity time scale into the Miocene and to develop an integrated magnetostratigraphy, multiple biostratigraphy, cyclostratigraphy and isotope stratigraphy for the late middle to late Miocene in the Mediterranean. In this paper, we focus on the detailed magnetostratigraphy of the Cretan sections, their cyclostratigraphy and the correlation to the CK92 geomagnetic polarity time scale. The precise correlation of the sedimentary cycles to the astronomical record will be subject of future studies.

Sections and sampling

All over Crete, a transition from sandy littoral deposits to open-marine marls is observed in the Tortonian. Generally, the marls are again overlain by shallow-marine beige to whitish marls and limestones of Messinian age. We extended and resampled in more detail the Faneromeni and Kastelli sections (Langereis, 1984) and part of the Skouloudhiana section (Langereis et al., 1984). Where possible and appropriate, we studied also the cyclostratigraphy of the - cyclically bedded - sections in detail, a study we had previously omitted.

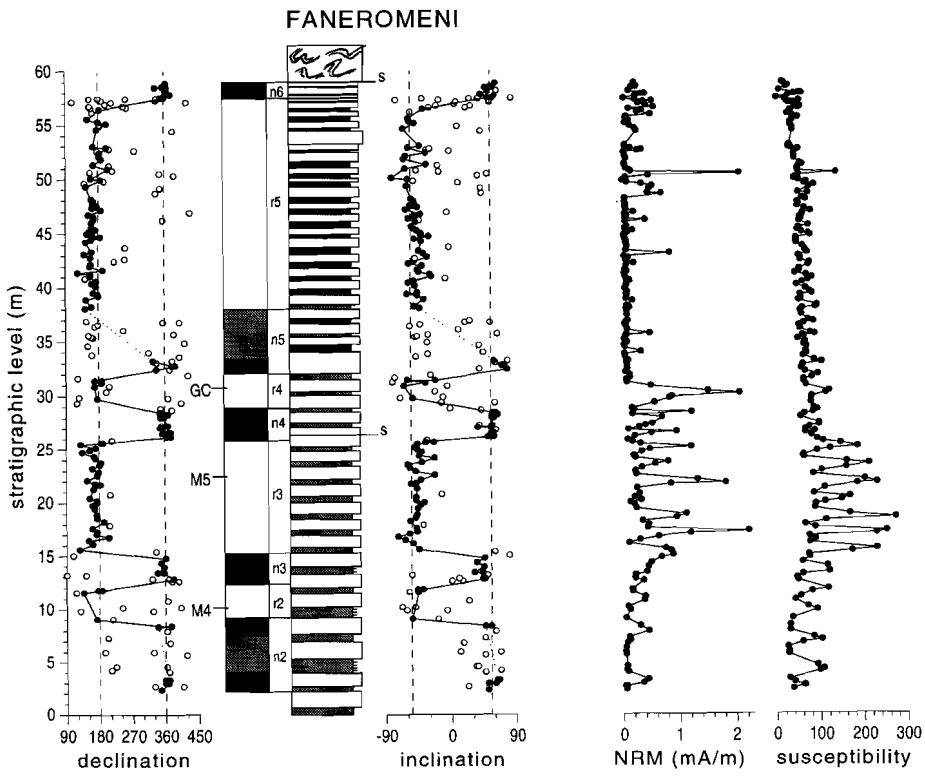

Figure 2. Magnetostratigraphy, lithology, susceptibility and NRM-intensities of the Faneromeni section. Solid symbols represent reliable directions, open symbols represent low intensity samples which are difficult to interpret. Dashed lines indicate declination and inclination of the geocentric axial dipole field for the present latitude of Crete. In the polarity column, black (white) denotes normal (reversed) polarity zones; shaded interval denotes zone with undefined polarity. The lithostratigraphic column displays cyclic sedimentary variations of white (white), grey (grey) and sapropeletic (black) layers Biostratigraphic datum levels are GC = FOD of *Globorotalia conomiozea*, M5 = FOD of *Globorotalia menardii* form 5, M4 = LOD of *Globorotalia menardii* form 4, s = bedding-parallel shear plane.

The Faneromeni section is located along the north coast of Crete, just west of Sitia (Fig. 1) and consists mainly of blue-grey marls. The section has a thickness of 60 m and is excellently exposed. It contains an undisturbed and complete succession except for a bedding-parallel shear plane in the middle part (fig 2). In the upper part of the section a 1.5 m thick slump level is present, which comprises a single sedimentary cycle. A transition from open-marine marls to shallow-marine carbonates marks the uppermost part of the section. Sampling was continued up to a bedding-parallel shearplane which forms the base of a major slump level.

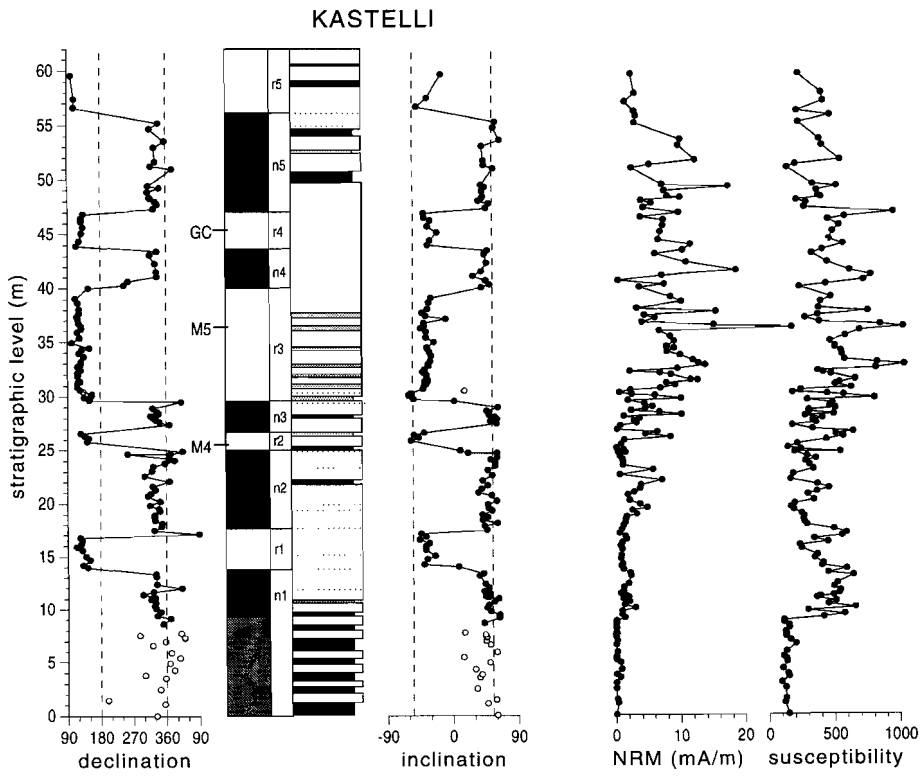

Figure 3. Magnetostratigraphy, lithology, susceptibility and NRM-intensities of the Kastelli section. See also caption to figure 2. ; dotted lines in the lithological column are sandy interbeds.

The Kastelli section on central Crete (Fig. 1) has a thickness of 60 m and consists of sediments similar to those of the Faneromeni section. The earlier sampled section (Langereis et al., 1984) has been resampled and extended downward (Fig. 3).

The sections on western Crete (Fig. 1) near the villages of Potamida and Skouloudhiana have previously been studied and sampled in detail (Langereis et al. 1984). We have not resampled the Potamida sections but constructed a composite section by combining Potamida 1 and 3 (Fig. 4). The Skouloudhiana section (Fig. 5) consists of a lower and upper part, separated by a non-exposed interval. We extended the upper Skouloudhiana section downward by several metres but did not succeed in closing the stratigraphic gap. Since we cannot exclude the existence of faults in the non-exposed interval, the relation between the two sections remains uncertain. In this paper, we only discuss the results of

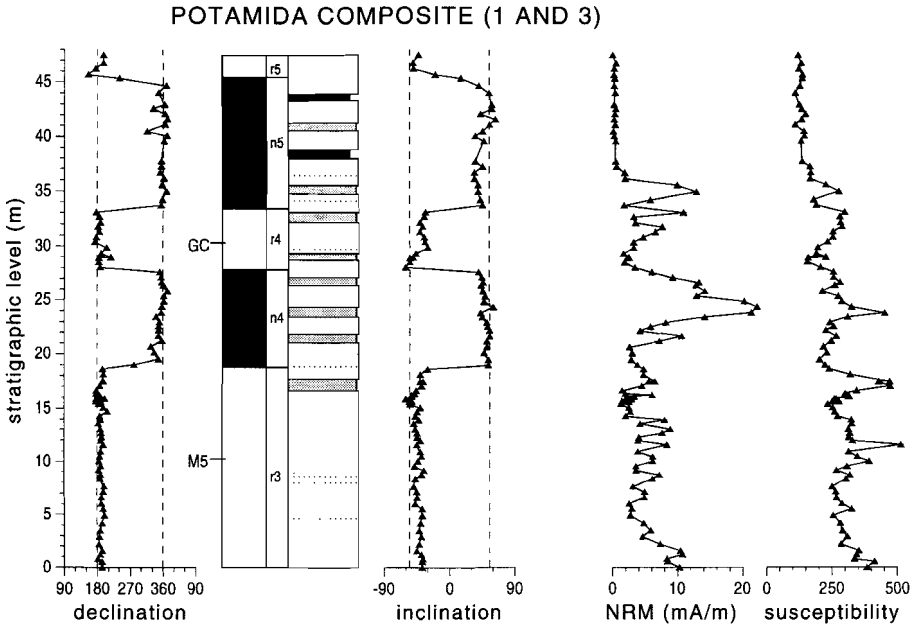

Figure 4. Magnetostratigraphy, lithology, susceptibility and NRM-intensities of the Potamida section. The data are from the thermally demagnetised specimens of the earlier sampling of Langereis et al. (1984). See captions to figures 2 and 3.

the upper Skouloudhiana section because it overlaps but also extends the composite Potamida section.

Paleomagnetic samples were taken with an average spacing of approximately 30 cm. This corresponds to 4-7 sample levels per sedimentary cycle. In the Faneromeni section, 208 levels were sampled, in the Kastelli section 164 levels. At each level, we took standard paleomagnetic cores (25 mm diameter) with an electric drill and a generator as power supply. As routine procedure, we removed the weathered surface in order to drill in sediments as fresh as possible. For the Potamida 1 and 3 sections and the upper Skouloudhiana section we have used the thermal demagnetisation data of Langereis et al. (1984). In the latter section, an additional 52 levels were sampled.

Biostratigraphy and cyclostratigraphy

The planktonic foraminiferal biostratigraphy used in this paper is the one employed in earlier papers and consists of the following sequence of bioevents (in stratigraphic order) : LOD of *Globorotalia menardii* form 4, FOD of *Globorotalia*

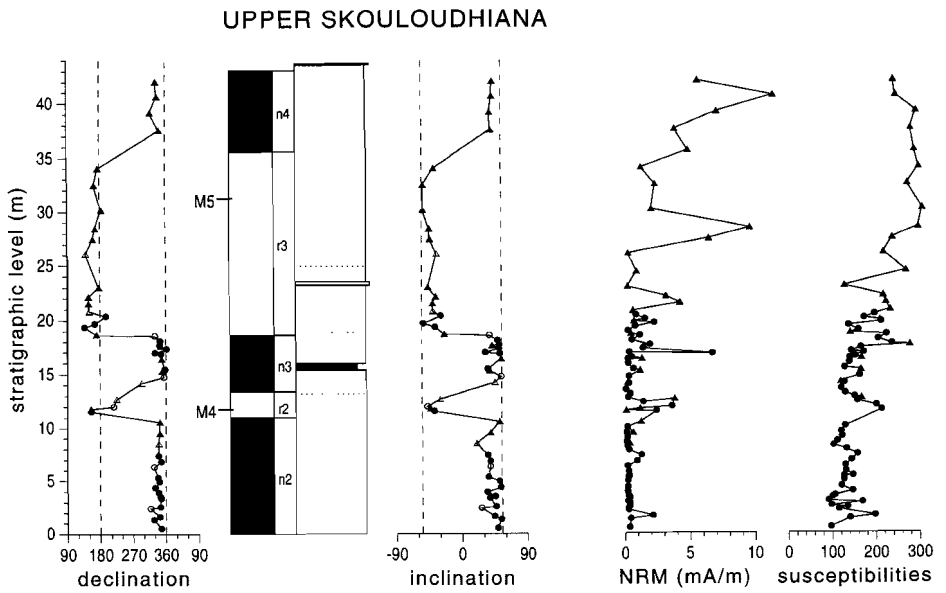

Figure 5. Magnetostratigraphy, lithology, susceptibility and NRM-intensities of the Skouloudhiana section. Triangles represent data derived from the thermally demagnetised specimens of the earlier sampling of Langereis et al. (1984); circles are from this study. See captions to figures 2 and 3.

menardii form 5, and FOD of the *Globorotalia conomiozea* group (Zachariasse, 1975, 1979; Langereis et al., 1984). These bioevents occur in three successive intervals of reversed polarity (r2, r3 and r4; see figs. 2-5) and provide a solid biostratigraphic framework for correlating upper Tortonian to lower Messinian sections over the entire length of the Mediterranean.

The position of the FOD of *Globorotalia menardii* form 5 in the resampled Faneromeni section is slightly below the position reported by Langereis (1984). This modification is caused by the much higher resolution in the present Faneromeni section.

All studied sections show a distinct cyclic bedding (see figs. 2-5). At Faneromeni, the sedimentary cycles consist of bipartite depositional sequences displaying distinct grey-white colour variations in which the grey beds are less indurated. In the upper half of the section, sapropels start to occur within, or completely substitute, grey beds (of the grey-white colour cycles). At Kastelli, sedimentary cycles mainly consist of sapropel-marl alternations. Sapropel containing intervals alternate with thick homogeneous marl intervals in which the cyclic bedding is less obvious. Nevertheless, variations in induration of the marls are present which resemble the bipartite grey-white colour cycles at

Faneromeni. Although not as distinct as at Faneromeni and Kastelli, also the Potamida composite section shows typical variations in colour and, more evident, in induration, especially in the middle and upper part of the section (Fig. 4). In the uppermost part, two distinct sapropel layers are present. In the lower part of the section, the variations in colour and induration are more difficult to interpret. Here, the vague colour variations have not been indicated in figure 4, but may point to quadripartite rather than to bipartite sedimentary cycles.

Together with the magnetostratigraphic and biostratigraphic results, a consistent and coherent cyclostratigraphy starts to emerge for the Mediterranean upper Miocene with the same potential as the well-established cyclostratigraphies for the Mediterranean Pliocene and lower Pleistocene (Hilgen, 1991a,b; Langereis and Hilgen, 1991) and the upper Pleistocene (Ryan, 1972). The two oldest sapropels in the Faneromeni section - which occur in polarity zone n5 (Fig. 2) - can be recognised in all sections except Skouloudhiana where this stratigraphic level is not reached. The three sapropels, which occur in the successive polarity zones n2, r2 and n3 at Kastelli and which alternate with regular grey-white cycles, provide another sapropel pattern. Although no sapropels are present in the correlative part of the Faneromeni section, three thick grey marlbeds, containing numerous thin sandbeds, can be correlated with these three sapropels (see Fig. 2).

Magnetostratigraphy

The bulk susceptibility of the samples was measured on a Kappabridge KLY-2. The natural remanent magnetisation (NRM) was measured on a 2G Enterprises cryogenic magnetometer. At least one specimen from each sampling level was progressively demagnetised by applying stepwise thermal demagnetisation with small (30-50 °C) temperature increments.

Eastern Crete : Faneromeni

In the Faneromeni section, the NRM shows very low intensities in the lower and upper part of the section, and relatively high intensities - one order of magnitude higher - in the middle part (fig 2). Thermal demagnetisation (Fig. 6a-f) shows that in most samples a small viscous and laboratory-induced component is removed at 100 °C. A relatively small secondary present-day field component is removed at 200-225 °C. A characteristic remanent magnatisation (ChRM) is usually totally removed at temperatures ranging from 300 °C to 400 °C. Further demagnetisation at higher temperatures mainly results in a randomly directed viscous magnetisations. Especially for the samples with relatively high NRM intensities, the ChRM direction can reliably be determined (Fig. 6a,b). The demagnetisation diagrams of samples with a lower NRM often show a cluster

with temperatures ranging from 240 °C to 390 °C (Fig. 6c,6d). Here, a characteristic direction cannot accurately be determined but the normal or reversed polarity is in most cases unambiguous. Several levels show results which are less reliable because of a very weak magnetic signal (fig 6e,f); the interpreted directions of these samples are plotted with an open circle in figure 2.

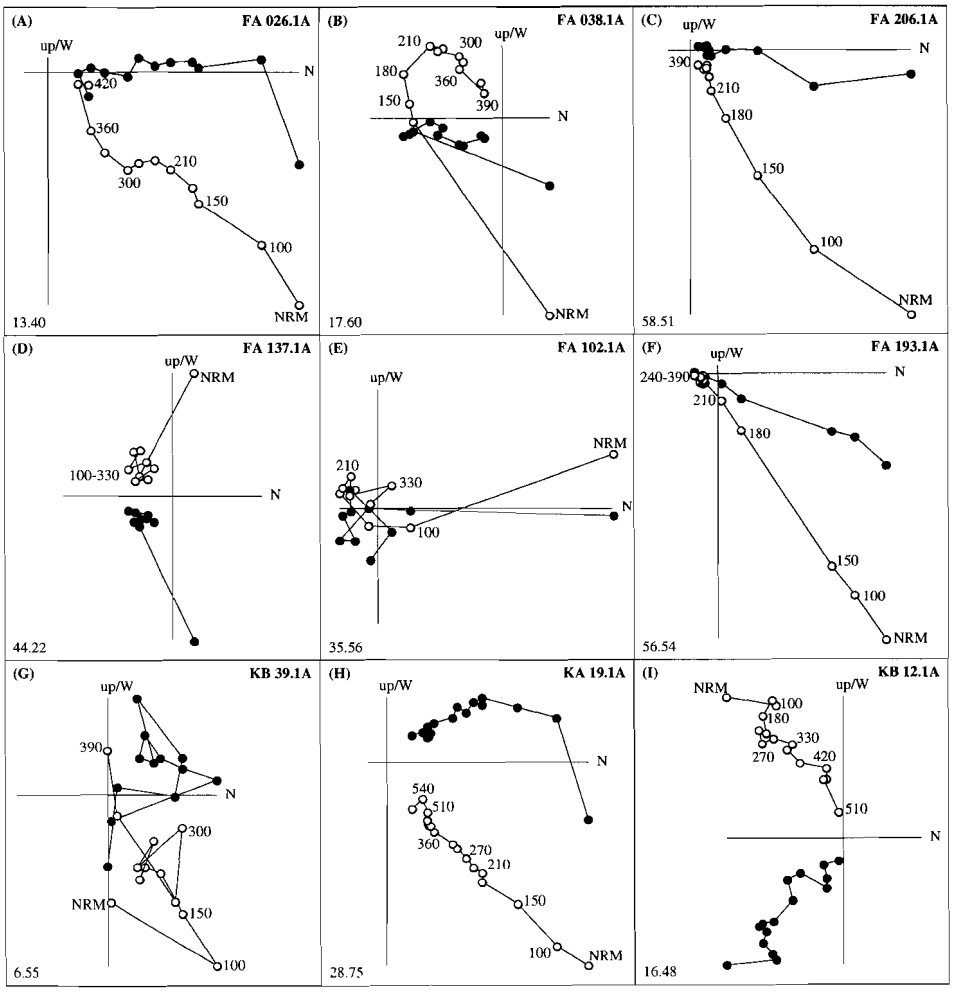

Figure 6. Orthogonal projections of stepwise thermal demagnetisation of selected samples from the Faneromeni (FA) and Kastelli (KA) sections. Solid (open) symbols represent the projection of the ChRM vector end-point on the horizontal (vertical) plane. Values represent temperatures in degrees Celcius; stratigraphic levels are in the lower left corner.

The ChRM directions and polarity zones (Fig. 2) show that eight polarity reversals are recorded in the Faneromeni section. Unfortunately, two intervals of the section show such a low intensity that directions and even polarities are uncertain. Especially in the interval above the normal zone n5, some samples tend to show - although inconsistently - a reversed polarity (Fig. 6e). Such a reversed polarity, however, is not in good agreement with the unambiguous results of the other time-equivalent Cretan sections. In the uppermost part of the section, the r5/r6 polarity reversal is accompanied by low intensities; the sedimentary cycles are in this part rather thin.

The susceptibility record of the Faneromeni section (Fig. 2) shows that maximum values of susceptibility coincide with the grey intervals of the sedimentary cycles. Hence, the susceptibility record can be used for estimating the number of cycles in parts of the sections in which the cyclic bedding is less distinct. We assume, for instance, that the maximum in susceptibility within the anomalously thick white interval just below the first sapropeletic layer in Faneromeni represents an extra 'grey interval'. This indicates that this white interval actually consists of two sedimentary cycles.

Central Crete : Kastelli

The NRM intensities in the Kastelli section are much higher than in the Faneromeni section and range from 1 to 20 mA/m. The highest intensities occur, just like in Faneromeni, in the magnetic zone r3 (Fig. 3). Thermal demagnetisation shows the same characteristics as in the previous study of Langereis et al. (1984). After removing a laboratory induced magnetisation at 100 °C, the demagnetisation diagrams generally reveal a stable and well-defined characteristic remanent magnetisation (Fig. 6h,6i). Since most of the magnetisation is removed at temperatures of approximately 580 °C, it can be concluded that magnetite is the main carrier of the remanence. In some samples, the remanence is only completely removed at temperatures above 600 °C, which suggests that some hematite or cation-deficient magnetite (Heider and Dunlop, 1986) is also present.

Nine polarity reversals are recorded in the Kastelli section. The biostratigraphic and magnetostratigraphic evidence indicates that the section contains two extra polarity zones that are older than the ones recorded in the Faneromeni section (n1,r1; Fig. 3). The ChRM-direction and polarity are mostly unmistakable (Fig. 6h,i), except for the lowermost part of the section where the results are less reliable (Fig. 6g). The large tectonic rotation of the area (42°; Langereis, 1984) helped us to distinguish primary from secondary normal components. The normal zones n2 and n5, which showed ambiguous results at Faneromeni, are here unequivocally established.

The susceptibility of the Kastelli section is higher than at Faneromeni (Fig. 3). Maximum values in susceptibility coincide also in Kastelli with the grey parts of

the sedimentary cycles. It allows us to estimate the number of sedimentary cycles in the parts of the section where lithological variations are less evident.

Western Crete : Potamida and Skouloudhiana

Both the Potamida and Skouloudhiana sections show in general excellent demagnetisation characteristics (Langereis et al., 1984). NRM intensities are rather high, especially in Potamida and the upper part of Skouloudhiana, which corresponds to the same magnetic polarity interval as in Faneromeni and Kastelli.

The magnetostratigraphic record of the Potamida section as well as the Skouloudhiana section reveals four polarity reversals. The position of the biostratigraphic datum levels show that the lowermost reversal boundary (R-N) in Potamida corresponds to the uppermost one in Skouloudhiana (figs. 4, 5).

Again, in the Potamida composite section, the greyish coloured, indurated beds correlate with relative maxima of susceptibility (Fig. 4). Therefore, they may be considered as the equivalent of the grey parts of the sedimentary cycles known from Faneromeni.

Discussion

The magnetostratigraphic results of the present study essentially confirm the earlier results of Langereis (1984). The upward extension of the Faneromeni section resulted in the registration of an extra polarity reversal (from R to N). The only evidence in all sections for hiatuses is the bedding-parallel shear-plane in polarity zone n4 of the Faneromeni section. This shearplane marks only a minor hiatus. The LOD of *G. menardii* form 4, the FOD of *G. menardii* form 5 and the FOD of *G. conomiozea*, are in all sections found in three (r2,r3,r4) successive periods of reversed polarity. Combining the results of the Cretan sections shows that the polarity patterns of all sections are in good agreement and that in total ten polarity reversals and hence nine complete polarity zones have been recorded.

Correlation with CK92

The first step is to find out whether we can correlate the Cretan polarity sequences to the new time scale (CK92) of Cande and Kent (1992) on the basis of the polarity pattern alone. The correlations of Langereis et al. (1984) and Berggren et al. (1985) of the Cretan polarity sequence to the commonly used GPTS (Lowrie and Alvarez, 1981; Berggren et al., 1985) have led to considerable controversy. However, the CK92 time scale shows more detail in the late Miocene with respect to the time scale of Berggren et al. (BKFV85). In particular, the former Chron 6 of BKFV85 contains two additional short normal subchrons in CK92. This

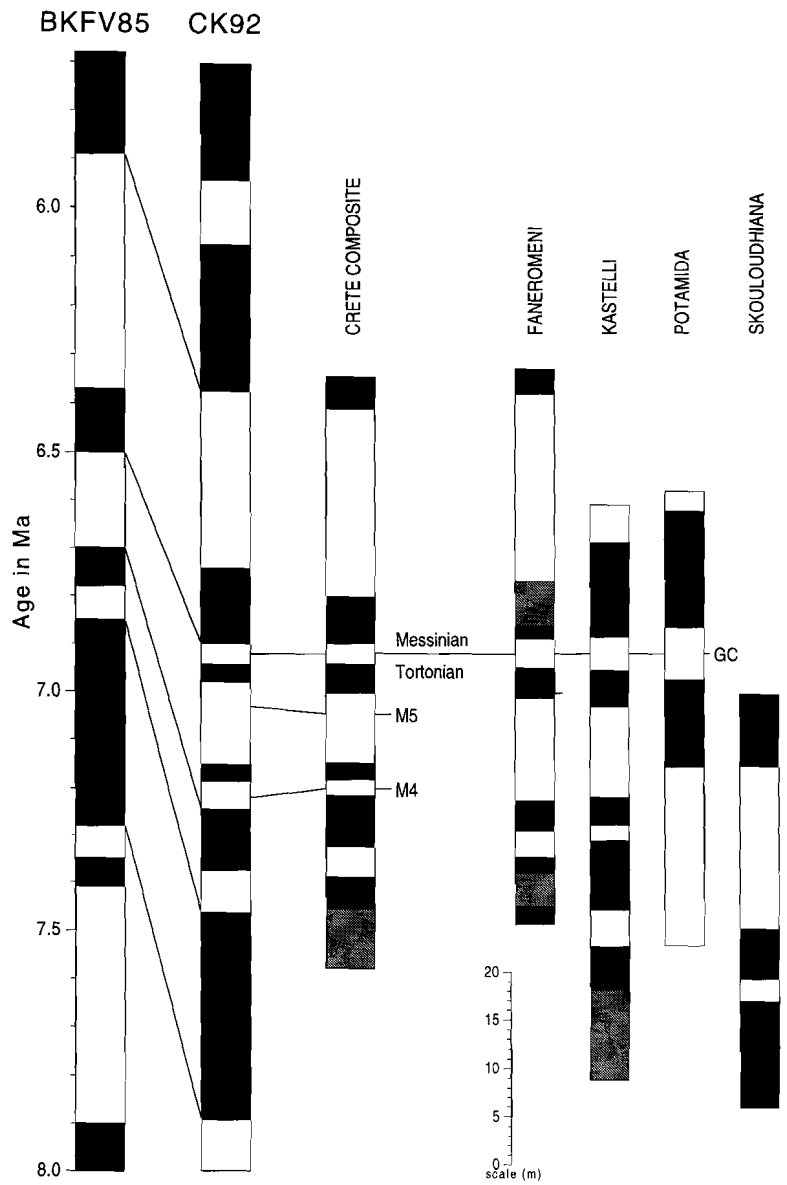

Figure 7. Correlation of the Cretan polarity sequences with the GPTS of Berggren et al. (BKFV85) (1985) and of Cande and Kent (CK92) (1992). Lines connect the same reversal boundaries and emphasise the difference in polarity pattern between the two time scales. The polarity zones of the Crete Composite column are given as astronomical durations derived from the number of precession related sedimentary cycles (Table 1.) Polarity zones of the four Cretan sections (Faneromeni, Kastelli, Potamida and Skouloudhiana) are given in stratigraphic distances. Biostratigraphic markers GC (= Tortonian/Messinian boundary), M5 and M4 as in caption to figure 2.

zone	nr. of cycles			duration (kyr)
	Faneromeni	Kastelli	West Crete	composite
n6	**>3**			**>65**
r5	**18**			**391**
n5	**4.5**	*4.5-5*	**4.5**	**98**
r4	**2**	*2-2.5*	**2**	**43**
n4	*2.75*	*2.5*	**2.75**	**60**
r3	**6.75**	*6.25*	*6.8*	**146**
n3	**1.5**	**1.5**	*1.5*	**33**
r2	**1.5**	**1.5**	*1.5*	**33**
n2	**>3**	*5*		*109*
r1		*3*		*65*
n1		**>9**		**>195**

Table 1. Number of sedimentary cycles in the Faneromeni, Kastelli and west Cretan (Potamida and Skouloudhiana) sections. Bold values represent the number of cycles counted directly from the lithological columns (figs. 2-5). Italic values represent the number of cycles estimated using the susceptibility record and/or a constant sedimentation rate. Zonation as in figs. 2-5. Astronomical durations for the individual polarity zones (right column) are estimated using an average periodicity of 21.7 kyr. for precession (Berger, 1984).

substantially modifies the polarity pattern during this time interval and allows an unambiguous correlation of the Cretan polarity sequences to CK92 (Fig. 7). Furthermore, it can now be concluded that neither the correlation of Langereis et al. (1984) nor the one of Berggren et al. (1985) was correct. Finally, Channell et al. (1990) appear to have missed the short reversed interval of anomaly C3Bn.1r in ODP Site 654, since they found the FOD of *G. conomiozea* in an interval of normal polarity.

The different and more detailed polarity pattern of CK92 for the late Miocene solves the previous correlation problems. The new correlation results in an age of 6.92 Ma for the FOD of *G. conomiozea*, and in ages of 7.03 Ma and 7.22 Ma for the FOD of *G. menardii* form 5 and the LOD of *G. menardii* form 4, respectively. Consequently, the age of the Tortonian/Messinian boundary arrives at 6.92 Ma according to the CK92 time scale. Since the age of the Miocene/Pliocene boundary is determined at an age of 5.16 Ma with respect to CK92, the duration of the Messinian is 1.76 Myr.

Comparison with astronomically derived durations

Additional support for our present correlation is provided by the sedimentary cycles, assuming that this cyclicity is controlled by the astronomical cycle of precession. This assumption is based on the fact that the observed sedimentary

Chron	polarity	duration (kyr) CK92	zone	duration (kyr) This study
	R	660		
C3An.1n	N	240		
	R	130		
C3An.2n	N	300	n6	>65
	R	**368**	r5	**391**
C3Bn	N	**157**	n5	**98**
	R	**45**	r4	**43**
C3Br.1n	N	**35**	n4	**60**
	R	**172**	r3	**146**
C3Br.2n	N	**34**	n3	**33**
	R	**58**	r2	**33**
C4n.1n	N	**131**	n2	**109**
	R	**88**	r1	**65**
C4n.2n	N	428	n1	>195
	R	155		
Total duration of the Cretan polarity sequence:		**1088**		**978**

Table 2. Comparison of the astronomically derived duration (right) of the individual polarity zones with the sea-floor spreading derived duration of the corresponding (sub)chrons in CK92 (left). Note the large difference between the astronomical duration and CK92 for the total Cretan polarity sequence.

cycles are similar to the sedimentary cycles found in the Mediterranean Plio-Pleistocene: these younger cycles proved to be invariably related to the precession cycle (Hilgen, 1991a,b). Combining the number of cycles in the Faneromeni section with the polarity reversal ages of CK92 enables us to calculate the average duration of the sedimentary cycles. The resulting 23.5 kyr strongly suggest that these cycles are indeed related to the precession cycle which has an average periodicity of 21.7 kyr (Berger, 1984). Any other correlation to CK92 leads to unrealistic (changes in) sedimentation rates and durations for the cycles. In those parts of the sections where the cyclic bedding is clearly developed, counting of the cycles in individual polarity zones is straightforward. Where sampling took place in sufficient detail, the susceptibility record can also be used. Where necessary, we derived an average thickness of the sedimentary cycles and estimated the number of cycles for those parts which showed no clear cyclic lithology. It appears that the number of cycles per individual polarity zone agrees very well (Table 1).

The next step is to use the 'true' average periodicity of 21.7 kyr (Berger, 1984) instead of the average periodicity of 23.5 kyr derived from CK92. This enables us to independently estimate the duration of the individual polarity zones in every section (Table 1). We have also used these durations to construct a composite

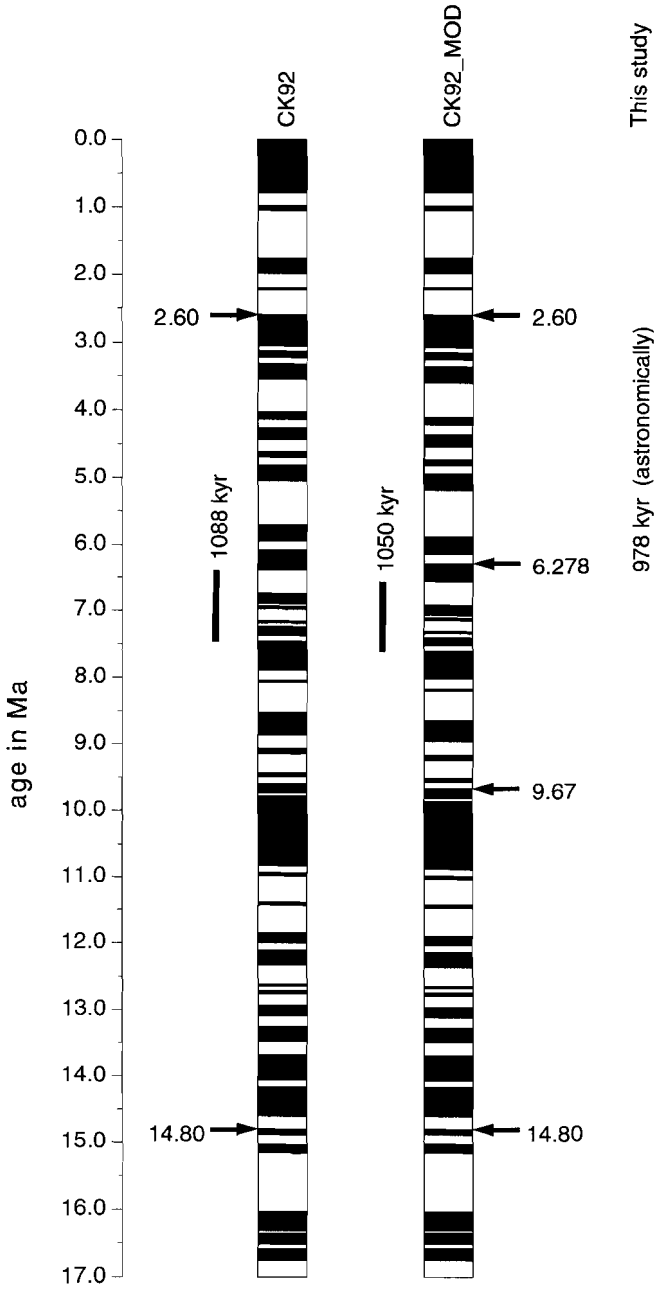

Figure 8. CK92 time scale (left column) and modified GPTS (CK92_MOD; right colomn) using new astronomical and radiometric calibration points. Further explanation and references see text. Small black columns indicate the total duration of the composite Cretan polarity sequence correlated straightforwardly to the GPTS. Astronomical duration is derived from the number of precession induced sedimentary cycles (Table 2).

Cretan 'astronomical' polarity time sequence (Fig. 7). A comparison of this polarity time sequence with the seafloor spreading derived durations of CK92 shows that there is in general a good agreement in the pattern, but the astronomically derived duration (978 kyr) for the complete polarity sequence is 110 kyr shorter than the correlative part in CK92 (1088 kyr; Table 2). This shorter astronomical duration is unexpected because for the Plio-Pleistocene astronomical ages (Shackleton et al. 1990; Hilgen, 1991a,b) proved to be invariably older (by 5-7%) than the ages in the conventional time scales. The variable period of precession - ranging from 14 to 28 kyr for individual cycles (Berger, 1984) - can be held responsible for discrepancies in the duration of individual polarity zones that are relatively short. But it does certainly not explain the 110 kyr discrepancy for the duration of the complete polarity sequence.

An explanation for this discrepancy in duration are errors in the ages of the calibration points of CK92 and/or differences in sea floor spreading rate between the calibration points. Cande and Kent used an astronomical age of 2.60 Ma for the Gauss/Matuyama boundary (C2An (y)) and a radiometric age of 14.8 Ma for the younger end of chron C5Bn.1n (y) (Miller et al., 1985) to construct the late Miocene part of CK92. Astronomically derived ages for polarity reversals in the Gilbert Chron and Chron 5, however, are approximately 180 kyr older than in CK92 (Hilgen, 1991b; Shackleton et al., 1993). Furthermore, Baksi (1993) obtained an $^{40}Ar/^{39}Ar$ age of 9.67 Ma for the younger end of chron C5n (y). This is only 80 kyr older than the interpolated age of 9.592 Ma for the same reversal in CK92.

Incorporating an astronomical age of 6.278 for the younger reversal boundary of chron C3An.2n (y) (Shackleton et al., 1993) and a radiometric age of 9.67 for

C5n (o) (Baksi, 1993) as age calibration points in the CK92 time scale enables us to re-estimate the ages of the polarity reversals. If we use linear interpolation between the two new calibration points, the correlation of the Cretan polarity sequence to the modified polarity pattern (CK92_MOD; Fig. 8) results in an age of 7.10 Ma for the FOD of *G. conomiozea* and hence also the Tortonian/Messinian boundary. This age agrees reasonably well with radiometric datings from the northern Apennines, where Vai et al. (1993) obtained an age of 7.33 ± 0.08 Ma biotite-rich layers a few metres below the FOD of *G. conomiozea.* They suggest an age of 7.26 ± 0.10 Ma for the Tortonian/Messinian boundary, based on the inferred sedimentation rate. Since the astronomical age of the Miocene/Pliocene boundary is accurately dated at 5.32 Ma (Hilgen, 1991b), the use of CK92_MOD provides a duration of the Messinian of 1.78 Myr. This duration does not deviate significantly from the 1.76 Myr duration according to CK92.

The modified CK92 time scale results in a reduction, but not in a complete elimination of the 110 kyr discrepancy between the astronomically derived duration of the Cretan polarity sequence and CK92 (Fig. 9). This problem can only be solved after the sedimentary cycles in the Cretan sections have been calibrated directly to the astronomical record.

Conclusions

We have established detailed magnetostratigraphic, biostratigraphic and cyclostratigraphic records for four upper Tortonian to lower Messinian sections on Crete. Combining these sections enables us to construct a composite polarity sequence which contains ten polarity reversals. The recognition of two additional short subchrons in the CK92 time scale, not recorded before in the commonly used time scales, solves the previous correlation problem of the late Miocene Cretan polarity sequence to the GPTS (Langereis et al., 1984; Berggren et al., 1985). Our correlation implies that the FOD of *G. conomiozea* and hence the Tortonian/Messinian boundary occurs in the short reversed polarity subchron C3Bn.1r of CK92 (or CK92_MOD), resulting in an age of 6.92 (or 7.10) Ma for the T/M boundary and a duration of 1.76 (or 1.78) Myr for the Messinian. Furthermore, new ages are derived for the FOD of *G. menardii* form 5 (7.03, or 7.20 Ma) and the LOD of *G. menardii* form 4 (7.22, or 7.38 Ma) which are found in successive periods of reversed polarity (C3Br.1r, C3Br.2r, respectively).

We used precession-controlled sedimentary cycles to independently estimate the duration of the late Miocene polarity sequence on Crete. It appears that the astronomically derived duration is 10% shorter than the duration of the same polarity sequence in CK92. If the most recent astronomical and $^{40}Ar/^{39}Ar$ radiometric age determinations are incorporated in the CK92 time scale as new calibration points, this discrepancy is reduced but not completely eliminated.

Acknowledgements

P.J. Verplak assisted in the field and also measured many of the samples. G.J. van 't Veld and G. Ittman prepared the micropaleontological samples. G. Postma, I.M. Villa, G.B. Vai and D.V. Kent read an earlier version of the manuscript and provided useful comments. The reviews by C. Laj and Y. Gallet are greatfully acknowledged. This study was partly funded by the Netherlands Organization of Scientific research (NWO). This is MIOMAR contribution no. 2.

Chapter 2

Late Miocene magnetostratigraphy, biostratigraphy and cyclostratigraphy in the Mediterranean

Abstract

A new chronology for the late Miocene of the Mediterranean is presented by combining magnetostratigraphic, biostratigraphic (planktonic foraminifera and dinoflagellates) and cyclostratigraphic data. Long and continuous upper Miocene sections on Gavdos (Metochia section) and Sicily (Gibliscemi section) display cyclic alternations of homogeneous marls and sapropels and can be correlated on the basis of their distinct cyclic patterns. The Metochia section yields a good paleomagnetic signal and the position of 17 polarity reversals can be determined. The resulting polarity sequence allows an unambiguous correlation to the geomagnetic polarity time scale (GPTS). The paleomagnetic signal in the Gibliscemi section is too weak to determine a reliable polarity sequence, except for the lowermost part of the section. Detailed biostratigraphic analysis results in the identification of 13 planktonic foraminiferal and 9 dinoflagellate bioevents, which can all be accurately dated. The Tortonian/Messinian boundary, defined by the First Regular Occurrence (FRO) of the *G. conomiozea* group is determined in chron C3Br.1r with an age of 7.12 Ma, according to the GPTS (CK95) of Cande and Kent (1995).

This chapter has been published as: W. Krijgsman, F.J. Hilgen, C.G. Langereis, A. Santarelli, W.J. Zachariasse, Late Miocene magnetostratigraphy, biostratigraphy and cyclostratigraphy in the Mediterranean, *Earth Planet. Sci. Lett.*, 136, 475-494, 1995.

Introduction

The chronology of the Mediterranean Pliocene and Pleistocene has improved substantially during the last decade since several integrated magnetostratigraphic and biostratigraphic studies have been published on land sections and deep sea cores in the eastern Mediterranean (Hilgen and Langereis 1988; Channell et al., 1988, 1990; Zijderveld et al., 1991; Langereis and Hilgen, 1991). All these sections reveal characteristic sedimentary cycle patterns, which were shown to be related to the Earth's orbital cycles of precession and eccentricity. These sections were used to construct an astronomically calibrated polarity time scale (APTS) for the Plio- and Pleistocene (Hilgen, 1991a,b). Such an APTS proved to be more accurate and to have a higher resolution than conventional time scales.

The chronology of the Mediterranean late Miocene, however, is still very poor and restricted to sediments of late Tortonian-early Messinian age. Suitable land-based sections consisting of open marine sediments are rare. On Crete, good paleomagnetic results were obtained from various sections consisting of cyclically bedded marine marls (Langereis, 1984; Langereis et al., 1984). These sections - displaying bipartite sedimentary cycles, do not extend further than 7.7 Ma (Krijgsman et al., 1994a). Paleomagnetic results from late Miocene sequences in Sicily and northern Italy are disappointing. Sections represent too short an interval (Langereis, 1984), have unsuitable paleomagnetic properties (Negri and Vigliotti, 1994) or are completely overprinted by a present day normal field component (Langereis and Dekkers, 1993). Finally, magnetostratigraphic studies from ODP site 654 in the Tyrrhenian sea gave reasonable results but again here the succession is restricted to sediments younger than 7 Ma (Channell et al., 1990).

Our present research aims at the development of a reliable and accurate chronostratigraphic framework for the late Miocene and the extension of the Plio-Pleistocene APTS into the Miocene. We have found long and continuous upper Miocene sections consisting of an alternation of marine marls and sapropels on the island of Gavdos (Greece) and on Sicily (Italy). These sections have been sampled in detail, within the framework of the EU sponsored MIOMAR project, and appeared to be very suitable as Mediterranean reference sections for the late Miocene.

In this paper, we present a new and detailed integrated magnetostratigraphy, biostratigraphy and cyclostratigraphy for the upper Miocene from these sections on Gavdos and Sicily. Furthermore, we incorporate earlier results from sections on Crete for the interval straddling the Tortonian/Messinian boundary (Krijgsman et al., 1994a). The direct calibration of the sedimentary cycles to the astronomical records and the resulting numerical ages for the individual polarity reversals and biostratigraphic datum planes is presented in Chapter 3.

Sections and sampling

The two main sections used in this study are the Metochia section on Gavdos and the Gibliscemi section on Sicily which both consist of open marine, cyclically bedded marl sequences (Fig. 1). Additional data are supplied by sections from Crete (Faneromeni, Kastelli) which have previously been studied (Langereis, 1984; Langereis et al., 1984; Krijgsman et al., 1994a). In all sections, sampling was aimed at a minimum of four levels per sedimentary (precession-related) cycle which corresponds to a resolution of approximately 5 kyr. At each level we took four cores; two standard-oriented paleomagnetic cores and two additional cores for biostratigraphical, sedimentological and geochemical purposes. At some levels, mainly in the laminated beds, it was impossible to drill an oriented core and we only took a non-oriented handsample for biostratigraphic analysis.

Gavdos: Metochia section

The island of Gavdos is located approximately 30 km south of Crete and represents the southernmost emerged part of the Hellenic arc system. The Metochia section is located on the northern part of the island and is composed of two subsections (Metochia B and C) which are separated by a normal fault (Fig. 1; de Stigter 1989). These subsections are correlated

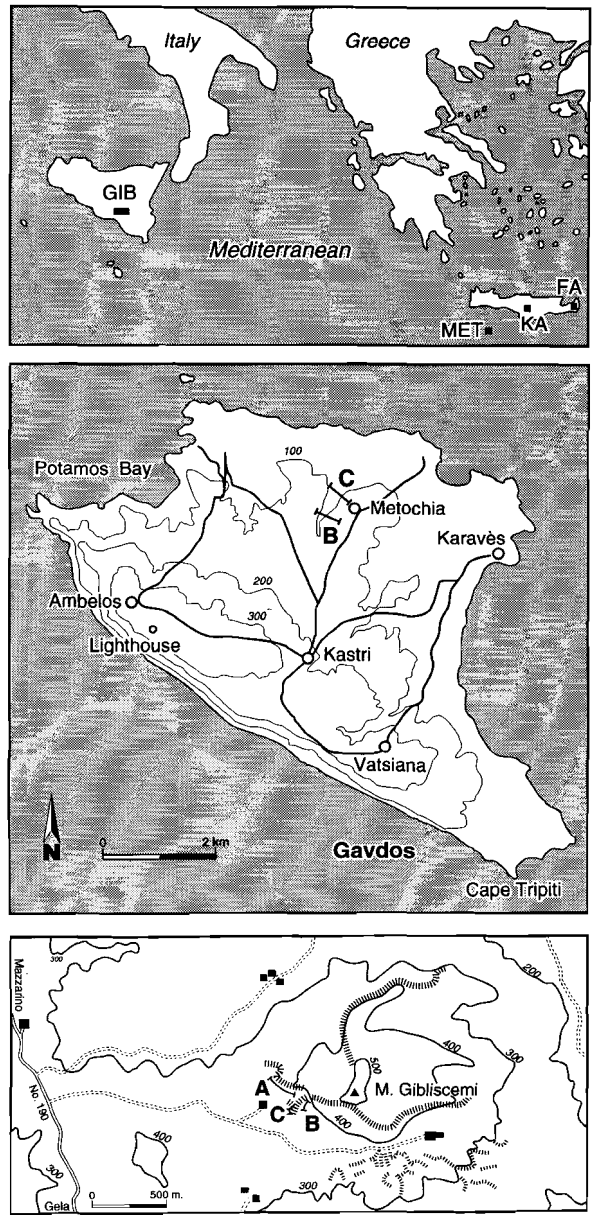

Figure 1. : Location map of the Metochia (MET), Gibliscemi (GIB), Kastelli (KA) and Faneromeni (FA) sections (top); detailed maps showing the trajectories of the subsections Metochia B and C (middle) and Gibliscemi A, B and C (bottom).

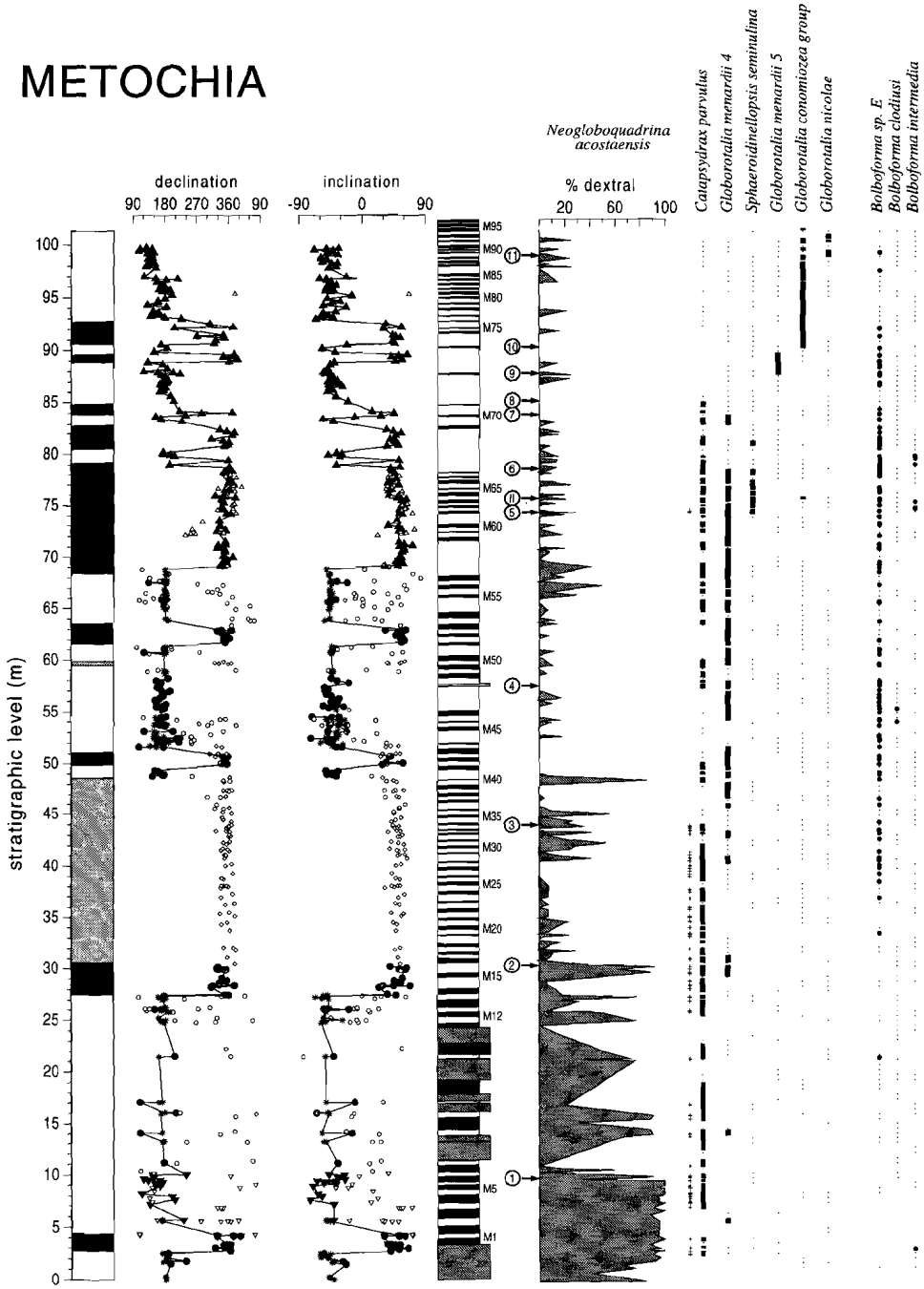
METOCHIA
declination
90 180 270 360 90
inclination
-90 0 90
Neogloboquadrina acostaensis
% dextral
20 60 100
stratigraphic level (m)
0 5 10 15 20 25 30 35 40 45 50 55 60 65 70 75 80 85 90 95 100
M95 M90 M85 M80 M75 M70 M65 M60 M55 M50 M45 M40 M35 M30 M25 M20 M15 M12 M5 M1
11 10 9 8 7 6 11 5 4 3 2 1
Catapsydrax parvulus
Globorotalia menardii 4
Sphaeroidinellopsis seminulina
Globorotalia menardii 5
Globorotalia conomiozea group
Globorotalia nicolae
Bolboforma sp. E
Bolboforma clodiusi
Bolboforma intermedia

on the basis of characteristic lithology patterns. The basal part of Metochia B is formed by a paleosol which is overlain by sediments characteristic of an estuarine environment and shallow marine sands rich in *Heterostegina*, echinoderma and molluscs. These so-called *Heterostegina* sands rapidly pass into deep marine (>200 m) sediments consisting of an alternation of hemipelagic marls and brownish laminated beds (sapropels) which are numbered M1 to M96 (Fig. 2). In the lower part of Metochia B (M7-M11) five successive turbiditic sequences occur within or entirely replace the sapropelitic intervals (Postma et al. 1993). In the part of the section below the turbidites we succeeded to drill in fresh (blue) coloured sediments after removing the weathered surface. The middle part of the Metochia B section is thoroughly weathered - many samples are characterised by rusty spots - and even after serious efforts no fresh samples could be drilled.

Metochia C predominantly consists of a rhythmically layered succession of hemipelagic marls and sapropels. In the upper part of the section the thickness of the sedimentary cycles decreases although several thin turbiditic beds are intercalated. Metochia C is sampled from cycle M36 to M96 resulting in an overlap of 20 cycles with Metochia B. The sediment is less weathered and brown rusty spots are absent. The sapropel-bearing succession in the Metochia section is overlain in stratigraphic continuity by cyclically bedded diatomites of Messinian age. These diatomites, which contain some 38 cycles, are not included in the present study.

We sampled 560 levels over a stratigraphic interval of approximately 100 m, which corresponds to an average spacing of 20 cm. A second sampling trip was organised to confirm several important polarity reversals and to resample the weathered part of Metochia B for magnetostratigraphic purposes only.

Figure 2. : Polarity zones, lithology, cycle numbers and ranges of planktonic foraminifera, *Bolboforma* and dinoflagellates of the Metochia section. In the polarity column black (white) denotes normal (reversed) polarity interval and shaded interval denotes zone of undefined (only secondary components) polarity. Closed (open) symbols denote reliable (unreliable) directions. ∇ = group A samples; ● = group B samples; ◆ = group C samples; Δ = group D samples; * = directions obtained by applying the great circle method (McPhadden and McElhinney, 1988). Lithology column shows cyclic alternations of homogeneous marls (white) and sapropels (black); shaded interval represents turbiditic intercalations (Postma et al., 1993). Right part of the figure shows biostratigraphic data given in terms of absence/presence. Numbered bioevents (encircled) refer to 1) highest regular occurrence (hro) of dextral *N. acostaensis*, 2) lowest common occurrence (lco) of *G. menardii* 4, 3) Last Common Occurence (LCO) of large-sized *C. parvulus*, 4) frequency shift (fs) in *C. parvulus*, 5) lowest regular occurrence (lro) of *S. seminulina*, 6) hro of *S. seminulina*, 7) LCO of *G. menardii 4*, 8) LO of *C. parvulus*, 9) First occurrence of *G. menardii 5* (FO), 10) First Regular Occurrence (FRO) of the *G. conomiozea* gr., and 11) FO of *G. nicolae*. Arrows indicate positions of bioevents. + = large sized types of *C. parvulus*.

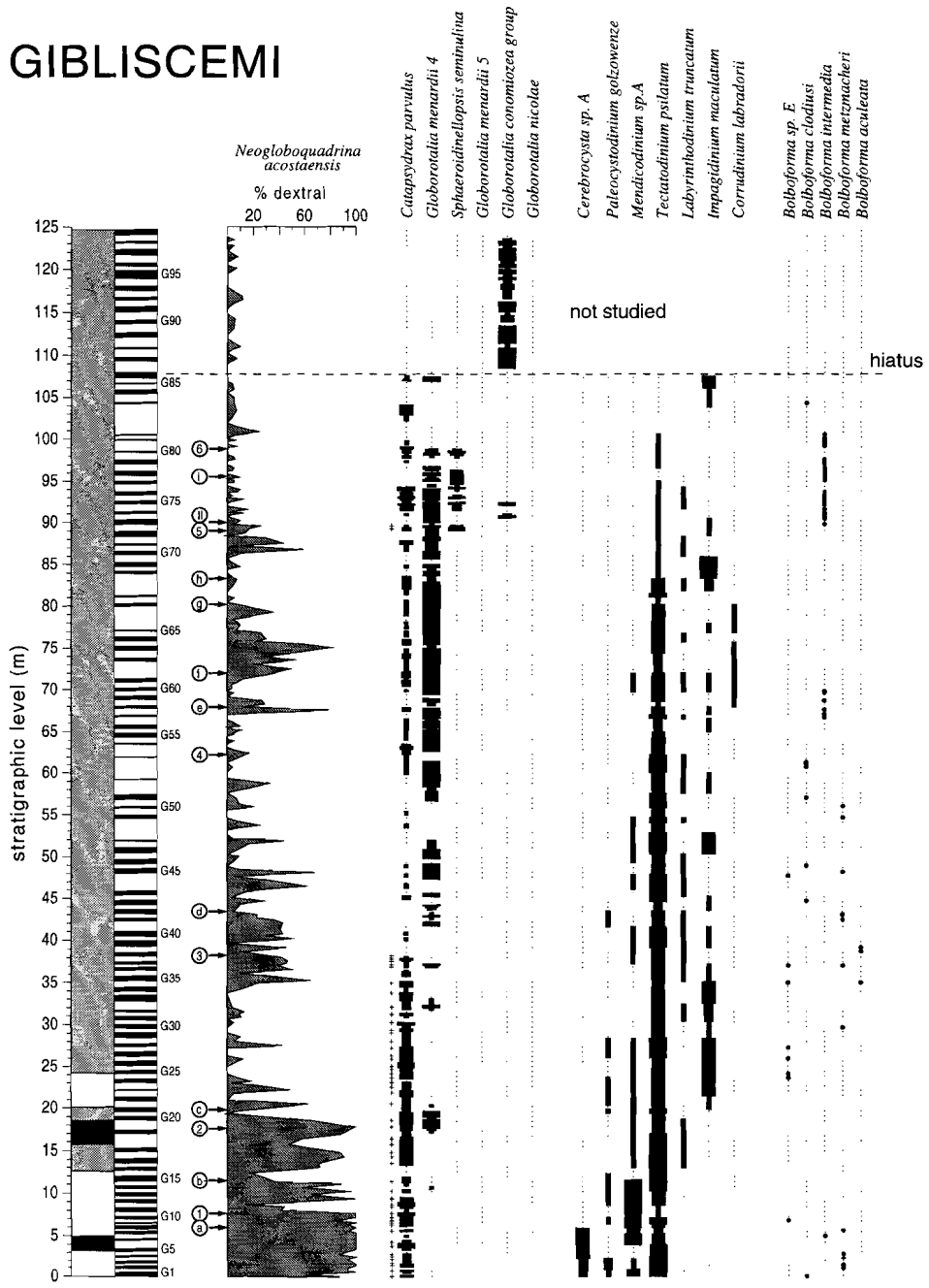
GIBLISCEMI
Neogloboquadrina acostaensis
% dextral
20 60 100
stratigraphic level (m)
0 5 10 15 20 25 30 35 40 45 50 55 60 65 70 75 80 85 90 95 100 105 110 115 120 125
G1 G5 G10 G15 G20 G25 G30 G35 G40 G45 G50 G55 G60 G65 G70 G75 G80 G85 G90 G95
a 1 b 2 c 3 d 4 e 1 5 g h 6 i j
Catapsydrax parvulus
Globorotalia menardii 4
Sphaeroidinellopsis seminulina
Globorotalia menardii 5
Globorotalia conomiozea group
Globorotalia nicolae
Cerebrocysta sp. A
Paleocystodinium golzowenze
Mendicodinium sp.A
Tectatodinium psilatum
Labyrinthodinium truncatum
Impagidinium maculatum
Corrudinium labradorii
Bolboforma sp. E
Bolboforma clodiusi
Bolboforma intermedia
Bolboforma metznacheri
Bolboforma aculeata
not studied
hiatus

Sicily: Gibliscemi section

The Gibliscemi section is located on the southern slope of Monte Gibliscemi on the southern part of the island of Sicily (Fig. 1). Here, upper Miocene sequences start with a cyclic alternation of homogeneous hemipelagic marls and sapropels, followed by the diatomites of the Tripoli Formation (Messinian) and capped by the Calcare di Base and evaporites (gypsum) of the Gessoso-Solfifera Formation.

The basal part of the Gibliscemi section is tectonically disturbed and overlies the so-called "argille-scagliose" which forms the decollement level of thrust nappes. Various shear planes cause important deformations/hiatuses and no continuous section could be sampled along a single trajectory. We succeeded in obtaining a relatively undisturbed and continuous succession - in which the sapropels are numbered (G1-G99, Fig. 3) - by sampling three separate subsections (Gibliscemi A, B and C; Fig. 1) which can be correlated on the basis of their distinct characteristic cyclic patterns. In our composite section, deformation is only bedding-parallel and (predominantly) restricted to sapropels. Only in the top part of the section, a shear plane is found which runs obliquely to the bedding, in the interval preceding the diatomites of the overlying Tripoli Formation.

A total of 620 levels has been sampled in the three subsections, corresponding to an average spacing of 20 cm. A second sampling trip was made to focus on the lowest part of the section. We resampled the interval comprising cycles G1-G25 in the Gibliscemi A and C sections to obtain a more reliable magnetostratigraphy.

Cyclostratigraphy

All sections consist of open-marine sediments that show cyclic alternations of either whitish-coloured carbonate-rich and grey-coloured carbonate-poor marls (Faneromeni section; lower part), or of homogeneous marls and brownish-

---

Figure 3. : Polarity zones, lithology, cycle numbers and ranges of planktonic foraminifera, *Bolboforma* and dinoflagellates of the Gibliscemi section. Biostratigraphic data of planktonic foraminiferal marker species are based on surveying a standard number of fields (27 out of 45) on a rectangular picking tray and semi-quantitatively presented in terms of absence, trace (<3 specimens per 9 fields of picking tray), rare (3-10), common (10-30) and frequent (>30) indicated by increasing bar thickness. For numbered foraminiferal bioevents see caption to Figure 2. Semi-quantitative distribution of dinoflagellate marker species is based on 200-counts and presented in terms of absence, trace (1-5%), rare (5-10), common (10-25) and frequent (>25) indicated by increasing bar thickness. Encircled dinoflagellate events refer to a) LO of *C. sp. A*, b) LCO of *M. sp. A*, c) FO of *I. maculatum*, d) LO of *P. golzowenze*, e) FO of *C. labradorii*, f) LO of *M. sp. A*, g) of LO *C. labradorii*, h) LCO of *T. psilatum*, and i) LO of *L. truncatum*.

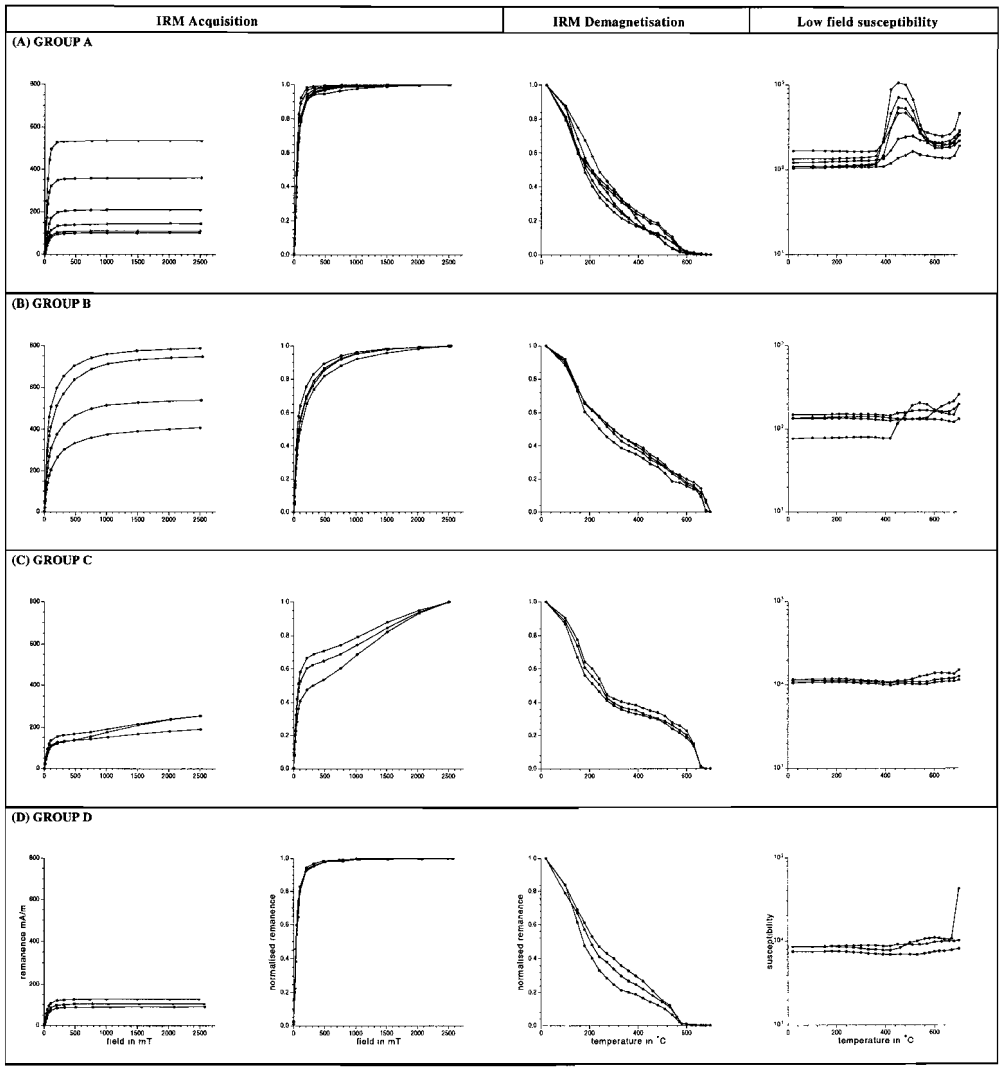

Figure 4. : Examples of rock magnetic tests for selected samples of the four groups (A,B,Cand D) of the Metochia section. In the IRM acquisition diagrams, the initial steep rise (0-300 mT) points to magnetite, the gradual increase at high fields suggests the presence of hematite (see especially group C). Stepwise thermal demagnetisation of the normalised NRM also show the presence of magnetite (A and D) and hematite (B and C). Low field susceptibilities display chemical reactions during thermal demagnetisation. Note the sudden increase at approximately 400 °C in group A.

coloured laminated beds termed sapropels (see Krijgsman et al., 1994a). Especially these sapropels reveal characteristic patterns - with both small-scale and large-scale clusters in addition to the individual sapropels - which allows the sections to be correlated (cyclostratigraphically) in detail. The sedimentary cycle patterns of the studied sections and their correlation to the astronomical target curves are discussed in detail in Chapter 3.

Magnetostratigraphy

Thermal demagnetisations were performed in a magnetically shielded, laboratory built furnace. The natural remanent magnetisation (NRM) was measured on a 2G Enterprises cryogenic magnetometer. At least one specimen per sampling level was thermally demagnetised using temperature increments of 30-50 °C. Furthermore, we performed some rock magnetic tests to identify the dominant carriers of the magnetism, including acquisition of an isothermal remanent magnetisation (IRM) and subsequent demagnetisation of this IRM. The IRM was induced in a pulse magnetiser and measured on a digitised spinner magnetometer based on a Jelinek JR3 driver unit. After each step we measured the low field susceptibility which was measured on a Kappabridge KLY-2.

Gavdos: Metochia section

Thermal demagnetisation of the samples from the Metochia section revealed that several intervals showed different types of demagnetisation behaviour, which appeared to be rather constant throughout the specific intervals. Viscous behaviour, when heated above temperatures of 400 °C, is shown by the marly interval below the turbidites (M1-M6). Good quality demagnetisation (linear decay) is observed in the *Heterostegina* sands, the turbidites and four following cycles (M7-M15), the upper part of Metochia B (M43-M56) and the lower part of Metochia C (M36-M56, with exception of M49). Low-intensity clusters at temperatures between 240-600 °C are observed in the middle part of Metochia B (M16-M42) and the upper part of Metochia C (M57-M93) but show different behaviour in these two subsections. We performed some rockmagnetic tests on a number of samples from each interval to characterise the magnetic properties and to distinguish primary from secondary components. On the basis of these experiments, we divided the samples in four groups (Fig. 4). For each group, all selected samples show the same typical behaviour. Therefore we assume that all samples showing the same demagnetisation behaviour can be attributed to the same group.

Group A: Group A is characterised by the dominance of a low coercivity mineral with maximum blocking temperatures below 600 °C (Fig. 4a) indicating the presence of magnetite. Heating of the samples to temperatures above 390 °C

results in a sudden increase of susceptibility which continues up to temperatures of 500 °C. This behaviour was observed earlier in suboxic to anoxic sediments and may be the result of oxidation of an iron sulphide like pyrite (Van Velzen, 1994). The decrease in susceptibility between 500 and 600 °C can be ascribed to oxidation of magnetite to hematite.

Samples attributed to group A are found in the lowermost 6 cycles (M1-M6) of Metochia B, between the *Heterostegina* sands and the turbidites. NRM intensities range from 0.04-2 mA/m, initial susceptibilities from 90-180*10^{-6} SI. The characteristic remanent magnetisation (ChRM) is usually largely removed at temperatures ranging from 300-390 °C. Demagnetisation diagrams for this interval show both normal and reversed polarities (Fig 5c,d) suggesting a primary origin for this component. Further demagnetisation at higher temperatures results in a mainly randomly directed viscous component.

Group B: IRM acquisition of group B samples indicate the presence of both a low coercivity (magnetite) and a high coercivity mineral (Fig. 4b). IRM demagnetisation shows that at least one component persisted at temperatures higher than 600 °C. Approximately at 680 °C the IRM is totally removed which indicates that the high coercivity mineral is hematite. Most samples show no significant change in susceptibility during the heating experiments. Samples which are attributed to group B are observed in the *Heterostegina* sands, cycles M7-15 and M43-56 in Metochia B and in cycles M36- M56 (except M49) in Metochia C.

NRM intensities range from 1-7 mA/m, susceptibilities 100-200*10^{-6} SI. Thermal demagnetisation diagrams show that in most samples a large secondary present-day field component is removed at 240 °C (Fig. 5a,j,k). Demagnetisation at higher temperatures reveals both normal and reversed components and again suggests a primary origin of the ChRM. Demagnetisation diagrams are generally of good quality and in most cases the polarity can reliably be determined. Some samples do not show a linear decay to the origin but move successively toward the reversed quadrant of the Zijderveld diagram (Fig. 5e). We assume that the primary component is partly overprinted by a secondary component caused by overlapping blocking temperature spectra. When plotted on an equal area diagram remanence vectors progressed along a great circle toward a southerly upward direction indicating removal of a normal phase from a reversed primary component. In these cases a best fitting great circle plane was used to estimate the characteristic directions according to the method of McFadden and McElhinny (1988) (Fig. 5f).

Group C: IRM acquisition and demagnetisation of group C samples show that the magnetisation is here dominated by a high-coercivity mineral (Fig. 4c). IRM-acquisition curves clearly differ from the group A and B curves. The blocking temperatures range from 660-680 °C which is characteristic for hematite. No major changes in susceptibility are observed during heating up to 700 °C. Samples of group C are found in cycles M16-M43 in Metochia B.

NRM intensities range from 1-3 mA/m, initial susceptibilities from 80-160*10^{-6}

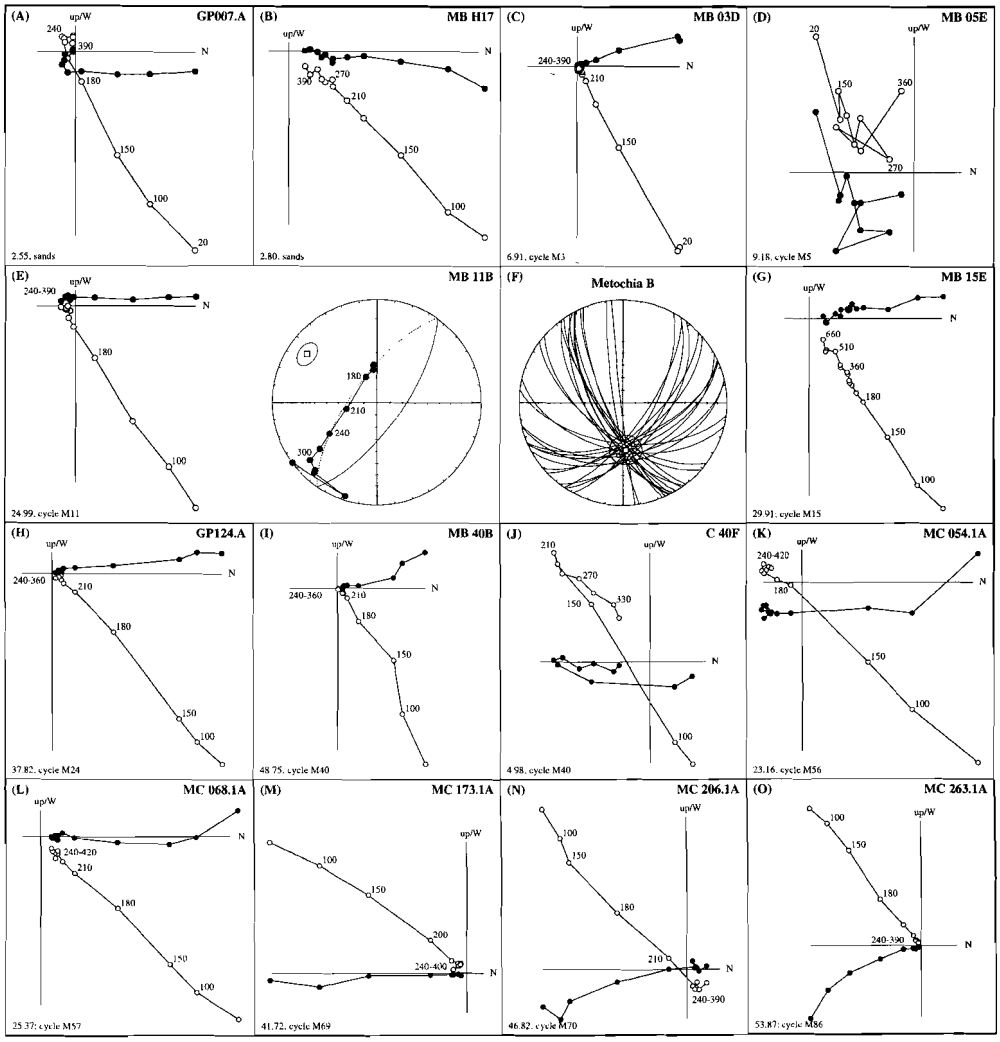

Figure 5. : Thermal demagnetisation diagrams for samples from the Metochia section. Closed (open) symbols represent the projection of the vector end-points on the horizontal (vertical) plane; values represent temperatures in °C; stratigraphic levels are in the lower left-hand corner. (E) Example showing no clear decay to the origin; the great circle in the equal- area projection suggests that a reversed ChRM is not fully resolved. = the normal to the plane with its error. (F) The intersections of all great circle planes as estimate of the primary directions.

SI. Demagnetisation diagrams show that a large normal component is removed at temperatures of 240 °C. At higher temperatures a low-intensity cluster is observed, always indicating normal magnetisation directions (Fig. 5h,i). The samples from cycles M40 and M43 in Metochia C, however, give clearly reversed primary directions whereas demagnetisation of the samples from the same cycles in Metochia B results in clusters which are characteristic for group C (Fig. 5i,j). This indicates that the high coercivity mineral (hematite) is of secondary origin and most likely generated by subrecent weathering of the sediment.

Group D: Samples attributed to group D again show a low coercivity mineral as the dominant carrier of the remanence (Fig. 4d). Maximum blocking temperatures of approximately 580 °C point to the presence of magnetite. The difference with group A is the response of susceptibility during heating of the sediment. In group D, no increase in low field susceptibilities is observed between temperatures of 390-500 °C. Samples attributed to group D are found in cycle M57 of Metochia B and in cycles M57-M91 of Metochia C.

NRM intensities range from 0.17-2.5 mA/m, susceptibilities from 35-150*10^{-6} SI. The lower values of the initial susceptibility are probably related to a higher $CaCO_3$ content. Demagnetisation diagrams show that a secondary low temperature (LT) component is removed at temperatures of 240 °C (Fig. 5k-o). In the lower part of the section this LT component has a normal present-day field direction, whereas in the upper part of the section this LT component has a reversed direction (Fig. 5m-o). After removing the LT component, a relatively small but well-determined high temperature (HT) component reveals a consistent pattern of both normal and reversed polarities (Fig. 5). We suggest that the HT component (> 240 °C) represents the primary ChRM component and the LT component a secondary post-depositional overprint. The reversed polarity of the LT component might be generated by late-diagenetic processes, for instance when the sediment became uplifted/exposed during a period of reversed polarity. The rock magnetic results indicate that the secondary component in Metochia C is a low coercivity (probably magnetite) component.

The ChRM directions and polarity zones of the composite Metochia section show that at least seventeen polarity reversals are recorded (Fig. 2; Table 1). The magnetostratigraphic results from the partly overlapping Metochia B and C sections confirm the cyclostratigraphic correlation. No primary components could be determined in the middle part of the Metochia B section (M16-M42). In this part of the section the secondary component totally overprints the primary component and hence no original polarity can be determined. The lower part of Metochia C is less weathered and yields good results for cycles M40-M42. The paleomagnetic signal of cycles M36-M39 is too weak to determine a reliable polarity.

Sicily: Gibliscemi section

The NRM intensities of the Gibliscemi section are very low, 50-150 μA/m and initial susceptibilities range from 100-200*10^{-6} SI. Only for the lower part of the section reliable magnetostratigraphic data could be derived (Fig. 3). The best demagnetisation diagrams were given by samples of the lowermost part (cycles G1-G25) of the section.

IRM acquisition and subsequent demagnetisation for selected samples of the lower part of Gibliscemi A indicate the presence of a low coercivity mineral with a maximum unblocking temperature of 560-600 °C (Fig. 6a). This suggests that magnetite is the dominant carrier of the magnetism. Heating of the samples results in an increase of the low field susceptibility between temperatures of 400-480 °C after which a decrease to 600 °C is observed. These results generally show the same characteristics as the samples of Group A of the Metochia section.

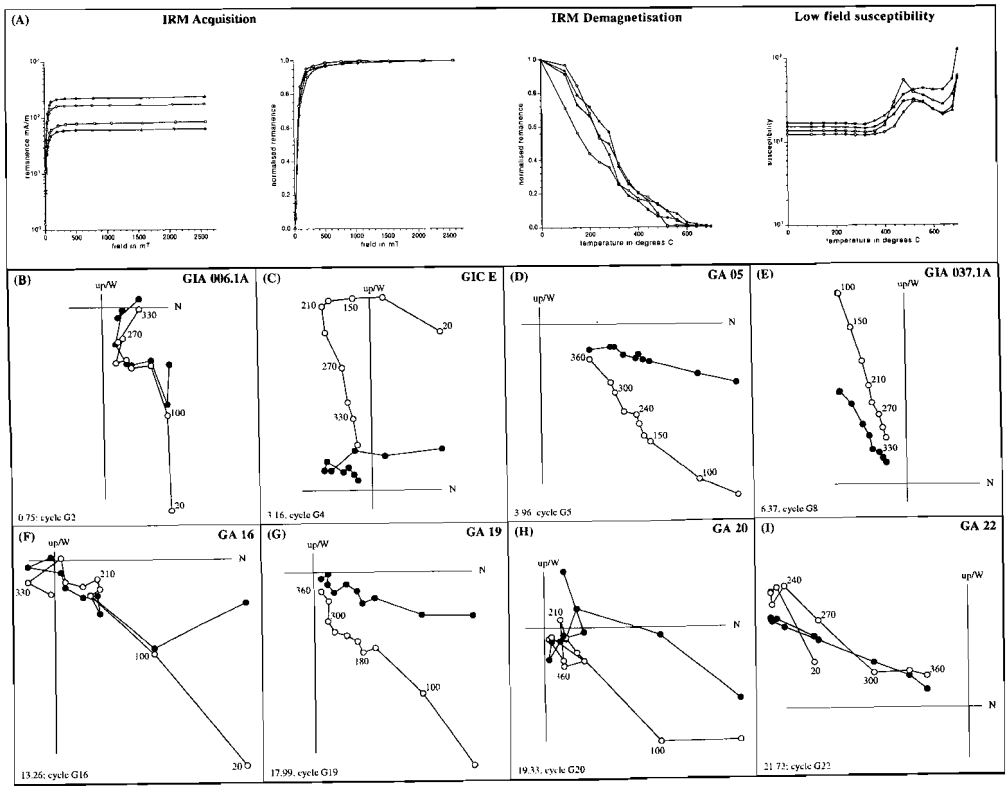

Figure 6. : (A) Examples of IRM acquisition, subsequent IRM demagnetisation and low-field susceptibilities for selected samples of the Gibliscemi section. (B-I) Thermal demagnetisation diagrams. See also captions to Figs. 4 and 5.

Thermal demagnetisation often reveals that a secondary, normally directed component is removed at a temperature of 240 °C (Fig. 6c) although this component is not always present (Fig. 6e). The ChRM component is subsequently demagnetised at temperatures of approximately 400 °C. Demagnetisation at higher temperatures results in a large and randomly directed viscous component, compatible with an increase in susceptibility probably caused by the oxidation of pyrite to magnetite (Van Velzen, 1994). Demagnetisation diagrams are often difficult to interpret because of the very weak NRM (Fig. 6b,f,h). We interpreted a direction as reliable only if a linear decay to the origin was observed. The reliable ChRM directions show an average clockwise rotation; 20° for the normal polarities and 25 ° for the reversed polarities. Clockwise rotations on Sicily have been found earlier by Scheepers and Langereis (1993) who estimated an average clockwise rotation of 34° for early Pliocene sections from the Caltanissetta basin.

Four polarity reversals are recorded in the lowest part of the section (Fig. 3; Table 1). The results from the Gibliscemi A and C sections are in agreement with each other and confirm the positions of the polarity reversals. Unfortunately, the upper two reversals cannot be pinpointed accurately in one sedimentary cycle because of the very weak paleomagnetic signal.

Biostratigraphy

Planktonic foraminiferal biostratigraphy played an essential role in confirming the cyclostratigraphic correlation between Gibliscemi and Metochia since magnetostratigraphic and dinoflagellate control is poor in one or the other section. Planktonic foraminiferal biostratigraphic correlations are based on the stratigraphic distribution of six species plus the coiling ratio of *N. acostaensis* in 337 samples from Gibliscemi and 553 from Metochia (see Figs. 2 and 3). The distribution of these six species is based on surveying a standard number of fields (27 out of 45) on a rectangular picking tray and specified in semi-quantitative terms (frequent, common, rare, trace) for Gibliscemi and in qualitative terms (presence, absence) for Metochia. Most species display an intermittent distribution pattern. This holds in particular for the sinistrally-coiled *G. menardii 4* in the lower part of both sections (G1-G50 and M1-M45). This species occurs more regularly between G51-G80 and M46-M68 but then vanished until its brief reoccurrence in G85 of Gibliscemi and in M69 of Metochia. The top of this brief reoccurrence event is equated with the LCO of *G. menardii 4* even though this species shows a final and extremely brief influx in the upper part of the range of *G. menardii 5* (Zachariasse, 1979). Fig. 2 shows that the sinistral *G. menardii 4* is followed in succession by the dextral *G. menardii 5* and the sinistral *G. conomiozea* group. This succession (although differently labeled) has been noticed in many locations in the Mediterranean (Zachariasse, 1975; Glacon et al., 1990; Sierro et al., 1993; Hodell et al., 1994), and the absence of *G. menardii 5* in Gibliscemi, therefore,

points to a major hiatus at 108 m (Fig. 3). The unkeeled globorotaliid group lacks systematic changes that can be used for correlating both sections. An exception is the FO of *Globorotalia nicolae* - a dextrally-coiled and biconvex form with inflated chambers - which is a useful bioevent for correlating lower Messinian sequences in the Mediterranean region. The FO of *G. nicolae* in Metochia shortly preceeds the first occurrence of diatomites and follows a relatively long interval in which unkeeled globorotaliids are absent. The top of Gibliscemi reaches into this absence interval. Another useful species is *Catapsydrax parvulus*, which is the last representative of the *Catapsydrax* group. *Catapsydrax parvulus* is a senior synomym of *Globorotalia falconarae*, which, in the Mediterranean ranges up into Zone N16 (Iaccarino, 1985; Chamley et al., 1986). *Catapsydrax parvulus* is common to frequent in cycles G1-G37 of Gibliscemi and in M1-M29 of Metochia and its maximum size is significantly larger than in any younger level (with the exception of a brief reoccurrence in G72 and M61, see Figs. 2 and 3). The LCO of these large-sized *C. parvulus* types is a useful bioevent for the (eastern) Mediterranean. *Catapsydrax parvulus* is extremely scarce from the LCO level of the large-sized types up to cycle G37 and M29, but becomes again more frequent from cycles G53 and M47 up to its LO level (M71) in Metochia (Figs 2 and 3).

Sphaeroidinellopsis seminulina is common to frequent in a discrete interval which ranges from G72 to G80 and from M61 to M68 (Figs. 2 and 3). The base of this interval coincides with the brief re-occurrence of large-sized *C. parvulus* types, while the top corresponds with the base of the longer-term absence interval of *G. menardii 4* preceding its LCO level. Scattered occurrences of *S. seminulina* are found beyond this interval in cycle M10 and M68-M69 (see also Fig. 8). The last species with biostratigraphic significance is *N. acostaensis*. Coiling of this species is dominant dextral from G1 to G10 and from M1 to M6, whereafter coiling changes in a series of high-amplitude fluctuations up to G19 in Gibliscemi and M15 in Metochia. Above that level dominant sinistral coiling prevails, although at some levels coiling reverts to dominant dextral.

The stratigraphic distribution of the species listed above provides 11 first-order bioevents (summarized in Table 2), which are perfectly isochronous compared to the cyclostratigraphic framework and which substantially improve the biostratigraphic resolution in this time span. However, many more isochronous surfaces can be drawn between both sections on the basis of second-order bioevents. Examples of such second-order bioevents are several short-term incursions of *Globoquadrina altispira*, the many short-term absence intervals of *Globorotalia menardii 4*, and the brief reoccurrence of large-sized *Catapsydrax parvulus* types. One of the most remarkable second-order bioevents is the single short incursion of abundant *Globoquadrina dehiscens* in cycle G32 of Gibliscemi and in the equivalent cycle M28 of Metochia.

Along with the planktonic foraminiferal analysis we recorded the absence and presence of 5 species of the calcareous microfossil group of *Bolboforma* (Protophyta, Spiegler and Rögl, 1992). Figs. 2 and 3 show that the sections Metochia and Gibliscemi have three species in common but their stratigraphic

distribution shows little similarity. This is surprising because the opposite is true for the distribution of the planktonic foraminifers. We conclude, therefore, that this group has little biostratigraphic significance in this part of the Mediterranean and for the time slice studied.

Dinoflagellate cysts are abundant in section Gibliscemi, but rare in Metochia. Actually, 75% of the samples in Metochia was barren possibly due to intense weathering. 200-counts on 72 samples from below the hiatus in Gibliscemi yielded 7 species with (potential) biostratigraphic significance (Fig. 3). The LO of *Cerebrocysta* sp. A in cycle G6 has also been recorded by Powell (1986) in the lower part of the Tortonian type section along the Rio Mazzapiedi-Castellania and might be a useful bioevent for (at least) the Mediterranean region. The LO of *Palaeocystodinium golzowense* in G41 seems to have (semi)global significance since it has been recorded in a number of late Miocene sequences from outside the Mediterranean as well (e.g. Edwards, 1984; Head et al., 1989). *Mendicodinium* sp. A has its LO in G61. The highest occurrence of *Labyrinthodinium truncatum* in G78 represent its true last occurrence since this species is absent in section Faneromeni, which covers the interval missing in Gibliscemi due to a hiatus. The LO of *Labyrinthodinium truncatum* is a useful bioevent since it has been recorded in a number of late Miocene sections from outside the Mediterranean as well (Edwards, 1984; Head et al., 1989). *Tectatodinium psilatum* ranges up into section Faneromeni but its frequency drop in G68 is a very distinct and probably useful bioevent. Whether the FO of *Impagidinium maculatum* in G21 and the limited range of *Corrudinium labradorii* (from G58 to G66) have biostratigraphic significance will become evident after studying additional late Miocene sections from within and outside the Mediterranean.

Integrated stratigraphic framework

The data presented in this paper provide a high-resolution integrated stratigraphic framework for the Mediterranean Upper Miocene. Since the Gibliscemi section recorded a large hiatus in its upper part and also did not provide a good magnetostratigraphy, we incorporated the earlier data from the Faneromeni and Kastelli sections of Crete which showed reliable results for the corresponding interval. (Langereis et al., 1984; Krijgsman et al., 1994a). In general, the magnetostratigraphic and biostratigraphic data are consistent with, and thus

---

Figure 7. : Stratigraphic framework showing the magnetostratigraphy, integrated biostratigraphy and cyclostratigraphy of the Kastelli, Faneromeni, Metochia and Gibliscemi sections and the correlation of the magnetostratigraphy to the geomagnetic polarity time scale of Cande and Kent (1995). Cyclostratigraphic correlations are based on sedimentary cycle pattern.

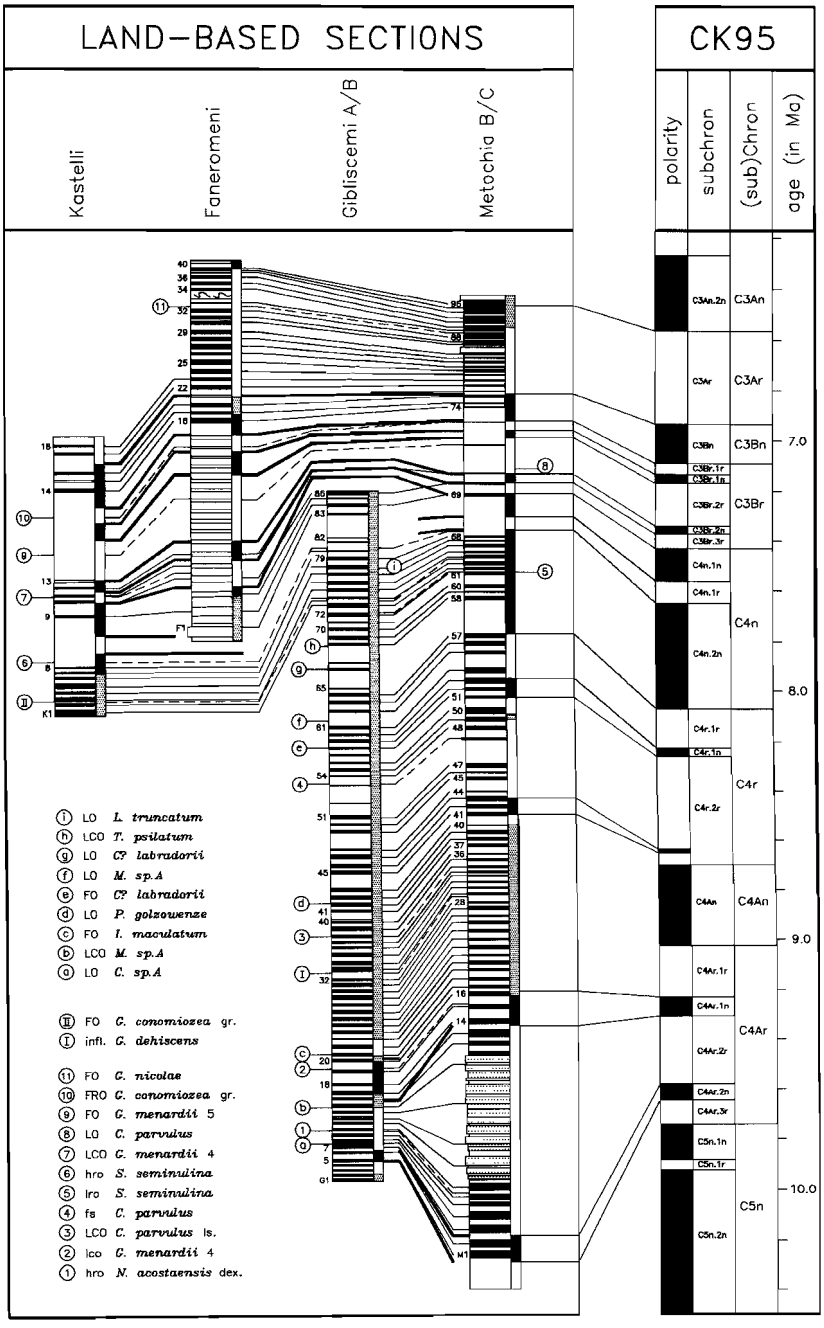
LAND–BASED SECTIONS
Kastelli
Faneromeni
Gibliscemi A/B
Metochia B/C
CK95
polarity
subchron
(sub)Chron
age (in Ma)
C3An.2n
C3An
C3Ar
C3Bn
C3Br
C4n
C4r
C4An
C4Ar
C5n
7.0
8.0
9.0
10.0
ⓘ LO L. truncatum
ⓗ LCO T. psilatrum
ⓖ LO C? labradorii
ⓕ LO M. sp.A
ⓔ FO C? labradorii
ⓓ LO P. golzowenze
ⓒ FO I. maculatrum
ⓑ LCO M. sp.A
ⓐ LO C. sp.A
Ⓘ FO G. conomiozea gr.
Ⓘ infl. G. dehiscens
⑪ FO C. nicolae
⑩ FRO G. conomiozea gr.
⑨ FO G. menardii 5
⑧ LO C. parvulus
⑦ LCO G. menardii 4
⑥ hro S. seminulina
⑤ lro S. seminulina
④ fs C. parvulus
③ LCO C. parvulus ls.
② lco G. menardii 4
① hro N. acostaensis dex.

essentially confirm, the cyclostratigraphic correlations, although minor discrepancies exist (Fig. 7). The polarity reversals of the upper part of the Metochia section are consistently found at a slightly lower (cyclo)stratigraphic position than at Faneromeni and Kastelli, as confirmed by the high-resolution biostratigraphic data. Furthermore, the consistent offset of generally 1/2 to 1 cycle suggest that this discrepancy is probably not caused by a misinterpretation of the paleomagnetic data. Diagenetic processes, related to the paleoredox conditions, may cause a delay of the acquisition of the NRM, which is dependent on the lithology of the sediment (Van Hoof et al., 1993). Such a delayed acquisition is a likely explanation for the observed discrepancies between Metochia and Crete.

Correlation to the GPTS

Since the results of all sections are generally in good agreement, we can use the polarity sequences to construct a chronostratigraphic framework and to assign absolute ages to the biostratigraphic events. Correlation of the established polarity patterns (Table 1) to the GPTS has been made by reference to the most recent published version CK95 (Cande and Kent; 1995). The results of the Cretan sections were correlated earlier to the older CK92 (Cande and Kent; 1992) time scale (Krijgsman et al.; 1994a). In CK95, the polarity patterns are identical to CK92; differences are caused by the incorporation of new and additional calibration points which results in slightly older ages for the polarity reversals. Hence, the correlation of the polarity patterns of the Faneromeni and Kastelli sections to CK95 remains the same but only results in a minor change in age (Fig. 9). This was also suggested by the modified CK92_MOD time scale of Krijgsman et al. (1994a).

In contrast to the Cretan sections, the Metochia section could be extended further downward which resulted in the recording of eight additional polarity reversals (Fig. 7). Correlation to CK95 shows that the long normal interval (M57-M68) corresponds to chron C4n.2n and the first short normal interval (M51-M53) to chron C4r.1n. The second short normal interval (M41-M42) cannot be correlated to any chron in CK95. It might correspond to the so-called cryptochron C4r.2r-1 which has a duration of 16 kyr according to CK95. This short polarity interval is also found in ODP Leg 138 (Schneider, 1994). The duration of this interval, estimated from thickness and sedimentation rate, ranges from 33-58 kyr in Schneider (1994), which is in agreement with our results that indicate a duration of 30-40 kyr (1.5-2 sedimentary cycles). Hence, a duration of 16 kyr in CK95, based on ocean floor anomaly patterns, seems too short. Schneider (1994) also records another cryptochron, which he calls C4r.1r-1, that is not recorded in the Cande and Kent (1992, 1995) time scale. According to our results, only reversed polarities are recorded in the corresponding time interval. There is one level (M49), however, for which we obtained normal polarities, but rock magnetic

CK95 chron	age	Faneromeni level in m	Kastelli level in m	Metochia level in m	Gibliscemi level in m
C3An.2n (o)	6.567	57.43 - 57.50			
C3Bn (y)	6.935	-	55.72 - 57.00	92.57 - 93.21	
C3Bn (o)	7.091	31.60 - 32.41	46.83 - 47.25	90.60 - 90.74	
C3Br.1n (y)	7.135	28.63 - 29.73	43.40 - 43.90	89.69 - 89.91	
C3Br.1n (o)	7.170	25.84 - 26.18	40.57 - 41.03	88.72 - 89.03	
C3Br.2n (y)	7.341	15.35 - 15.60	29.19 - 29.67	84.91 - 85.02	
C3Br.2n (o)	7.375	11.80 - 13.40	26.79 - 27.39	83.89 - 84.00	
C4n.1n (y)	7.432	8.35 - 9.00	24.25 - 25.40	83.09 - 83.28	
C4n.1n (o)	7.562		16.75 - 17.39	80.23 - 80.87	
C4n.2n (y)	7.650		13.29 - 13.97	78.83 - 79.87	
C4n.2n (o)	8.072			68.86 - 69.26	
C4r.1n (y)	8.225			62.99 - 63.90	
C4r.1n (o)	8.257			61.36 - 61.82	
C4r.2r-1 (y)	8.635			50.79 - 51.60	
C4r.2r-1 (o)	8.651			49.29 - 49.90	
C4An (y)	8.699				
C4An (o)	9.025				
C4Ar.1n (y)	9.230				17.99 - 20.46
C4Ar.1n (o)	9.308			27.35 - 27.41	12.09 - 14.25
C4Ar.2n (y)	9.580			5.63 - 5.73	4.55 - 5.05
C4Ar.2n (o)	9.642			2.55 - 3.10	3.05 - 3.41

Table 1. : Stratigraphic levels of polarity reversals recorded in the studied sections.

experiments suggest that we are dealing here with a normal (hematite; group B) overprint. This level thus reveals the same rock magnetic characteristics as the long remagnetised interval (M16-M39) in Metochia B. This remagnetised interval is marked by the (regular) occurrence of numerous sapropels whereas the remagnetised M49 level occurs in a small group (M48-M50) of sapropels. In this respect, it is suspect that two short normal polarity intervals coincide with small sapropel groups (i.e. M41-M44 and M51-M54). Their rock magnetic characteristics, however, suggest a primary origin of these normal polarities.

No reliable data are derived from the middle part of the Metochia B section (M16-M39) because the primary component is probably totally overprinted by a normally directed secondary weathering component. Also in the Gibliscemi section no polarities could be determined for the time-equivalent interval. The combined results of Gibliscemi and Metochia show that four polarity reversals are recorded at the base of the sections, which determine two short normal polarity intervals. The only likely correlation to CK95 of the 20 kyr (M1; G5) and 50 kyr (M14-M15; G18-G19) normal polarity intervals is to the subchrons C4Ar.1n and C4Ar.2n (Fig. 7). According to this correlation, it appears that we did not

no.	species	event	Faneromeni level in m	Faneromeni age in Ma	Kastelli level in m	Kastelli age in Ma	Metochia level in m	Metochia age in Ma	Gibliscemi level in m	Gibliscemi age in Ma	CK95 chron	CK95 age in Ma
11	*G. nicolae*	FO	51.76 - 52.05	6.676 - 6.687			99.25 - 99.35				**C3Ar**	**6.68 ± 0.01**
10	*G. conomiozea gr.*	FRO	30.18 - 30.33	7.110 - 7.128	44.35 - 45.05	7.114 - 7.129	90.25 - 90.33	7.104 - 7.117			**C3Br.1r**	**7.12 ± 0.01**
9	*G. menardii 5*	FO	22.08 - 22.55	7.224 - 7.236	36.72 - 37.10	7.222 - 7.235	87.90 - 87.97	7.204 - 7.218			**C3Br.2r**	**7.23 ± 0.01**
8	*C. parvulus*	LO					85.20 - 85.69	7.306 - 7.333			**C3Br.2r**	**7.32 ± 0.01**
7	*G. menardii 4*	LCO	10.10 - 10.75	7.392 - 7.418	25.40 - 25.81	7.397 - 7.432	84.12 - 84.24	7.363 - 7.371			**C3Br.3r**	**7.40 ± 0.02**
6	*S. seminulina*	hro			11.58 - 11.94		79.06 - 79.31	7.630 - 7.682	98.74 - 99.04	*7.591 - 7.621*	**C4n.2n(y)**	**7.65 ± 0.03**
5	*S. seminulina*	lro					74.44 - 74.60	7.829 - 7.866	88.81 - 89.28	*7.799 - 7.828*	**C4n.2n**	**7.85 ± 0.02**
4	*C. parvulus*	fs					57.31 - 57.84	8.383 - 8.424	62.14 - 62.49	*8.283 - 8.301*	**C4r.2r**	**8.40 ± 0.02**
3	*C. parvulus (ls)*	LCO					44.10 - 44.27	8.801 - 8.820	38.25 - 38.40	*8.835 - 8.864*	-	**8.81± 0.01**
2	*G. menardii 4*	lco					29.35 - 29.76	9.236 - 9.250	17.43 - 17.76	*9.234 - 9.292*	**C4Ar.1n(y)**	**9.24 ± 0.01**
1	*N. acostaensis dex*	hro					9.81 - 9.93	9.526 - 9.529	7.63 - 8.01	9.455 - 9.504	**C4Ar.2r**	**9.53 ± 0.01**
II	*G. conomiozea gr*	FO					75.78 - 75.90	7.774 - 7.813	90.48 - 90.67	*7.770 - 7.791*	**C4n.2n**	**7.78 ± 0.01**
1	*G. dehiscens*	influx					40.91 - 41.15	8.895 - 8.913	32.35 - 33.03	*8.939 - 8.986*	-	**8.90 ± 0.01**
i	*L. truncatum*	LO							95.30 - 95.90	*7.658 - 7.692*	*C4n.2n*	*7.67 ± 0.02*
h	*T. psilatum*	LCO							82.01 - 84.62	*7.899 - 7.966*	*C4n.2n*	*7.93 ± 0.03*
g	*C? labradorii*	LO							79.76 - 80.66	*7.983 - 8.013*	*C4n.2n*	*8.00 ± 0.02*
f	*M. sp. A*	LO							70.87 - 73.11	*8.144 - 8.198*	*C4r.1r*	*8.17 ± 0.03*
e	*C? labradorii*	FO							67.41 - 68.55	*8.230 - 8.238*	*C4r.2r/C4r.1n*	*8.23 ± 0.01*
d	*P. golzowenze*	LO							42.83 - 44.02	*8.727 - 8.770*	-	*8.75 ± 0.02*
c	*I. maculatum*	FO							19.52 - 20.19	*9.187 - 9.249*	*C4Ar.1r*	*9.22 ± 0.03*
b	*M. sp. A*	LCO							11.07 - 11.88	9.316 - 9.402	**C4Ar.2r**	**9.36 ± 0.04**
a	*C. sp. A*	LO							5.53 - 6.28	9.518 - 9.566	**C4Ar.2r**	**9.54 ± 0.02**

Table 2. : Position, age and (sub)chron designation of biostratigraphic events according to CK95. Ages have been obtained by linear interpolation of the sedimentation rate between dated reversal boundaries (see Table 1). (Sub)chron designation is given in italics if based on cyclostratigraphic correlations to section with magnetostratigraphy.

record the upper and lower reversal boundaries of chron C4An. Our correlation is furthermore confirmed by the duration of the interval between the reversal boundaries C4r.1n (o) and C4Ar.1n (y), which is 973 kyr in CK95 and 1040 kyr based on the estimated number of (± 50 precession related) sedimentary cycles.

The established magnetostratigraphic correlation results in accurate ages, according to the CK95 time scale, for the following bioevents (Table 2); (1) highest regular occurrence (hro) of dexral *N. acostaensis* (chron C4Ar.2r; 9.53 ± 0.01 Ma), (2) lowest common occurrence (lco) of *G. menardii 4* coincident with the last of a series of high-amplitude changes in % dextral *N. acostaensis* (C4Ar.1n (y); 9.24 ± 0.01 Ma); (3) LCO of large sized *C. parvulus* types (8.81 ± 0.01 Ma); (4) frequency shift in *C. parvulus* from nearly absent to commonness (C4r.2r; 8.40 ± 0.02 Ma); (5) the lro of *S. seminulina*, coincident with a brief re-occurrence of large-sized *C. parvulus* types (C4n.2n; 7.85 ± 0.02 Ma); (6) the highest regular occurrence (hco) of *S. seminulina*, coincident with the temporary disappearance of *G. menardii 4* preceding its LCO (C4n.2n(y); 7.65 ± 0.03 Ma); (7) the LCO of *G. menardii* form 4 (C3Br.3r; 7.40 ± 0.02 Ma), (8) the last occurrence (LO) of *C. parvulus* (C3Br.2r; 7.32 ± 0.01 Ma), (9) the FO of *G. menardii* form 5 (C3Br.2r; 7.23 ± 0.01 Ma); (10) the First Regular Occurrence (FRO) of the *Globorotalia conomiozea* group (C3Br.1r; 7.12 ± 0.01 Ma), (11) the FO of *G. nicolae* (C3Ar; 6.68 ± 0.01 Ma). The dinoflagellate bioevents are only determined in the Gibliscemi section which could not be directly dated since this section did not provide a good magnetostratigraphy. Numerical ages for these events are calculated after a cyclostratigraphic correlation of the polarity reversals of the Metochia section to their corresponding position in Gibliscemi (see Table 2).

The age of the T/M boundary

The level at 6 meter below the base of the Tripoli Formation in section Falconara (Sicily) has been proposed in 1979 by Colalongo et al. as the Global Stratotype Section and Point (GSSP) for the Tortonian/Messinian (T/M) boundary and serves as such already for 16 years but the boundary has never been formally defined. The position of the proposed GSSP for the T/M boundary is marked by the FO of *Globorotalia conomiozea* (Colalongo et al., 1979).

G. conomiozea belongs to a late Miocene group of keeled globorotaliids characterized by sinistral coiling and a reniform chamber outline in spiral view (Zachariasse, 1979). Relatively flat morphotypes are named *G. dalii* and *G. miotumida* (with *G. dalii* being a junior synomym of *G. miotumida*),whereas conical forms are labeled *G. conoidea*, *G. conomiozea*, *G. sphericomiozea*, *G. saphoa*, and *G. mediterranea* depending on the degree of test thickness, axial angularity, and the number of chambers. All these morphotypes, however, completely intergrade, which - in addition to the similarity in chamber outline and coiling - is the reason why they all have been lumped into one single category called the *G. conomiozea* group (Zachariasse, 1979) or the *G. miotumida* group (Sierro et al., 1993).

The late Miocene *G. conomiozea* group lived at the mid- to high-latitudes of both hemispheres (Berggren, 1984) and invaded the Mediterranean near the T/M boundary in response to increased climatic cooling (Zachariasse and Spaak, 1983; Sierro et al., 1993). This invasion is preceded, however, by an earlier short-term invasion of thick-shelled and conical representatives of this group at two closely spaced levels slightly above the lowest regular occurrence of *S. seminulina* (Figs. 2 and 3). The *G. conomiozea* group coexisted with *G. menardii 4* during the first invasion, but was the sole keeled globorotaliid in the Mediterranean during the second invasion near the T/M boundary. The sudden spreading of the *G. conomiozea* group in the Mediterranean during this second invasion (= FRO) of the *G. conomiozea* group) is taken by Langereis et al. (1984), Sierro et al. (1993), and Krijgsman et al. (1994a) to mark the T/M boundary. The earliest representatives of the *G. conomiozea* group during this second invasion consist of the flat *G. miotumida* type (Glacon et al., 1990; Sierro et al., 1993; Hodell et al., 1994). The first conical types arrived later and that is the reason why some authors (e.g. Glacon et al., 1990; Hodell et al., 1994) place the T/M boundary at the first occurrence level of these conical (= *G. conomiozea*) types in accordance with the original proposal of Colalongo et al. (1979). The first conical types in section Metochia show up in cycle M73, shortly after the FRO of the *G. conomiozea* group, but their regular occurrence starts in cycle M76 in the upper part of chron C3Bn. Hodell et al. (1994) might have equated last level with the T/M boundary, which would explain why they placed this boundary in Chron 3Bn, whereas Langereis et al. (1984) and Krijgsman et al. (1994a) placed the T/M boundary midway chron C3Br.1r. The earliest representatives of the *G. conomiozea* group at the proposed T/M boundary level in section Falconara contain already some conical types, but their regular occurrence starts at about 8 m above the proposed boundary level. This suggests that the proposed T/M boundary level in Falconara is associated with a small hiatus and, therefore, might not be a suitable candidate for defining the T/M boundary. In anticipation of a formal definition we place the T/M boundary at the FRO of the *G. conomiozea* group (in accordance with Langereis et al., 1984 and Krijgsman et al., 1994a) because this bioevent reflects the most pronounced change in late Miocene globorotaliids and is - irrespective of species concept and labeling procedures - easy to identify within and immediately outside the Mediterranean. The T/M boundary defined in this way has an age of 7.12 Ma based on linear interpolation between the younger end of chron C3Br.1n (y) and the older end of chron C3Bn (o) in CK95.

Conclusions

A high-resolution stratigraphic framework for the late Miocene in the (eastern) Mediterranean is established by combining magnetostratigraphic, biostratigraphic and cyclostratigraphic data from marine sections on Gavdos, Sicily and Crete. Seventeen polarity reversals are recorded which allows an

unambiguous correlation to CK95 (Fig. 7). This correlation is used to calculate ages for eleven major planktonic foraminiferal and nine dinoflagellate bioevents (Table 2). The Tortonian/Messinian boundary, placed at the FRO of the *Globorotalia conomiozea* gr., is determined in chron C3Br.1r and has an age of 7.12 Ma according to CK95.

Acknowledgements

T. van Hoof, G. Postma, P.-J. Verplak, H. Zijderveld, A. Antonarakou, and F. van Welderen Rengers are greatfuly acknowledged for their help in the field. We thank H. de Stigter is for using his field data of Gavdos and D. Spiegler (GEOMAR, Kiel) for assisting in determining the *Bolboforma* species. We also thank the Damorakis family and Georgos Tsigonakis for the good times we had on Gavdos. G. van 't Veld and G. Ittman prepared the micropaleontological samples. This study was partly supported by The Netherlands Geosciences Foundation (GOA) with financial aid from the Netherlands Organization of Scientific Research (NWO) and the EU HCM program. This is MIOMAR contribution no. 3.

Chapter 3

Extending the astronomical (polarity) time scale into the Miocene

Abstract

An astronomical time scale is presented for the late Miocene based on the correlation of characteristic sedimentary cycle patterns in marine sections in the Mediterranean to the 65° N summer insolation curve of La90 with present-day values for the dynamical ellipticity of the Earth and tidal dissipation by the moon (Laskar, 1990; Laskar et al., 1993). This correlation yields ages for all sedimentary cycles and hence also for the recorded polarity reversals, and planktonic foraminiferal and dinoflagellate events.

The Tortonian/Messinian (T/M) boundary placed at the first regular occurrence of the *Globorotalia conomiozea* group in the Mediterranean is dated at 7.24 Ma. The duration of the Messinian stage arrives at 1.91 Myr because the Miocene/Pliocene boundary has been dated previously at 5.33 Ma (Lourens et al., 1995).

The new time scale is confirmed by $^{40}Ar/^{39}Ar$ ages of volcanic beds and by the number of sedimentary cycles in the younger part of the Mediterranean Messinian.

This chapter has been published as: F.J. Hilgen, W. Krijgsman, C.G. Langereis, L.J. Lourens, A. Santarelli, W.J. Zachariasse, Extending the astronomical (polarity) time scale into the Miocene, *Earth Planet. Sci. Lett.*, 136, 495-510, 1995.

Introduction

A recently developed method to construct geological time scales involves the calibration of sedimentary cycles, or other cyclic variations in geological records, to computed time series of the quasi-periodic variations of the Earth's orbit. Following early tuning attempts for the late Pleistocene during the 1960's and early 1970's (Emiliani, 1966; Shackleton and Opdyke, 1973; Hays et al., 1976), the astronomical time scale is now firmly established for the last 6 Myr (Shackleton et al., 1990, 1995; Hilgen, 1991a,b; Tiedemann et al., 1994). This time scale deviates considerably from earlier time scales based on K/Ar dating, and it has subsequently been confirmed by radiometric ages using the $^{40}Ar/^{39}Ar$ (single crystal) laser fusion dating technique. The new time scale has been succesfully applied in paleoclimatic studies (Lourens et al., 1992) and in studies of seafloor spreading history (Wilson, 1993). In addition, the age of fluence monitor standards in radiometric ($^{40}Ar/^{39}Ar$) dating has been calibrated independently of absolute isotopic abundance measurements by comparison of astronomical and $^{40}Ar/^{39}Ar$ ages for seven polarity reversals over the last 3.5 Myr (Renne et al., 1994).

In this study, we aim at extending the astronomical time scale back in time, into the Miocene. Earlier, Shackleton et al. (1994) carried out a preliminary and partial astronomical tuning of GRAPE (Gamma Ray Attenuation Porosity Evaluation) records of ODP Leg 138 sites for the interval between 6 and 10 Ma, while Krijgsman et al. (1994) calculated an astronomical duration for a late Miocene polarity sequence on Crete by multiplying the number of sedimentary cycles with the average 21.7 kyr period of precession. The duration of the latter sequence is approximately 10 % shorter than that of the correlative part in the geomagnetic polarity time scale (GPTS) of Cande and Kent (1992). Here, we calibrate the sedimentary cycles of the sections from Crete (Krijgsman et al., 1994a) and of older sections from Gavdos and Sicily (Krijgsman et al., 1995) directly to astronomical target curves. This calibration provides astronomical ages for all sedimentary cycles and hence for the polarity reversals and biostratigraphic datum planes recorded in these Mediterranean sections.

The resulting time scale is then compared with the most recent polarity time scales of Cande and Kent (1995; CK95) and Shackleton et al. (1995; SCHPS95), with radiometric ($^{40}Ar/^{39}Ar$) ages of volcanic beds, and with the number of sedimentary cycles in the younger, partly evaporitic, part of the Mediterranean Messinian.

Cyclostratigraphy of the sections

We have used four Mediterranean sections for the construction of our time scale, namely the Metochia section on Gavdos, the Gibliscemi section on Sicily and the Faneromeni and Kastelli sections on Crete (see Fig. 1 in Chapter 2 for exact location). The magnetostratigraphy and biostratigraphy of the sections, and

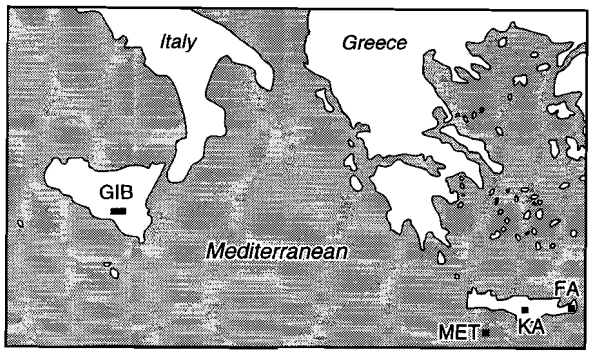

Figure 1. Locations of sections Gibliscemi (GIB), Metochia (MET), Faneromeni (FA) and Kastelli (KA). See Chapter 2 for a detailed map.

the correlation of the magnetostratigraphy to the GPTS of Cande and Kent (1995; CK95) are discussed in detail by Krijgsman et al. (1994a, 1995; Chapter 2): They showed that the succession starts above chron C5n and continues into chron C3An, and ranges from 9.7 to 6.5 Ma according to CK95. The cyclostratigraphic details and the correlation of the sedimentary cycle patterns to the astronomical solutions are presented in this paper.

All sections consist of open marine sediments that show cyclic alternations of either whitish-coloured carbonate-rich and grey-coloured carbonate-poor marls (Faneromeni, lower part), or of homogeneous marls and brownish-coloured beds termed sapropels. Sapropels (and the related grey beds) have been labeled in stratigraphical order per section. Their characteristic pattern allows the sections to be correlated in detail. These cyclostratigraphic ("bed-to-bed") correlations are confirmed by the magnetostratigraphy and biostratigraphy (Chapter 2). They reveal minor differences in the number and expression of the cycles, for instance the Gibliscemi section contains additional (thin) sapropels in intervals which correspond to thick homogeneous marly intervals on Gavdos (Fig. 2).

Sapropels in particular display characteristic cycle patterns. A prominent feature is the occurrence of sapropels in both small-scale clusters and large-scale clusters (Figs. 2, 3). Small-scale clusters typically contain 3 or 4 sapropels and are separated from adjacent (small-scale) clusters by a thin, poorly developed sapropel and/or a homogeneous marl bed which is thicker - approximately two times - than a regular homogeneous marl bed. Large-scale clusters typically contain 3 or 4 small-scale clusters and are separated from adjacent clusters by thick homogeneous intervals which only occasionally contain additional thin sapropels. Large-scale clusters are given a roman numerical (see also Fig. 3). The grouping of sapropels into clusters is usually straightforward, but sometimes arbitrary; their stratigraphical range and characteristics are summarised below,where "G" refers to Gibliscemi, "M" to Metochia, "K" to Kastelli and "F" to Faneromeni (informal labeling):

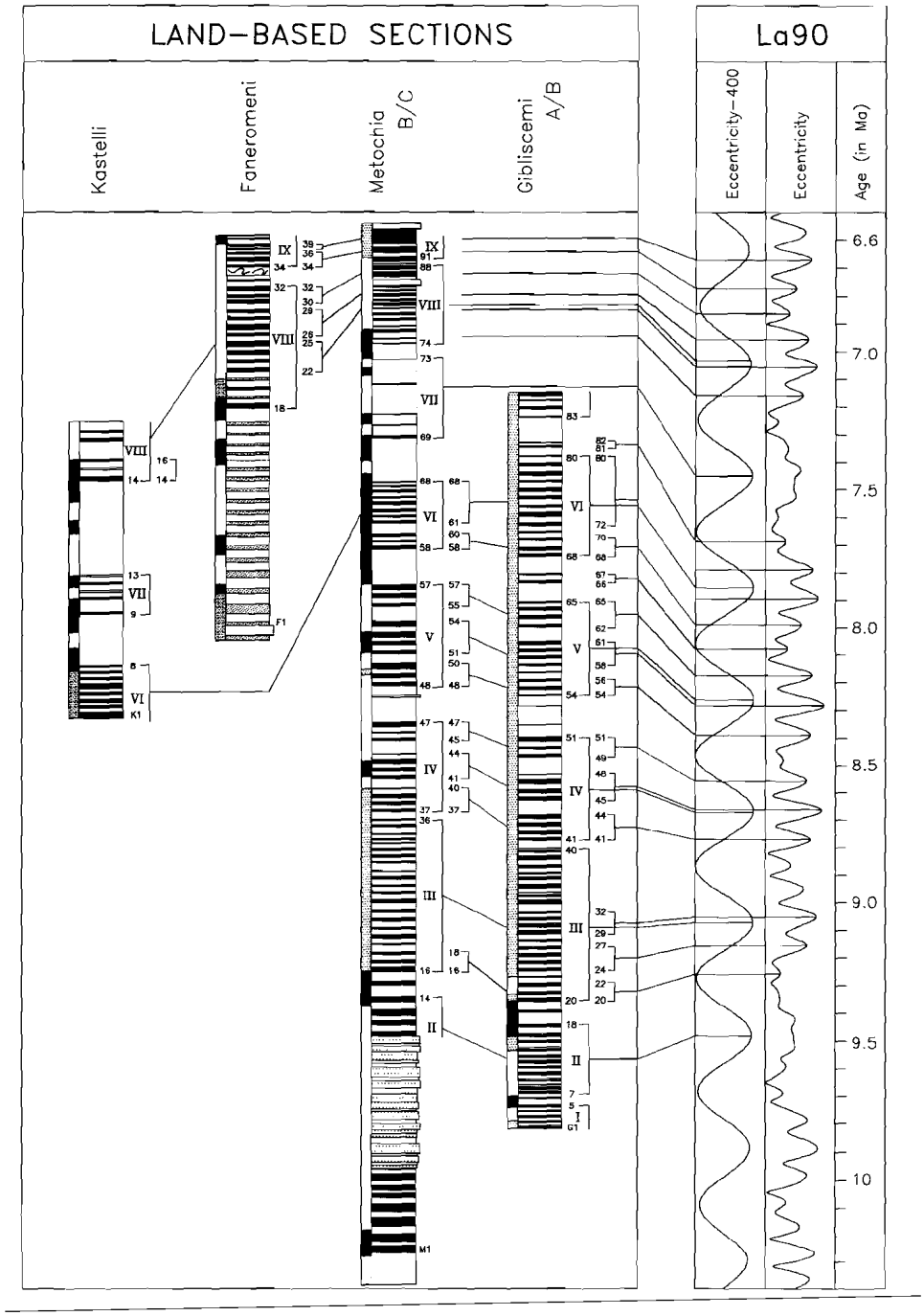
LAND–BASED SECTIONS
La90
Kastelli
Faneromeni
Metochia B/C
Gibliscemi A/B
Eccentricity–400
Eccentricity
Age (in Ma)
6.6
7.0
7.5
8.0
8.5
9.0
9.5
10
M1
F1
K1
G1

cluster I is incomplete; cluster II ranges from sapropel (of cycle) G7 to sapropel G18 (M14). No small-scale clusters could be distinguished;

cluster III ranges from sapropel G20 to sapropel G40 (M16 to M36). The presence of the thinner and less distinct sapropels G23, G28 and G32 allows the recognition of three small-scale clusters at Gibliscemi;

cluster IV ranges from sapropel G41 to sapropel G51 (M37 to M47) and contains three distinct small-scale clusters. It is separated from cluster III by a thick marl bed overlying a poorly developed sapropel (G40/M36);

cluster V ranges from sapropel G54 to sapropel G65 (M48 to M57) and similarly to cluster IV contains three small-scale clusters. At Gibliscemi, a thin sapropel (G57) is present between the lower and middle small-scale cluster which is not developed in the Metochia section (between M50 and M51). Also the upper small-scale cluster in section Gibliscemi contains an additional sapropel (G65);

cluster VI contains one typical small-scale cluster of 3 sapropels (G68-70, M58-60) and an atypical cluster which includes as many as 8 successive sapropels in the Gibliscemi and Metochia sections (G72-79, M61-68). At Gibliscemi, this atypical cluster contains an extra cycle (grey layer; G80) which is also recognised in the Kastelli section (K8). Also at Gibliscemi, a thin sapropel (G71) is found between the two clusters which is absent in Metochia (between M60 and M61). In addition, two extra thin sapropels are present in the thick homogeneous interval which separates clusters V and VI (G66 and G67). They constitute an additional small-scale cluster;

cluster VII represents an aberrant large-scale cluster. At Metochia, this cluster comprises 5 (thin) sapropels (M69-73) of which only the lowermost 3 are apparently grouped in a single small-scale cluster. But the homogeneous marl beds in between these three sapropels are twice as thick as the marl beds of cycles in the large-scale clusters VI and VIII. Hence, these cycles show a deviating pattern which is confirmed by the cycle patterns in the other sections (see Fig. 2). In contrast to Metochia and Kastelli, two extra thin sapropels (G81 and G82) are present in the thick homogeneous interval which separates clusters VI and VIII. They constitute an additional small-scale cluster;

cluster VIII is separated from cluster IX by the thick homogeneous marl bed of cycle F32 in combination with the extremely poorly-developed sapropel (i.e. grey marl bed) of cycle F33. The relatively thick homogeneous marl beds of cycles F25and F29 allows recognition of three small-scale clusters (containing 4,4, and 3 sapropels, respectively) in the interval ranging from sapropel F22 to F32. These small-scale clusters cannot be distinguished in the Metochia section. An extra small-scale cluster can be recognised at Kastelli (K14-16):

Figure 2. First-order and second-order correlations of the sedimentary cycles to the astronomical record: correlation of sapropel clusters to eccentricity maxima. Large-scale clusters have been correlated to 400-kyr eccentricity maxima (first-order correlations) and small-scale clusters to 100-kyr maxima (second-order correlations). The 400-kyr eccentricity cycle has been filtered from the eccentricity time series of solution La90 (Laskar, 1990).

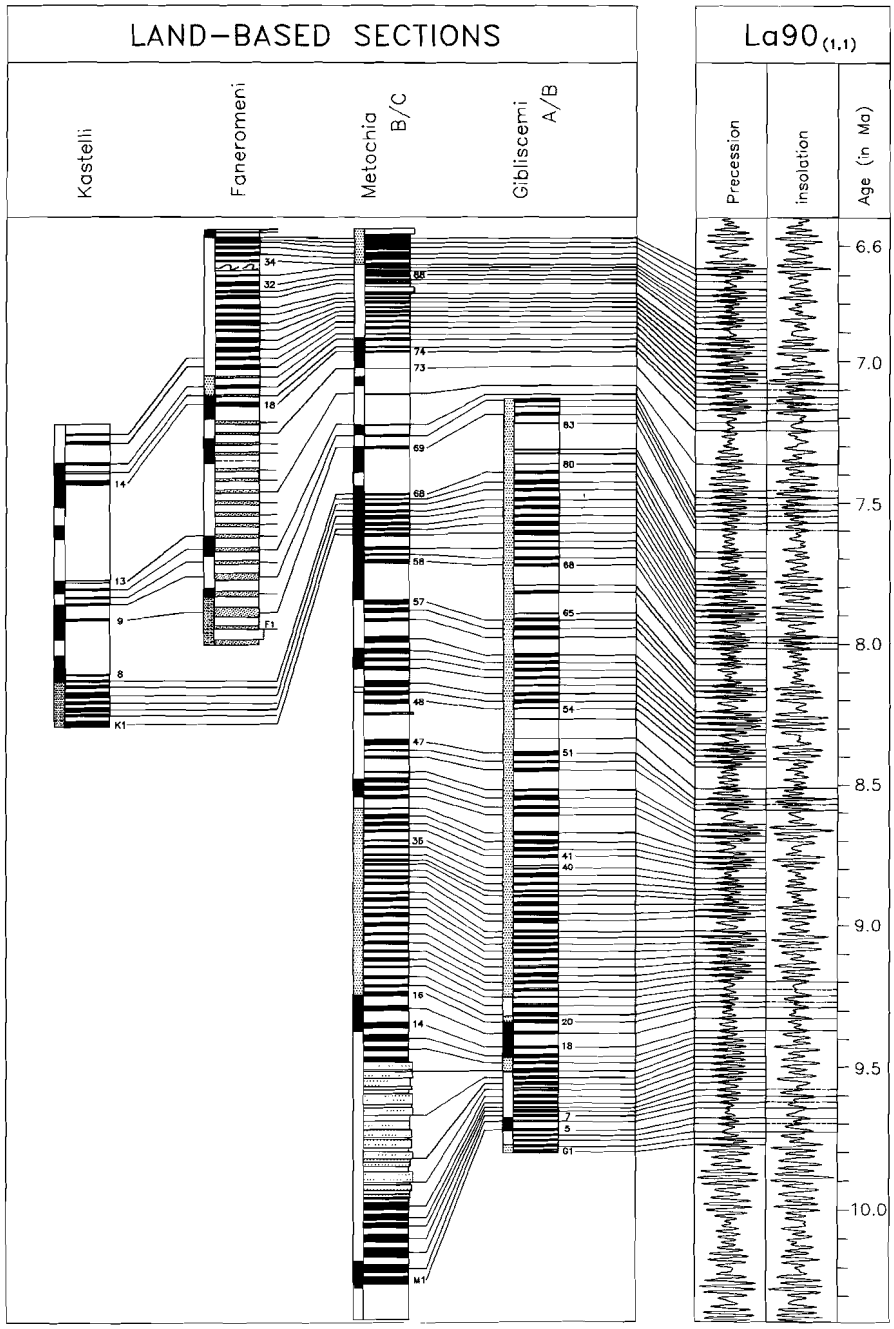
LAND–BASED SECTIONS
La90(1,1)
Kastelli
Faneromeni
Metochia B/C
Gibliscemi A/B
Precession
insolation
Age (in Ma)
6.6
7.0
7.5
8.0
8.5
9.0
9.5
10.0

cluster IX is incomplete; it includes at least two small-scale clusters which contain sapropels F34-36 and grey marlbeds F37-39, respectively.

Sapropels further reveal patterns which cannot be regarded as clusters. These patterns - with sapropels being alternatingly thick/thin or present/absent - are confined to specific intervals. The stratigraphic range and characteristics of these intervals are summarised below (in stratigraphic order):

sapropels G18-24 (M14-20). This interval displays a characteristic pattern which is markedly similar in the Gibliscemi and Metochia sections (Fig. 3). The homogeneous marlbeds of cycles G18 (M14) and G19 (M15) are twice as thick as the marlbeds of the cycles below and above. Furthermore the marlbed of cycle G18 (M14) is slightly thicker than that of cycle G19 (M15). These two extraordinary thick cycles are followed by an interval in which the well-developed and thick sapropels G20, G22 and G24 (M16, M18 and M20) alternate with the thin and poorly-developed sapropels G21 and G23 (M17 and M19), where G23 (M19) is less prominent than G21 (M17);

sapropels G49 to G51 (M45 to M47) and M58-60. These sapropels define small-scale clusters of 3 sapropels of which the middle sapropel is thinner and less prominent (Fig. 2,3).

sapropels G83 to G86 (M69 to 71); carbonate cycles F2-6. These cycles belong to (large-scale) cluster VII. On Gavdos, the homogeneous marlbeds in between sapropels M69-71 are twice as thick as the marlbeds of regular cycles below and above (Fig. 2,3). Hence, these cycles may represent composite ("double") cycles, i.e. cycles which contain an extra cycle that lacks sedimentary expression. This interpretation is confirmed by the sedimentary cycle patterns in the other sections. At Faneromeni, the grey beds of the correlative cycles F2, F4 and F6 are thicker (and contain thin sand layers) than the grey beds of adjacent cycles. An alternation of thick (G83 and G85) and thin (G82 and G84) sapropels is found. At Kastelli (Fig. 2,3), one distinct (K9) and two less distinct sapropels (K10 and K12) are separated by a thick homogeneous marlbed (between K9 and K10) and a poorly-developed grey bed (K11). Finally, an alternation of thick (G84 and G86) and thin (G83 and G85) sapropels is found just below the shearplane which marks the hiatus in the Gibliscemi section (see Chapter 2).

sapropels M74-M78, F18-F22 and K14-K17 form a characteristic pattern which can be recognised all over Crete. It consists of three well-developed and thick sapropels (M74, M76 and M78; F18, F20 and F22; and K14, K16 and K17) which alternate either with thin sapropels (M75 and M77) or with sedimentary cycles that lack a sapropel but contain a grey marl instead (F19 and F21; K15). Sapropels K16 and K17 are separated by a thick homogeneous marlbed.

Figure 3. Third-order correlations of the individual sedimentary cycles to precession minima and of alternatingly thick/thin sapropels/cycles to interference patterns of precession and obliquity as reflected in the 65° N summer insolation curve of solution La90 with present-day values for the dynamical ellipticity of the Earth and tidal dissipation by the moon.

Sedimentary cycle				age 1	age 2	Cycle			age 1	age 2	Cycle		age 1	age 2
Kas	Gib	Met	Fan	p	i	Kas	Gib	Met	p	i	Gib	Met	p	i
		M96	F39	6.654	6.654		G81		7.694	7.693	G40	M36	8.829	8.829
		M95	F38	6.675	6.675	K8	G80		7.743	7.743	G39	M35	8.849	8.849
		M94	F37	6.696	6.696	K7	G79	M68	7.766	7.766	G38	M34	8.869	8.869
		M93	F36	6.748	6.749	K6	G78	M67	7.787	7.787	G37	M33	8.889	8.889
		M92	F35	6.769	6.768	K5	G77	M66	7.809	7.808	G36	M32	8.904	8.905
		M91	F34	6.789	6.789	K4	G76	M65	7.833	7.834	G35	M31	8.923	8.923
		M90	F33	6.808	6.807	K3	G75	M64	7.858	7.857	G34	M30	8.944	8.944
		M89		6.825	6.826	K2	G74	M63	7.880	7.880	G33	M29	8.965	8.965
		M88	F32	6.845	6.844	K1	G73	M62	7.901	7.901	G32	M28	9.015	9.015
		M87	F31	6.865	6.866		G72	M61	7.923	7.923	G31	M27	9.037	9.037
		M86	F30	6.886	6.884		G71		7.950	7.950	G30	M26	9.058	9.058
		M85	F29	6.917	6.917		G70	M60	7.973	7.973	G29	M25	9.080	9.080
		M84	F28	6.938	6.938		G69	M59	7.994	7.994	G28	M24	9.104	9.105
		M83	F27	6.960	6.960		G68	M58	8.015	8.015	G27	M23	9.130	9.129
		M82	F26	6.982	6.982		G67		8.051	8.051	G26	M22	9.151	9.152
		M81	F25	7.008	7.005		G66		8.070	8.069	G25	M21	9.173	9.172
		M80	F24	7.031	7.032		G65		8.125	8.125	G24	M20	9.195	9.195
K18		M79	F23	7.053	7.052		G64	M57	8.145	8.144	G23	M19	9.222	9.225
K17		M78	F22	7.074	7.075		G63	M56	8.165	8.165	G22	M18	9.246	9.245
		M77	F21	7.097	7.097		G62	M55	8.186	8.186	G21	M17	9.266	9.267
K16		M76	F20	7.123	7.123		G61	M54	8.237	8.236	G20	M16	9.285	9.284
K15		M75	F19	7.146	7.146		G60	M53	8.258	8.258	G19	M15	9.322	9.322
K14		M74	F18	7.167	7.167		G59	M52	8.279	8.279	G18	M14	9.368	9.367
			F17	7.212	7.207		G58	M51	8.300	8.300	G17	M13	9.393	9.394
		M73	F16	7.242	7.242		G57		8.322	8.323	G16	M12	9.415	9.414
			F15	7.262	7.263		G56	M50	8.352	8.351	G15	M11	9.437	9.438
			F14	7.280	7.280		G55	M49	8.373	8.373	G14	M10	9.461	9.460
			F13	7.316	7.317		G54	M48	8.394	8.393	G13	M9	9.484	9.484
			F12	7.339	7.338		G53		8.433	8.432	G12	M8	9.507	9.507
		M72	F11	7.361	7.361		G52		8.507	8.507	G11	M7	9.529	9.528
			F10	7.385	7.386		G51	M47	8.545	8.545	G10	M6	9.552	9.554
			F9	7.409	7.408		G50	M46	8.565	8.566	G9	M5	9.577	9.576
			F8	7.431	7.431		G49	M45	8.587	8.586	G8	M4	9.599	9.600
K13			F7	7.454	7.453		G48	M44	8.638	8.638	G7	M3	9.621	9.619
K12		M71	F6	7.477	7.478		G47	M43	8.659	8.659	G6	M2	9.641	9.642
K11			F5	7.500	7.500		G46	M42	8.680	8.680	G5	M1?	9.676	9.677
K10	G86	M70	F4	7.523	7.523		G45	M41	8.702	8.702	G4		9.697	9.696
	G85		F3	7.545	7.545		G44	M40	8.731	8.732	G3		9.725	9.724
K9	G84	M69	F2	7.569	7.567		G43	M39	8.753	8.753	G2		9.748	9.749
	G83		F1	7.593	7.594		G42	M38	8.774	8.774	G1		9.770	9.770
	G82			7.673	7.674		G41	M37	8.794	8.794				

Phase relations and astronomical solutions

The sedimentary cycle patterns described here are very similar to the patterns in the Mediterranean Plio-Pleistocene which are related to the Earth's orbital cycles of precession, eccentricity and obliquity (Rossignol-Strick, 1983; Hilgen, 1987, 1991a,b; Lourens et al., 1995). This similarity argues for an analogous interpretation of the Miocene cycle patterns and it implies that individual sapropels are related to precession, while sapropel clusters are related to eccentricity. Deviating patterns - with sapropels being alternatingly thick/thin or present/absent - reflect interference between precession and obliquity. Similar to the Plio-Pleistocene, Miocene cycle patterns are dominantly controlled by eccentricity (sapropel clusters) and precession (individual sapropels). This astronomical interpretation of the Miocene patterns has independently been confirmed by Krijgsman et al. (1994a) who correlated polarity sequences of upper Miocene sections on Crete to CK92. This correlation yielded a periodicity (of 23.5 kyr) for individual sedimentary cycles which is close to the 21.7 kyr average periodicity of astronomical precession.

First results of detailed micropaleontological and geochemical studies further point to a single mechanism for sapropel formation throughout the Mediterranean Neogene (Nijenhuis and Schenau, 1995). We may thus safely assume that the Plio-Pleistocene phase relations between sedimentary cycles and astronomical cycles can be employed to calibrate the Miocene cycles to the astronomical record as well. As a consequence, the individual sapropels of late Miocene age correspond to precession minima, small-scale sapropel clusters correspond to 100 kyr eccentricity maxima, large-scale clusters correspond to 400 kyr eccentricity maxima and "amplified" (thick) sapropels correspond to obliquity maxima (Hilgen, 1991a; Lourens et al., 1995).

For our calibration we have used the 65°N summer insolation curve of astronomical solution La90 (Laskar, 1990; Laskar et al., 1993) with present-day values for the dynamical ellipticity of the Earth and the tidal dissipation by the moon. We selected this target curve because it shows the best agreement with sedimentary cycle patterns and orbitally controlled frequency components in climatic proxy records in the Mediterranean Pliocene-Pleistocene (Lourens et al., 1995). The reader is referred to the latter paper for a discussion on the selection of the La90 solution and the 65°N summer insolation curve (as target), and on the potential influence of obliquity on low latitudes.

Table 1. Astronomical ages of individual sedimentary cycles. Ages refer to the mid-points of sapropels and/or grey layers and represent 3-kyr lagged ages of the correlative precession minima (p) or the summer insolation maxima (i) based on the third-order correlations of the sedimentary cycles to the astronomical record shown in figure 4. The 3-kyr lag is based on the difference in age between the youngest Holocene sapropel in the Mediterranean and the correlative precession minimum / insolation maximum.

Calibration to the astronomical record

The astronomical calibration of the sequence of Pliocene cycles in the Mediterranean (Hilgen, 1991a,b) cannot simply be extended to the sequence of Miocene cycles because of the intervening interval of Messinian evaporites and fresh- to brackish water deposits. Hence, the astronomical calibration of the Miocene cycles is not straightforward, and several procedures can be followed to solve this problem. One procedure is to use radioisotopic age constraints from high-precision $^{40}Ar/^{39}Ar$ dating, e.g. that of C5n (y) at 9.67 (Baksi et al., 1993) or the Tortonian-Messinian boundary at 7.26 Ma (Vai et al., 1993). We refrained from using this approach because we prefer to build an astronomical time scale that does not depend on radiometric dating. Another procedure would be to start from the astronomically dated Miocene-Pliocene boundary (Hilgen, 1991b) and use the number of assumedly astronomically controlled evaporite cycles in the Mediterranean Messinian, and thus to estimate the age of the top of our upper Miocene sequence. A third procedure would be to start from the age of the youngest polarity reversal identified in our sections according to the most recent geomagnetic polarity time scales CK95 and SCHPS95. Both these time scales include astronomically derived ages for reversal boundaries in the Plio-Pleistocene. We have used the last approach, but application of the other procedures would have resulted in the same astronomical calibration. We discuss this further (below) where we test the validity of the proposed astronomical calibration.

By using high-resolution GRAPE density and stable isotope records from ODP Leg 138 in the eastern tropical Pacific, Shackleton et al. (1993) obtained a preliminary astronomical age of 6.278 Ma for C3An.2n (y). This age is 9 kyr older than the age (6.269 Ma) for the same polarity reversal in CK95. We simply added this age difference to the age of 6.567 Ma for the next older reversal in CK95 (C3An.2n (o)) to obtain a first approximation - of 6.576 Ma - for the astronomical age of the youngest polarity reversal recorded in our sections (Fig. 2).

We then proceeded by attempting to correlate first the sapropel clusters to eccentricity. No straightforward correlation is found, however, if we use the age of 6.576 Ma for C3An.2n (o) as starting point. We then proceeded by slightly adjusting the age of this calibration point. The minimum adjustment necessary to establish a consistent correlation between sapropel clusters and eccentricity maxima is shifting the age ± 100 kyr towards older levels. The resulting correlations of large-scale sapropel clusters to 400 kyr eccentricity maxima and of small-scale clusters to 100 kyr maxima are presented in figure 3. The validity of these first-order and second-order correlations is supported by the atypical large-scale clusters (II and VII) which lack a clear subdivision in small-scale clusters. These large-scale clusters correlate well with two 400-kyr eccentricity cycles at 7.4 and 9.5 Ma that lack the usually pronounced expression of the 100-kyr cycle (see fig. 3). Moreover, the large-scale clusters IV and V, which reveal the most distinct subdivision in small-scale clusters, correlate with 400-kyr eccentricity maxima, at

8.3 and 8.7 Ma, that show the most pronounced expression of the 100-kyr cycle (Fig. 3). Such variations in the expression - or "amplitude" - of the 100-kyr cycle reflect a longer-term eccentricity cycle with a period near 2 Myr. We then used the low-order correlations to establish (third-order) correlations between individual sapropels and precession minima and between individual sapropels and insolation maxima (Fig. 4). All correlations shown in figures 3 and 4 are internally consistent and there is still a good to excellent agreement between sapropel patterns and interference patterns of precession and obliquity back to 9.7 Ma. Only the exact calibration of the sedimentary cycles of the atypical cluster VII remains uncertain. These cycles may actually correlate with precession minima - and the corresponding insolation maxima - that are 20 to 40 kyr younger (i.e., one to two precession cycles). This alternative option implies that the unusually thick cycles F13 and F17 do not represent composite ("double") cycles, i.e., cycles which contain an extra cycle that lacks sedimentary expression, but must be considered as regular ("single") cycles.

Alternative calibrations would necessitate shifting the age of the sedimentary cycle record 400 kyr in either direction as is inherent in applying the 400 kyr eccentricity cycle for a first-order astronomical calibration.

The most likely alternative calibration is by shifting the cycle record 400 kyr towards younger levels which would imply a 300 kyr (=400-100) adjustment of our initial age of 6.576 Ma for C3An.2n (o). We superficially explored this alternative calibration and a very limited number of other alternatives. All these exercises resulted in correlations which are not convincing and less consistent than the correlations presented in figures 3 and 4. Summarizing, we are convinced that the proposed astronomical calibration is essentially correct and that it is based on continuous sedimentary successions.

The calibration of the sedimentary cycle record to precession (Fig. 4) was used to establish an astronomical time scale for the late Miocene. It results in ages for the individual sedimentary cycles, and hence for all biostratigraphic datum planes and polarity reversals recorded in our sections (see tables 1-3). The age of the Tortonian/Messinian boundary placed at the level of the first regular occurrence of the *G. conomiozea* group arrives at 7.24 Ma. Since the age of the Miocene-Pliocene boundary is 5.33 Ma (Lourens et al., 1995), the duration of the Messinian is 1.91 Myr. Note that the alternative option for the astronomical calibration of the sedimentary cycles in large-scale cluster VII (see above) results in slightly younger ages for all reversals and bioevents between 7.6 and 7.2 Ma. According to this option, the age of the T/M boundary is 7.21 Ma and the duration of the Messinian 1.88 Myr.

The exact accuracy of astronomical solutions and hence of our astronomical ages is difficult to determine (Berger and Loutre, 1993; Quinn et al., 1991) also because other factors, i.e., the tidal dissipation by the moon and the dynamical ellipticity of the Earth, which are influenced by glacial cycles, start to play a role (Laskar et al., 1993). The analytical solution La90 is in excellent agreement with the numerical solution QTD90 (Quinn et al., 1991) once the same term for the

magnetic reversal	Gibliscemi	Metochia	Kastelli	Faneromeni	range	chron	age
C3An.2n (o)				6.675-6.678	6.675-6.678		**6.677**
C3Bn (y)		*7.106-7.133*	7.094-7.108	-	7.094-7.108		**7.101**
C3Bn (o)		*7.216-7.223*	*7.208-7.214*	7.203-7.218	7.203-7.218		**7.210**
C3Br.1n (y)		*7.257-7.268*	*7.255-7.262*	7.249-7.264	7.249-7.264		**7.256**
C3Br.1n (o)		*7.301-7.316*	*7.296-7.302*	7.299-7.304	7.299-7.304		**7.301**
C3Br.2n (y)		*7.474-7.478*	7.455-7.462	7.452-7.455	7.455		**7.455**
C3Br.2n (o)		*7.517-7.522*	7.488-7.496	7.480-7.499	7.488-7.496		**7.492**
C4n.1n (y)		*7.545-7.552*	7.519-7.536	7.529-7.535	7.529-7.535		**7.532**
C4n.1n (o)		*7.649-7.678*	7.639-7.649		7.639-7.649		**7.644**
C4n.2n (y)		*7.695-7.742*	7.692-7.703		7.692-7.703		**7.697**
C4n.2n (o)		8.102-8.116			8.102-8.116		**8.109**
C4r.1n (y)		8.247-8.267			8.247-8.267		**8.257**
C4r.1n (o)		8.296-8.310			8.296-8.310		**8.303**
C4r.2r-1 (y)		8.648-8.670			8.648-8.670		**8.659**
C4r.2r-1 (o)		8.694-8.710			8.694-8.710		**8.702**
C4An (y)		-					-
C4An (o)		-					-
C4Ar.1n (y)	9.256-9.304	-			9.256-9.304		**9.280**
C4Ar.1n (o)	*9.384-9.430*	9.376-9.378			9.376-9.378		**9.377**
C4Ar.2n (y)	9.627-9.642	9.628-9.630			9.628-9.630		**9.629**
C4Ar.2n (o)	9.675-9.684	*9.696-9.714*			9.675-9.684		**9.679**

planktonic foram	**event**							
11) *G. nicolae*	FO		6.826-6.831		6.822-6.831	6.826-6.831	**C3Ar**	**6.829**
10) *G. conomiozea gr.*	FRO		7.237-7.241	*7.239-7.249*	7.240-7.243	7.240-7.241	**C3Br.1r**	**7.240**
9) *G. menardii 5*	FO		7.353-7.356	*7.351-7.356*	7.353-7.359	7.353-7.356	**C3Br.2r**	**7.355**
8) *C. parvulus*	LO		7.446-7.466	-	-	7.446-7.466	**C3Br.2r**	**7.456**
7) *G. menardii 4*	LCO		7.507-7.512	7.512-7.519	7.511-7.519	7.512	**C3Br.3r**	**7.512**
6) *S. seminulina*	hro	7.719-7.727	7.720-7.731	7.724-7.729		7.724-7.727	**C4n.2n**	**7.726**
5) *S. seminulina*	lro	7.913-7.921	7.915-7.921			7.915-7.921	**C4n.2n**	**7.918**
4) *C. parvulus*	fs	8.420-8.429	8.420-8.442			8.420-8.429	**C4r.2r**	**8.425**
3) *C. parvulus (ls)*	LCO	8.869-8.872	8.863-8.868			8.863-8.868	-	**8.865**
2) *G. menardii 4*	lco	9.309-9.316	9.312-9.324			9.312-9.316	**C4Ar.1n(y)**	**9.314**
1) *N. acostaensis dex*	hro	9.531-9.541	9.546-9.549			9.546-9.549	**C4Ar.2r**	**9.548**
II) *G. conomiozea gr.*	FO	7.890-7.893	*7.863-7.867*	*7.864-7.869*		7.890-7.893	**C4n.2n**	**7.892**
I) *G. dehiscens*	influx	8.969-8.990	8.970-8.984			8.970-8.984	-	**8.977**

dinoflagellate								
i) *L. truncatum*	LO	7.789-7.800				7.789-7.800	**C4n.2n**	**7.795**
h) *T. psilatum*	LCO	8.003-8.041				8.003-8.041	**C4n.2n**	**8.022**
g) *C? labradorii*	LO	8.061-8.077				8.061-8.077	**C4n.2n**	**8.069**
f) *M. sp. A*	LO	8.197-8.243				8.197-8.243	**C4r.1r**	**8.220**
e) *C? labradorii*	FO	8.289-8.312				8.289-8.312	**C4r.2r/C4r.1n**	**8.300**
d) *P. golzowense*	LO	8.762-8.785				8.762-8.785	-	**8.774**
c) *I. maculatum*	FO	9.260-9.272				9.260-9.272	**C4Ar.1r**	**9.266**
b) *M. sp. A*	LCO	9.435-9.452				9.435-9.452	**C4Ar.2r**	**9.444**
a) *C. sp. A*	LO	9.586-9.614				9.586-9.614	**C4Ar.2r**	**9.600**

tidal dissipation is introduced. The latter solution is supposedly very accurate, but was not computed for the time intervals older than 3 million years. Also the excellent agreement with sedimentary cycle patterns in the Mediterranean Pliocene suggests that the selected target curve -La90 $_{(1,1)}$ summer insolation - is very accurate (Lourens et al., in press). The error in the astronomical ages can roughly be estimated to be in the order of 5 kyr at 5.0 Ma. This error may well increase to 10-20 kyr around 10.0 Ma.

Our astronomical ages of the polarity reversals are invariably older than the ages in recent polarity time scales (Table 4). It is remarkable that the discrepancies with CK95 are largest for the youngest reversals dated (up to 166 kyr) and decrease gradually to values between 25 and 70 kyr for older reversals. Discrepancies with SCHPS95 further indicate that our astronomical calibration is not in agreement with the preliminary and partial astronomical tuning of GRAPE records from ODP leg 138 for the interval between 6.0 and 10.0 Ma (Shackleton et al., 1995). Unpublished work on ODP leg 154 sediments (Shackleton, pers. comm., 1995) also shows that the late Miocene age estimates of Shackleton et al. (1995) are too young.

Testing the validity of the astronomical calibration

In this chapter, we attempt to test the validity of the new time scale. Independent tests must either come from astronomical calibration of other, preferably extra-Mediterranean records or from high-precision radioisotopic dating. In addition, the number of sedimentary cycles in the remaining younger part of the Mediterranean Messinian may provide important constraints.

Radiometric age constraints

The time scale can be tested by comparing astronomical ages of polarity reversals or biostratigraphic datum planes with radioisotopic age constraints for the same events. Recent radioisotopic results include an age of 9.51 Ma for C4Ar.2n (o) (Baksi et al., 1993) and an age of 7.07 Ma for the Tortonian/Messinian boundary (Vai and Laurenzi, 1994). We did not include K/Ar ages (e.g. from Iceland; McDougall et al., 1984) because radioisotopic dating of lavas often yield ages that are too young. We have sampled ashbeds that are intercalated in section Metochia and in parallel sections on Crete (e.g. Faneromeni, Kastelli) for

Table 2. Astronomical ages of biostratigraphic datum planes and polarity reversals. Ages have been obtained by linear interpolation of the sedimentation rate between astronomically-dated calibration points shown in table 1. We used the 3-kyr lagged ages of insolation maxima for the sapropels as starting point.

reversal	our age	CK95	Δ	SBP90 SCHPS95	Δ
C1n		0.780		0.780	
C1r.1n (y)		0.990		0.990	
C1r.1n (o)		1.070		1.070	
C2n (y)	**1.785**	1.770	*0.015*	1.770	*0.015*
C2n (o)	**1.942**	1.950	*-0.008*	1.950	*-0.008*
C2r.1n (y)	**2.129**	2.140	*-0.011*		
C2r.1n (o)	**2.149**	2.150	*-0.001*		
C2An.1n (y)	**2.582**	2.600	*-0.018*	2.600	*-0.018*
C2An.1n (o)	**3.032**	3.040	*-0.008*	3.046	*-0.014*
C2An.2n (y)	**3.116**	3.110	*0.006*	3.131	*-0.015*
C2An.2n (o)	**3.207**	3.220	*-0.013*	3.233	*-0.026*
C2An.3n (y)	**3.330**	3.330	*0.000*	3.331	*-0.001*
C2An.3n (o)	**3.596**	3.580	*0.016*	3.594	*0.002*
C3n.1n (y)	**4.188**	4.180	*0.008*	4.199	*-0.011*
C3n.1n (o)	**4.300**	4.290	*0.010*	4.316	*-0.016*
C3n.2n (y)	**4.493**	4.480	*0.013*	4.479	*0.014*
C3n.2n (o)	**4.632**	4.620	*0.012*	4.623	*0.009*
C3n.3n (y)	**4.799**	4.800	*-0.001*	4.781	*0.018*
C3n.3n (o)	**4.896**	4.890	*0.006*	4.878	*0.018*
C3n.4n (y)	**4.998**	4.980	*0.018*	4.977	*0.021*
C3n.4n (o)	**5.236**	5.230	*0.006*	5.232	*0.004*
C3An.1n (y)	*5.952*	5.894	*0.059*	5.875	*0.077*
C3An.1n (o)	*6.214*	6.137	*0.079*	6.122	*0.092*
C3An.2n (y)	*6.356*	6.269	*0.089*	6.256	*0.100*
C3An.2n (o)	**6.677**	6.567	*0.110*	6.555	*0.122*
C3Bn (y)	**7.101**	6.935	*0.166*	6.919	*0.182*
C3Bn (o)	**7.210**	7.091	*0.119*	7.072	*0.138*
C3Br.1n (y)	**7.256**	7.135	*0.121*		
C3Br.1n (o)	**7.301**	7.170	*0.131*		
C3Br.2n (y)	**7.455**	7.341	*0.114*		
C3Br.2n (o)	**7.492**	7.375	*0.117*		
C4n.1n (y)	**7.532**	7.432	*0.100*	7.406	*0.126*
C4n.1n (o)	**7.644**	7.562	*0.082*	7.533	*0.111*
C4n.2n (y)	**7.697**	7.650	*0.047*	7.618	*0.079*
C4n.2n (o)	**8.109**	8.072	*0.037*	8.027	*0.082*
C4r.1n (y)	**8.257**	8.225	*0.032*	8.174	*0.083*
C4r.1n (o)	**8.303**	8.257	*0.046*	8.205	*0.098*
C4r.2r-1 (y)	**8.659**	8.635	*0.024*		
C4r.2r-1 (o)	**8.702**	8.651	*0.051*		
C4An (y)	*8.750*	8.699	*0.051*	8.631	*0.119*
C4An (o)	*9.075*	9.025	*0.050*	8.945	*0.130*
C4Ar.1n (y)	**9.280**	9.230	*0.050*	9.142	*0.138*
C4Ar.1n (o)	**9.377**	9.308	*0.069*	9.218	*0.159*
C4Ar.2n (y)	**9.629**	9.580	*0.049*	9.482	*0.147*
C4Ar.2n (o)	**9.679**	9.642	*0.037*	9.543	*0.136*
C5n.1n (y)		9.740		9.639	

Table 3. Comparison of the astronomical ages of reversal boundaries with the ages of the corresponding reversals in recently advanced polarity time scales of Cande and Kent (1995; CK95) and Shackleton et al. (1995; SCHPS95). Ages of reversals which could not be dated directly because of their late Messinian age or of poor magnetostratigraphic results in our sections have been obtained by linear interpolation of seafloor-spreading rates between the nearest younger and older astronomically dated reversals in the synthetic anomaly profile of Cande and Kent (1992). These ages are shown in italics. Ages of younger polarity reversals - of Plio-Pleistocene age - have been included. They are taken from Cande and Kent (1995; CK95), Shackleton et al. (1990; SBP90 and 1995; SCHPS95) and Lourens et al. (in press). CK95 included astronomical ages of Shackleton et al., (1990) and Hilgen et al. (1991b) for this time interval. In this chapter, the same astronomical solution and target curve is used as the one preferred by Lourens et al., (in press).

datum	radiometric age	FCT age 27.95	FCT age 28.03	astronomical age
T/M boundary	7.07 ± 0.05	7.17	7.19	**7.240**
C4Ar.2n (y)	9.51 ± 0.05	9.51	9.54	**9.679**

Table 4. Comparison of astronomical and Ar/Ar ages for C4Ar.2n (o) and the Tortonian-Messinian boundary. Ar/Ar ages have been recalculated to ages of 27.95 and 28.03 Ma for the Fish Canyon Tuff sanidine following the formula given in Dalrymple et al. (1993).

$^{40}Ar/^{39}Ar$ dating (Chapter 5).

Baksi et al. (1993) carried out $^{40}Ar/^{39}Ar$ incremental heating studies on whole rock basalts of a number of lava flows from Akaroa Volcano, New Zealand. These lava flows span two successive field reversals. The lower normal to reversed (N-R) transition is assumed to represent the termination of chron C5. This boundary was previously dated at 8.9 Ma by Evans (1970) who used the K/Ar method. The new results yielded a weighted mean plateau age of 9.67 ± 0.05 Ma for this boundary, while the younger (R-N) reversal was dated at 9.51 ± 0.05 Ma. The latter age is slightly younger than our astronomical age of 9.66 Ma for the same reversal. Although Berggren et al. (1995) point out that the lower transition at Akaroa can also be correlated with either chron C5n.1r/C5n.2n or chron C4Ar.2r/n boundary, any other option than the one preferred by Evans (1970) and Baksi (1993) would increase the discrepancy with the astronomical age for C4Ar.2n (o).

Using K/Ar dating on biotite and a single Ar/Ar dating on plagioclase, Vai et al. (1993) dated several volcanogenic beds intercalated in upper Tortonian - lower Messinian marine sequences in the northern Apennines. They obtained an age of 7.26 Ma for the Tortonian/Messinian boundary through linear extrapolation of the sedimentation rate over a short distance. Recently, Vai and Laurenzi (1994) provided a series of additional Ar/Ar datings of biotite-rich ash layers spanning the Tortonian/Messinian boundary in the Monte di Casino section. They arrived at a revised age of 7.07 ± 0.05 Ma for the boundary which is younger than their previous estimate of 7.26 Ma and also younger than our astronomical age of 7.24 Ma.

A straightforward comparison between the radioisotopic and astronomical ages, however, should be viewed with caution because of the age uncertainty of fluence monitor standards in radioisotopic dating. For example, the age of the Fish Canyon Tuff (FCT), which provides one of the most widely used standards for age calibration in radioisotopic dating, varies between 27.55 and 27.95 Ma (Izett et al., 1992; Baksi, 1993; Renne et al., 1994). This age uncertainty results in a

potential error of 1.5 %. To eliminate this uncertainty, Renne et al. (1994) compared Ar/Ar ages with astronomical ages for seven polarity reversals over the last 3.5 Myrs and they derived a best age estimate of of 27.95 (or 28.03) Ma for the FCT sanidine.

Baksi et al. (1993) used an age of 27.95 Ma for Fish Canyon Tuff biotite whereas Vai et al. (1993) and Vai and Laurenzi (1994) used 27.55 Ma. In table 4, we compared the $^{40}Ar/^{39}Ar$ ages of both C4Ar.2n (o) and the Tortonian/ Messinian boundary - recalculated to ages of 27.95 and 28.03 Ma for the Fish Canyon Tuff - with the astronomical ages. This comparison shows that the Ar/Ar ages are now in better agreement with the astronomical ages. In particular, they support our preferred astronomical calibration because they are totally inconsistent with ages that are 400 kyr younger (or older) than our astronomical ages. The age difference for the T/M boundary is further reduced considering that Vai and Laurenzi (1994) equate the boundary with a level above the first regular occurrence (FRO) of the *G. conomiozea* group (i.e., the first occurrence level of *G. conomiozea* types), whereas we use the FRO level of the *G. conomiozea* group (see Chapter 2). The use of the alternative option to astronomically calibrate the sedimentary cycles of large-scale cluster VII (see above) results in a reduction of this discrepancy as well.

Cyclostratigraphic framework of Messinian evaporites

Cyclic bedding is not restricted to the pre-evaporitic part of the Mediterranean Messinian, since the evaporites often show a pronounced cyclic bedding as well. Here, we investigate whether the number of sedimentary cycles in the younger part of the Mediterranean Messinian is consistent with what we might expect from the astronomical calibrations.

The standard succession of the Messinian evaporites comes from the Caltanissetta Basin on Sicily (Decima and Wezel, 1973). In stratigraphical order, this succession includes diatomites of the Tripoli Formation, partly evaporitic limestones of the Calcare di Base, massive gypsum and halite of the Lower Evaporites, gypsum arenites, and selenitic gypsum of the Upper Evaporites. All units except the Tripoli diatomites belong to the Gessoso-Solfifera Formation. Because no literature data are presently available on the number of cycles for all units, we included information from Gavdos and from basins other than the Caltanissetta Basin, in particular the Ciminna Basin on northern Sicily (Bommarito and Catalano, 1973) and the Vena del Gesso and Romagna-Marche Basins in the northern Apennines (Vai and Ricci Lucchi, 1976; Vai, 1989, 1995).

The number of sedimentary cycles has been summarised per stratigraphic unit and per basin in table 5. The consistent number of evaporite cycles in all basins suggests that disturbing effects of hiatuses on the continuity of the evaporite sequences is small. Also, the disturbing effect of lateral facies changes will be small because most of the cyclically bedded sequences have been logged in stratigraphic succession.

lithostrat. unit	Calta-nissetta	Ciminna	Vena del Gesso	Romagna Marche	Gavdos	comp.
Upper evaporites	7-8	6-8		6-8		8
Intermediate marls		1				1
Lower evaporites		15/16	16	15		16
Calcare di Base	4-13	4	4 (±2)			4 (±2)
Tripoli diatomites	>34				38	38
Total						67 (±2)
No. of astronomical precession cycles:						67

Table 5. Number of sedimentary cycles per stratigraphic unit and per evaporite basin. For the Ciminna Basin, we included both the "lower selenite gysum" and the "laminated gypsum" of Bommarito and Catalano (1973) in the Lower Evaporites. In that case, the transition from "lower selenite" to "laminated gypsum" would correspond with the transition from major (thicker) to minor (thinner) evaporite cycles in the Vena del Gesso Basin (see Vai, 1989) and the major discontinuity in the evaporite sequences would invariably separate the Lower from the Upper Evaporites. In the Romagna-Marche basin, the Upper Evaporites do not exhibit the usual gypsum-bearing cycles but consist of a cyclic alternation of thin evaporitic limestone beds and marly clays of the Colombacci Fm. In the total number count of the sedimentary cycles, we preferred to use the 38 diatomite cycles from Gavdos because they are tectonically less disturbed than the diatomites in the Falconara section. Moreover, they are in stratigraphic continuity with our Metochia section, thus excluding discrepancies as a consequence of a diachronous base of the diatomites (e.g. Gersonde, 1978). The large numbers of 6-9 and 4-13 cycles of the Calcare di Base in the Caltanissetta Basin as reported by Pedley and Grasso (1993) and Decima et al. (1988) have not been used because these cycles represent at least partly the lateral (= marginal) equivalent of the lower evaporites and/or the top of the Tripoli diatomites (see Butler et al., 1995).

The best current estimate for the total number of sedimentary cycles in our composite evaporite sequence of the Mediterranean Messinian, including the pre-evaporitic diatomites, is 67 ± 2. For the composite, we preferred to use the 38 diatomite cycles from Gavdos because they are tectonically less disturbed than the diatomites in the Falconara section. Moreover, they are in stratigraphic continuity with our Metochia section, thus excluding discrepancies as a consequence of a diachronous base of the diatomites (e.g. Gersonde, 1978). Here, we assume that all cycles are related to precession. This assumption is based on - both observed as well as inferred - lithological relationships between the different types of sedimentary cycles (Vai and Ricci Lucchi, 1976; authors field observations). Field observations for instance clearly reveal that sapropels pass

into diatomites of the Tripoli Formation and that the diatomite cycles are replaced by cycles of the Calcare di Base.

The number of 67 can now be compared with the number of precession cycles in the same time interval, i.e. between the base of the diatomites, dated at 6.70 Ma, and the Miocene/Pliocene boundary, dated at 5.33 Ma. This interval contains 67 precession cycles. This number is in excellent agreement with our estimate of 67 ± 2 for the total number of sedimentary cycles even though the exact number remains uncertain. Using this cyclostratigraphic framework, we obtained preliminary ages of 5.95 Ma for the base of the Calcare di Base, and of 5.87 and 5.52 Ma for the base of the Lower Evaporites and Upper Evaporites, respectively.

Our framework differs from that of Vai (1995) by the larger number of sedimentary cycles in the pre-evaporitic Messinian, and that we held precession rather than obliquity responsible for the formation of cycles in the Upper Evaporites. Evidence for the precessional forcing of these cycles comes from Ar/Ar ages of 5.4 ± 0.06 and 5.5 ± 0.05 Ma for an ash layer intercalated directly below the first limestone ("Colombaccio") marker bed in the northern Apennines (Odin, 1995 as referred to by Vai, 1995). These ages are in good agreement with our age of 5.52 Ma for the base of the Upper Evaporites, but they are too young in case the Upper Evaporite cycles are obliquity controlled.

Another consequence of our framework is that the onset of evaporite formation is younger than 6.0 Ma and even postdates the Gilbert/Chron 5 boundary tentatively dated at 5.955 Ma (see Table 3). This outcome is in agreement with Gaultier et al. (1994) who, based on the magnetostratigraphy of the Sorbas section in Spain, placed the onset of evaporite formation in the early Gilbert as well. This onset now closely coincides with the most extreme glacial stages TG 20 and 22 in the high-resolution stable isotope records of ODP Site 846 from the equatorial Pacific (Shackleton et al., 1995b) and Atlantic Morocco (Hodell et al., 1994) suggesting at least a partial glacio-eustatic control on the final isolation of the Mediterranean during the latest Miocene.

Conclusions

Marine sequences exposed in Mediteranean land-based sections allow the construction of an astronomical time scale for the late Miocene by correlating characteristic sedimentary cycle patterns to target curves of astronomical solution La90 with present-day values for the dynamical ellipticity of the Earth and the tidal dissipation by the moon. This correlation yields ages for the individual sedimentary cycles, and for the polarity reversals and planktonic foraminiferal and dinoflagellate events recorded. The Tortonian/Messinian boundary is dated at 7.24 Ma (or 7.21 Ma).

Astronomical ages of the polarity reversals are older (up to 182 kyr) than the ages of the corresponding reversals in the most recent geomagnetic polarity time scales of CK95 and SCHPS95. Discrepancies with CK95 are largest for the

youngest reversals dated (up to 166 kyr) and decrease gradually to values between 25 and 70 kyr for older reversals. Discrepancies with SCHPS95 indicate that our calibration is not in agreement with the preliminary and partial astronomical tuning of GRAPE records from ODP leg 138 for the interval between 6.0 and 10.0 Ma (Shackleton et al., 1995).

The new time scale is consistent with recent $^{40}Ar/^{39}Ar$ ages of volcanic beds and with the number of sedimentary cycles in the younger partly evaporitic part of the Mediterranean Messinian.

Acknowledgements

This study was partly supported by the Netherlands Geosciences Foundation (GOA) with financial aid from the Netherlands Organization of Scientific Research (NWO) and the EU-HCM program. This is MIOMAR project contribution no. 4.

Chapter 4

The Monte del Casino section (Northern Apennines, Italy): a potential Tortonian/Messinian boundary stratotype?

Abstract

Results are presented from a high-resolution integrated stratigraphic study of the Monte del Casino section, which is considered as a candidate boundary stratotype section for the Tortonian/Messinian (T/M) boundary. The section yields a good to excellent cyclostratigraphy, tephrastratigraphy and planktonic foraminiferal and nannofossil biostratigraphy. It can be correlated in detail to other Mediterranean sections using cyclostratigraphic patterns in combination with the planktonic foraminiferal biostratigraphy. These correlations indicate that the succession of the Monte del Casino composite section is continuous in the T/M boundary interval and that all sedimentary cycles, volcanic ash layers and bio-events can be accurately dated by tuning the sedimentary cycles to astronomical target curves.

The quality of the paleomagnetic signal varies considerably throughout the section. A reliable magnetostratigraphy cannot be established for the T/M boundary interval because of a secondary magnetisation carried by iron sulphides. Cyclostratigraphic correlations indicate that discrepancies exist between the position of the reversals recorded here and those found in earlier magnetostratigraphic studies. Comparison of $^{40}Ar/^{39}Ar$ ages of ash layers with their astronomical ages, show that biotite ages give a good approximation of the age of the section, but are not suitable for high-resolution chronology. Despite these short-comings the Monte del Casino section is a suitable candidate to define the T/M boundary, but its qualities should be critically weighted against those of other sections.

This chapter has been submitted for publication as: W. Krijgsman, F.J. Hilgen, A. Negri, J.R. Wijbrans, W.J. Zachariasse, The Monte del Casino section (Northern Apennines, Italy): a potential Tortonian/Messinian stratotype?, *Palaeogeogr. Palaeoclimatol. Palaeoecol.*, 1996.

Introduction

The Tortonian/Messinian (T/M) boundary is at present defined at the first occurrence level of *Globorotalia conomiozea* in the Falconara section on Sicily (Colalongo et al., 1979). Subsequent studies revealed however that this section is unsuitable to define this boundary according to criteria formulated by the International Commission on Stratigraphy (Cowie et al., 1986): the section is completely remagnetised (Langereis and Dekkers, 1992) and seriously deformed tectonically in the critical interval (field observations and unpublished data). Better sections for defining the T/M boundary stratotype are to be found on Crete and Gavdos, in Morocco and in Northern Italy.

The Potamida and Faneromeni sections on Crete and the Metochia section on Gavdos yielded a good to excellent magnetostratigraphy, planktonic foraminiferal biostratigraphy and cyclostratigraphy (Langereis et al., 1984; Krijgsman et al., 1994; 1995). The polarity sequence only recently allowed a straightforward and unambiguous calibration to the Geomagnetic Polarity Time Scale (GPTS) of Cande and Kent (1992). All sections are correlated in detail using sedimentary cycle patterns in combination with the magnetostratigraphy and a high-resolution planktonic foraminiferal biostratigraphy (Krijgsman et al., 1995). Calibration of the cycle patterns to astronomical target curves resulted, among others, in an age of 7.24 Ma for the T/M boundary (Hilgen et al., 1995).

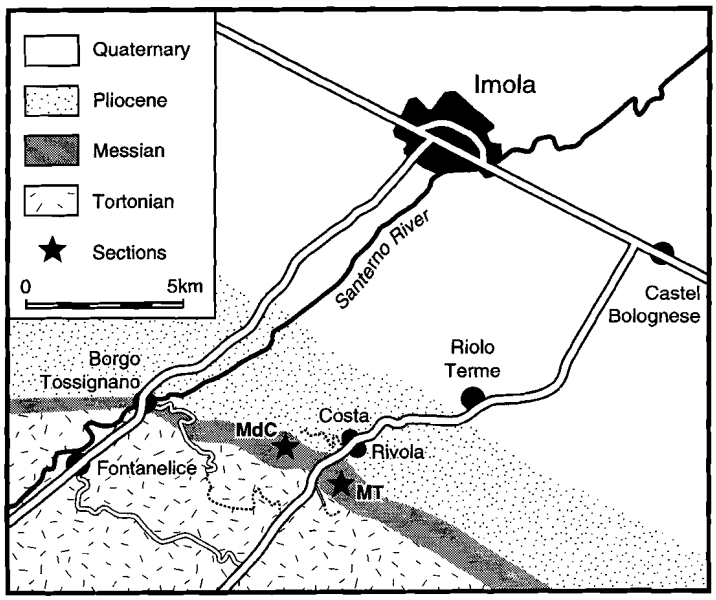

Figure 1. : Location map of the Monte del Casino (MdC) and Monte Tondo (MT) sections in the Vena del Gesso basin of the Northern Apennines (Italy).

The Oued Akrech section in Morocco (Benson et al., 1991, 1995) has the advantage that it is located at the Atlantic side of the Riffean corridor, thus facilitating correlations to the open ocean. The section provided a good paleomagnetic signal and shows a distinct cyclic bedding (Benson et al., 1995; own field observations). It therefore has the potential to be correlated to the astronomical solutions (see also Benson et al., 1995).

Vai et al. (1993) proposed the Monte del Casino section in Northern Italy as a potential alternative type section, even though this section is tectonically deformed and a reliable magnetostratigraphy is lacking (Negri and Vigliotti, in press). A clear advantage of this section is the large number of biotite-rich ash layers. Radiometric dating of these ash layers resulted in an age of 7.07 ± 0.05 Ma for the T/M boundary (Vai and Laurenzi, 1994). There are, however, problems in correlating the sedimentary cycles from Monte del Casino I to Monte del Casino II, and to the Monte Tondo section located 8 km to the SE (Vai et al., 1993). This unsuitability of the sedimentary cycle patterns for high-resolution time-stratigraphic correlations is in contrast to results of integrated stratigraphic studies of coeval marine sections on Crete and Sicily (Krijgsman et al., 1993; 1995). Therefore, we decided to study the Monte del Casino section in detail. The aim of this study is twofold: firstly, to test the cyclostratigraphic, biostratigraphic and magnetostratigraphic potential of this section, and secondly, to compare the radiometric ($^{40}Ar/^{39}Ar$) ages of the volcanic ash layers with astronomically derived ages for the same events. We determined $^{40}Ar/^{39}Ar$ ages of several ash layers ourselves in addition to the ages made already available by Laurenzi et al. (in press). Finally, all results will be used to evaluate critically the Monte del Casino section as a potential T/M boundary stratotype.

Sections

The Monte del Casino and Monte Tondo sections are situated 8 km apart, in the foothills of the Northern Apennines (Fig.1). Both sections consist of open marine grey to blue coloured marly clays with numerous intercalations of biotite-rich ash layers and brown to black coloured, organic-rich, laminated sediments termed sapropels (Calieri, 1992; Vai et al., 1993). The clays are of late Tortonian - early Messinian age, overlie turbidites of the Formazione Marnoso-Arenacea and are overlain by Messinian limestones of the Calcare di Base and gypsum of the Lower Evaporites.

In the present study, we focus on the stratigraphic interval which straddles the T/M boundary. We studied essentially the same interval as Vai et al. (1993) but did not include the deformed top part of the section. The section can be extended downward to reach the turbidites. This extension contains an additional 14 sapropels, but is not included in the present study. For this reason, the first sapropel in the lithological log is numbered C15.

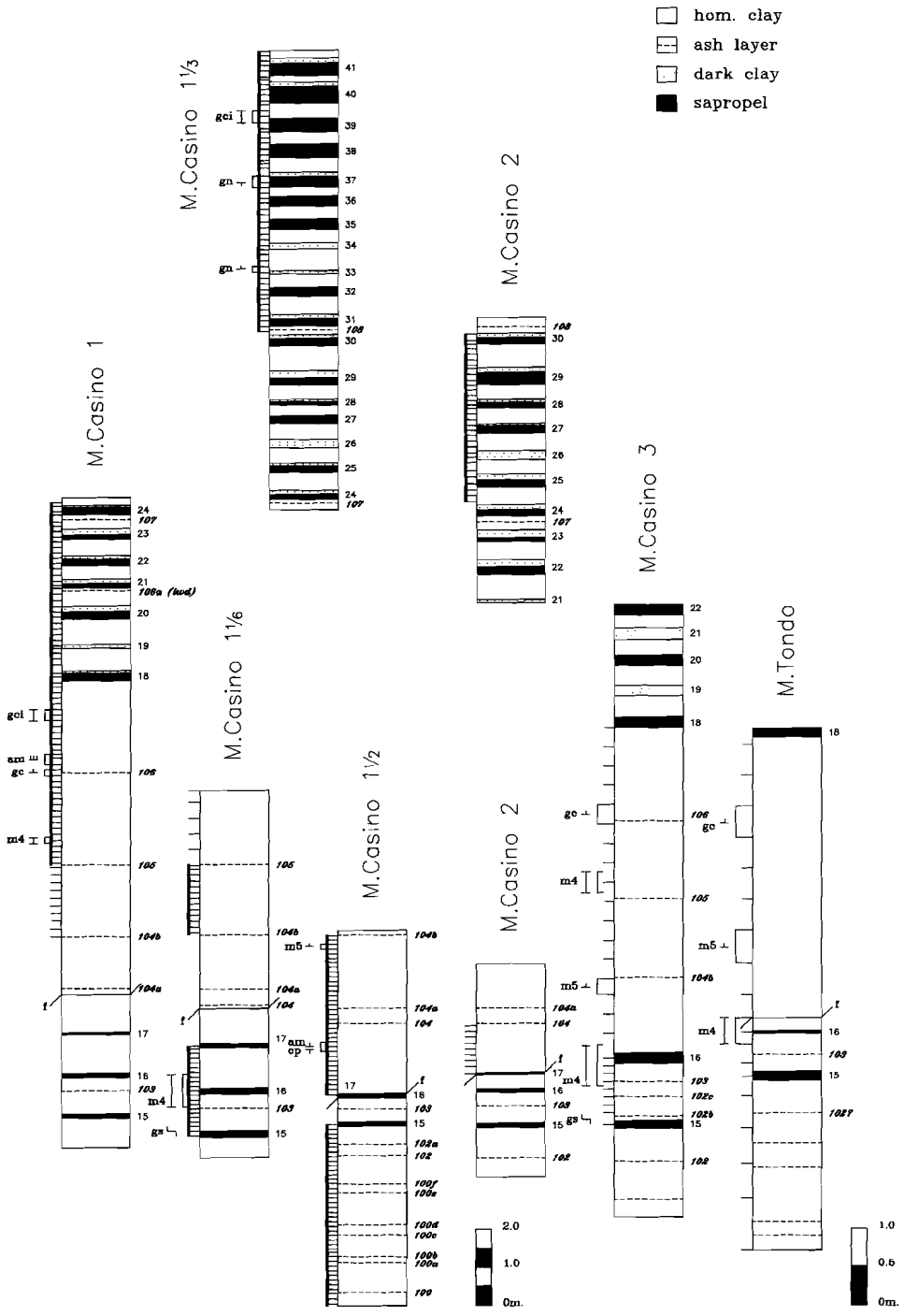
hom. clay
ash layer
dark clay
sapropel
M.Casino 1
M.Casino 1⅓
M.Casino 1⅙
M.Casino 1½
M.Casino 2
M.Casino 2
M.Casino 3
M.Tondo
gci
gn
am
gc
m4
m5
ep
gs
t
2.0
1.0
0m.
1.0
0.5
0m.

Discrete low angle shearplanes between C15 and ash 104a seriously disturb the stratigraphic continuity. The deformation was almost completely avoided in our composite section (see Fig. 2). The middle part of the section, including the T/M boundary interval, is relatively undisturbed. Deformation - in the form of bedding parallel shearplanes - becomes again more intense towards the top of the section (from C40 onwards). In comparison with Monte del Casino, the Monte Tondo section is tectonically more strongly deformed. Like at Monte del Casino, deformation is related to NE-ward directed thrusting in combination with the presence of competent stratigraphic units higher in the succession (i.e. evaporites)

Cyclostratigraphy and tephrastratigraphy

The succession shows a distinct cyclic bedding. Sedimentary cycles typically consist of a grey to blue coloured homogeneous marly clay (lithofacies A1 of Vai et al., 1993) and a brown to black coloured, laminated layer which is enriched in organic matter and termed sapropel (E1). A distinct grey non-laminated layer is found on top of most sapropels (E2). Sapropels are not found throughout the section, but occur in distinct intervals. Three lower sapropels (C15-C17) are followed by a thick homogeneous interval. This homogeneous interval is in turn succeeded by a regular and cyclic alternation of sapropels and clays which continues to the top of the section. In this upper part, some characteristic cycle patterns can be distinguished in addition to the basic cyclic repetition. Cycles with distinct sapropels (C18, C20 and C22) alternate with cycles in which sapropels are weakly developed (C21) or even absent (C19). Sapropels are further absent in cycles C26 and C33-34. The homogeneous bed of cycle C29 is anomalously thick. The homogeneous bed of C41 is very prominent and distinctly white coloured.

The Monte del Casino section contains 19 biotite-rich layers which appear as mm to 1cm thick partings (Fig. 2). In addition to abundant biotite flakes, these layers contain labradoritic plagioclase and quartz (Vai et al., 1993; Laurenzi et al., in press). Disperse biotite flakes are found in a 4 to 6 cm thick sedimentary interval straddling the ash layers. Biotite crystals are well-preserved with an idiomorphic hexagonal outline, suggesting a volcanic origin as fallout deposits (Vai et al., 1993). The numbering of the ash layers is after Laurenzi et al. (in press).

Figure 2. : Monte del Casino (MdC) subsections are found in the different gullies of the badland exposure. MdC 1 is located directly SE of MdC I of Vai et al. (1993) whereas MdC 2 corresponds to (part of) MdC II of Vai et al. (1993). Where possible lateral tracing of marker-beds was used to physically correlate subsections: MdC $1^1/_2$ and $1^1/_6$ (ash 104b), MdC $1^1/_2$ and 2 (ashes 102-103; sapropels C15-16) and MdC 2 and 3 (ash 103). The position of samples and bio-events have been indicated: for numbering see table 2. The MdC composite section is indicated by the samples connected by the thick line. Sapropels and grey beds have been numbered - from 15 to 41 - in stratigraphical order.

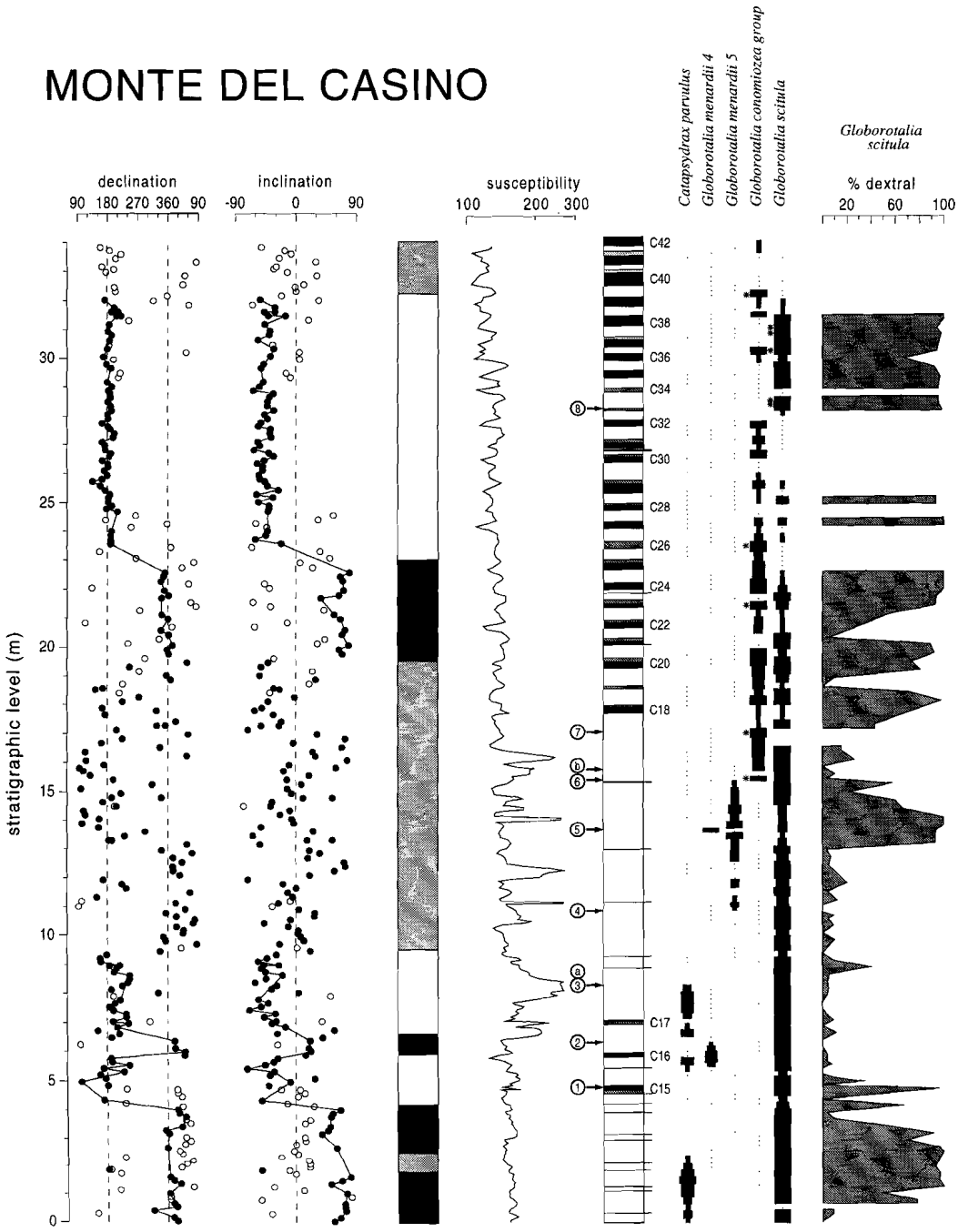
MONTE DEL CASINO
declination
90 180 270 360 90
inclination
-90 0 90
susceptibility
100 200 300
Catapsydrax parvulus
Globorotalia menardii 4
Globorotalia menardii 5
Globoroitalia conomiozea group
Globoroitalia scitula
Globorotalia scitula
% dextral
20 60 100
stratigraphic level (m)
0
5
10
15
20
25
30
C42
C40
C38
C36
C34
C32
C30
C28
C26
C24
C22
C20
C18
C17
C16
C15

Biostratigraphy

Planktonic foraminifera

Planktonic foraminiferal biostratigraphy of the Monte del Casino composite section is based on the semi-quantitative distribution of 5 taxa plus the coiling ratio of non-keeled globorotaliids in 130 samples (Fig. 3). Additional samples were - qualitatively - analysed from overlapping parts of the MdC (sub)sections and from Monte Tondo to check cyclostratigraphic and tephrastratigraphic correlations (Fig. 2).

Keeled globorotaliids provide the most useful biostratigraphic events (Fig. 3). A short but prominent influx of the left-coiled *Globorotalia menardii 4* occurs around sapropel C16. Keeled globorotaliids then become absent again up to the first occurrence (FO) level of the right-coiled *Globorotalia menardii 5* directly below ash 104b. The interval in which *G. menardii 5* is the dominant keeled globorotaliid is punctuated by a very short but distinct influx of *G. menardii 4* slightly above ash 105. At ash layer 106, *G. menardii 5* is definitively replaced by left-coiled assemblages of keeled globorotaliids characterised by a reniform chamber outline in spiral view. These assemblages are termed the *Globorotalia conomiozea* group by Zachariasse (1979) and the *Globorotalia miotumida* group by Sierro (1985) and Sierro et al. (1993). Although the earliest representatives of the *G. conomiozea* group usually show flat tests typical of *G. miotumida*, the first sample directly above 106 already contains an assemblage that is dominated by conical forms usually labelled as *G. conomiozea*, *G. conoidea*, *G. saphoa* or *G. mediterranea*. The next sample dominated by these conical forms is found higher up in the succession, below sapropel C18. A last major influx of the *G. conomiozea* group is found in cycle 39 (Fig. 3).

Coiling changes of the unkeeled globorotaliids, collectively labelled the *G. scitula* group, provide some additional bio-events. A persistent change in coiling direction - from dextral (via mixed dextral/sinistral) to sinistral - coincides with sapropel C15. Dominantly left-coiling assemblages are found to a level

Figure 3.: Polarity zones, susceptibility, lithology, cycle numbers and ranges of planktonic foraminifera of the Monte del Casino section. In the polarity column black (white) denotes normal (reversed) polarity interval and shaded interval denotes zone of undefined (only secondary components) polarity. Closed (open) symbols denote reliable (unreliable) directions. Lithology column shows cyclic alternations of homogeneous marls/marly clays (white) and sapropels (black); shaded interval represents grey layers. Biostratigraphic data of planktonic foraminiferal marker species are based on surveying a standard number of fields (27 out of 45) on a rectangular picking tray and semi-quantitatively presented in terms of absence, trace (<3 specimens per 9 fields of picking tray), rare (3-10), common (10-30) and frequent (>30) indicated by increasing bar thickness. Bioevents are indicated (encircled): see table 2.Arrows indicate positions of bioevents.

approximately 1 m above ash 105 (Fig. 3). This level corresponds to the middle part of the range of *G. menardii 5*. The coiling direction then switches back to an alternating mode. Dominantly right-coiling representatives of the *G. scitula* group are intermittently found in low numbers from sapropel C23 upwards but become abundant again from the grey bed of cycle 33 to sapropel C38. Bottom and top of this interval correspond with the FO and LO (last occurrence) of *G. nicolae*, a dextrally-coiled and biconvex form with inflated chambers of the *G. scitula* group. The FO of *G. nicolae* thus follows a relatively long interval in which unkeeled globorolaliids are rare or absent (Fig. 3).

Another useful bioevent is the LO of *Catapsydrax parvulus*. This event is found above sapropel C17. Neogloboquadrinids show dominant left coiling throughout the section. A change in coiling direction (i.e from sinistral to dextral) has been reported by Vai et al. (1993) from a level well above the top of our section.

Calcareous nannofossils

Preparation of the calcareous nannofossil samples followed standard techniques: no centrifugation was done to retain the original composition in the assemblage and a smear slide was mounted with Norland optical adhesive. Analyses were done according to the semi-quantitative methodology of Rio et al. (1990), to define the first occurrence of the *Amaurolithus* group. Nannofossil counts are based on surveying a standard number of fields (1000) using a light microscope with 1250x magnification. All samples show an abundant and moderately to well-preserved nannoflora. In general, the best preserved nannoflora occur in sapropel layers together with abundant pyrite. The assemblage mainly consists of *Reticulofenestra* spp. with many levels showing abundant "small" (less than 3 μm) *Reticulofenestra, Coccolithus pelagicus, Reticulofenestra pseudoumbilicus* (specimens of 7-10 μm), *Sphenolithus moriformis* and *Sphenolithus abies*. Further, *Syracosphaera pulchra, Syracosphaera* spp., *Triquetrorhabdulus rugosus, Rhabdosphaera* spp. and *Scyphosphaera* spp. are commonly recorded. *Reticulofenestra rotaria* is rare in the higher part of the section.

The genus *Discoaster* is generally abundant, but preservation varies from very poor to good; again, the best preserved specimens occur in sapropel layers. Most of the specimens belong to *D. variabilis* and *D. pentaradiatus. Discoaster brouweri* and *D. intercalaris* are commonly recorded, while *D. challengeri* and *D. icarus* are rare. In the lower part of the section few specimens of *D. loeblichii* have been observed. The occurrence of *D. tamalis* and *D. asymmetricus* is remarkable. Both species are recorded in the early Pliocene: the FO of *D. asymmetricus* marks the base of the NN 14 zone of Martini (1971), and the FO of *D. tamalis* is recorded by Perch Nielsen (1985) in the NN 15 zone.

The genus *Helicosphaera* is well-represented by *H. carteri* and *H. intermedia. H. orientalis, H. stalis* and *H. walbersdorfensis* (the "small" Helicosphaera group

according to Negri and Vigliotti, in press) are almost continuously recorded in the lower part of the section, but become more scattered towards the top.

The occurrence of the genus *Amaurolithus* is rare and discontinuous, especially in the early part of its range. Hence, for biostratigraphic events we refer to the *Amaurolithus* spp. group. The FO of *Amaurolithus* spp. is recorded between 8.13 and 8.37 m, i.e well below ash 104. Rare *A. primus* and *A. amplificus* are recorded discontinuously in the interval between 8.37 and 15.56 m. Between 15.81 and 23.07 m, *Amaurolithus* spp. is more abundant and continuous, and consists mainly of *A. delicatus*. Representatives of this group become scattered again from 24.55 m to nearly absent toward the top of the section. This pattern has also been recorded in the Monte Tondo section (Negri and Vigliotti, in press) and probably allows to discriminate two events in the *Amaurolithus* group: the FO and an "acme" interval, probably caused by favourable environmental conditions in the basin.

Magnetostratigraphy

Methods

To establish the magnetostratigraphy for the Monte del Casino section, at least one specimen per sampling level was thermally demagnetised. Thermal demagnetisation was applied with small temperature increments of 20-30 °C up to a maximum temperature of 420 °C, in a magnetically shielded, laboratory-built, furnace. The natural remanent magnetisation (NRM) was measured on a 2G Enterprises DC SQUID cryogenic magnetometer. Furthermore, several rock magnetic experiments were performed to identify the carriers of the magnetisation. The initial susceptibility and the anisotropy were measured on a Kappabridge KLY-2. An isothermal remanent magnetisation (IRM) was acquired on a PM4 pulse magnetiser up to a maximum field of 2000 mT. The IRM was subsequently thermally demagnetised, and after each temperature step the bulk susceptibility was measured. Finally, thermomagnetic runs were recorded with a modified horizontal translation Curie balance making use of a cycling field (Mullender et al., 1993).

Thermal demagnetisation

Throughout the whole section, thermal demagnetisation diagrams are of mixed quality. The relatively large dip (40°) of the section was useful to distinquish between primary and secondary components. The lowermost part of the section (0-4 m) predominantly shows normal polarities after bedding plane correction (Fig. 3, 4a). NRM-intensities generally range from 0.01-1 mA/m. The remanence is usually largely removed at temperatures below 400 °C. Further

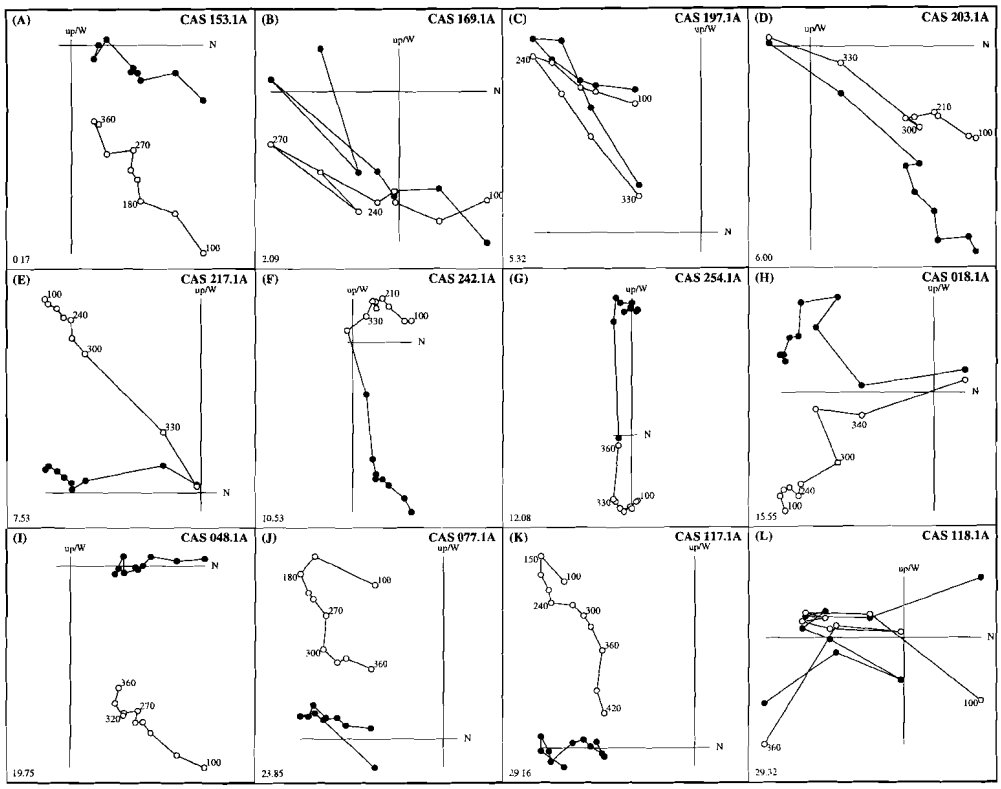

Figure 4 : Thermal demagnetisation diagrams for samples of the Monte del Casino section. Closed (open) symbols represent the projection of the vector end-points on the horizontal (vertical) plane; values represent temperatures in °C; stratigraphic levels are in lower left-hand corner.

demagnetisation at higher temperatures results in a mainly randomly directed viscous component. For several levels in this interval, however, directions and polarities cannot be determined (Fig. 3,4b). The following interval (4-9.5 m) shows mainly reversed polarities except for several samples between 6 and 7 metres which give only normal directions (Fig. 3). Demagnetisation diagrams show that a normal polarity component is removed at temperatures below 200 °C and a reversed component between 200-400 °C (Fig. 4c). This normal component has a present-day field direction before bedding plane correction and can thus be regarded as a secondary overprint, probably caused by subrecent weathering. In some cases, this overprint is even absent indicating that we sampled in fresh (unaltered) sediments (Fig. 4e). The presence of both N and R directions for the magnetic component in the 200-400 °C range confirms the suggestion of a primary origin of the magnetisation.

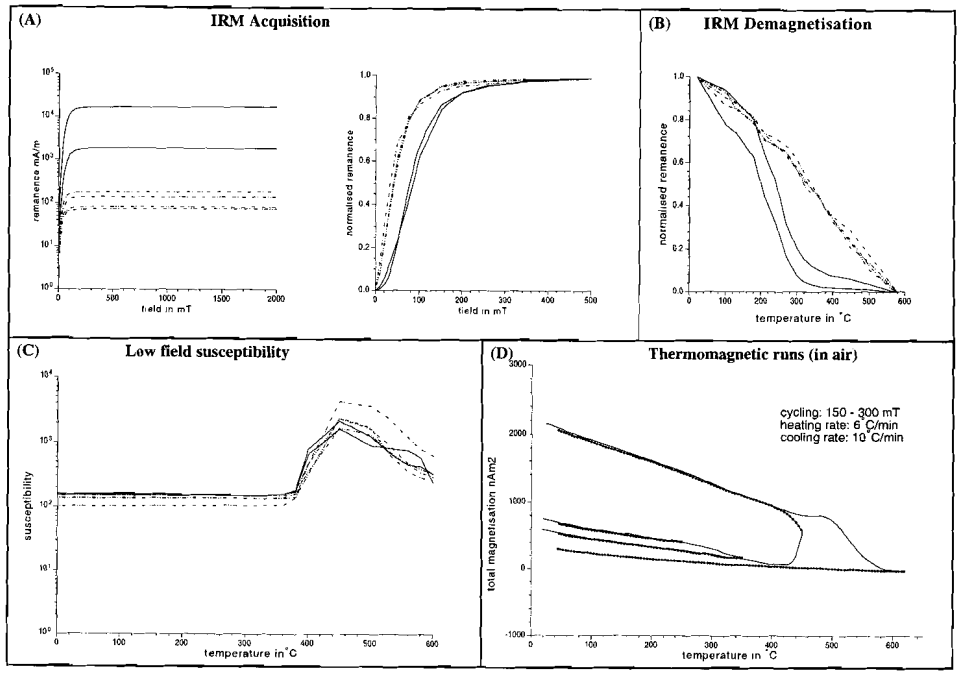

Figure 5 : (A) Examples of IRM acquisition of samples of the Monte del Casino section. The initial steep rise points to magnetite, the gradual increase at lowest fields suggest the presence of iron sulfides like pyrrhotite or greighite. (B) Stepwise thermal demagnetisation of the normalised IRM also show the presence of both iron sulfides and magnetite. (C) Low-field susceptibility during thermal demagnetisation; the increase in susceptibility between 400-500 °C is probably related to the oxidation of pyrite to magnetite. (D) Example of a thermomagnetic run in air showing a faint Curie point at a temperature of 320 °C, suggesting the presence of pyrrhotite.

The middle part of the section revealed different types of demagnetisation behaviour. NRM intensities are much higher and range from 0.1-10 mA/m. Thermal demagnetisation between 100 and 300 °C gradually removes the magnetisation. At temperatures higher than 300 °C the remanence is almost totally removed and only a small viscous component is left (Fig. 3; 4f-h). This indicates the presence of a magnetic carrier with a Curie point slightly above 300 °C, probably an iron sulphide like greigite or pyrrhotite. Most directions are neither normal nor reversed indicating a secondary (diagenetic) origin for this component.

The upper (cyclic) part of the section shows demagnetisation diagrams of good quality (Fig. 3; 4i-k). NRM intensities range from 0.01-1 mA/m. A secondary present-day field component is generally removed below 240 °C. Demagnetisation at higher temperatures reveals consistently normal and reversed directions and again suggests a near primary origin of the

magnetisation. Demagnetisation diagrams are of good quality in the homogeneous marls and the polarities can reliably be determined. The NRM is very low in the sapropeletic beds and the uppermost part of the section. Reliable directions cannot be determined and demagnetisation diagrams only show scatter after removing the 240 °C component (Fig. 4l). Remarkably, in some cases, the diagrams give a much better defined reversed component without bedding plane correction.

Rock magnetic results

The IRM acquisition curves indicate the presence of two different components (Fig. 5a). A general steep rise between 0 and 100 mT and saturation at 200 mT indicates the presence of a low-coercivity mineral like magnetite or maghemite. These curves are characteristic for samples of the upper and lowermost part of the section. Samples from the middle part show a less prominent rise at the lowest fields (0-50 mT) and saturation at approximately 500 mT, suggesting the presence of iron sulphides. The IRM demagnetisation curves confirm the presence of these components. An unblocking temperature of 580 °C for the low-coercivity dominated samples is characteristic for magnetite (Fig. 5b). The higher-coercivity dominated samples show a strong decrease at temperatures between 240 and 320 °C which is indicative for iron sulphides which have Curie temperatures of 320-325 °C for pyrrhotite (Dekkers, 1989) and 333 °C for greigite (Spender et al., 1972; see also Roberts, 1995).

During thermal demagnetisation of the IRM we also measured the bulk susceptibility after each temperature increment (Fig. 5c). No significant changes in the susceptibility are observed below 380 °C. Heating to higher temperatures results in a large increase of susceptibility which continues up to temperatures of 450 °C. This behaviour was observed earlier in sediments from suboxic to anoxic environments and is likely the result of oxidation of pyrite (Van Velzen, 1993). The subsequent decrease in susceptibility between 450 and 600 °C can be ascribed to oxidation of magnetite to hematite. The thermomagnetic runs partly confirm these observations, but show an increase in magnetisation at temperatures of 420 °C, thus slightly higher than in the susceptibility records (Fig. 5d). The 350 °C run shows a (weakly developed) Curie point at approximately 320 °C suggesting that the iron sulphide is pyrrhotite, because greigite would begin to break down above 282 °C (Skinner et al., 1964; Roberts, 1995) and has, in addition, a slightly higher Curie temperature of 333 °C (Spender et al., 1972).

Susceptibility and anisotropy

The initial susceptibility (χ_{in}) of the sediment is strongly dependent on the concentration of paramagnetic clayminerals. The results from the Monte del Casino section show that a clear relation with the cyclicity exists in the upper part

of the section (Fig. 3). The lowest values of χ_{in} are dominantly observed at the bottom of the sapropels, the highest values at the bottom of the homogeneous marls; at the top of the grey intervals.

The anisotropy of the magnetic susceptibility (AMS) can be used to provide information on the tectonic deformation of the sediment (Kissel et al., 1986; Scheepers, 1994). There is often a clear relation between the AMS and the regional stress field in the area; a magnetic lineation may develop perpendicular to the regional stress field. The anisotropy at Monte del Casino (determined for 30% of the samples) is generally 1-2%. After bedding plane correction, the minimum axes are all vertical, the intermediate and maximum axes are randomly oriented in the horizontal plane. Furthermore, it shows that the fabric causing the anisotropy is entirely foliated (oblate). Some degree of lineation is observed in the tectonically disturbed interval between sapropels C15 and C17. The tectonic deformation at Monte del Casino obviously had no major influence on the magnetic fabric. The strong oblateness of the fabric, and the absence of lineation, indicates that deposition had taken place on a horizontal plane in a very quiet sedimentation environment.

Ar/Ar dating

Methods

Argon geochronology was carried out using laser fusion and incremental heating techniques. A detailed description of techniques was published earlier (Wijbrans et al., 1995); here we describe the sample preparation and experimental conditions pertinent to this study. The ash layers contain well-preserved euhedral biotite crystals and a slightly milky feldspar fraction. From the biotites, we separated the largest crystal fraction (250 - 500 μm). In cases where the yield in this size fraction was insufficient, a smaller crystal fraction (125-250 μm) was added. The feldspar fraction was prepared using standard heavy liquid and magnet separating techniques. For the Monte del Casino ashes, the feldspar fractions consisted mainly of plagioclase. For both the plagioclase and the biotite, approximately 20 mg aliquots were packaged in Al-foil, and loaded in a 5 mm ID quartz tube with the flux monitors (USGS standard 85G003 TCR sanidine, K/Ar age 27.92 Ma) packaged in Cu-foil. Individual packages were approximately 1 mm thick, and standards were loaded between each set of 5 unknowns. Irradiation with fast neutrons was carried out in the CLICIT facility in the Oregon State University TRIGA reactor (Dodd and Anderson, 1994). After irradiation, the samples were loaded in a Cu-tray (60 mm diameter) with 2 mm diameter holes for each individual experiment. For both the standards and the unknowns, we applied a single fusion technique where for each sample 5 replicates (>1.0 mg

Sample	mineral	40Ar/39Ar	isochron	n	MSWD
MCA 9	Biotite	7.30 ± 0.05	7.27 ± 0.06	3	1.64
	Plagioclase	7.89 ± 0.07	8.17 ± 0.08	4	1.70
MCA 3	Biotite	7.70 ± 0.03	7.27 ± 0.08	5	20.9
	Plagioclase	7.48 ± 0.05	7.41 ± 0.04	4	2.79
MCA 2a	Biotite	7.49 ± 0.01	7.51 ± 0.03	5	1.28
	B-plateau	7.56 ± 0.07	7.51 ± 0.02	9	0.07
	Plagioclase	9.55 ± 0.07	7.17 ± 0.09	4	23.3
MCA 1	Biotite	7.53 ± 0.01	7.30 ± 0.10	4	1.06
	B-plateau	7.48 ± 0.02	7.58 ± 0.05	13	0.02
	Plagioclase	8.34 ± 0.12	7.46 ± 0.18	3	3.12
MCA 0	Biotite	7.47 ± 0.02	7.32 ± 0.15	4	2.07

Table 1: Argon ages of ash layers. The age monitor used for these experiments was the USGS standard 85G003 TCR sanidine, with an age of 27.92 Ma.

each) were analysed. The biotites and plagioclase samples were preheated to approximately 500 °C in order to remove some of the atmospheric argon that interferes with accurate analysis of the radiogenic argon component in young samples. In addition, biotites MCA1 and MCA2a were analysed using an incremental heating technique, using a defocussed laser beam and stepping up of the power of the laser beam for each subsequent degassing step until fusion of the biotite sample occurred.

The argon gas was measured isotopically using a double focussing noblegas mass spectrometer (MAP215-50) in static mode. Beam intensities were measured on a secundary elecron multiplier detector (gain 60,000) and switchable preamplifier resistor settings (109, 108 and 107 Ohm) by peak jumping at half mass intervals down from mass 40 to 35.5. System blanks were measured at least between every set of 5 unknowns. In general, the blank correction was the average of the blanks run before and after the unknown. System blanks in a laser fusion sytem tend to be predictable and usually show a slight increase during the day. For the main isotopes ^{40}Ar and ^{39}Ar, sample to blank ratios were always less than 100. The blanks for this project were typically in the range m/e:40 6.0-2.0*10^{-16} moles, m/e:39 3.0-1.5*10^{-17} moles, m/e:38 2.0-1.0*10^{-17} moles, m/e:37 2.5-2.0*10^{-16} moles, m/e:36 4.0-3.0*10^{-17} moles. System mass discrimination was measured

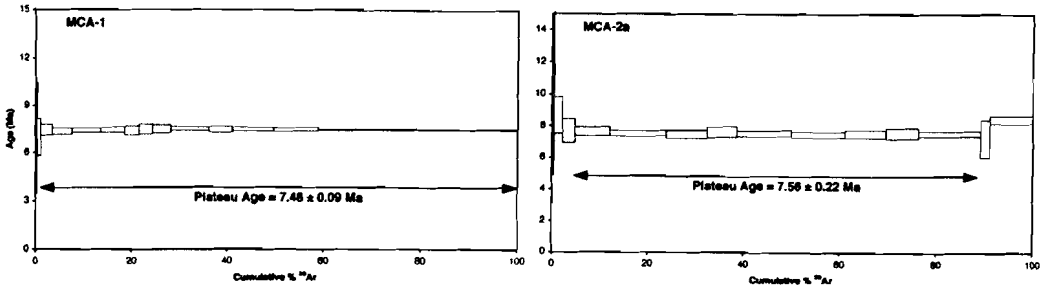

Figure 6: $^{40}Ar/^{39}Ar$ age spectra for biotite samples of ash layers 102 (MCA-1) and 103 (MCA-2a).

by letting clean air argon (approximately $5.0*10^{-14}$ moles ^{40}Ar) into the mass spectrometer from a 10 l reservoir using a 1 ml gas pipette.

Results

The results of argon dating are summarised in table 1, the age spectra for MCA1a, and 2 are given in figure 6. Apparently, weighted mean ages of single fusion datings do not match the stratigraphic order, while in addition discrepancies exist between biotite and plagioclase ages for the same level. Biotite ages are all in the same range, whereas in some cases plagioclase ages are considerably older. These plagioclase ages appear to be affected by varying amounts of excess argon.

It is commonly assumed that before eruption silicic magmas contain fluids that include some argon, but in many cases most of this fluid is liberated during extrusion, effectively resetting the argon geochronometer. Our data shows that degassing of the plagioclase during eruption of the magma was not complete. As plagioclase contains less K than biotite, the effect of incorporation of excess argon in plagioclase is more dramatic, but we must assume that the biotite ages are affected to some degree as well.

In argon geochronology there are two techniques that may help to assess the effects of excess argon in the system. When the isotopic data are regressed in an isotope correlation diagram, no assumptions are made concerning the isotopic composition of the non-radiogenic component on the argon gas. It can be seen (table 1), that for the plagioclase samples the regression ages are consistently younger than the mean age of the single fusion experiments, confirming the presence of excess argon. The relatively large uncertainty of the regression ages prevents us from using these age for high-resolution chronology. The biotite regression ages also tend to be slightly younger than the mean of the single fusion ages, which is consistent with the presence of some excess argon in the biotites, although the effect is so small that the results of both calculations overlap at the 2 sd level.

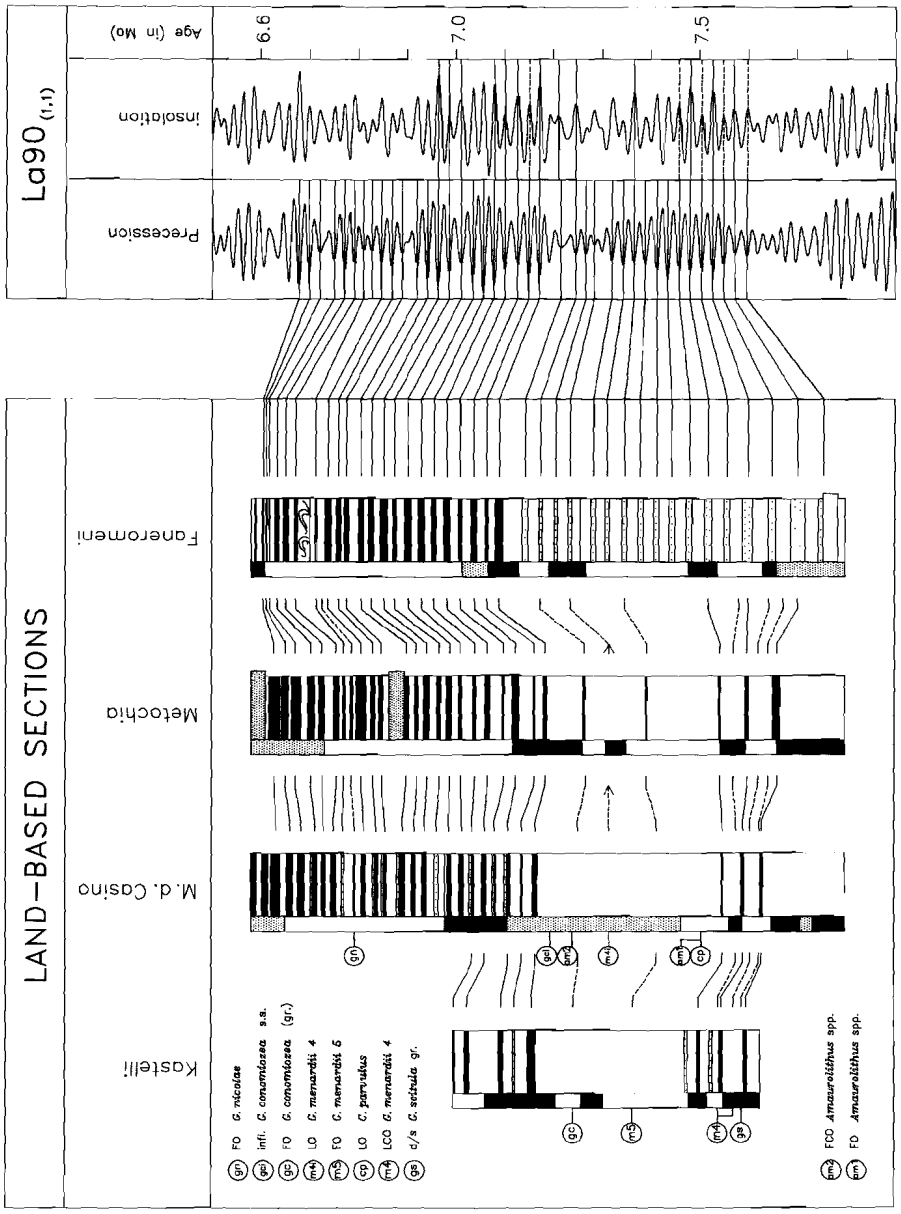

Figure 7 : Cyclostratigraphic and (planktonic foraminiferal) correlations of the MdC section to previously studied sections on Crete and Gavdos. Also shown are the correlations of the sedimentary cycles (sapropels, grey beds) to astronomical target curves (precession and 65° Nlat summer insolation) derived from solution La90 (Laskar et al., 1993; see Hilgen et al., 1995 and Lourens et al., in press for more details).

The second method to test for disturbance of the argon in minerals is by carrying out incremental heating experiments (Fig. 6). Pristine undisturbed systems will give identical ages for each temperature step within error, allowing the calculation of a plateau age over most of the gas released during the experiment. In favorable cases, excess argon can be recognised from anomalously high ages in the first steps, and ages decreasing to a plateau in the higher temperature steps. The effects of weathering of the biotite may also cause disturbance of the gas release, preventing the calculation of a plateau age. The age spectrum of MCA1 shows the effect of some minor excess argon in the initial steps and an excellent plateau of over the remaining 98% of the gas release. The effect appears to be very minor and confined to the first few steps of the experiment. The age spectrum of MCA2a is more disturbed both at the low temperature end and at the high temperature end of the experiment. Nevertheless, the experiment allows the calculation of a plateau age that meets commonly accepted criteria.

However, multiple single fusion ages, plateau ages and isochron ages of the biotites are inconsistent and neither match the stratigraphic order. Furthermore, we note that there is a potential problem with excess argon as documented from the plagioclase analyses.

Discussion and conclusions

Integrated stratigraphic framework

The results of the planktonic foraminiferal biostratigraphic analysis confirm the cyclostratigraphic and tephrastratigraphic correlations between the Monte del Casino subsections and between the Monte del Casino composite section and Monte Tondo (Fig. 2). The Monte del Casino sapropel pattern and planktonic foraminiferal events can straightforwardly be correlated to previously studied sections on Crete and Gavdos (Fig. 7). The correlations show that the same succession of (first-order) bio-events can be recognised as elsewhere in the Mediterranean (see also Sierro et al., 1993). The consistency of the cyclostratigraphic and biostratigraphic correlations indicate that - in agreement with the field evidence - the succession in the Monte del Casino composite section is (nearly) continuous. All sapropels, bio-events and ash layers can thus be astronomically dated since the sedimentary cycles in the other sections were already calibrated to astronomical target curves (Hilgen et al., 1995; see also Fig. 7). This calibration reveals that - like in the other sections - grey beds and less prominent sapropels correlate with insolation maxima that are reduced in amplitude due to interference of precession and obliquity. The aberrantly thick

no.	species	event	level in m	age range	age 1	age 2
	planktonic forams					
8	*G. nicolae*	FO	28.11-28.35	6.822-6.832	6.827	6.829
7	*G. conomiozea*	influx	17.01	---	7.192	---
6	*G. conomiozea gr.*	FO	15.28-15.46	7.236-7.241	7.239	7.240
5	*G. menardii 4*	influx	13.63	---	7.289	*7.280*
4	*G. menardii 5*	FO	10.77-10.89	7.367-7.371	7.369	7.355
3	*C. parvulus*	LO	8.13-8.37	7.440-7.446	7.443	7.456
2	*G. menardii 4*	LCO	6.24-6.36	7.504-7.509	7.507	7.512
1	*G. scitula gr.*	d/s coiling	4.73-4.85	7.564-7.568	7.566	*7.553*
	calcareous nanno's					
b	*Amaurolithus spp.*	FCO	15.61-15.86	7.225-7.232	7.228	---
a	*Amaurolithus spp.*	FO	8.13-8.37	7.440-7.446	7.443	---

Table 2: Stratigraphic position and astronomically derived ages for calcareous plankton events in the Monte del Casino section (age 1) and comparison with astronomical ages for the same events according to Hilgen et al. (1995; age 2). Ages 2 in italics are based on additional biostratigraphic analysis of samples from the Faneromeni section on Crete.

cycle 28 represents a double cycle, i.e. a cycle which contains an extra cycle that lacks lithological expression.

Our correlations also demonstrate that second-order events such as changes in coiling direction and short-term influxes can be very helpful to enhance the temporal resolution of biostratigraphic correlations on at least a regional (Mediterranean) scale. For instance, the last short influx of *G. menardii 4* within the range of *G. menardii 5* has been detected also in the Potamida and Faneromeni sections on Crete, and is astronomically dated at 7.28 Ma (table 2). The (second) influx of the *G. conomiozea* group, dominated by conical types, below C18 has been reported from below the same correlative sapropel in the Potamida section (Zachariasse, 1979). The astronomical age of this influx is 7.19 Ma. Apparently, this very short influx - as well as the first influx - has been missed in other sections because of a too low sample resolution. It shows that the replacement of *G. menardii 5* by the *G. conomiozea* group is a more suitable biostratigraphic criterion to define the T/M than the first occurrence of dominant *G. conomiozea* types (Krijgsman et al., 1995). Moreover, our results from Monte del Casino show that both boundary criteria actually result in the same position for the T/M boundary because keeled globorotaliids in the first sample containing the *G. conomiozea* group are already dominated by conical shells. Thusfar, this coincidence has not been reported from other T/M boundary sections. Finally,

the persistent change in coiling direction of the *G. scitula* group - from alternatingly sinistral/dextral to sinistral - might prove to be a useful bio-event in the Mediterranean.

Most of the planktonic foraminiferal events are useful for (time-)stratigraphic correlations on a regional scale, but are less suitable for correlations on a wider preferably global scale although certain events can easily be recognised in the adjacent Atlantic (Sierro et al., 1993; Hodell et al., 1994). An event with a potential for global correlations is the FO of *Amaurolithus* spp. In the present study, this event is found below ash 104. Comparison with magnetostratigraphically well-constrained sections (Fig. 7) shows that event is slightly younger than the younger end of C3Br.2n. In a previous study of the Monte del Casino section, Negri and Vigliotti (in press) reported the first rare *Amaurolithus* from a lower level, approximately 1 m. below ash 102. This would correspond to a position within C4n.1n, which is slightly older than the oldest occurrence of this genus reported from the equatorial Pacific (Raffi et al., 1995; Shackleton et al., 1995). Moreover, the rare and discontinuous occurrence of *Amaurolithus* in the early part of its range makes the FO (of *Amaurolithus*) unsuitable for long-distance time-stratigraphic correlations.

The magnetostratigraphy, on the other hand, is only partly consistent with the cyclostratigraphic and biostratigraphic correlations. Positions of the polarity reversals recorded in the lower part of the section (C4n.1n(y), C3Br.2n(o) and C3Br.2n(y)) are in good agreement with the results from the Metochia section on Gavdos, but show a consistent offset of 1/2 to 1 sedimentary cycle compared to the position in the Faneromeni and Kastelli sections on Crete (Fig. 7). This offset was earlier explained by diagenetic processes causing a delay in NRM acquisition (Van Hoof et al., 1993). The position of the reversal recorded in the upper part of the section (C3Bn(y)) is well-defined in cycle C25; i.e. 4 to 5 cycles younger than its position observed on Gavdos and Crete. Delayed acquisition processes can certainly not explain the younger age found at Monte del Casino because sedimentary remanence acquisition mechanisms can make the reversal appear older, but not younger. Remarkably, the difference between astronomical ages of polarity reversals and the ages according to CK95 is exceptionally large - 166 kyr - for C3Bn(y) (Hilgen et al., 1995). A position at cycle C25 in Monte del Casino will significantly reduce this discrepancy to approximately 70 kyr.

Comparison of Ar/Ar ages and astronomical ages

The astronomical ages of sapropels and ash layers are obtained independently from radiometric dating methods and can be compared with our $^{40}Ar/^{39}Ar$ ages from Monte del Casino. Our data were calculated against USGS standard TCR with an age of 27.92 Ma, intercalibrated to an age of 28.09 ± 0.10 Ma for the FCT#3 biotite (Wijbrans et al., 1995). Previous argon datings on the Monte del Casino ashes have been reported by Vai et al., (1993) and Laurenzi et al. (in press) who

Sample code	ash layer	astronomical age 1	astronomical age 2	mineral	This study 40Ar/39Ar	This study isochron	Laurenzi et al., (in press) plateau	Laurenzi et al., (in press) isochron
	108	**6.874**						
MCA 9	**107**	**7.040**		Biotite	7.26 ± 0.05	7.23 ± 0.06	7.12 ± 0.03	7.11 ± 0.04
				Plagioclase	7.85 ± 0.07	8.13 ± 0.08		
	106a	**7.101**						
	106	**7.239**	**7.241**				7.39 ± 0.04	7.33 ± 0.19
MCA 3	**105**	**7.308**	**7.299**	Biotite	7.66 ± 0.03	7.23 ± 0.08	7.51 ± 0.04	7.47 ± 0.06
				Plagioclase	7.44 ± 0.05	7.37 ± 0.04		
	104b	**7.360**	**7.347**					
	104a	**7.414**	**7.406**					
	104	**7.426**	**7.419**					
MCA 2a	**103**	**7.539**		Biotite	7.45 ± 0.01	7.47 ± 0.03		
				B-plateau	7.52 ± 0.07	7.47 ± 0.02		
				Plagioclase	9.50 ± 0.07	7.13 ± 0.09		7.04
	102c	**7.548**						
	102b	**7.562**						
A	**102a**	**7.581**	**7.575**					
MCA 1	**102**	**7.589**	**7.579**	Biotite	7.49 ± 0.01	7.26 ± 0.10		
				B-plateau	7.44 ± 0.02	7.54 ± 0.05	7.39 ± 0.04	7.38 ± 0.04
				Plagioclase	8.30 ± 0.12	7.42 ± 0.18		
b	**100f**	**7.608**	**7.589**					
MCA 0	**100e**	**7.615**	**7.593**	Biotite	7.43 ± 0.02	7.28 ± 0.15		
D	**100d**	**7.636**	**7.604**					
E	**100c**	**7.643**	**7.608**					
F	**100b**	**7.658**	**7.616**					
G	**100a**	**7.661**	**7.618**					
H	**100**	**7.681**	**7.628**					

Table 3: Astronomically derived ages of ash layers and comparison with $^{40}Ar/^{39}Ar$ ages. To ensure a meaningful comparison, all radiometric ages are recalculated to an age of 27.95 Ma for the FCT biotite (see Renne et al., 1994). The first astronomical age (age 1) was obtained by linear interpolation of the sedimentation rate between astronomically dated calibration points, i.e. the sapropel mid-points (see Hilgen et al., 1995 for exact ages). Ages of ash layers older than sapropel 15 were calculated in this way (the preliminary log and biostratigraphy show that sapropel 13 is found 14.35 m. below sapropel 15 and that this sapropel corresponds to sapropel K7/M68/G79 in Hilgen et al., 1995) and by linear downward extrapolation of the sedimentation rate taking the stratigraphic distance from sapropel 15 to 16 in the MdC 3 subsection as starting point (age 2). The age of the ash layers is expected to fall within the calculated age range because of a downward increase in sedimentation rate. The second age (age 2) of ash layers intercalated between sapropel 17 and 18 was calculated by including additional age calibration points based on (the position of) certain bio-events (FO *G. menardii 5*, last influx *G. menardii 4* and FO *G. conomiozea*) which have been dated astronomically in the continuously cyclically bedded Faneromeni section. These ages are considered more reliable because this approach corrects (in a thick homogeneous interval) for intra-formational changes in sedimentation rate, disturbances in stratigraphic thicknesses as a consequence of tectonic deformation and inaccuracies in logging exact stratigraphic distances.

used the FCT#3 biotite, with an age of 27.55 ± 0.08 Ma (Lanphere et al., 1990), as their principal standard. Consequently, there would be an offset between the two data sets caused by these discrepant ages of the FCT biotite. Renne et al. (1994) demonstrated, by comparing astronomical and $^{40}Ar/^{39}Ar$ ages of seven polarity reversals during the last 3.5 Myr, that the best estimate for the age of the FCT sanidine is 27.95 Ma. We recalculated all argon ages from Monte del Casino to an age of 27.95 for FCT biotite to ensure a meaningful comparison with the astronomical ages (table 3). The weighted mean ages of the plagioclase are without exception too old, which is caused by excess argon since isochron ages are younger. Discrepancies with the single fusion ages of biotite are smaller and range from -180 kyr to +350 kyr. Comparison of the astronomical ages with the (younger) biotite isochron ages does not result in a reduction of the discrepancies (-330 kyr to +190 kyr).

The plateau age of MCA2a is in good agreement with the astronomical age, whereas the plateau age of MCA1, which shows a much better age spectrum, is not. Our plateau age of MCA1 can also be compared with the plateau age of ash 102 of Laurenzi et al. (in press), which shows that these ages obtained by two different labs are only slightly different (table 3).

Chemical analyses by Laurenzi et al. (in press) on the Monte del Casino biotite crystals show that chemical alteration of the biotite can be excluded because the potassium content is high in all samples. Furthermore, homogeneous compositions of the biotite in most ashes indicate that contamination by detrital components can be neglected.

In conclusion, the comparison with the astronomical ages shows that the $^{40}Ar/^{39}Ar$ datings on the Monte del Casino biotites are not suitable for accurately dating the sedimentary succession - and hence the T/M boundary - even if statistically acceptable ages are obtained. Moreover, these datings do not match the stratigraphic order and their reproducibility is poor since weighted mean ages of total fusion, isochron ages and plateau ages are inconsistent. Nevertheless, they gave a good approximation of the age of the section with an average and maximum deviation of 0.16 and 0.36 Myr, respectively.

The Monte del Casino section: a potential T/M boundary stratotype?

Vai et al. (1993) have argued that de Monte del Casino section is a suitable GSSP for the T/M boundary. The excellent correlation between this section and time-equivalent sections on Crete and Gavdos indicates that the Monte del Casino section is continuous, without tectonic complications or stratigraphic hiatuses in the boundary interval. These correlations provide a set of astronomical ages for all sedimentary cycles, ash layers and bio-events in the Monte del Casino section (table 2, 3).

This indicates that the Monte del Casino section is indeed a suitable GSSP for the T/M boundary. The large number of ash layers could be an extra recommendation, but they are not suitable for an accurate and precise dating of

the boundary. A more serious short-coming is the poor paleomagnetic signal in the critical interval. However, the boundary is magnetostratigraphically well-constraint in sections on Crete and occurs within chron C3Br.1r (Krijgsman et al., 1995). A final concern is the permanence of exposure. The (natural) outcrop has changed considerably during the last years (R. Calieri, pers.comm.) and there is at present no guarantee that the section is long lasting.

In conclusion, the Monte del Casino section is a suitable GSSP for the T/M boundary, but its qualities as a boundary stratotype should be critically weighted against those of other candidate sections. This evaluation, however, is beyond the scope of the present paper.

Acknowledgements

We thank Gian Vai and Roberta Calieri for discussing the Monte del Casino section in the field. Gerrit van 't Veld and Geert Ittman processed the micropaleontological samples. Henk Meijer assisted with the paleomagnetic measurements. The presence of Lucas Lourens in the field was of crucial importance because without his ability in constructing tents it would have been impossible to have sampled the section in the rain and mud. This is MIOMAR contribution 5.

Chapter 5

Comparison of astronomical and $^{40}Ar/^{39}Ar$ ages of late Miocene ash beds: consequences for the age of mineral dating standards

Abstract

In this paper we present the first results of $^{40}Ar/^{39}Ar$ multiple single fusion datings on biotites and feldspars from two volcanic ash beds found on the islands of Crete, Gavdos and Koufonisi (Greece). These ash beds are intercalated in cyclically bedded marine sequences of late Miocene age which have been independently dated by correlating the sedimentary cycles to computed astronomical target curves. This calibration allows the $^{40}Ar/^{39}Ar$ ages to be compared directly with astronomical ages.

In general, our $^{40}Ar/^{39}Ar$ ages - calculated against TCR sanidine with an age of 27.92 Ma, intercalibrated to an age of 28.09 Ma for the FCT#3 biotite and an age of 24.99 Ma for the DRA sanidine - are consistent with the stratigraphic order and are in good agreement with the astronomical ages. The most reliably $^{40}Ar/^{39}Ar$ age - of 6.936 ± 0.006 Ma - is obtained from a sanidine separate of the lowermost ash in the Faneromeni section; this ash layer has an astronomical age of 6.941 Ma. The best fit - with the astronomical age - is obtained when the age of the TCR sanidine is increased slightly to 27.94 Ma, the age of the FCT#3 biotite to 28.11 Ma and the age of the DRA sanidine to 25.01 Ma.

This chapter has been submitted for publication as: F.J. Hilgen, W. Krijgsman, J.R. Wijbrans, Comparison of astronomical and $^{40}Ar/^{39}Ar$ ages of late Miocene ash beds: consequences for the age of mineral dating standards, *Geophys. Res. Lett.*, 1996.

Introduction

The age uncertainty of the neutron fluence monitors, or mineral dating standards, is the factor presently limiting the accuracy in $^{40}Ar/^{39}Ar$ dating. This uncertainty results in a 1 to 1.5 % error as compared with a 0.3 % precision of modern $^{40}Ar/^{39}Ar$ dating techniques. For instance, generally accepted ages for the Fish Canyon Tuff (FCT) sanidine, one of the most widely used dating standards, range from 27.55 to 28.09 Ma (Izett et al., 1991; Swisher et al., 1992). One solution to reduce the uncertainty is to determine the absolute air calibration of the ^{38}Ar tracer for isotope dilution determination of ^{40}Ar more precisely (Kunk et al., 1994). Further carefull comparison of different techniques applied to various minerals from ash horizons has been used with success in older parts of the timescale (Baadsgaard et al., 1992).

An alternative solution is to compare radiometric ($^{40}Ar/^{39}Ar$) ages with ages that have been obtained independently by astronomical dating. This dating method is based on the correlation or tuning of cyclic variations in the geological record to computed astronomical time series of orbital variations. Renne et al. (1994) recalculated published $^{40}Ar/^{39}Ar$ ages for 7 polarity reversals younger than 3.5 million years to fit them to astronomical ages for the same reversals. The best fit was obtained when they adopted an age of 27.95 ± 0.18 (or 28.03 ± 0.18) Ma for the FCT sanidine, dependent on the exact stratigraphic position of astronomically dated polarity reversals.

A disadvantage of the study by Renne et al. (1994) is that the $^{40}Ar/^{39}Ar$ ages for 5 (out of 7) polarity reversals had to be calculated by linear interpolation of sediment accumulation rates between dated volcanic beds thereby assuming a constant sedimentation rate in depositional settings where this is not very likely. Moreover, the exact positions of reversal boundaries are not always exactly known due to lack of sample density and/or post-depositional remagnetization (Van Hoof et al., 1993; Lourens et al., 1996). Finally, the precise $^{40}Ar/^{39}Ar$ age of these reversals is still an area of active research (e.g. Pringle et al., 1993; Renne et al., 1993). Such potential short-comings are avoided by dating ash beds in sedimentary sequences that have been dated astronomically. This approach ensures $^{40}Ar/^{39}Ar$ ages to be compared (more) directly with the astronomical ages.

In this paper we present the first results of $^{40}Ar/^{39}Ar$ datings of volcanic ash beds intercalated in cyclically bedded marine successions of late Miocene age in the Mediterranean. These successions have been astronomically dated (Hilgen et al., 1995) resulting in an astronomical (polarity) time scale for the Mediterranean late Miocene. This time scale is significantly older than CK95 and Shackleton et al. (1995) but is at least partly confirmed by independent astronomical tuning of ODP Leg 154 sites (Shackleton, pers. comm.).

Sections and stratigraphy

For our study we selected the Faneromeni, Kastelli and Agios Ioannis sections on Crete, the Metochia section on Gavdos and the Koufonisi section on Koufonisi. These open marine sections consist of cyclic alternations of white coloured homogeneous marls and brown coloured often well-laminated, organic-rich beds (termed sapropels) with minor intercalations of turbidites and volcanic ashbeds (Krijgsman et al., 1995). All sections have been correlated in detail using a combination of cyclostratigraphy and high-resolution planktonic foraminiferal biostratigraphy (Fig. 1; Van Gessel, 1994). The resulting bed-to-bed correlations are confirmed by the stratigraphic position of the volcanic ashbeds.

Three prominent ash beds are present in the Kastelli and Agios Ioannis sections and have been labelled a1, a2 and a3. They generally contain feldspar, quartz and glass shards. The a1 and a3 ashes in addition contain abundant biotite, whereas the a2 contains no (or minor) biotite; this ash is rich in hornblende phenocrysts. The a1 - but not the a2 and a3 - is found in all sections studied. Additional thin volcanogenic beds are found in most of the sections. In these ashes the crystals are badly preserved and minerals are rounded indicating substantial post-depositional transport.

$^{40}Ar/^{39}Ar$ dating

Radiometric dating focussed on the biotite and feldspar populations of the a1, a2 and a3 ashbeds, because of the good preservation and (sub-)euhedric shape of individual crystals. These three ash beds are interpreted as primary fall-outs (a1 in section Metochia) or to have undergone only limited post-depositional transport. Considerable effort was made to collect fresh unweathered material. The samples were washed and seived to separate the >125 μ fraction. In addition, microprobe analyses were performed on a Geol-JXA 86000 superprobe, to investigate the composition and homogeneity of the biotites and feldspars.

Methods

The largest biotite fractions (> 125 μm) were mechanically separated using a Faul vibration table. This separation was followed by microscopic examination and hand-picking of individual crystals using euhedric shape and preservation as selection criteria. Feldspar crystals (>200 μm) were separated by sieving, Faul vibration table, magnetic separator and hand-picking under the microscope. Heavy liquid separation was applied to the seived fraction of the Faneromeni a1-ash. This resulted in the isolation of sanidine crystals with densities between 2.58 and 2.625 gr/cm^3.

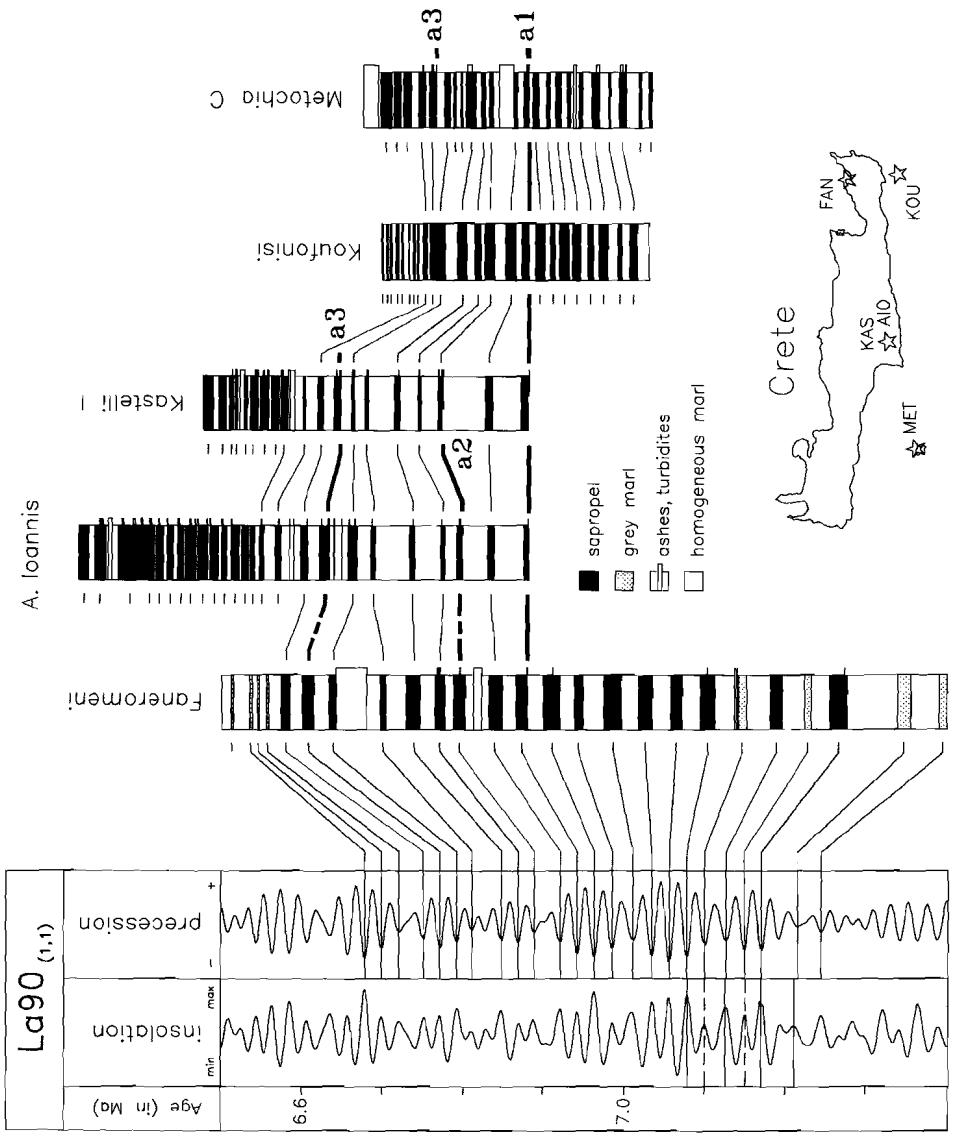

Figure 1.: Cyclostratigraphic correlations between the studied sections and calibration of the sedimentary cycles to astronomical target curves (after Hilgen et al., 1995). The cyclostratigraphic correlations have been confirmed by the tephrastratigraphy and the planktonic foraminiferal biostratigraphy (Van Gessel, 1994). A gross location map of the studied sections is included.

Argon geochronology was carried out using laser fusion of several replicate samples (usually n=5). A detailed description of techniques was published elsewhere (Wijbrans et al., 1995). In summary, approximately 20 mg aliquots of both feldspar and biotite were packaged in Al-foil, and loaded with the flux monitors (USGS standard 85G003 TCR sanidine, K/Ar age 27.92 Ma) that were packaged in Cu-foil, in a 5 mm ID quartz tube. Individual packages were approximately 1 mm thick, and standards were loaded between each set of 5 unknowns. Irradiation with fast neutrons was carried out in the B3 facility in the Oregon State University TRIGA reactor. After irradiation, the samples were loaded in a Cu tray (60 mm diameter) with 2 mm diameter holes for each individual experiment. For both the standards and the unknowns, we applied a single fusion technique where for each sample 5 replicates were analysed. The biotites and feldspar samples were preheated to approximately 500 C in order to remove some of the atmospheric argon that interferes with accurate analysis of the radiogenic argon component in young samples. The argon gas was measured isotopically using a double focussing noblegas mass spectrometer (MAP215-50) in static mode. Beam intensities were measured on a secundary elecron multiplier detector (gain 10,000) by peak jumping at half mass intervals down from mass 40 to 35.5. System blanks were measured at least between every set of 5 unknowns. In general, the blank correction applied was the average of the blanks run before and after the unknown. System blanks in a laser fusion sytem tend to be predictable and usually show a slight increase during the day. The blanks for this project were in the range m/e:40 0.5 -1.2 exp-16 moles, m/e:39 5 exp-19 moles, m/e:38 4 exp-19 moles, m/e:37 6 exp -18 moles, m/e:36 1.0 exp-18 moles for the VU7 series run in 1994, and in the range m/e:40 2.0 - 6.0 exp-16 moles, m/e:39 1.5 - 3.0 exp-18 moles, m/e:38 1.0 - 2.0 exp-18 moles, m/e:37 2.0 - 2.5 exp -17 moles, m/e:36 3.0 - 4.0 exp-18 moles for the VU10 series run in 1995. System mass discrimination was measured by letting clean into the mass spectrometer from a 10 l reservoir using a 1 ml gas pipette.

Results

Results of the Microprobe analyses are shown in table 1. Figure 2 shows that the biotites cluster in two groups which correspond to the a1 and a3 ash layers (a2 does not contain (or only minor) biotite). Only biotites of the a1 from Kastelli and Koufonisi diverge from the a1 cluster. The lower amount of K atoms per 22 O atoms in the Kastelli biotite may indicate that this biotite is partly altered to chlorite. The overall good clustering points to a homogeneity of the biotite populations, excludes the presence of detrital contaminants and confirms the cyclostratigraphic correlations between the sections.

Results of the microprobe analysis in addition revealed major differences in the feldspar populations of the two dated ash layers (a1 and a3). The a1 contains a mixed sanidine-plagioclase population (although no sanidine was actually

ash	section	SiO2	TiO2	Al2O3	FeO	CaO	MgO	K2O	Na2O	F	MnO
	Biotite										
	Agios Ioannis	36.53	4.46	13.72	16.78	0.02	13.56	8.58	0.63	0.34	0.04
A3	Kastelli	37.14	4.58	13.87	17.34	0.02	13.87	8.71	0.62	0.30	0.09
	Metochia	36.62	4.35	13.64	16.66	0.03	13.31	8.23	0.78	0.31	0.03
	Agios Ioannis	37.00	3.95	13.07	16.22	0.01	14.41	8.76	0.47	0.69	0.19
	Kastelli	39.84	4.10	12.81	15.58	0.03	13.43	8.17	0.31	0.71	0.15
A1	Faneromeni	37.78	3.99	13.73	16.66	0.01	14.70	9.01	0.46	0.64	0.29
	Koufonisi	36.27	3.94	15.45	15.78	0.04	14.38	8.65	0.53	0.54	0.13
	Metochia	37.52	4.12	13.55	16.53	0.06	14.58	8.93	0.47	0.73	0.17
	Plagioclase										
	Agios Ioannis	59.89	0.01	25.50	0.24	7.29	0.00	0.72	6.97	0.04	0.00
A3	Kastelli	59.23	0.02	25.85	0.27	7.87	0.00	0.66	6.76	0.06	0.00
	Metochia	59.90	0.01	25.26	0.21	7.35	0.00	0.74	6.83	0.03	0.00
	Agios Ioannis	60.37	0.00	24.84	0.25	6.35	0.00	0.88	7.49	0.02	0.00
	Kastelli	57.51	0.00	26.70	0.41	8.66	0.00	0.48	6.44	0.02	0.00
A1	Faneromeni	60.86	0.01	24.77	0.33	6.17	0.00	0.84	7.66	0.05	0.00
	Koufonisi	64.78	0.00	23.28	0.41	4.73	0.00	1.11	6.43	0.00	0.00
	Metochia	58.35	0.00	25.70	0.70	7.57	0.00	0.49	6.85	0.05	0.00
	Sanidine										
	Agios Ioannis	-	-	-	-	-	-	-	-	-	-
	Kastelli	65.45	0.02	18.95	0.05	0.18	0.00	11.53	3.51	0.03	0.00
A1	Faneromeni	64.52	0.01	19.05	0.17	0.22	0.00	11.28	3.50	0.02	0.00
	Koufonisi	65.86	0.02	19.06	0.20	0.19	0.00	11.55	3.39	0.01	0.00
	Metochia	68.62	0.05	18.04	0.37	0.17	0.95	9.19	3.06	0.05	0.00

Table 1.: Results of analyses of biotites, plagioclases and sanidines from the a1- and a3-ash layers in the different sections. Data represent averaged values of measurements of individual crystals.

measured from this ash in section Agios Ioannis) whereas the a3 contains only plagioclase. Again these results confirm the cyclostratigraphic correlations.

The results of the $^{40}Ar/^{39}Ar$ dating have been summarized in table 2. The $^{40}Ar/^{39}Ar$ ages are in agreement with the stratigraphic succession because ages of the a1-ash are consistently older than the ages of the a3-ash apart from the age of the a1-biotite from Kastelli. This exceptionally young age can best be explained by the influence of weathering.

Biotites and feldspars yielded consistent ages for the same sample except for the a1-ash in the Kastelli and Koufonisi sections. Inconsistency in the Kastelli-a1 ages is caused most likely by weathering which preferentially affected the biotite ages which is confirmed by concomittant reduction in K content. For the moment

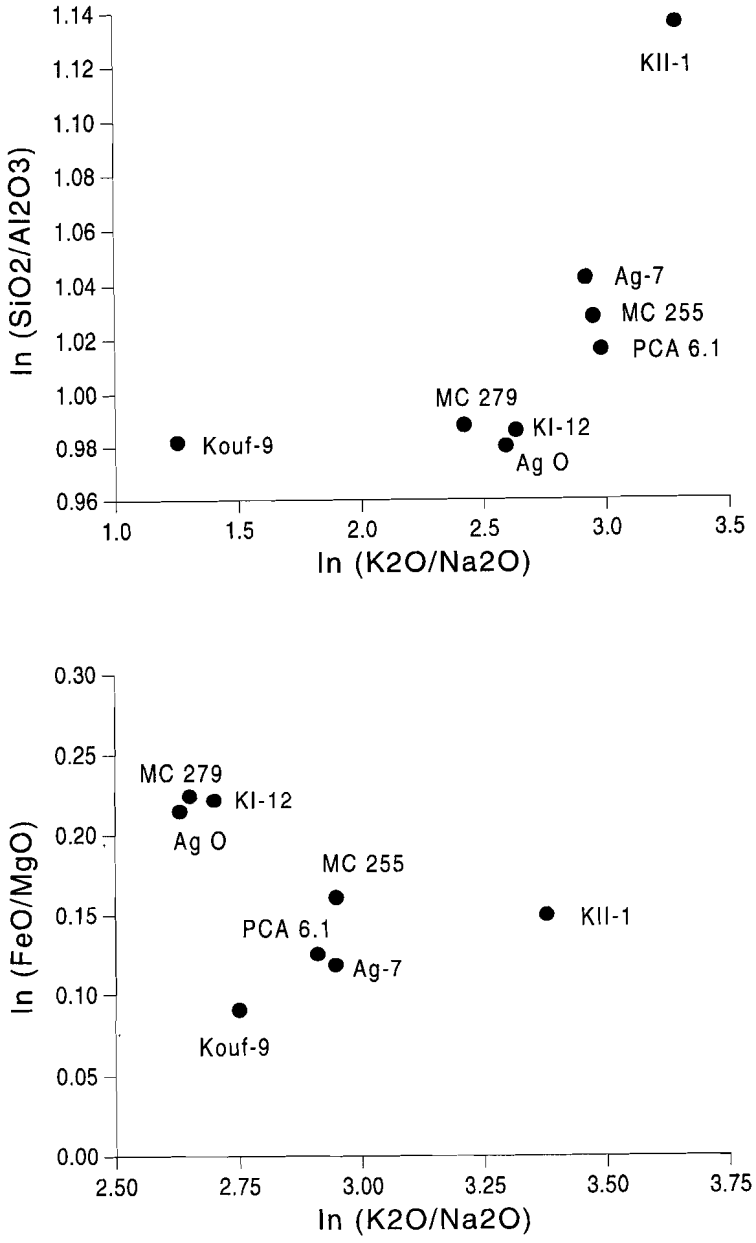

Figure 2.: Plots of Ln SiO_2/Al_2O_3 and Ln FeO/MgO versus Ln K_2O/Na_2O for biotites of the a1 and a3 ash layers in the different sections. Data points represent averaged values for measurements of individual biotite crystals (n between 7 and 20). MC 255 (Metochia), PCA 6.1 (Faneromeni), Ag -7 (Agios Ioannis), KII-1 (Kastelli) and Kouf -9 (Koufonisi) are derived from the a1-ash layer and MC 279, KI-12 and Ag 0 from the a3-ash layer.

we do not have an explanation for the inconsistency in the ages for the a1-ash from Koufonisi.

Despite some minor discrepancies, ages for the same ash layer in the different sections are also in good agreement with one another if we disregard the discrepant young age of the Kastelli-a1 biotite and the discrepant old age of the Koufonisi-a1 feldspar. Older biotite age for an ash may be considered more reliable than slightly younger ages because of the (potential) influence of weathering (see discussion above). This approach would result in an age of 6.934 Ma for the a1 and of 6.747 Ma for the a3. Our feldspar ages are considered less reliable than the biotite ages because they have been obtained from plagioclase (a3) or from mixed plagioclase/sanidine (a1) populations. Only the Faneromeni-a1 feldspar age - of 6.936 Ma - is derived from a pure sanidine separate and hence this age is considered the most reliable for the a1. It is in excellent agreement with the biotite age - of 6.934 Ma - for this ash.

Comparison with astronomical ages

Biotite and plagioclase - present in the mixed feldspar populations - are less suitable to accurately determine the $^{40}Ar/^{39}Ar$ age of a sample. Despite minor influence of weathering - as indicated by the major element compositions - the biotites yield more scatter in the argon ages, hence they are less suitable for high-precision chronostratigraphy. The plagioclase is better preserved, but due to the lower K content precise measurements of the radiogenic ^{40}Ar is more difficult because of the combined effects of a larger proportion of atmospheric argon and possible problems with excess ^{40}Ar (see Krijgsman et al., 1996). We therefore selected the single sanidine age of 6.936 ± 0.006 Ma for the a1-ash in the Faneromeni section to determine the age of Taylor Creek Rhyolite sanidine, FCT#3 biotite and DRA mineral standards (Dalrymple and Duffield, 1988; Izett et al., 1991; Wijbrans et al., 1995) via intercalibration with astronomical time.

The a1-ash is intercalated at the base of a sapropel which is dated astronomically at 6.938 Ma (Hilgen et al., 1995). The astronomical age of the a1 arrives at 6.941 Ma because the age of 6.938 Ma refers to the sapropel mid-point and the presently best estimate for the duration of a well-developed sapropel is in the order of 5-6 kyr.

Our $^{40}Ar/^{39}Ar$ data were calculated against USGS standard TCR sanidine with an age of 27.92 Ma intercalibrated to an age of 28.09 ± 0.10 Ma for the FCT#3 biotite and of 24.99 Ma for the DRA sanidine (Wijbrans et al., 1995). Although these ages are to within the analytical uncertainty consistent with the astronomically derived age for the Faneromeni a1 ash bed, the best fit with the astronomical age is obtained when the age of the TCR sanidine is increased slightly from 27.92 to 27.94 Ma, the age of the DRA sanidine from 24.99 to 25.01 and the age of the FCT#3 biotite from 28.09 to 28.11 Ma. The latter age is

ash no.	Astron. Ages	mineral	sections				
			Agios Ioannis	Kastelli	Faneromeni	Koufonisi	Metochia
a3	6.771	biotite	6.747 ± 0.014	6.668 ± 0.010			6.632 ± 0.021
		plagioclase	6.776 ± 0.066	6.749 ± 0.044			
a2	6.887	?					
a1	6.941	biotite	6.893 ± 0.013	5.691 ± 0.055	6.934 ± 0.016	6.813 ± 0.012	6.768 ± 0.025
		feldspar	6.923 ± 0.013	6.844 ± 0.008		7.164 ± 0.032	6.786 ± 0.027
		sanidine			6.936 ± 0.006		

Table 2.: $^{40}Ar/^{39}Ar$ and astronomical ages for the a1, a2 and a3 ash layers. No radiometric ages were obtained for the a2 layer due to unsuitability of the material. The astronomical age of the ash layers was calculated by adding 3 kyr to the insolation age given by Hilgen et al. (1995) for the mid-point of sapropels in which the ash layers are intercalated at the base. The value of 3 kyr is based on the presently best estimate for the duration of a well-developed sapropel, which is in the order of 5-6 kyr

consistent with the age of 27.95 ± 0.18 Ma, or 28.03 ± 0.18 Ma, obtained by Renne et al. (1994) for the FCT sanidine via intercalibration with astronomical time.

The ages we obtained here for monitor dating standards via intercalibration with astronomical time should be considered preliminary because they are based on just a limited number (5) of single fusion experiments on the Faneromeni a1-sanidine. Future research will focus on the a1-ash by dating sanidine separates from at least 4 different sections and using step-wise heating in addition to multiple (>30) single fusion dating experiments. This study aims to determine the age of the monitor dating standards more accurately and to reduce the analytical error, currently being 0.018 Myr (1sd). Finally, a direct intercalibration against the widely used FCT#3 sanidine standard is desirable (e.g. Renne et al., 1994).

Acknowledgements

We thank Lodewijk IJlst for his help with the mineral separation and Timo Nijland for discussions on the biotites. Pim, Tirza, Serge and Rolf logged the Agios Ioannis and Kastelli I sections. Malcolm Pringle carried out the first argon datings on the Metochia a1-ash. This study was partly supported by the Netherlands Geosciences Foundation (GOA) with financial aid from the Netherlands Organization of Scientific Research (NWO) and the EU-HCM program. This is MIOMAR-project contribution no. 6.

Chapter 6

Magnetostratigraphic dating of the middle Miocene climate change in the continental deposits of the Aragonian type area in the Calatayud-Teruel basin (Central Spain)

Abstract

The exceptionally dense mammalian faunal record of the Aragonian type area in Central Spain shows that an important climate change towards a cooler and more humid climate is recorded during the Neogene Mammal Zone MN 5 (Van der Meulen and Daams, 1992). The magnetostratigraphic results from mammal-bearing middle Miocene continental sections in the Aragonian type area indicate that the onset of this climate change, at the MN 4/MN 5 boundary, occurs in the reversed chron C5ACr and has an age of 14.1 Ma, according to the geomagnetic polarity time scale (GPTS) of Cande and Kent (1995). This age is consistent with the age estimate of 14.1-14.05 Ma for the main increase in $\delta^{18}O$ in the marine record (Flower and Kennett, 1993). These independent observations of time-equivalent cooling in both continental and marine records confirm and accurately date a global cooling event in the middle Miocene.

The age of 14.1 Ma for the MN 4/MN 5 boundary is significantly younger than previously recorded in continental time scales (Berggren et al., 1985; Steininger et al., 1990). This results in a longer duration of the MN 4 zone by approximately 3 Myr, which is consistent with the many important faunal changes occuring in MN 4. Furthermore, the MN 5/MN 6 boundary occurs in chron C5ACn (13.8-13.9 Ma) and the MN 6/MN 7-8 boundary in the interval C5Ar.1n-C5Ar.3r (12.7-13.0 Ma).

This chapter has been published as: W. Krijgsman, C.G. Langereis, R. Daams, A.J. van der Meulen, Magnetostratigraphic dating of the middle Miocene climate change in the continental deposits of the Aragonian type area in the Calatayud-Teruel basin (Central Spain), *Earth Planet. Sci. Lett.*, 128, 513-526, 1994.

Introduction

The Aragonian land mammal stage was defined at the International Symposium of Mammalian Stratigraphy of the European Tertiary (Munich 1975) between the first appearances (FA) of the equids *Anchitherium* and *Hipparion* in Europe (Fahlbusch, 1976). Later, the lower (Ramblian/Aragonian) boundary was moved upward to the FA of *Democricetodon*, the first modern cricitid in (central and) western Europe (Daams et al., 1987). The Aragonian stage comprises the Neogene Mammal zones MN 4, 5, 6, 7 and 8 in the nomenclature of Mein (1975, 1990) and De Bruijn et al. (1992). In the type area of the Aragonian, a local zonation has been made in Zones B to G3 (Van der Meulen and Daams, 1992; Daams and Freudenthal, 1988). Two new zones are recognised here: Zone Dc is charcterised by *Megacricetodon collongensis, Fahlbushia koenigswaldi* and *Pseudofahlbushia* (Cricetidae, hamsters), which are common components associated with *Pseudodryomys simpliciders* and *P. ibericus* (Gliridae, dormice); zone Dd contains mainly the same species as Dc, although *Peridyromys rex* is also present. Chronostratigraphic control of Aragonian sediments is only based on indirect correlations of MN zones with marine biostratigraphy. In the Tertiary basins of central Spain there are no possibilities to correlate the continental successions to the marine scale because of the scarcity of marine intercalations. Radiometric calibration to the absolute time scale is impossible by the absence of intercalated rocks of volcanic origin. Since there are no reliable age determinations, controversies exist about almost all biostratigraphic zones and boundaries (Steininger et al., 1990).

The oldest Aragonian faunas are placed in the Neogene Mammal Zone MN 4. The MN 3/MN 4 boundary - by definition the Ramblian/Aragonian boundary - is not directly dated, but its age is based on the correlation with marine planktonic zones. In recent literature, this boundary - based on an ambiguous correlation with nannofossil zones in Portugal - is set at 17.8 Ma (Steininger et al., 1990) or at 18.5 (Van der Meulen and Daams, 1992).

The position of the upper (Aragonian/Vallesian) boundary has been a subject of debate, since the FA of *Hipparion* seems to be a clear example of diachrony. Berggren et al. (1985) placed this boundary at 12.5 Ma based on radiometric dates on sites from Germany. Sen (1990) has suggested that *Hipparion* appears in the Mediterranean at approximately 11.5 Ma, within chron C5R. The FA of *Hipparion* in the Siwaliks of Pakistan is magnetostratigraphically dated (in chron C5n) at 10 Ma (Johnson et al., 1982). Finally, Steininger et al. (1990) place the Aragonian/Vallesian boundary at 11.5 Ma.

The marine records clearly show that major paleoceanographic and paleoclimatic changes have occurred in the middle Miocene. These changes represent an important step towards near-modern oceanographic conditions. Foraminiferal assemblages established in the middle Miocene persisted through the late Neogene (Miller and Katz, 1987; Kurihara and Kennett, 1992). A change in the rate of $^{87}Sr/^{86}Sr$ increase is thought to have occurred at 14.6-14.8 Ma and

was interpreted as the development of a permanent Antarctic ice cap (Miller et al., 1991a). Global increases in $\delta^{18}O$ from 16.2 to 12 Ma are considered to reflect major ice sheet growth on Antarctica (Shackleton and Kennett, 1975; Savin et al., 1975; Miller et al., 1991b; Woodruff and Savin, 1991, Wright et al., 1992). Flower and Kennett (1993) showed that the main increase of $\delta^{18}O$ in the middle Miocene (event Mi3; Miller et al., 1991a) occurred between 14.5 and 14.0 Ma with a major increase between 14.1 and 14.05 Ma. The dating of this event was based on magnetostratigraphic (Barton, 1985), biostratigraphic (Barron et al., 1985) and isotopic (Woodruff and Savin, 1991) data.

The middle Miocene climate change is well-documented in the marine record, but the effects of the climate change on the continental fauna record is poorly known. The scarcity of fossil localities and the rather scattered outcrops makes it difficult to study large scale climatic changes on land. The Aragonian type area, however, shows abundant fossiliferous levels covering successive Neogene mammal zones (see Fig. 7). The dense mammalian faunal record of the Aragonian makes it possible to apply principal component analyses on the rodent assemblages from the Ramblian and Aragonian (Van der Meulen and Daams, 1992). An important result was the recognition of a major cooling phase in the middle Aragonian during Zone E which is correlative to Zone MN 5. According to Steininger et al. (1990), MN 5 spans the interval from 17 to 16 Ma, which suggests that the climate change to a colder state on land significantly predates the changes in the marine record by several Myr. Van der Meulen and Daams (1992) bracketed the cooling event between 15 and 13 Ma, based on paleomagnetic data by Dijksman (1977) and marine-continental tiepoints in Portugal. Age determinations, especially for the mammal zones, however, are still ambiguous (Steininger et al., 1990).

The stratigraphic position of the middle Miocene (MN 5) climate change is accurately tied into the Aragonian type section. To make a direct correlation of the climate change to the GPTS we have sampled the Aragonian type section for magnetostratigraphic purposes. To obtain a reliable chronostratigraphic framework for the standard mammal zonations of the middle Miocene Aragonian stage we have also sampled a time-equivalent section near the village of Calatayud which we could extend to older levels. In the present paper, we present the magnetic polarity stratigraphy of the two sections in the Aragonian type area and their correlation to the geomagnetic polarity time scale (GPTS).

Sections and sampling

The Aragonian stage was defined in the Calatayud-Teruel basin of Central Spain (Daams et al., 1977), located in the Iberian range between the Western and Eastern Iberian Chains (Fig. 1). Sediments in the type area mainly consist of breccias, conglomerates, sands, silts, clays, lacustrine limestones and gypsum. Throughout the area, the reddish coloured fluviatile-lacustrine sediments are

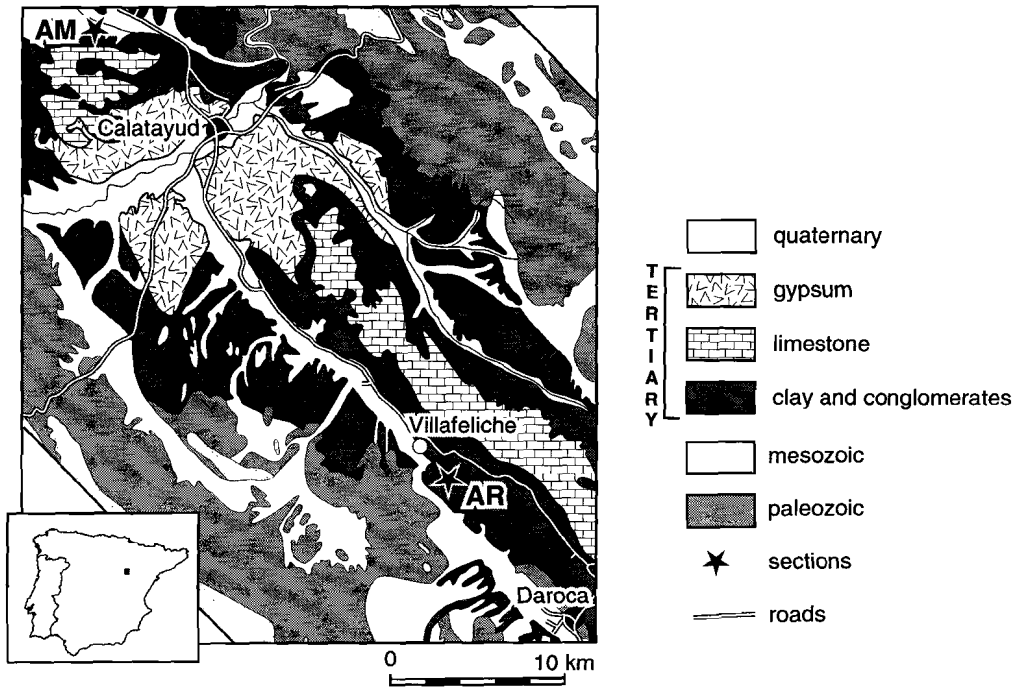

Figure 1. Location of the Aragon (AR) and Armantes (AM) sections in the type area of the Aragonian in the Calatayud-Teruel basin of central Spain (slightly modified after Dijksman 1977).

capped by a thick formation of alternating white-greyish marls and white limestones. This formation is thought to be partly of Vallesian age, because laterally found fossil localities contain Vallesian faunas (Daams et al., 1977). The most favourable sediments for fossil accumulation were in general clays, silts and marls in particular those with lignitic contents and/or concentrations of fresh water or terrestrial molluscs.

The Aragon section

The Aragon section has a thickness of 170 metres and comprises the partly overlapping Valdemoros (VA), Las Umbrias (LUM) and Las Planas (LP) sections (Daams et al., 1977). The section is located at approximately one km SE of the village of Villafeliche (Fig. 1). The base of the section consists of red silts and clays containing red conglomerate (channel fills) and white limestone beds and it discordantly overlies the Cambrian basement. The number of limestone beds gradually increases higher up in the section while the reddish colour diminishes. The middle part of the section consists of whitish limestones and white/grey

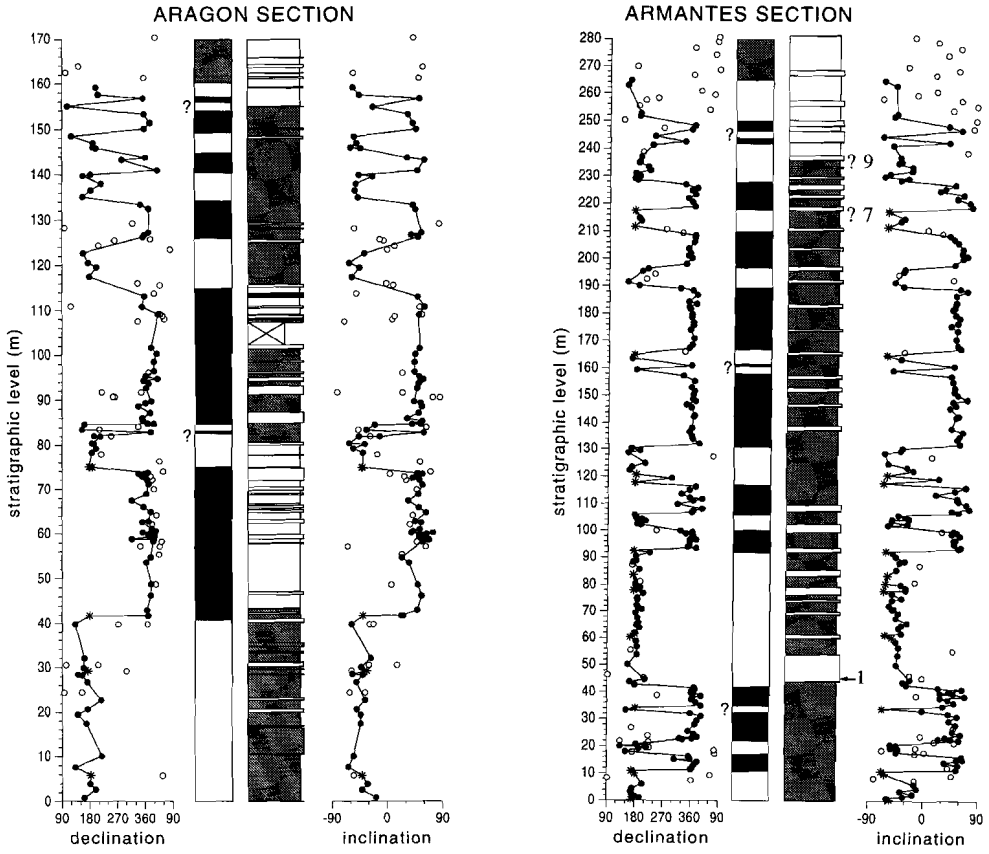

Figure 2 and 3. Magnetostratigraphy and lithology of the Aragon and Armantes sections. Solid dots represent reliable directions, circles represent low intensity samples which are difficult to interpret. Stars represent directions obtained by applying the great circle method. In the polarity column, black (white) denotes normal (reversed) polarity zones; shaded interval denotes a zone of uncertain polarity. Question marks denote polarity intervals based on a single level. The lithology column displays variations of red coloured silts and conglomerates (shaded) and greyish-white coloured marls and limestones (white). Arrow indicates position of fossil locality Armantes 1; question marks denote uncertain positions of fossil localities Armantes 7 and 9, in the upper part of the section (Dijksman, 1977).

marls with limestone beds up to 3 m in thickness (Fig. 2). A second unit composed of red silty clays with some pebbly interbeds and white limestones overlies the white marl/limestone interval. The upper part of this unit consists of thick, up to 10 m, red clay beds in which some limestone beds are intercalated (Fig. 2). These clays are in turn capped by a formation of white limestones.

In the Aragonian section, 143 sites were sampled with an average spacing of approximately 1.5 metres. At each site two paleomagnetic cores were drilled after

first removing the weathered surface. We attempted to sample the section as long and continuously as possible to obtain a maximum number of polarity zones. Unfortunately, the uppermost part of the section was sampled in less detail because of fewer levels with a suitable lithology.

The Armantes section

The Armantes section, named after the mountain range the Sierra de Armantes, is located a few kilometres NW of the village of Calatayud (Fig. 1). The Armantes section is 280 metres thick and was sampled along the northern slope of the mountains (Fig. 1). The base of the section (Armantes A; De Bruijn, 1965, or Ribota; Dijksman, 1977) consists of a unit of red silts and sands, while the top is formed by a unit of 10 metres of white limestones (44-54 m in Fig. 3). The major part of the Armantes section consists of a rhythmic alternation of red clays and pink-white limestones (Fig. 3). This alternation is remarkably continuous and throughout the whole section limestone beds are observed, which is especially evident in the more weathered parts of the section. Between the thick limestone beds, smaller beds are observed at irregular distances and at several levels thin conglomerates are intercalated. The regular cyclicity observed in the section suggests that a relation exists with climatic changes induced by astronomical cycles of the Earth's orbit. The upper part of the section (Armantes B; De Bruijn, 1965 or Calatayud; Dijksman, 1977) is overlain by a thick series of white limestones and dolomites with some rare intercalations of reddish coloured sediments (Fig. 3).

The Armantes 1 fossil locality is directly located in the sampled section. Two other localities, Armantes 7 and 9, are located three and one km southwest of the sampled section; Dijksman (1977) tentatively correlated these to an approximate position at the top of the Armantes section (Fig. 3).

Paleomagnetic samples are taken with an average spacing of approximately 1 to 1.5 metres. At each site we drilled two standard paleomagnetic cores. The section could not be sampled at evenly spaced intervals, because the red silts were often impossible to drill. We succeeded, however, in drilling several levels between all thick limestone beds.

Rock magnetic properties

We performed some rock magnetic experiments on selected samples of both the Aragon and Armantes section to identify the carriers of the NRM components. These rock magnetic experiments include acquisition of an isothermal remanent magnetisation (IRM) on a PM 4 pulse magnetiser (of H. Böhnel) and subsequent thermal demagnetisation. Susceptibilities were measured after each temperature step on a Kappabridge KLY-2. Finally, some

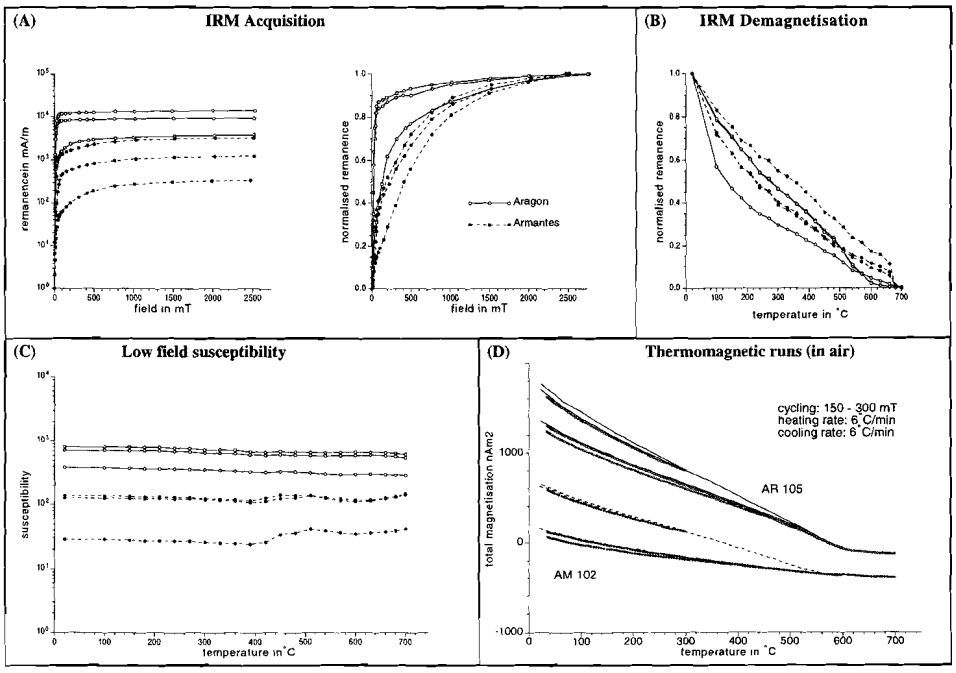

Figure 4. (A): Examples of IRM acquisition of samples of the Aragon and the Armantes section. The initial steep rise points to magnetite, the gradual increase at high fields suggests the additional presence of hematite. (B): Stepwise thermal demagnetisation of the normalised IRM also show the presence of both magnetite and hematite. (C): Low field susceptibility during thermal demagnetisation. (D): Examples of thermomagnetic runs in air.

thermomagnetic runs were recorded with a modified horizontal translation Curie balance making use of a cycling field (Mullender et al., 1993).

Both in the samples of the Aragon and Armantes section, the acquisition of the IRM shows an initial steep rise until 100/200 mT, suggesting the presence of a low-coercivity mineral like magnetite or maghemite, after which the IRM gradually increases (Fig. 4a). Saturation is generally not reached in the highest fields (2500 mT) which indicates the additional presence of a high-coercivity mineral like goethite or hematite. The unblocking temperatures after thermal demagnetisation of the IRM (Fig. 4b) support the presence of magnetite and, especially for the Armantes section, hematite as the dominant magnetic carriers. The rapid decay at low temperatures in some samples suggests the occasional presence of goethite.

The initial susceptibility shows no important changes for the samples of the Aragon section when heated up to 700 °C (Fig. 4c), indicating that no additional magnetic minerals are produced during heating of the samples. Some samples of the Armantes section show a small increase in susceptibility at temperatures

higher than 400 °C (Fig. 4c). The thermomagnetic runs on the Curie balance also imply that no additional magnetic material is produced during heating to 700 °C (Fig. 4d). The sample of the Aragon section indicates the presence of magnetite, because the results reveal a Curie point of 580 °C. The rock magnetic experiments suggest that the main carriers of the magnetisation are hematite and magnetite but that also small amounts of goethite may be present.

Paleomagnetic results: magnetostratigraphy

The natural remanent magnetisation (NRM) was measured on a 2G Enterprises cryogenic magnetometer. The total NRM intensities are generally high, ranging from 0.1 to 10 mA/m, and are strongly related to the lithology. Generally, the reddish silts and clays show much higher intensities than the white limesones and marls. The low-field susceptibility ranges from 50-1500 * 10^{-6} SI. At least one specimen from each sample site was progressively demagnetised using 30 °C temperature steps.

Aragon section

In the Aragon section, thermal demagnetisation of the samples reveals that the total NRM is generally composed of three components. A small viscous and randomly oriented component disappears at temperatures of 100 °C. A relatively large secondary component is generally removed at temperatures of 240 °C (Fig. 5a). It has approximately a present-day field direction before bedding tilt correction and is therefore of recent origin and most probably caused by weathering of the sediments. A characteristic remanent magnetisation (ChRM) is generally removed at temperatures below 580 °C. Demagnetisation diagrams are generally of good quality and in most cases the characteristic directions can reliably be determined (Fig. 5b,c). Only in the white limestones, several levels show less reliable results because of a very weak magnetic signal, although the (N/R) polarity is usually clear (Fig. 2).

Some samples do not show a simple linear decay to the origin, even if the polarity is clear. It is assumed that the primary component is partly overprinted by a secondary component caused by overlapping unblocking temperature spectra. In these cases, a best fitting plane is calculated through the datapoints according to the method of McFadden and McElhinny (1988).

The ChRM directions and polarity zones (Fig. 2) show that fifteen polarity intervals have been recorded. Unfortunately, the uppermost polarity intervals are only determined by a few samples and must therefore be considered as less reliable. The most conspicuous characteristics of the Aragon polarity sequence are the two long normal intervals in the middle part of the section which are

separated by a relatively short reversed interval. Within this reversed interval, one level is observed which shows a normal polarity.

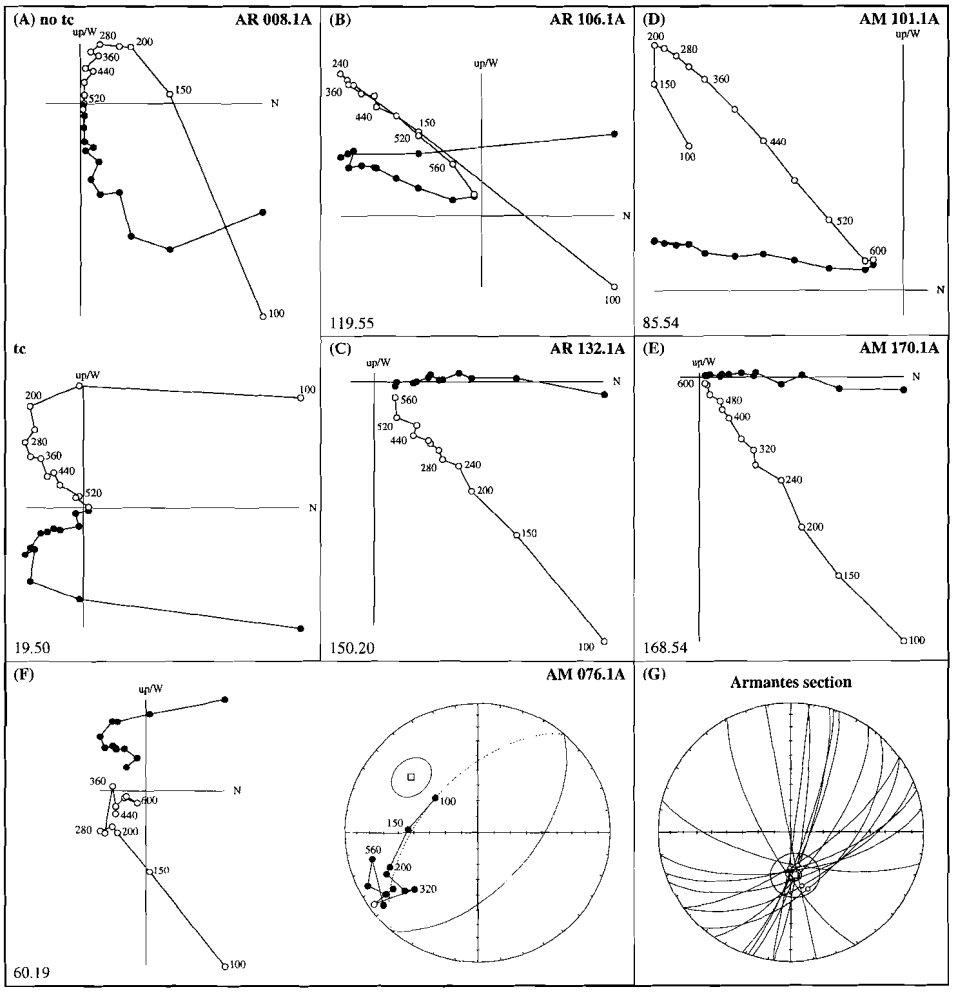

Figure 5. Thermal demagnetisation diagrams of samples from the Aragon and Armantes section. Closed (open) circles denote the projection on the horizontal (vertical) plane; values are temperature steps in °C; stratigraphic levels are in the lower left corner. (A) is an example from the steeply dipping lower part of the section, displaying at low temperatures a present-day field component before tilt correction (no tc) and at high temperatures a characteristic primary component after tilt correction (tc). (F) is an example showing no clear linear decay to the origin; the great circle in the equal area projection suggests that a reversed ChRM is not fully resolved. Open square denotes the normal to the plane with its error. Diagram (G) shows the intersections of all great circle planes as estimates of the primary directions.

Armantes section

Similar to the Aragon section, the thermal demagnetisation diagrams of the Armantes section reveal a stable and well-defined ChRM component after removing a secondary present day field component at 240 °C. Susceptibilities as well as ChRM-intensities are lower than in the Aragon section. Polarities are evident and characteristic directions can often reliably be determined (Fig. 5d,e). Generally, the total remanence is not entirely removed at temperatures of 600 °C and probably hematite contributes to the characteristic magnetisation. Best fitting planes (McFadden and McElhinny, 1988) for the samples without a clear linear decay to the origin (Fig. 5f) were used to estimate the characteristic directions (Fig. 5g). Some samples in the Armantes section show demagnetisation diagrams that are impossible to interpret or, like the limestones in the upper part of the section, have such low intensities that characteristic directions cannot accurately be determined (Fig. 3).

Twenty-five polarity intervals have been recorded in the Armantes section. The uppermost polarity intervals are composed of only a few samples and are hence less reliable. In the middle part of the section a single normal polarity level is observed in a reversed interval. In this case, it is not clear whether this sample is totally overprinted by a normally directed weathering component or that it represents a very small normal interval. It does occur in the same reversed interval as the single normal level of the Aragon section, although their relative positions are different.

Correlation to the GPTS

Correlation of the Aragonian sections to the GPTS has been made by reference to the most recent published version (CK95). Since the polarity sequence of the Armantes section contains twenty-five polarity intervals and the regular cyclic sedimentary patterns suggest a fairly constant sedimentation rate, it makes this section very suitable for correlation to the GPTS. Clearly, only one unambiguous correlation can be made (Fig. 6); all other correlations result in sudden and unlikely changes in sedimentation rate. It shows that the Armantes section covers a continuous time interval of almost 5 Myr. The base of the section corresponds to

Figure 6. Correlation of the Armantes and Aragon sections to the GPTS of Cande and Kent (1992). Lines connect corresponding reversal boundaries. The polarity zones of the Aragon and Armantes sections are in metres. Arrow at the left side indicates the stratigraphic position of the climate change as observed in the biostratigraphic record in the Aragon section (see also Figure 6.). Right columns display mammal zones and stages. Ages of the Zone and Stage boundaries (solid lines) are from this study (see table 1). Asterisks (* (Van der Meulen and Daams, (1992), ** (Steininger et al., (1990)) represent literature ages for zone boundaries (dashed lines).

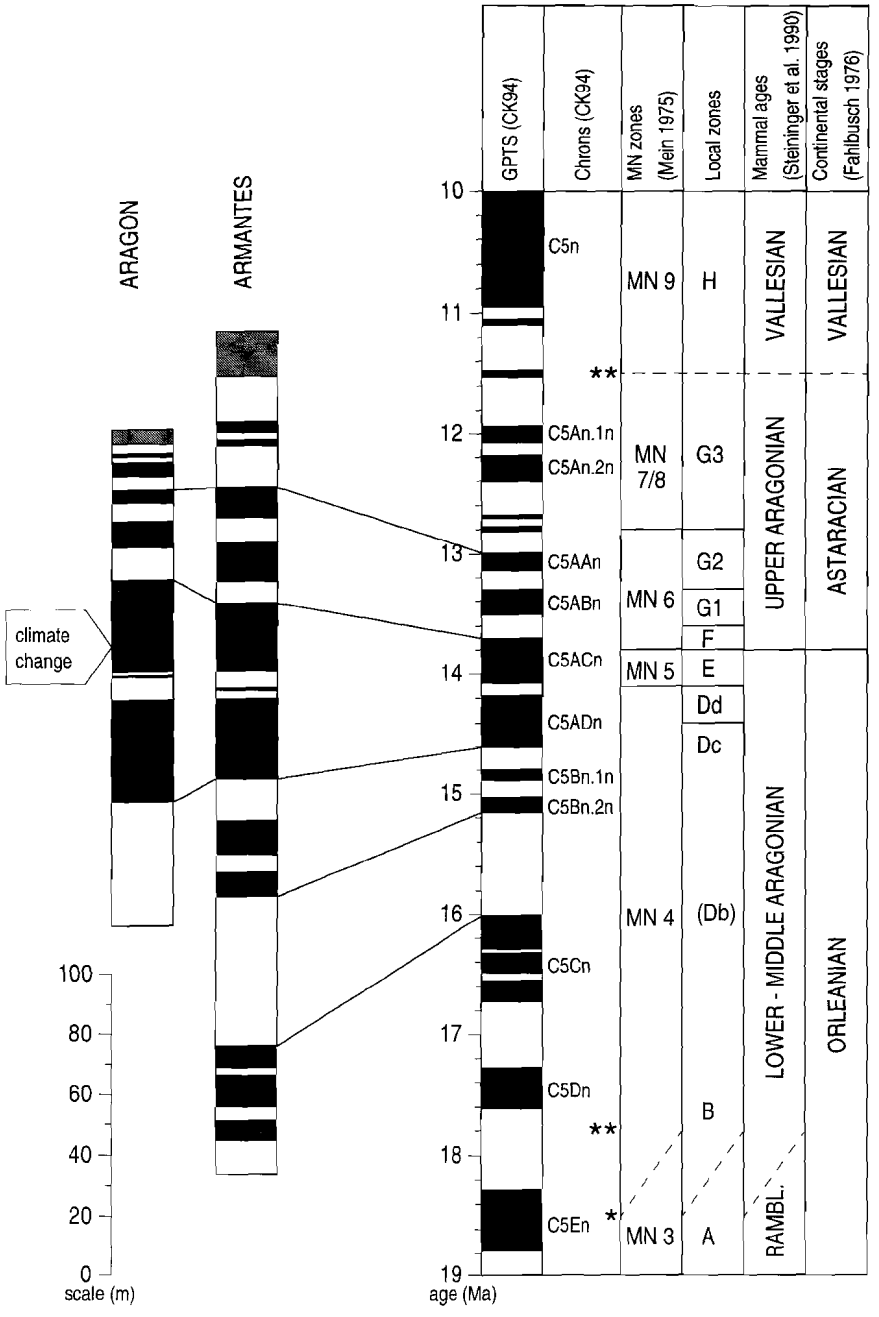
ARAGON
ARMANTES
climate change
100
80
60
40
20
0
scale (m)
10
11
12
13
14
15
16
17
18
19
age (Ma)
GPTS (CK94)
Chrons (CK94)
C5n
**
C5An.1n
C5An.2n
C5AAn
C5ABn
C5ACn
C5ADn
C5Bn.1n
C5Bn.2n
C5Cn
C5Dn
**
C5En
*
MN zones (Mein 1975)
MN 9
MN 7/8
MN 6
MN 5
MN 4
MN 3
Local zones
H
G3
G2
G1
F
E
Dd
Dc
(Db)
B
A
Mammal ages (Steininger et al. 1990)
VALLESIAN
UPPER ARAGONIAN
LOWER - MIDDLE ARAGONIAN
RAMBL.
Continental stages (Fahlbusch 1976)
VALLESIAN
ASTARACIAN
ORLEANIAN

BOUNDARY		CHRON	AGE in Ma
MN zones	Local zones	(CK94)	(CK94)
MN 7-8/MN 9	G3/H	--	11.5**
MN 6/MN 7-8	G2/G3	C5An.1n - C5Ar.3r	12.7 - 13.0
	G1/G2	C5AAr - C5ABn	13.1 - 13.5
	F/G1	C5ABr	13.5 - 13.7
MN 5/MN 6	E/F	C5ACn (0.2 - 0.6)	13.8 - 13.9
MN 4/MN 5	Dd/E	C5ACr (0.4)	14.1
	Dc/Dd	C5ADn (0.3)	14.3
MN 3/MN 4	A/B	--	17.8** - 18.5*

Table 1. Positions (or ranges) of MN and local zone boundaries and their ages with respect to the GPTS [2]. Asterisks represent ages from literature (* [1], ** [5]). Decimal fraction denotes position within a (sub)chron as taken from the younger end.

chron C5Cr and has an age of 17.0 Ma, the top of the section is estimated at 12.4 Ma according to CK95. Furthermore, it appears that every polarity zone is recorded and that no significant hiatuses exist. This makes the Armantes section a unique and important continental reference section for the middle Miocene.

Although the different lithologies of the Aragon section suggest changing sedimentation rates, the correlation to the Armantes section and hence to the GPTS is unequivocal (Fig. 6). The Aragon section is biostratigraphically younger than than the Armantes 1 fossil locality, whereas the top of the Aragon section is biostratigraphically time-equivalent with the top of the Armantes section. This results in only one posssible correlation, with the two long normal intervals to the middle part of the Armantes section, corresponding to chrons C5ACn and C5ADn and. The base of the Aragon section occurs in chron C5ADr at 14.8 Ma and the top in chron C5An.2r at approximately 12.5 Ma. The lowermost polarity zone of the Aragon section seems to be relatively long, but a higher sedimentation rate is in agreement with the presence of many conglomerate beds.

Since the Armantes section is now well-dated, reliable time constraints can be applied to the sedimentary sequence. The regular rhythmic alternation of red silts and white limestones suggests that the general depositional setting of the Armantes section in the middle Miocene has faithfully recorded climatic changes in the sedimentary patterns. The distinctly cyclic middle part of the section (54-235 m) contains 27 cycles and covers approximately 3 Myr. The resulting average periodicity of 111 kyr suggests that these sedimentary cycles are related to the ~100 kyr eccentricity cycle of the Earth's orbit.

Ages of the main biostratigraphic zone boundaries

Four Neogene Mammal (MN 4, 5, 6 and 7-8) zones are recognised in the biostratigraphic record of the Aragonian type section (Fig. 7). Our present correlation of the Aragonian polarity sequence to CK94 provides accurate age determinations for the boundaries of these successive MN Zones (table 1). The important MN 4/MN 5 boundary represents a major climate change (Van der Meulen and Daams, 1992) and occurs in chron C5ACr with an age of 14.1 Ma. The MN 5/MN 6 boundary occurs in chron C5ACn (13.8 - 13.9 Ma) and the MN 6/MN 7-8 boundary occurs in the interval C5Ar.1n - C5Ar.3r (12.7 - 13.0 Ma). These ages differ significantly from the ages in the most recent continental biostratigraphic time scale (Steininger et al., 1990) and they have important implications for biostratigraphic correlations.

Lower Aragonian: MN 4

The MN 3/MN 4 boundary is recognised by the FO of *Democricetodon* which is assumed to be more or less contemporanous with the entry of the mastodonts in Europe (Mein, 1990; Bulot, 1988). The age of the MN 3/MN 4 (Ramblian/Aragonian) boundary is still ambiguous (Van der Meulen and Daams, 1992; Steininger et al., 1990). For the MN 4/MN 5 boundary an accurate age of 14.1 Ma is now found (table 1). This is in large contrast with Steininger et al. (1990) who place this boundary at 17.0 Ma, based on indirect correlations with marine biostratigraphy. Our results indicate a significantly longer duration of the MN 4 zone of approximately 3 Myr (= ca. 350%). Indeed, a longer duration of MN 4 much better explains the many important changes in the continental faunal record during the early Aragonian. In the Aragonian type area MN 4 is bdivided in six local zones, significantly more than MN 5 (one), MN 6 (three) and MN 7-8 (one) (Van der Meulen and Daams, 1992).

In the Aragon section only two local zones (Dc and Dd) are present which correspond to MN 4. The Dc/Dd boundary occurs in chron C5ADn and has an age of 14.3 Ma. Additional information on the other local zones is provided by the Armantes section where the locality Armantes 1 (=zone Db) is magnetostratigraphically dated at 16.0 Ma. The large difference in age between Db and Dc of 1.2 Myr, agrees with the rather drastic change in fauna between Db and Dc and indicates that the time interval between 16.0 and 14.8 Ma is not represented in the fossil record.

Middle Miocene climate change: MN 5

The principal component analyses on the faunal record of the Aragonian type area have been interpreted using individual rodent taxa as environmental indicators (Van der Meulen and Daams, 1992). The result is an important cooling

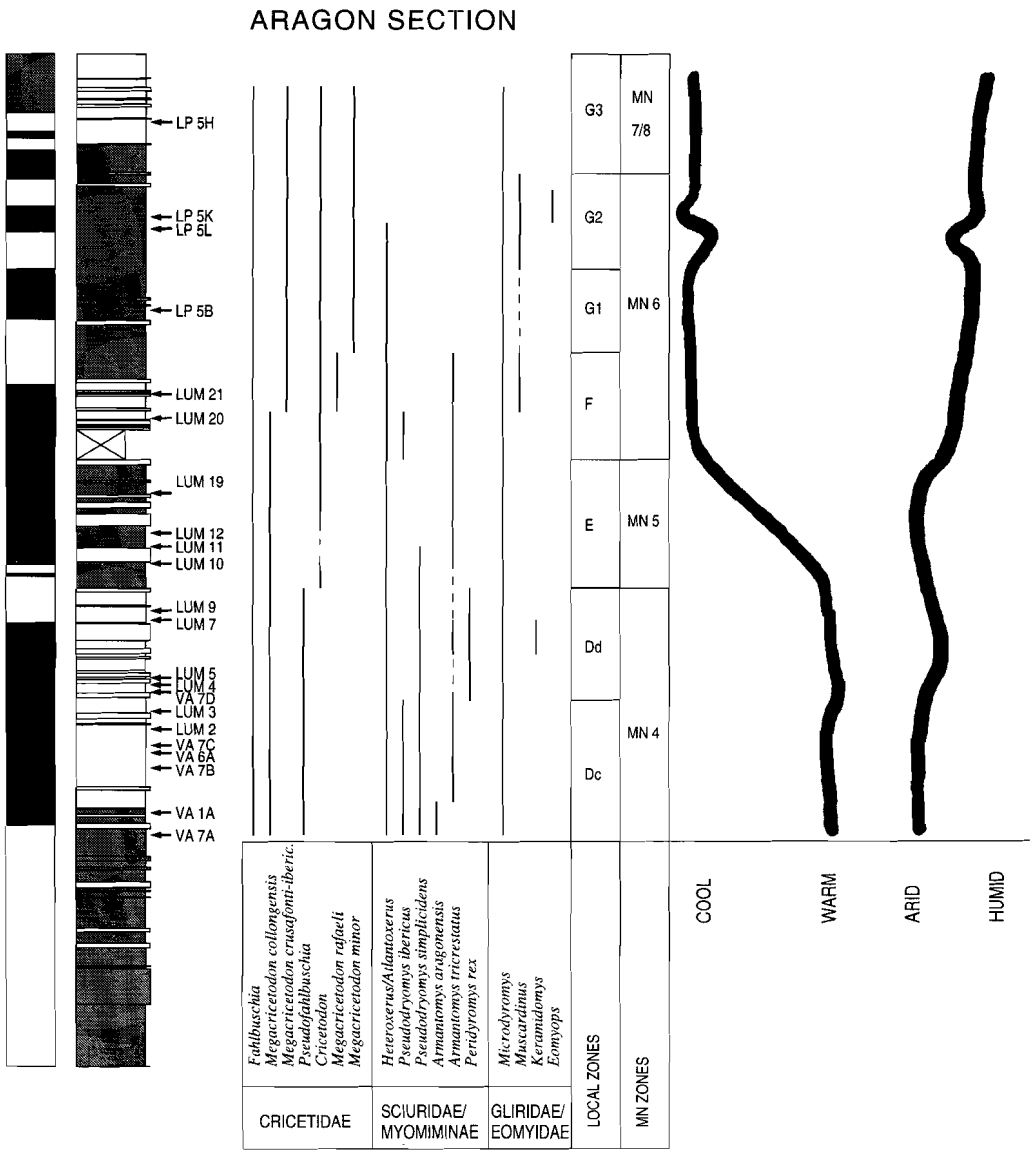

Figure 7. Biostratigraphy and local biozonations (Dc to G3) of the Aragon section and corresponding MN zones. For the magnetostratigraphy and lithology column see also caption to Figure 2. Arrows denote fossil localities (VA = Valdemoros, LUM = Las Umbrias and LP = Las Planas). Relative temperature and humidity curves are from Van der Meulen and Daams (1992).

event during zone E (MN 5). This cooling phase is assumed to have taken place on the basis of decreasing proportions of *Fahlbuschia*, which is considered as a high temperature proxy. In Zone F, *Fahlbuschia* has dropped to very low percentages representing the lowest temperatures (Fig. 7).

The onset of this cooling event can thus be dated to occur in chron C5ACr, at 14.1 Ma, corresponding to the lower boundary of MN 5. The MN 5/MN 6 boundary is dated in chron C5ACn at 13.8-13.9 Ma which indicates that the cooling event has a duration of approximately 300 kyr. The age of 14.1 Ma is identical to the most recent datings of the climatic changes (cooling) in the paleoceanographic record: Flower and Kennett (1993) showed that the major increase in $\delta^{18}O$ in foraminiferal tests, related to major ice sheet growth on Antarctica, had occurred between 14.1 and 14.05 Ma. We conclude that a major cooling event has taken place in the middle Miocene at 14.1 Ma both in the marine and the continental environment, indicating the global importance of this event.

Upper Aragonian: MN 6

Sofar, there has been no accurate dating of the MN 5/MN 6 boundary, which is placed somewhere between 16 and 15 Ma (Steininger et al., 1990). The MN 5/MN 6 boundary is by definition the Orleanian/Astaracian and also the local Aragonian E/F boundary. MN 6 comprises three local zones F, G1 and G2, which are well-defined in the Aragon type section. Our correlation results in a position of the MN 5/MN 6 boundary in chron C5ACn at 13.8-13.9 Ma (table 1). Furthermore, the local zone boundaries F/G1 and G1/G2 are found in chron C5ABr (13.5-13.7) and in the interval C5AAr-C5ABn (13.1-13.5 Ma), respectively.

The paleomagnetic results from the uppermost part of the Aragon as well as the Armantes section are less reliable and zones can either not be defined or by only a few, or even one sample level(s) (Figs. 2,3). The MN 6/MN 7-8 boundary was previously positioned at 13.8 Ma (Steininger et al., 1990). Our results from the Aragon section show that this boundary occurs somewhere in the interval C5Ar.1n-C5Ar.3r (12.7-13.0 Ma). Since there is no clear evidence that the Vallesian has been reached, we are restricted to use the somewhat controversial age of 11.5 Ma for the MN 7-8 /MN 9 and hence the Aragonian/Vallesian boundary, based on the possibly diachronous FA of *Hipparion* (Steininger et al.; Sen, 1990).

Conclusions

We have established detailed magnetostratigraphic records for two mammal-bearing continental sections of middle Miocene age in the type area of the Aragonian Stage. The polarity sequence of the Armantes section, with twenty-five polarity intervals, allows an unambiguous correlation to the GPTS (Cande

and Kent, 1995). Combining the magnetostratigraphy from the time-equivalent Aragon section with its dense biostratigraphic record results in the correlation of three successive Neogene Mammal (MN) Zone boundaries and six local Aragonian Zone boundaries to the GPTS.

Our correlations implie that the MN 4/MN 5 boundary occurs in the normal chron C5ACr, resulting in an age of 14.1 Ma. Multivariate analyses of the faunal record of the Aragonian indicate that an important climatic change has occurred during the MN 5 zone (Van der Meulen and Daams, 1992). Hence, the onset of this climatic cooling is dated at 14.1 Ma, which is in excellent agreement with the 14.1-14.05 Ma for the major increase in $\delta^{18}O$ in the marine record (Flower and Kennett, 1993). Van der Meulen and Daams (1992) suggest that during MN 5 the climate changed to a cooler and in MN 6 to a more humid climate, while the main increase in $\delta^{18}O$ is considered to be the result of ice-sheet growth on Antarctica. These independent observations of a time-equivalent climate change in both marine and continental records confirm the existence of a cooling event of global importance in the middle-Miocene.

The new age for the MN 4/MN 5 boundary is significantly younger than assumed in the previous conventional time scales (Berggren et al., 1985; Steininger et al., 1990) and indicates a much longer duration (by 3 Myr) of the MN 4 Zone. This is consistent with the many important faunal changes occuring in MN 4, in which six local Aragonian Zones are present. Finally, new ages are derived for the MN 5/MN 6 and the MN 6/MN 7-8 boundaries (table 1).

Acknowledgements

We thank Ton van Hoof, Jan van Dam, Hans Zijderveld and especially François Lévèque for their help in the field; Mark Dekkers and Hans de Bruijn for useful discussions. We greatfully acknowledge the constructive comments of W.A. Berggren and two anonymous reviewers. This study was supported by The Netherlands Geosciences Foundation (GOA/NWO). The paleontologists gratefully acknowledge financial support of the Commission of the European Communities, JOULE programme (1989-1992) of the DGCYT, project No. PB92-0013.

Chapter 7

A new chronology for the middle to late Miocene continental record in Spain

Abstract

The first detailed chronology for the middle to late Miocene continental record in Spain is presented, based on dense biostratigraphic and high-resolution magnetostratigraphic data of mammal-bearing sections which were studied in several basins (Calatayud-Daroca, Teruel, Vallès-Penedès, Duero and Júcar-Cabriel). Our results indicate that these sections compose an almost complete magnetostratigraphic succession from the lower Aragonian (MN 4) to the middle Turolian (MN 12). Seven successive Mammal Neogene (MN) zone boundaries are directly dated in these sections which often contain faunas of two successive zones in superposition. The three oldest boundaries are dated in the Aragonian type area (Calatayud-Daroca basin). The MN 4/MN 5 boundary (Vargas section) occurs in chron C5Cr(o) with a corresponding age of 17.26 ± 0.01 Ma, the MN 5/MN 6 boundary (Aragon section) in chron C5ACn(0.8) with an age of 13.75 ± 0.03 Ma and the MN 6/MN 7-8 boundary (Aragon section) in the interval C5Ar.1n-C5Ar.3r with an age of 12.75 ± 0.25 Ma. The MN 7-8/MN 9 (Aragonian/Vallesian) boundary, occurring in chron C5r.1n at 11.1 Ma, and the MN 9/MN 10 boundary, in chron C4Ar.3r at 9.7 ± 0.1 Ma, are recorded in the Vallès-Penèdes basin (Vallesian type area) and are supported by the results from the Duero basin (Torremormojón section). In the Turolian type area (Teruel basin), the MN 10/MN 11 (Vallesian/Turolian) boundary (La Gloria section) occurs in chron C4An(y) at 8.70 ± 0.01 Ma. Taking into account the pre-existing data from the Júcar-Cabriel basin, the MN 11/MN 12 boundary (Cabriel Valley section) is recalibrated to C4n.1n at an age of 7.5 ± 0.1 Ma.

This chapter has been accepted for publication as: W. Krijgsman, M. Garcés, C.G. Langereis, R. Daams, J. van Dam, A.J. van der Meulen, J. Agustí and L. Cabrera, A new chronology for the middle to Late Miocene continental record in Spain, *Earth Planet. Sci. Lett.*, 1996.

Introduction

The continental biostratigraphic time scale for the European Miocene still lacks a reliable chronological framework. Correlation of Mammal Neogene (MN) zones - with corresponding faunal assemblages and significant bioevents - to the absolute time scale is mainly based on correlation with marine biostratigraphy and regional zonation (e.g. Paratethys Stages; Steininger et al., 1990). Radiometric dating of intercalated volcanic sediments is rare and nearly always requires extrapolation over a large stratigraphic interval to the position of the fossil

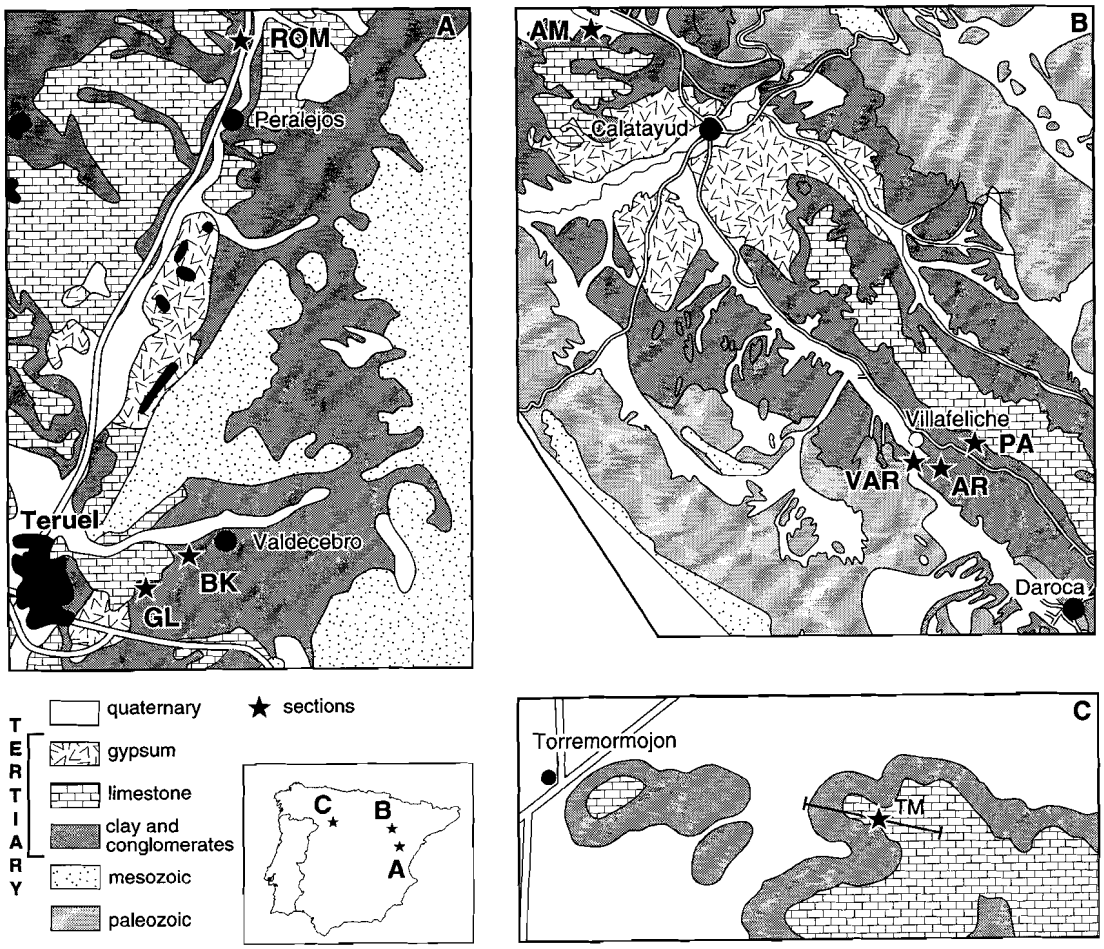

Figure 1. : Locations of the sections in the Calatayud-Daroca basin (A), Teruel basin (B) and Duero basin (C). AM = Armantes, AR = Aragon, VAR = Vargas, PA = Paje, ROM = La Roma, GL = La Gloria, BK = EL Bunker, TM = Torremormojón (road C612). For locations of sections in the Vallès-Penedès basin one is referred to Garcés (1995); for the Cabriel Valley section in the Júcar-Cabriel basin to (Opdyke et al. (1990).

locality. Magnetostratigraphy of long, continuous non-marine sequences has been proposed as an alternative to these approaches, but magnetostratigraphic studies of continental deposits are often thought to be hampered by the abundance of hiatuses and (unknown) changes of sediment-ation rates and the scarcity of long continuous outcrops. The comparison of continental fossil localities or regional continental zonations and the marine time scale remains ambiguous if there are no reliable age determinations. It follows that ages of Continental Stage and MN zone boundaries should preferably be determined in single sections which comprise as many as possible fossil-mammal faunas in superposition. For the European Miocene, direct magnetostratigraphic dating of such stage boundary sections have recently been established in Spain (Opdyke et al., 1990; Barbera et al., 1994; Krijgsman et al., 1994b; Garcés, 1995; Garcés et al., 1996). Good magnetostratigraphic results were also obtained from the Siwaliks in Pakistan (Johnson et al., 1982; Tauxe et al., 1982) and from the Kastellios Hill section of Central Crete (Sen et al., 1986).

In this paper, we present the magnetostratigraphic results of our middle to late Miocene sections from Spain and their correlation to the geomagnetic polarity time scale (GPTS). On this basis, we establish a detailed biochronology for the middle to late Miocene continental record in Spain. A well-dated chronostratigraphic framework for the continental biostratigraphy allows correlation to the marine biostratigraphy and the stable isotope records. Furthermore, paleoclimatological and paleoenvironmental changes on land can be compared to those from the marine realm. In earlier studies, the Aragonian faunal record showed an important climatic change to a cooler and more humid climate during the middle Miocene MN 5 zone (Van der Meulen and Daams, 1992). Magnetostratigraphic dating indicated this cooling event to occur at 14.1 Ma (Krijgsman et al., 1994b), and correlation to the marine record showed a time-equivalent increase in $\delta^{18}O$ (Flower and Kennett, 1993). Accurate and high-resolution dating thus provides evidence for (global) climatic events.

Geological setting and research strategy

Thick non-marine (alluvial and lacustrine) Miocene sequences in Spain were deposited as a consequence of the tectonic evolution of the Iberian plate (Anadón et al., 1989; Calvo et al., 1993) which resulted in a variety of tectonic settings (i.e., extensional half-grabens, compressional and strike-slip fault bounded basins, and foreland peripheral basins linked to the major thrust-fold belts). Some of these tectonically influenced, thick basin infills include stratigraphic sequences which fit quite well the conditions necessary to carry out high-resolution paleomagnetic studies.

To establish a high-resolution magneto-biochronology for the middle to late Miocene, the Calatayud-Daroca and Teruel basins of central Spain are among the most favourable areas because of their detailed fossil record and their long,

continuous sections. These basins comprise the type localities of the Ramblian (Daams et al., 1987), the Aragonian (Daams et al., 1977) and the Turolian (Crusafont, 1965; Marks, 1971). We selected several suitable sections for a new, complementary magnetostratigraphic study and we added biostratigraphic sampling where necessary. Biostratigraphic results indicate that our sections in the Calatayud-Daroca and Teruel basins range from the early to late Aragonian and from the late Vallesian to middle Turolian. In these basins, the lower Vallesian is mainly represented by isolated localities and suitable continuous sections are not found. Late Aragonian and Vallesian faunal assemblages in a continuous stratigraphic succession are known from the Vallès-Penedès basin (NE Spain), the type area of the Vallesian (Crusafont, 1951), and from the Duero basin (W Spain) (López et al., 1987; Garcia, 1987). For establishing the chronology of the Vallesian, we incorporated the magnetostratigraphic and biostratigraphic results from sections in the western Vallès area (Vallès-Penedès half graben) (Garcés, 1995) and carried out a magnetostratigraphic study on the Torremormojón section (Duero foreland basin). Both the Aragonian/Vallesian (MN 8/MN 9) and the lower to upper Vallesian boundaries are present in these sections.

To complete the upper part of the stratigraphic range of late Miocene sequences, a previous magnetostratigraphic study in central Spain by Opdyke et al. (1990) on the late Turolian Cabriel Valley section (Júcar-Cabriel basin) is also incorporated into the final chronology.

New sections and sampling

Earlier biostratigraphic and magnetostratigraphic work on the middle to late Miocene sequences in Spain provided a chronological framework for a large part of the Aragonian (middle Miocene) (Krijgsman et al., 1994b) and, recently, also for the Vallesian (late Miocene) (Garcés, 1995). To complete these earlier contributions and to extend our chronology to most of the middle and late Miocene, it was necessary to study new sections in the Calatayud-Daroca (Vargas and Paje sections), Teruel (La Roma, La Gloria and El Bunker sections) and Duero (Torremormojón section) basins.

The Aragonian type area is located in the Calatayud-Daroca basin of central Spain near the village of Villafeliche (Fig. 1) (Daams et al., 1977). An earlier study showed good paleomagnetic results for the Armantes and Aragon sections which range biostratigraphically from MN 5 (former MN 4b) to MN 7-8 (Krijgsman et al., 1994b). The new MN 4/MN 5 boundary is determined in the Vargas section, situated approximately 500 m west of the Aragon section (Fig. 1, 2). The Vargas section consists of the same type of sediments as in the Aragon section; red and multi-coloured silts and clays and greyish-white marly limestones which are deposited in distal alluvial and palustrine-lacustrine paleoenvironments.

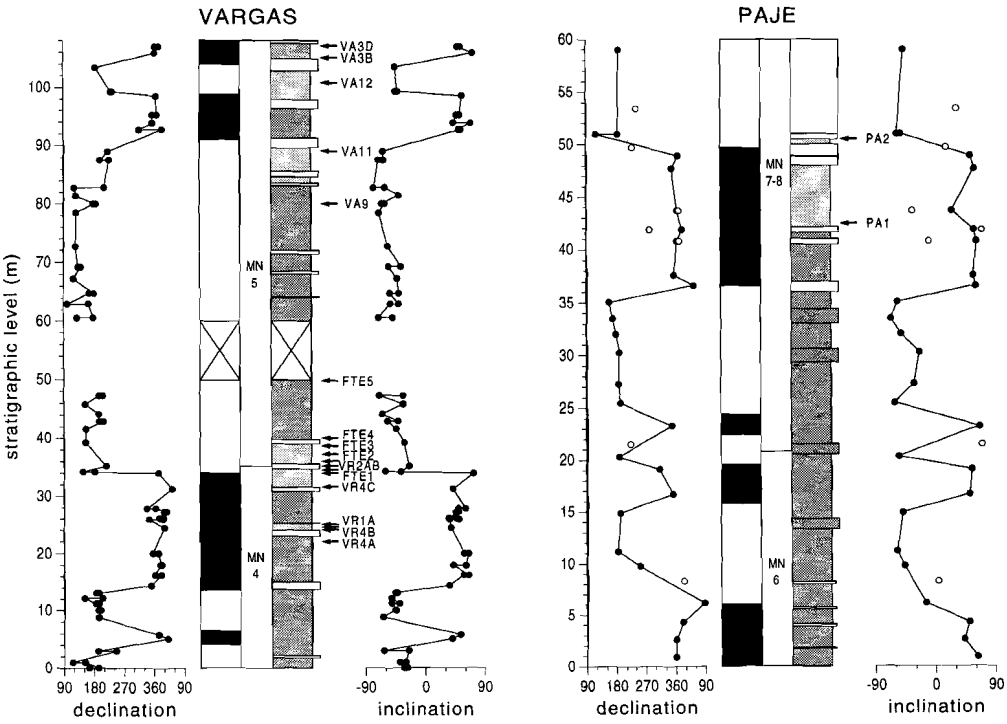

Figure 2. : Polarity zones, MN zonation and lithology of the Vargas and Paje sections (Calatayud-Daroca basin). Arrows indicate positions of fossil localities. VR = Vargas, FTE = Fuente Sierra en nog wat, VA = Valdemoros, PA = Paje. In the polarity column black (white) denotes normal (reversed) polarity interval. Closed (open) symbols denote reliable (unreliable) directions. The MN 4/MN 5 boundary is determined between localities FTE1 and FTE2. The MN 6/MN 7-8 boundary is after the Aragon section (Krijgsman et al. (1994b). The lithology column displays variations of reddish and multi-coloured silts and marls (dark shaded), greyish marls (shaded) and limestones (white).

The magnetostratigraphic results for the top of the Aragon section were hampered by the scarcity of suitable lithologies (Krijgsman et al., 1994b). In the Paje section, 500 m southeast of the top of the Aragon section (Fig. 1), reddish silts which were earlier shown to have good paleomagnetic properties, are continuously exposed and reach higher levels than in the Aragon section. The reddish fluviatile and lacustrine sediments in the Paje section are capped by a thick formation of alternating white-grey marls and white lacustrine limestones (Fig. 2). Two new fossil localities (MN 7-8) are present in the limestone unit at a higher stratigraphic position than the youngest locality in the Aragon section.

The Torremormojón section, located in the Duero Basin (Fig. 1) comprises a biostratigraphic succession ranging from late Aragonian (MN 7-8) to late Vallesian (MN 10) and incorporates the MN 7-8/MN 9 (Aragonian/Vallesian)

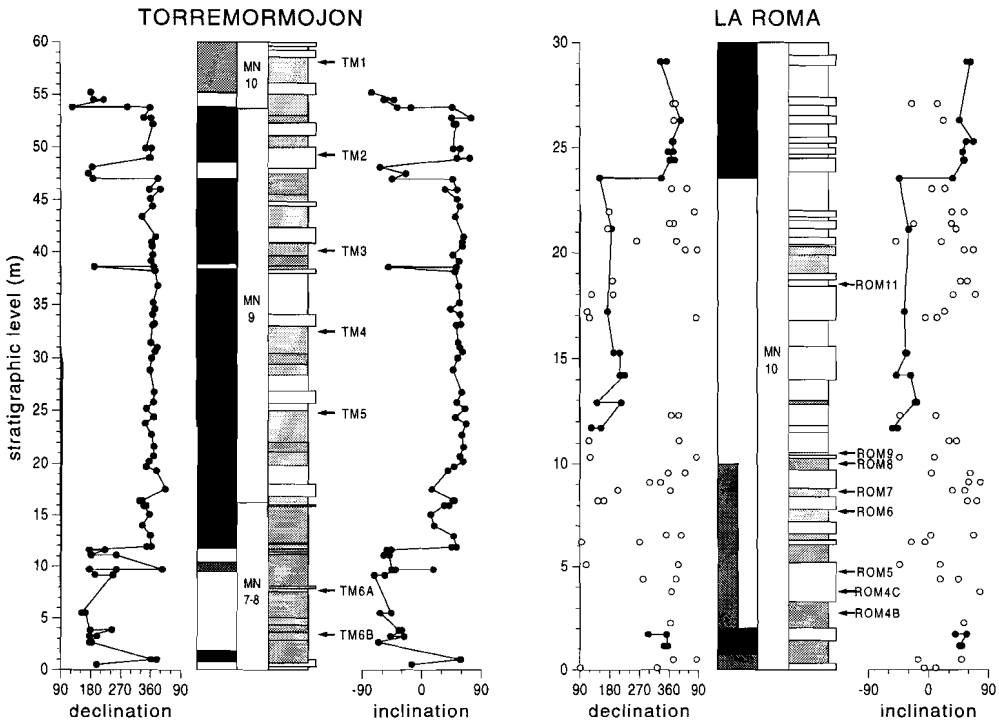

Figure 3. : Polarity zones, MN zonation and lithology of the Torremormojón (Duero basin) and La Roma (Teruel basin) sections. TM = Torremormojón, ROM = La Roma. The MN 7-8/MN 9 boundary is determined between localities TM6a and TM5, the MN 9/MN 10 boundary between TM2 ans TM1. See also captions to figure 2.

boundary and the MN 9/MN 10 boundary (Alvarez Sierra et al., 1990). This study is complementary to those of the Vallesian sequences in the Vallès-Penedès basin (Garcés, 1995). Earlier studies in Torremormojón investigated micromammals (López and Sanchiz, 1982; Alvarez Sierra, 1983; Garcia, 1983), pollen (Rivas and Valle, 1986), gastropods, ostracods and foraminifera (González et al., 1986). The lower part of the Torremormojón section (0-18 m) predominantly consists of ocre-coloured detrital sediments (clays and silts) alternating with white-grey marls and limestones (Fig. 3). In the upper part of the section, white limestones dominate and ocre-coloured sediments are rare. The approximately 60-m thick section comprises seven well-described fossil localities which are mainly found in dark-grey marls with abundant gastropods (Fig. 3; Garcia, 1983).

The type area of the Turolian is the Los Mansuetos area (Teruel Basin), located east of the town of Teruel (Fig. 1; Crusafont, 1965; Marks, 1971). The La Roma section contains eight MN 10 localities in superposition (Fig. 3). The section consists of white marls and limestones which are well-bedded and contain

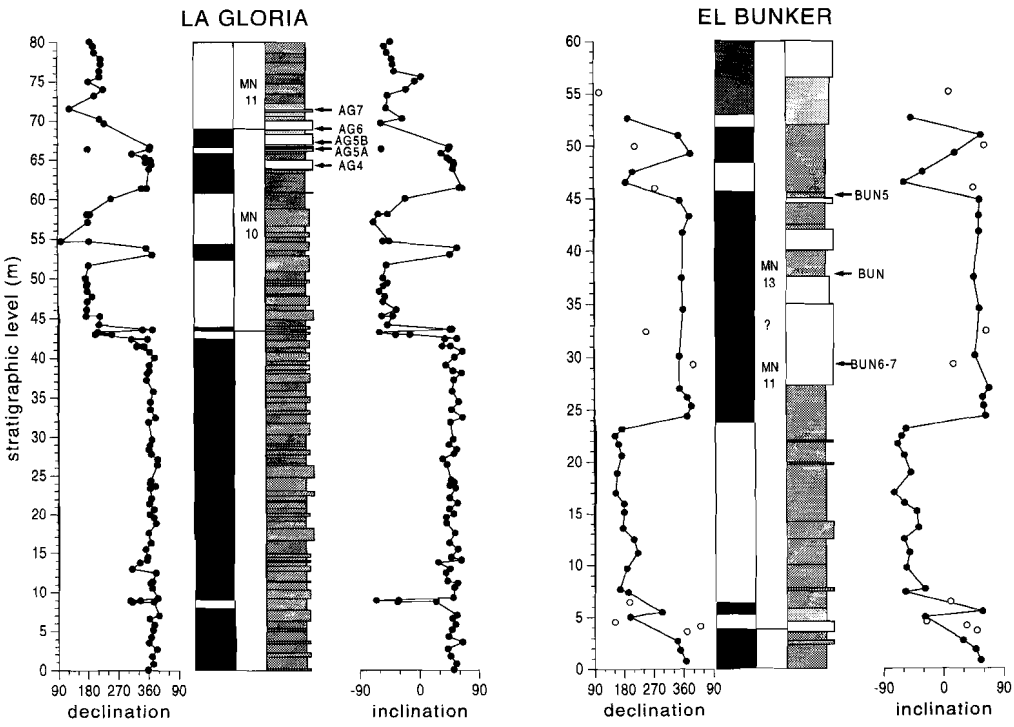

Figure 4. : Polarity zones, MN zonation and lithology of the La Gloria and El Bunker sections. AG = Los Aguanaces, BUN = El Bunker. The MN 10/MN 11 boundary is determined between fossil localities AG5b and AG7. See also captions to figures 2 and 3.

intercalations of dark-grey lignitic marls. The La Gloria and El Bunker sections (Fig. 4) mainly consist of red silty clays with intercalations of red sands, conglomerates (channel fills) and white lacustrine limestones. The regular alternation of dark red silty clays with lighter-coloured more calcareous silts, similar to that observed in the Armantes section (Krijgsman et al., 1994b), suggests a relation with astronomically induced cyclic climate changes. In the upper part of the sections white limestones are intercalated, which appeared to be favourable for fossil preservation and contain several levels with micromammal assemblages (Fig. 4). The Vallesian/Turolian boundary is located in the thick limestone unit of the La Gloria section. The base of the El Bunker section is equivalent with the top of the La Gloria section, but the middle and upper parts of the El Bunker section extend to higher stratigraphic levels and contain MN 11 and MN 13 localities (Fig. 4).

The magnetostratigraphic samples were taken by drilling oriented paleomagnetic cores with an electric drill and a generator as power supply, using water as a coolant. Considerable efforts were taken to remove the weathered

surface and to sample in sediments as fresh as possible. If the lithology was unsuitable for drilling with water, we took standard oriented handsamples which were drilled with compressed air in the laboratory.

The micromammal samples were dried and washed, and the residues were picked with a microscope for fossil remains. The biochronology we use is after De Bruijn et al. (1992) with the exception that we follow the decision reached in Salzburg (March 1995) to extend unit MN 5 downwards to include former sub-unit MN 4b (Mein, 1990).

Paleomagnetic results

At least one specimen per sampling level was progressively demagnetised by applying stepwise heating with small (40 °C) temperature increments in a laboratory built, shielded furnace. The thermal demagnetisation process was initiated by heating the samples to 100 °C to remove a randomly directed viscous component which was previously shown to be present in the continental sediments of central Spain (Krijgsman et al., 1994b). After each temperature step, the natural remanent magnetisation (NRM) was measured on a 2G Enterprises DC SQUID cryogenic magnetometer. Furthermore, we performed some rock magnetic analyses on selected samples from the Torremormojón and Gloria sections to identify the carriers of the NRM components. These experiments include acquisition of an isothermal remanent magnetisation (IRM) on a PM 4 pulse magnetiser and subsequent thermal demagnetisation of this IRM. Low field susceptibilities were measured after each temperature step on a Kappabridge KLY-2.

The widely varying lithologies in the sections nearly all give good paleomagnetic results. The silts and clays show relatively high characteristic remanent magnetisation (ChRM) intensities (0.1-10 A/m) and initial susceptibilities (50-1000 x 10^{-6} SI). Demagnetisation diagrams are of good quality and reveal stable ChRM components which show a linear decay to the origin during thermal demagnetisation (Fig. 5). A secondary normal present-day field component was totally removed at 200-240 °C; the ChRM component was usually largely removed at 600 °C, although in most samples some magnetic component remained up to temperatures of 680 °C. IRM-acquisition and subsequent demagnetisation indicate that hematite and magnetite are the dominant carriers of the magnetisation, but goethite is often also present (Fig. 6). The whitish limestones show much lower ChRM intensities (0.01-0.1 A/m) and susceptibilities (0-100 x 10^{-6} SI). Demagnetisation diagrams are difficult to interpret and in some cases, it was even not possible to determine the polarity.

Both normal and reversed components are revealed in all sections which demonstrates a primary origin of the magnetic components. At the intervals of the section in which the polarity changes, some specimens show a more complex thermal behaviour. Between temperatures of 240 °C and 600 °C, these samples

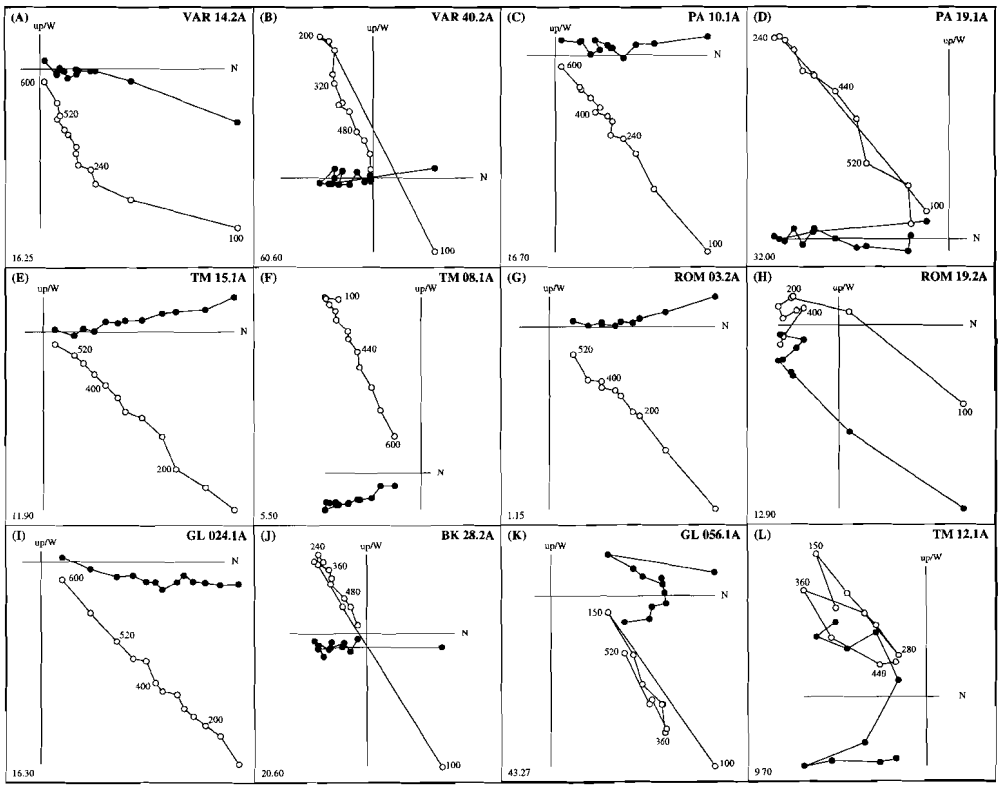

Figure 5. : Thermal demagnetisation diagrams for samples from the new studied sections in the Calatayud-Daroca, Teruel and Duero basins. Closed (open) symbols represent the projection of the vector end-points on the horizontal (vertical) plane; values represent temperatures in °C; stratigraphic levels are in the lower left-hand corner. (K) and (L) are examples showing demagnetisation of two components between temperatures of 150-600 °C. We believe that in these cases an early diagenetic component partly overprints the earlier acquired component.

show both a normal and a reversed component (Fig. 5k,l). We believe that in these cases early diagenetic processes cause a delayed acquisition and a (partial) overprint of the original (earlier acquired) component. Hence, the direction of the following (younger) polarity interval will overprint the original direction of the studied level. Diagenetic processes might also cause an overprint of the smallest subchrons and cryptochrons.

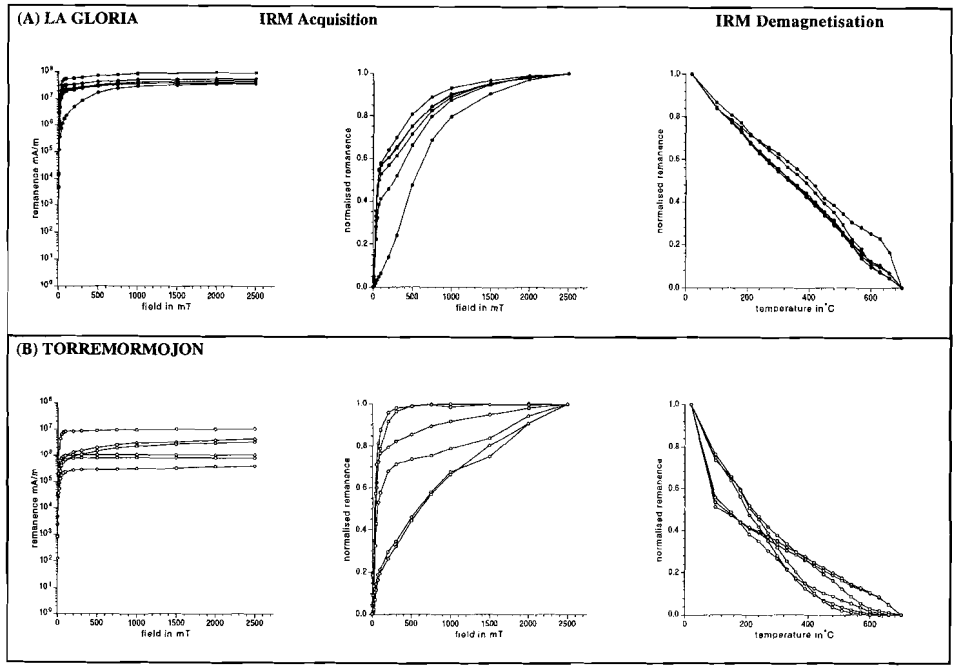

Figure 6. : Examples of IRM acquisition (absolute and normalised values) of samples of the La Gloria (A) and Torremormojón (B) sections. The initial steep rise (< 200 mT) points to magnetite, the gradual increase at high fields (> 200 mT) suggests the additional presence of hematite. Stepwise thermal demagnetisation of the normalised IRM also show the presence of both magnetite (580 °C) and hematite (680 °C).

Correlation to the GPTS

The new data resulting from this work, together with those from earlier contributions (Opdyke et al., 1990; Krijgsman et al., 1994b; Garcés, 1995), allow the correlation of the polarity sequences of all studied sections to CK95, the GPTS of Cande and Kent (1995). Some of the previous correlations are confirmed or refined. The magnetostratigraphic results from the Armantes and Aragon sections showed unambiguous correlations to CK95 (Fig. 7; Krijgsman et al., 1994b). The top of the Vargas section is biostratigraphically correlated with fossil locality AM 1 of the Armantes section. Hence, the upper two normal polarity intervals of the Vargas section correlate to chrons C5Cn.2n and C5Cn.3n. The large normal polarity interval in the lower part of the section correlates to chron C5Dn (Fig. 7). The small normal polarity interval, represented by only two levels, most likely corresponds to the so-called cryptochron C5Dr-1, also recorded in CK95. The MN4/MN5 boundary is determined in the reversed interval C5Cr

(Table 1). The successive two MN zone boundaries are determined in the Aragon section; MN5/MN6 at C5ACn(0.8) and MN6/MN7-8 in the interval C5Ar.1n-C5Ar.3n. The position of the MN5/MN6 boundary slightly differs from in our earlier work: it is now more precisely determined between localities LUM 20 and LUM 21 (Krijgsman et al., 1994b).

The Paje section is time-equivalent to the top of the Aragon section and the fossil localities Paje 1 and 2 are biostratigraphically younger than LP5H, the youngest fossil locality of the Aragon section (Krijgsman et al., 1994b). The most likely correlation to CK95 is that the normal polarity interval at the base of the section corresponds to chron C5AAn and that the normal polarity interval at the top of the section correspond to chron C5An.2n (Fig. 7).

The upper alluvial successions in the Les Fonts-Montagut sections (Vallès-Penedès half graben) record a complete sequence of Vallesian mammal assemblages. Ages of MN 9 and MN 10 units are based on biostratigraphic and magnetostratigraphic correlation of four composite sections showing stratigraphic superposition of biozones (Garcés, 1995). The observed reversal pattern allows an unambiguous correlation to the GPTS, mainly based on the presence of the long distinctive normal chron C5n. The MN 7-8/MN 9 and MN 9/MN 10 boundaries are determined in chrons C5r.1n and C4Ar.3r, respectively.

The major part of the Torremormojón section (Duero basin) shows predominantly normal polarities, which suggests a correlation to the long normal chron C5n.2n. The lowermost two short normal polarity intervals might then correlate to C5r.1n and C5r.2n. One level in the long normal part of the section shows a reversed polarity. This level probably corresponds to a cryptochron of chron C5n.2n; assuming a constant sedimentation rate, the most likely one is C5n.2n-1. No other cryptochrons are recorded, probably because of a low sampling density. Our correlation of the Torremormojon polarity sequence to CK95 indicates a duration of 2 Myr and a sample resolution of approximately 30 kyr. Since the duration of all these cryptochrons is shorter than 20 kyr, it is not surprising that they are not all recognised in our magnetostratigraphy. The MN7-8/MN9 - Aragonian/Vallesian - boundary is located between C5r.2r (TM 6a) and C5n.2n (TM 5). The MN9/MN10 boundary is determined between C5n.1n (TM 2) and C4Ar.2n (TM 1).

The La Gloria section (Teruel basin) also contains a long interval of normal polarity which is correlative with chron C5n.2n. The uppermost normal interval then most likely corresponds to C4An, which implies that chron C4Ar.1n was probably missed under our density of magnetostratigraphic samples. This correlation indicates a duration of 2.4 Myr and a sample resolution of approximately 24 kyr for the La Gloria section. A possible cryptochron is recorded in the lower part of the section (chron C5n.2n). The polarity intervals correlative to the subchrons C4Ar.2n and C5n.1n are partly or totally overprinted by a later, oppositely directed, magnetic component. The MN10/MN11 - Vallesian/Turolian - boundary occurs between localities AG5b and AG7 and is therefore placed in CK95 at the top of chron C4An.

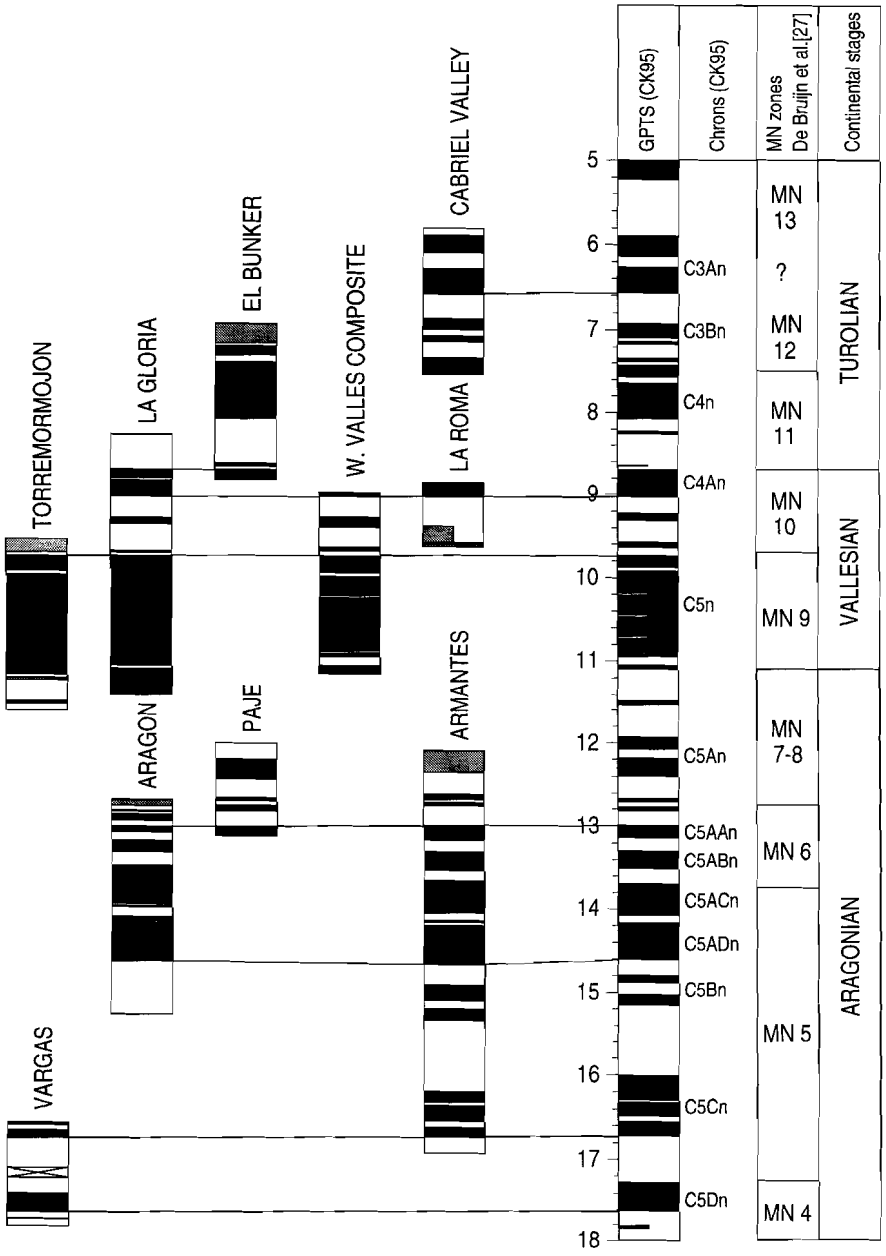
TORREMORMOJON
LA GLORIA
EL BUNKER
W. VALLES COMPOSITE
CABRIEL VALLEY
LA ROMA
ARAGON
PAJE
ARMANTES
VARGAS
GPTS (CK95)
Chrons (CK95)
MN zones De Bruijn et al.[27]
Continental stages
5
6
7
8
9
10
11
12
13
14
15
16
17
18
C3An
C3Bn
C4n
C4An
C5n
C5An
C5AAn
C5ABn
C5ACn
C5ADn
C5Bn
C5Cn
C5Dn
MN 13
?
MN 12
MN 11
MN 10
MN 9
MN 7-8
MN 6
MN 5
MN 4
TUROLIAN
VALLESIAN
ARAGONIAN

zone boundary	basin	section	chron (CK95)	age in (Ma)
MN11/MN12	Jucar-Cabriel	Cabriel Valley	C4n.1n	7.5 ± 0.1
MN10/MN11	Teruel	La Gloria	C4An(y)	8.7 ± 0.1
MN9/MN10	Valles-Penedes	Montagut	C4Ar.3r	9.7 ± 0.1
MN7-8/MN9	Valles-Penedes	Montagut	C5r.1n	11.1
MN6/MN7-8	Calatayud-Daroca	Aragon	C5Ar.1n-C5Ar.3i	12.5-13.0
MN5/MN6	Calatayud-Daroca	Aragon	C5ACn(0.8)	13.75 ± 0.03
MN4/MN5	Calatayud-Daroca	Vargas	C5Cr(o)	17.26 ± 0.01

Table 1. : Positions (or ranges) in the boundary sections of MN zone boundaries and their ages with respect to the GPTS [29]. Decimal fraction denotes position within a (sub)chron as taken from the younger end.

The results from the partly overlapping El Bunker section (Teruel basin) are in agreement with the polarity pattern of the La Gloria section. Hence, the normal polarity base of the El Bunker section correlates to C4An, the second normal interval most likely to C4n.2n. The results from the upper part of the section are difficult to interpret, probably because of large changes in sedimentation rate and major hiatuses which are suggested by the observation of MN13 faunas at the top of the section.

The La Roma section (Teruel Basin) contains only MN 10 faunas and its predominantly reversed polarities suggest a correlation to chron C4Ar (Fig. 7). The length of the upper normal interval indicates that the best correlation is to chron C4An which means that chron C4Ar.1n is not recorded in the low-intensity middle part of the section.

A previous magnetostratigraphic study in Central Spain by Opdyke et al. (1990) concerns the late Turolian Cabriel Valley section (Júcar-Cabriel basin) with the MN12 fossil locality Fuente Podrida (Mein et al., 1978) at the base. Furthermore, the MN11 locality Balneario is located 300 m to the east and estimated to be roughly 10 m stratigraphically lower (Opdyke et al., 1990). Even if unambiguous, it gives a constraint for the position of the MN11/MN12 boundary. Because this MN boundary is not defined in our sections we

Figure 7. : Correlation of the polarity sequences of the spanish sections to the GPTS of Cande and Kent [29]. Lines connect corresponding reversal boundaries. Right-hand columns display mammalian zones and stages. Ages of the zone and stage boundaries are from this study (Table 1).

incorporate the magnetostratigaraphic results of the Cabriel Valley section and recalibrate the polarity pattern to CK95 (Fig. 7), whereas the former calibration was to the GPTS of Berggren et al. (1985). Our new correlation of the MN11/MN12 boundary is to chron C4n.1n.

Chronology

The new magnetostratigraphic and biochronological data presented in this paper and those available from earlier (Opdyke et al., 1990; Krijgsman et al., 1994b) and more recent (Garcés, 1995) contributions enable the establishment of a chronological framework for the middle to late Miocene non-marine record in Spain.

Aragonian (MN 4 - MN 7-8)

The base of the Aragonian (MN 3/MN 4) is defined by the first appearance of the cricetid *Democricetodon* in central and western Europe (Daams et al., 1987). The oldest MN zone boundary found in our sections is the recently revised MN 4/MN 5 boundary, documented in the Vargas section and correlated to chron C5Cr. Our correlation results in an age of 17.26 ± 0.01 Ma, which is so far the only date on this newly defined boundary. The previous magnetostratigraphic dating of the MN 4/MN 5 boundary in the Aragon section, resulting in an age of 14.1 Ma, was based on the older biostratigraphic definition (Krijgsman et al., 1994b). The time-equivalent onset of a global mid-Miocene cooling event at 14.1 Ma should now be placed in the upper part of zone MN 5.

For the MN 5/MN 6 boundary, by definition the middle/late Aragonian and Orleanian/Astaracian boundary (Mein, 1975), no new magnetostratigraphic data are obtained. The earlier results from the Aragon section (Krijgsman et al., 1994b) show that the MN 5/MN 6 boundary is located in chron C5ACn with a corresponding age of 13.75 ± 0.03 Ma. Also for the MN 6/MN 7-8 boundary, we incorporate the results from the Aragon section which show that the boundary occurs somewhere in the interval C5Ar.1n-C5Ar.3r with an age of 12.5-13.0 Ma (Krijgsman et al., 1994b).

Vallesian (MN 9 and MN 10)

The lower Vallesian boundary was defined by Crusafont (1951) as the first appearance datum (FAD) of the equid *Hipparion* in western Europe. This FAD of *Hipparion* (or the "*Hipparion* datum") was originally assumed to be a synchronous event (Berggren and Van Couvering, 1974; 1978). This assumption was questioned by Sen (1990), who stated that ecological and paleogeographical factors had not been taken into account and suggested the *Hipparion* datum to be

a diachronous event. So far, however, neither synchrony or diachrony of the *Hipparion* datum has been proven because of the lack of reliable chronological data and limits of biostratigraphic resolution of large mammal faunas.

The main arguments for the assumed diachrony of the *Hipparion* event were related to radiometric dating from sites in Germany (Höwenegg) and Algeria (Bou Hanifia). The Höwenegg locality yielded two radiometric datings; 12.4 ± 1 Ma on hornblende (Lippolt et al., 1963) and 10.8 ± 0.4 Ma on whole rock analysis (Baranyi et al., 1976). It was already stated by Sen (1990) that the radiometric dating of the hornblende is rather questionable and the age of 10.8 ± 0.4 Ma is preferred. At Bou Hanifia, biotite rich ash layers were dated 12.18 ± 1.03 Ma (Chabbar-Ameur, 1976) and later redated at 12.03 ± 0.25 Ma, but they only indicate a maximum age for the Bou Hanifia Formation. An extrapolation to the *Hipparion*-bearing horizon is impossible because of a large stratigraphic gap of approximately 100 m between the ash layer and the fossil locality. The radiometric datings at Bou Hanifia can therefore not be used in discussing the age of the Aragonian/Vallesian boundary.

In the Vallès-Penedès basin, the association of *Hipparion* with *Megacricetodon ibericus* in localities CCN-20, CCN-22 and RK11 (Montagut section) indicates a lowermost Vallesian age. There the earliest occurrence of *Hipparion*, marking the lower MN9 boundary, occurs in chron C5r.1n, at 11.1 Ma (Garcés, 1995). In Torremormojón, the first record of *Hipparion* occurs in association with *Cricetulodon* in chron C5n.2n at an age of 10.3 Ma. Appearance of a typically Vallesian rodent fauna is, however, recorded in the same section somewhat earlier, between fossil localities TM2 and TM1, indicating an age of 10.9 +/- 0.3 Ma. The magnetostratigraphic results in both basins are in good agreement and indicate that the best age estimate for the MN 7-8/MN 9 boundary is in chron C5r.1n at 11.1 ± 0.1 Ma.

The MN9/MN10 (lower/upper Vallesian) boundary is associated with the entry of *Progonomys hispanicus* (Van de Weerd, 1976; Mein, 1990). The so-called Vallesian event corresponds to a major biotic crisis with numerous extinctions and radiations which affected diverse orders of mammals in different ways (Agustí and Moyà-Solà, 1990). This abrupt faunal change is most evident for the rodents. The Vallesian event profoundly affected three families of middle Miocene rodents (cricetids, glirids and eomyids), and a number of eastern (Asian) macromammal elements appear in western Europe at the same time. The MN 9/MN 10 boundary is well recorded in the Les Fonts and Montagut sections (Vallès-Penedès basin) in chron C4Ar.3r, at 9.7 Ma (Garcés, 1995). The results again agree with the one obtained from Torremormojón, where the MN9/MN10 boundary is recognised between localities TM 5 and TM 6a, giving an age of 9.7 ± 0.1 Ma.

Turolian (MN 11 - MN 13)

The base of the Turolian coincides with the base of MN 11. In the La Gloria section, MN 10 and MN 11 associations allowed the determination of the MN 10/MN 11 (Vallesian/ Turolian) boundary at an age of 8.70 ± 0.1 Ma. So far, this is the only direct age determination for this boundary and it is in agreement with previous dating of lowermost MN 11 faunas. The Kayadibi locality (lowermost MN 11) in Turkey is estimated between two radiometrically (K-Ar) dated ignimbrites of 9.4 ± 0.2 Ma and 7.95 ± 0.25 Ma (Becker-Platen et al., 1975). Quarry X from Samos (Greece) has a radiometric age near 8.5 Ma (Weidmann et al., 1984). Turolian faunas are not dated in Vallès-Penedès, but uppermost MN10 faunas with *Hipparion* cf. *mediterraneum* are correlated to the lower part of chron C4An, at about 9.0 Ma. This age closely fits with that of the base of the Turolian as determined in Teruel basin.

The MN 11/MN 12 boundary is correlated to magnetostratigraphy in the Cabriel Valley section (Opdyke et al., 1990) and recalibration to CK95 gives an age of 7.5 ± 0.1 Ma.

9. Conclusions

The good magnetostratigraphic results from ten sections in Spain show that an almost complete stratigraphic record is present from approximately 18 to 6 Myr (Fig. 7). The biostratigraphic record in this succession is extremely rich and dense which facilitates the construction of a detailed biozonation and the study of paleoclimatological and paleoenvironmental changes during the middle to late Miocene. Correlation of the magnetic polarity patterns of our sections to the GPTS of CK95 is generally straightforward, except for the top of the El Bunker section where major hiatuses or significant changes in sedimentation rate must have taken place.

For the first time, we have established a detailed chronology for the middle to late Miocene continental record in Spain. Seven successive MN zone boundaries are determined and dated in sections which contain faunas of two or more successive zones in superpositon (Table 1, Fig. 7). The previous magneto-stratigraphic dating of the onset of a global mid-Miocene 14.1 Ma cooling event (Krijgsman et al., 1994b) is confirmed, although this event is now considered as placed in the upper part of zone MN 5, following its new definition. The major biotic crisis, marked by the paleofaunal changes, on which the distinction between MN 9 and MN 10 is based (intra-Vallesian crisis (Agustí and Moyà-Solà, 1990) and which includes the entry of *Progonomys* into western Europe is well dated in chron C4Ar.3r at 9.7 Ma (Garcés, 1995).

Acknowledgements

We thank Luis Alcalá, Pablo Pelaez Campomanes, Lola Garcés, Ton van Hoof, Charon Duermeijer and François Lévèque for their help in the field. Henk Meijer assisted with the paleomagnetic measurements. This study was supported by the Netherlands Geosciences Foundation (GOA/NWO). RD, JvD and Av/dM gratefully acknowledge financial support of the CEE, JOULE programme DGICYT, PB92-0013. The contributions to the Vallesian magnetostratigraphy were supported by the projects CICYT GEO89-083, CAICYT PB94-1265 and DGICYT PB91-0096 from SMES.

Chapter 8

Cyclicity and NRM acquisition in a continental red bed sequence (Miocene, Spain): potential for an Astronomical Polarity Time Scale

Abstract

The Armantes section in the Calatayud-Daroca basin is a red-bed sequence consisting of a regular alternation (10 m scale) of reddish silts and pink/white limestones. In between these limestones a smaller-scale bedding (2-3 m scale) is intercalated, characterised by varying carbonate content and related differences in erosion resistance. Correlation of the magnetic polarity sequence to the geomagnetic polarity time scale (GPTS) suggests a periodicity of 111 kyr for the large-scale cyclicity, indicative of a relation with the ~100 kyr eccentricity period of the Earth's orbit.

Rock magnetic experiments show that the NRM in the Armantes section results from the presence of hematite and magnetite and/or maghemite. The relative contribution of hematite is strongly related to the lithology. Hematite is the dominant carrier in the limestones, while in the silts magnetite/maghemite is of major importance. The polarity reversals can easily be determined, even though the reversals of the magnetite and hematite components appear to be recorded at slightly different positions.

The astronomical solutions of La90 for the correlative interval show two peak values at periodicities of 95 and 125 kyr, with an average of 110 kyr. This is in excellent agreement with the magnetostratigraphically determined periodicities and confirms the suggestion that the large-scale cyclicity is related to eccentricity. The precipitation of the carbonates is most likely related to rising ground-water levels and to a related increase of evaporation which suggests that the thick limestone beds correlate to eccentricity maxima. The small-scale interbeds most likely reflect the influence of the precession cycle.

This chapter has been submitted for publication as: W. Krijgsman, W. Delahaije, C.G. Langereis, P.L. de Boer, Cyclicity and NRM acquisition in a continental red bed sequence (Miocene Spain): potential for an Astronomical polarity time scale. *J. Geophys. Res.*, 1996.

Introduction

Time is an indispensible tool in geology for constraining all kinds of processes and rates of change. A major break-through in chronology - with a resolution and accuracy of several kyr - recently came from marine studies directed at establishing an astronomical polarity time scale (APTS) (Shackleton et al., 1990, 1995; Hilgen 1991a,b, Hilgen et al., 1995). The construction of such a time scale involves the calibration (or "tuning") of astronomically induced sedimentary cycles or other cyclic variations in sedimentary sequences to computed astronomical time series of past variations in the Earth's orbit or to derived target curves (e.g. insolation, ice sheet volume). For paleoclimate and paleoenvironment reconstructions, the APTS is fundamental, but the construction of the APTS is, as yet, entirely based on open- marine sequences. The inclusion of the continental record would be helpful since a comprehensive understanding of paleo-climate and paleoclimate change is only achieved by accurate and high-resolution time-stratigraphic correlations between the continental and the marine record. In fact, the terrestrial sedimentary record seems to be the logical first place to look for Milankovitch cycles because, in the absence of oceanographic processes with their intrinsic and complicated non-linear (feed-back) mechanisms, a more direct registration of orbitally induced changes of climate may be expected (De Boer and Smith, 1994).

A potential serious drawback of using continental successions is the usual lack of a direct and sufficient time control, also because of the assumed common occurrence of hiatuses which may result from intermittent erosion caused by tectonic activity, base-level changes and autocyclic processes. High-resolution magnetostratigraphic studies on continental sections in the Calatayud-Teruel basin of Spain, however, showed that a continuous sedimentation - without major hiatuses - has taken place during the Miocene, providing accurate time constraints (Krijgsman et al., 1994b; 1996). The mammal biostratigraphic record of these sections is extremely dense and rich, and offers a resolution of 30 kyr for some intervals. The series ranges from the Neogene Mammal zone MN 4 (18 Ma; Aragonian) to MN 11 (8 Ma; Turolian) (Krijgsman et al., 1994b; 1996). Principal component analyses of the detailed rodent assemblages from the Ramblian and Aragonian (Van der Meulen and Daams, 1992) revealed that major climate changes can be recognised in this continental biostratigraphic record. The construction of an APTS in the Calatayud-Teruel basin will allow the incorporation of this part of the continental record in a global and astronomically tuned cyclostratigraphic and magnetostratigraphic framework. This, in turn, will allow the establishment of high-resolution time-stratigraphic correlations between the continental and the marine record needed for a comprehensive understanding of paleoclimate and paleoclimate change.

Sections with a continuous cyclic sedimentation pattern and good paleo-magnetic properties are needed for investigating the potential of constructing an APTS. For this study, we selected the Armantes section, a typical example of a

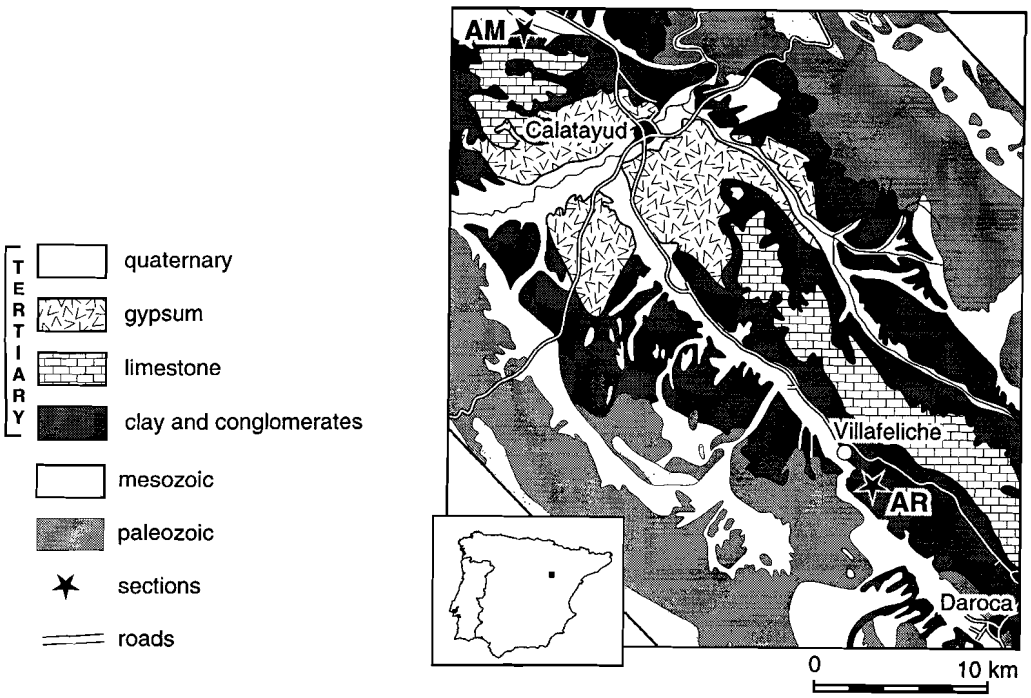

Figure 1: Location of the Armantes (AM) section in the Daroca-Calatayud graben. The Aragon section (AR) is time-equivalent with the Armantes section and has a very detailed biostratigraphic record (see Krijgsman et al., 1994b). Note that the depocenter of the Tertiary basin around Calatayud is characterised by gypsum deposits, while towards the margins lacustrine carbonates silts and coarse clastics occur.

red bed sequence. Correlation of the Armantes magnetic polarity sequence to the geomagnetic polarity time scale CK95 of Cande and Kent (1995) showed that sedimentation has been continuous over a 5 Myr interval (Krijgsman et al. 1994b). A 10-m-scale cyclic bedding of alternating reddish silts (red beds) and whitish limestones is very pronounced and, in addition, smaller-scale (2-3 m) variations in lithology are expressed as laterally continuous alternations of slightly more and slightly less erosion-resistent siltstones. The magnetostratigraphic results further showed that the 10-m-scale cyclic bedding has an average periodicity of 111 kyr (27 cycles in approximately 3 Myr), according to CK95, which strongly suggests that it is related to the ~100 kyr eccentricity cycle of the Earth's orbit (Krijgsman et al. 1994b).

Considering published data on red beds, there has always been a serious doubt on their value for magnetostratigraphic and paleomagnetic studies. The remanence of red beds resides for a large part in hematite grains which are often considered to be of chemical and thus post-depositional origin (Walker et al., 1981). However, as shown by Van den Ende (1977), hematite grains in red beds can also be of synsedimentary origin and contain a depositional remanent

magnetisation (DRM) In that case, they are capable of displaying paleosecular variations. If hematite carries a chemical remanent magnetisation (CRM), there are several possibilities for the origin of the hematite and its remanent magnetisation. Hematite can be created during early diagenesis or even recently during weathering (Roy and Park, 1972; Walker et al., 1981; Channel et al., 1982). Hematite can also be introduced into sediments by ground-water currents (Langereis and Dekkers 1992). Hence, CRM acquisition of hematite can be considered a long-term process, so that the CRM may comprise different paleomagnetic components and thus may not always be accurately dated. If, however, the hematite and its CRM has been created within a relatively short time interval, then the secondary paleomagnetic directions can be interpreted as delayed primary signals. Previous rock magnetic results from the Armantes section show that the natural remanent magnetisation (NRM) is defined by the two components hematite and magnetite (Dijksman, 1977; Krijgsman et al., 1994b). Throughout the section, there are variations in the relative amount of these two components which, in addition, are known to show a possible delay in acquisition (Dijksman, 1977).

To test the hypothesis of an astronomical origin of the distinct rhythmic bedding in the Armantes section, and to study the possible relation between the cyclic lithology variations and the acquisition of the NRM in these sediments, we sampled in detail a short stratigraphic interval. This interval contains three indurated limestone beds, which we infer to reflect the influence of the 100-kyr eccentricity cycle, and nine less distinct indurated beds in between.

The Armantes section

Geological setting and sampling

The Calatayud-Daroca basin is located in the Iberian Range, between the western and eastern Iberian Chains. The mountains adjacent to the basin consist of folded and faulted Paleozoic and Mesozoic rocks. Between Calatayud and Daroca, the basin is bordered by steeply dipping NW-SE trending normal faults with a dip towards the basin. Sediments in this area consist of conglomerates (along the borders of the basin), sands, silts, clays, and in the central part also lacustrine limestones and gypsum. The large body of evaporites (mainly gypsum) and limestones near the city of Calatayud, indicates that a lake existed in the deepest part of the graben, while red silts and intercalated white/pink limestones were deposited in the floodplain around the lake.

The Armantes section, approximately 12 km northwest of the city of Calatayud (Fig. 1), was first studied by De Bruijn (1965) for paleontological purposes and later by Dijksman (1977) and Krijgsman et al. (1994b), who showed

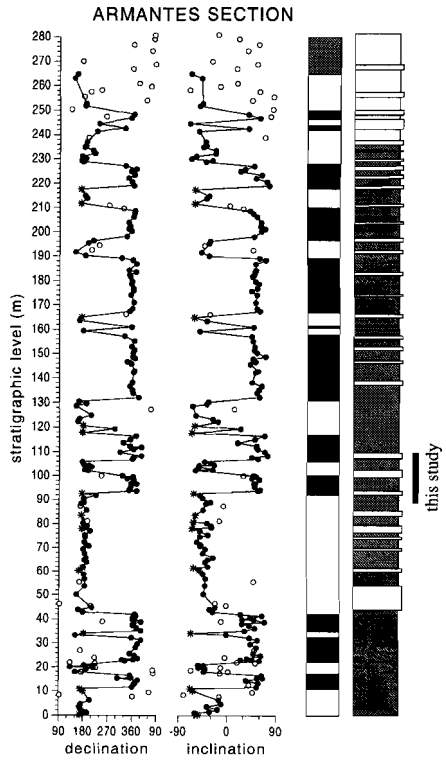

Figure 2. : Magnetostratigraphy and lithology of the Armantes section. Solid dots represent reliable directions, circles represent low intensity samples which are difficult to interpret. Asterisks represent directions obtained by applying the great circle method. In the polarity column, black (white) denotes normal (reversed) polarity zones; the shaded interval in the top of the section denotes a zone of uncertain polarity.The lithology column displays variations of red coloured silts and conglomerates (shaded) and pink/white-coloured limestones (white).

that the sediments have paleomagnetic properties suitable for magnetostratigraphy. Correlation of the magnetic polarity sequence to CK95 (Cande and Kent, 1995) showed that a continuous succession from 17 to 12.5 Ma is present (Fig. 2; Krijgsman et al. 1994b). The Armantes section predominantly consists of a regular alternation of red silts and pink/white limestones. The nearly complete absence of primary sedimentary structures indicates that pedoturbation (desiccation, burrowing, rooting, paleosol development) has been intensive. Clear sedimentary structures were only found locally in rapidly deposited coarse-grained channel fills higher in the sequence, some 5 m above the top of the interval discussed here. The limestones are interpreted as "caliche horizons" and palustrine/lacustrine carbonates. The observed alternation is remarkably continuous both laterally and vertically. Throughout the section 27 indurated limestone beds have been recognised. For a detailed sampling, we selected

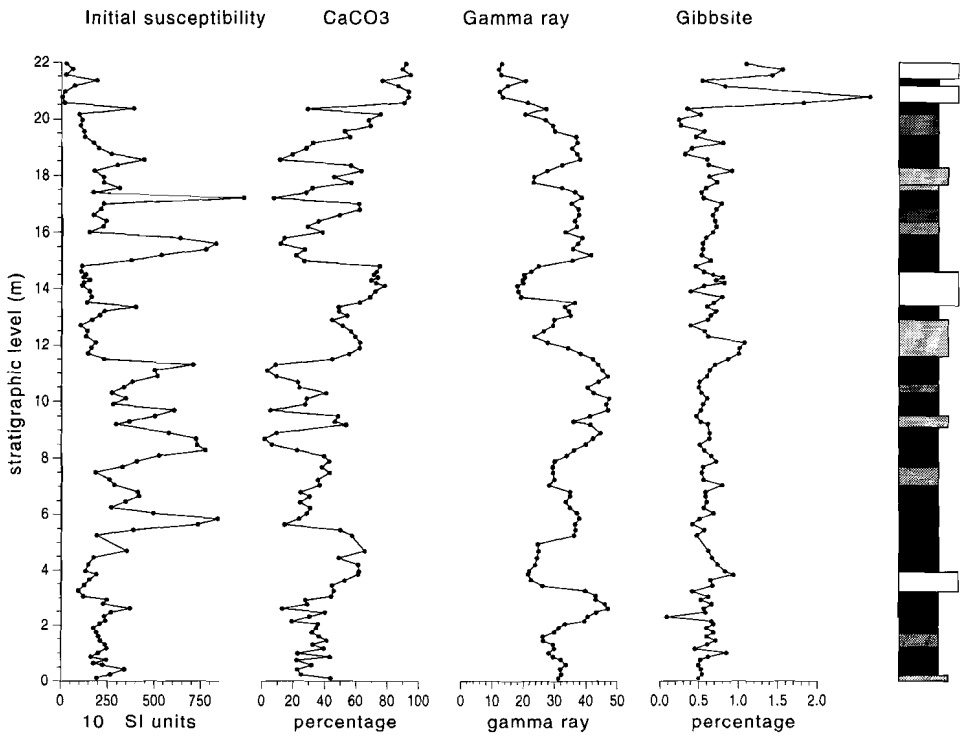

Figure 3. : Initial susceptibility, carbonate concentration, gamma-ray intensity and gibbsite content of the studied interval of the Armantes section. The lithology column displays red silts (dark shaded) smaller-scale bedding (shaded) and pink/white limestones (white). All records show a clear relation with the lithology. In the silts, the initial susceptibility and the gamma-ray intensity is relatively high while the carbonate concentration is low. Note also the increasing trend in the carbonate concentration from bottom to top.

the interval between limestone beds 7-9 because it is continuously exposed and accessible, because a smaller-scale cyclicity is well-developed, and because it contains three magnetic reversals. Correlation to CK95 shows that it concerns the chron interval C5Bn.1n-C5Br with an age from 15.2 to 14.9 Ma.

Over a stratigraphic distance of 22 m we sampled at 119 levels which corresponds to an average resolution of 18 cm (2.5 kyr). At each level we aimed to drill two oriented standard paleomagnetic cores. Some levels were impossible to drill and unoriented handsamples were taken.

Initial susceptibility and anisotropy

The initial susceptibility (χ_{in}) and the magnetic anisotropy of the samples were measured on a Kappabridge KLY-2. The χ_{in} is strongly dependent on the

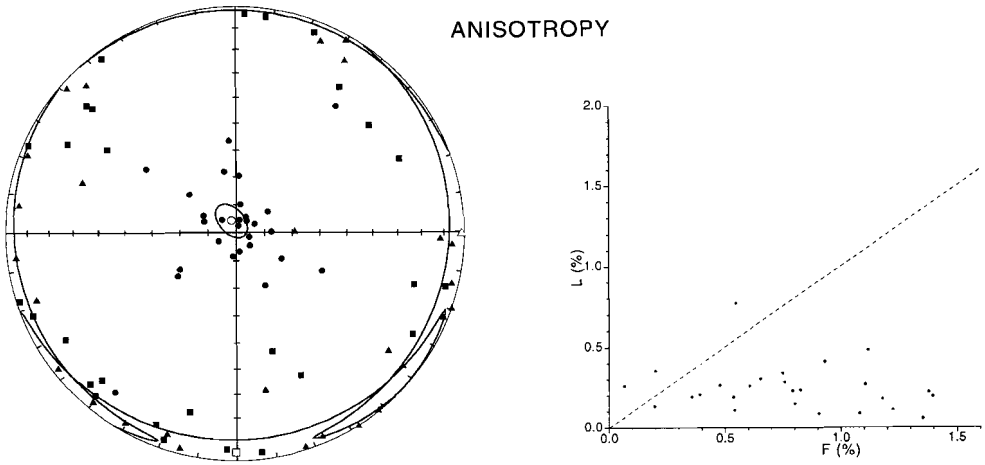

Figure 4 : Anisotropy of the initial susceptibility. (A) Principal axes of the anisotropy; dots denote minimum axis, triangles intermediate axis and squares maximum axis. Open symbols denote the mean direction of the principal axes. (B) Flinn diagram; L = lineation, F = foliation. The magnetic fabric is oblate which indicates that deposition has taken place on a horizontal plane in a quiet sedimentary environment without any currents.

concentration of paramagnetic (clay) minerals, on the concentration of ferrimagnetic minerals, and on the grain size and the type of magnetic mineral. The results from the Armantes section show that a clear relation exists between χ_{in} and lithology. The red silt beds show a relatively high χ_{in}, up to a maximum of 950 x 10^{-6} (SI), while the white limestone beds show a lower χ_{in} of 200-300 x 10^{-6}. The smaller-scale light red intercalations show intermediate values (Fig. 3).

For the oriented samples, the magnetic anisotropy of the initial susceptibility was determined. The anisotropy is generally 1-2 %, the minimum χ_{in} axes are on average vertical, the intermediate and maximum axes are randomly oriented in a horizontal plane (Fig. 4). The anisotropy can be caused by a large contribution of paramagnetic clay minerals or by hematite, which has a high intrinsic anisotropy. The Flinn diagram shows that the fabric causing the anisotropy is entirely foliated (oblate), and has no superimposed lineation. This strong oblateness of the fabric indicates that deposition has taken place on a horizontal surface in a quiet sedimentary environment.

Carbonate concentration and clay minerals

The carbonate concentration was determined in the laboratory by measuring the quantity of hydrochloric acid (1N HCl) needed to dissolve the carbonate. After dissolution of the carbonate, the clay minerals were analysed using thermogravimetric analysis (TGA). For some levels X-ray diffraction analyses

were made. The carbonate concentration of the samples displays a strong correlation with the observed lithology and erosion resistance in the field. It ranges between approximately 5-40 % for the red silt beds and 60-95 % for the pink/white limestone beds. The smaller-scale rhythmites have carbonate concentrations between 40 and 60 %. A general increase of carbonate content is observed from the bottom to the top of the section, and accompanies an increase of thickness of erosion-resistent beds (Fig. 3).

The X-ray diffraction analysis shows that the clay minerals predominantly consist of illite and to a lesser extent of kaolinite. Few samples possibly contain small amounts of chlorite and smectite. A TGA peak, observed around 300 °C, is ascribed to gibbsite. X-ray diffraction indeed reveals a weak and scattered signal around 4.85 Å. Gibbsite is an aluminum-hydroxide which is produced in soils under humid and warm conditions (Füchtbauer, 1988). Al can be dissolved in fluids with a pH of 7-8.5, a common range for water associated with carbonate deposits (Hay and Wiggins, 1980). The concentration of gibbsite displays a relation with the lithology, relatively high values occuring just beneath and within the bottom part of the thick limestone beds (Fig. 3). This suggests that these limestone beds were deposited under humid and warm conditions.

Gamma ray

The gamma ray signal at each level was measured in the field with a WG 135 differential Gamma Spectrometer. The gamma-ray record generally reflects the amount of clay minerals in the sediment. As expected, it reveals relatively high values for the clayey silt beds and low values for the limestone beds, thus showing a clear negative correlation with the carbonate concentration (Fig. 3). The gamma-ray record shows a much smoother function than the carbonate and χ_{in} records. This is caused by scattering of gamma-ray radiation from adjacent beds. A decreasing trend from bottom to top of the sampled interval is in agreement with the gradually increasing carbonate content and the decreasing susceptibility.

Paleomagnetic results

Methods

We performed some rock magnetic experiments to investigate the influence of the type of lithology on the NRM acquisition. An isothermal remanent magnetisation (IRM) was acquired on a PM4 pulse magnetiser up to maximum fields of 2400 mT and was measured on a JR5 spinner magnetometer. Hysteresis loops and (remanent) coercive-force values (Hc, Hcr) of all samples were

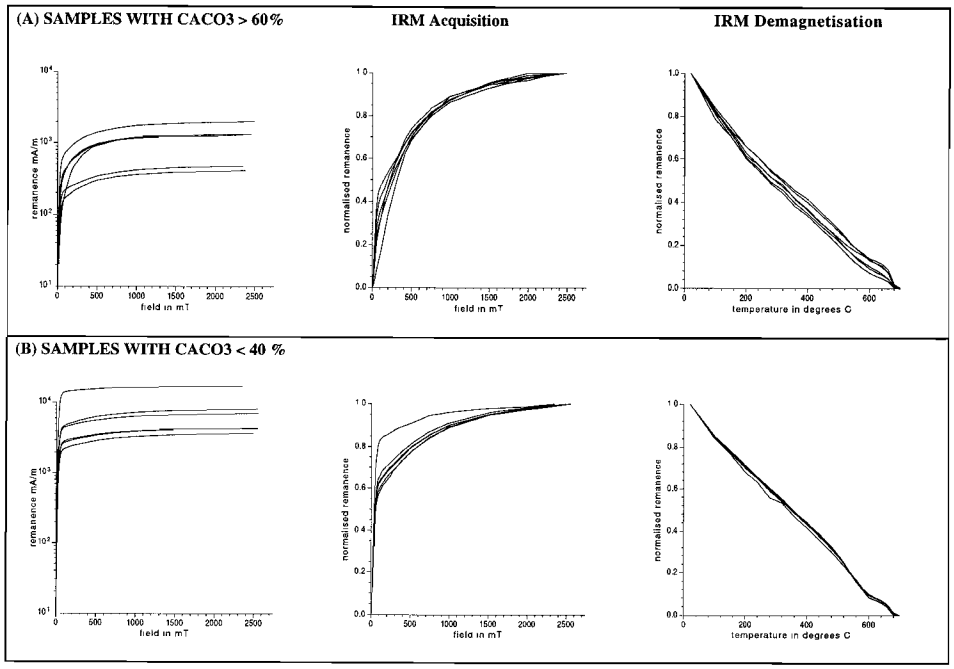

Figure 5. : Examples of IRM acquisition (absolute and normalised values) of samples from limestones with carbonate concentration > 60%, and from silts with carbonate concentration < 40%. The initial steep rise (< 200 mT) points to magnetite, the gradual increase at high fields (> 200 mT) suggests the additional presence of hematite. Stepwise thermal demagnetisation of the normalised IRM also shows the presence of both magnetite or partially oxidised magnetite (maghemite) (580-600 °C) and hematite (680 °C), particularly in the silts.

measured on a alternating-gradient-force magnetometer model 2900. Both the NRM and the IRM were thermally demagnetised in a laboratory-built shielded furnace, with small temperature increments of 30-50 °C, up to a maximum of 700 °C. The NRM was measured on a 2G Enterprises horizontal cryogenic magnetometer equipped with DC SQUIDS. Susceptibility was measured after each temperature step on a Kappabridge KLY-2.

IRM acquisition and subsequent demagnetisation

IRM acquisition curves were determined for all drilled samples. They indicate the presence of two different components (Fig. 5). A steep rise between 0 and 100-200 mT suggests the presence of a low-coercivity mineral like magnetite or maghemite. At higher fields, the IRM acquisition curves increase gradually. Even at the highest field values of 2400 mT, saturation is generally not reached. This

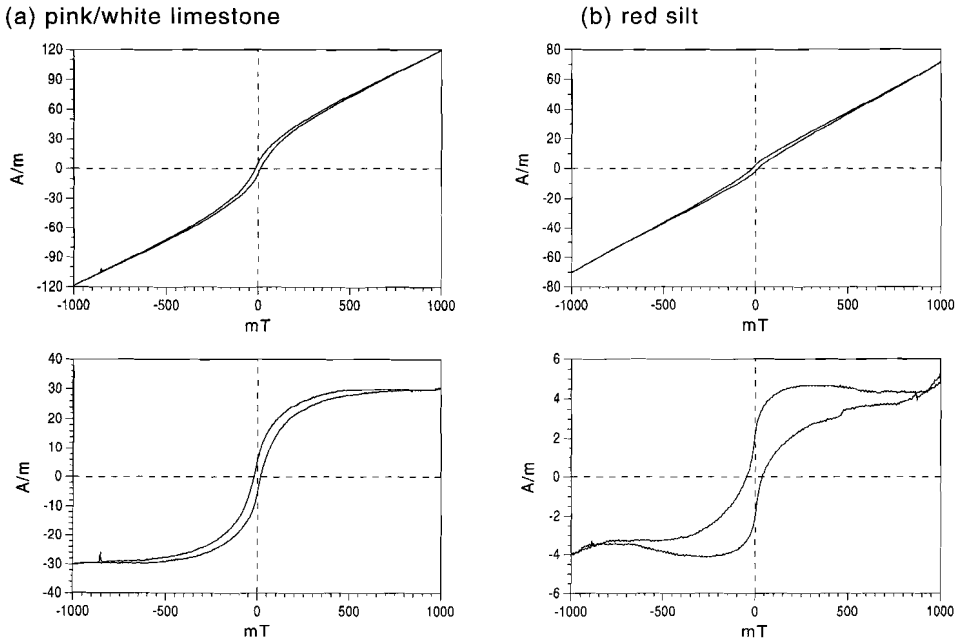

Figure 6: Hysteresis loop and corrected (for paramagnetic contribution) hysteresis loop of a selected sample from the limestones and from the silts. The strong increase at low magnetic fields points to magnetite, the fact that saturation is not achieved in the highest possible field of 1 Tesla suggests the presence of hematite.

indicates the presence of a high-coercivity mineral like hematite and/or goethite. The relative part of the IRM which is caused by the high-coercivity mineral was estimated by extrapolation to the relative intensity axis, from the point where the low coercivity mineral is saturated. For the silts it shows that the IRM mainly (60-85%) consists of the low-coercivity component. For the limestones the contribution of the low-coercivity minerals to the IRM is relatively low (0-20%), and the IRM is dominated by the high-coercivity mineral.

The IRM demagnetisation curves confirm the presence of two different components. An unblocking temperature of 580-600 °C, which is clearly visible in the curves of the silt beds, is somewhat high for magnetite and could indicate the presence of partially oxidised magnetite (maghemite) (Fig. 5). All curves show an additional unblocking temperature of 680 °C which indicates the presence of hematite as the high-coercivity mineral. The IRM demagnetisation curves show no significant decrease below 100 °C which suggests that the contribution of goethite is negligible.

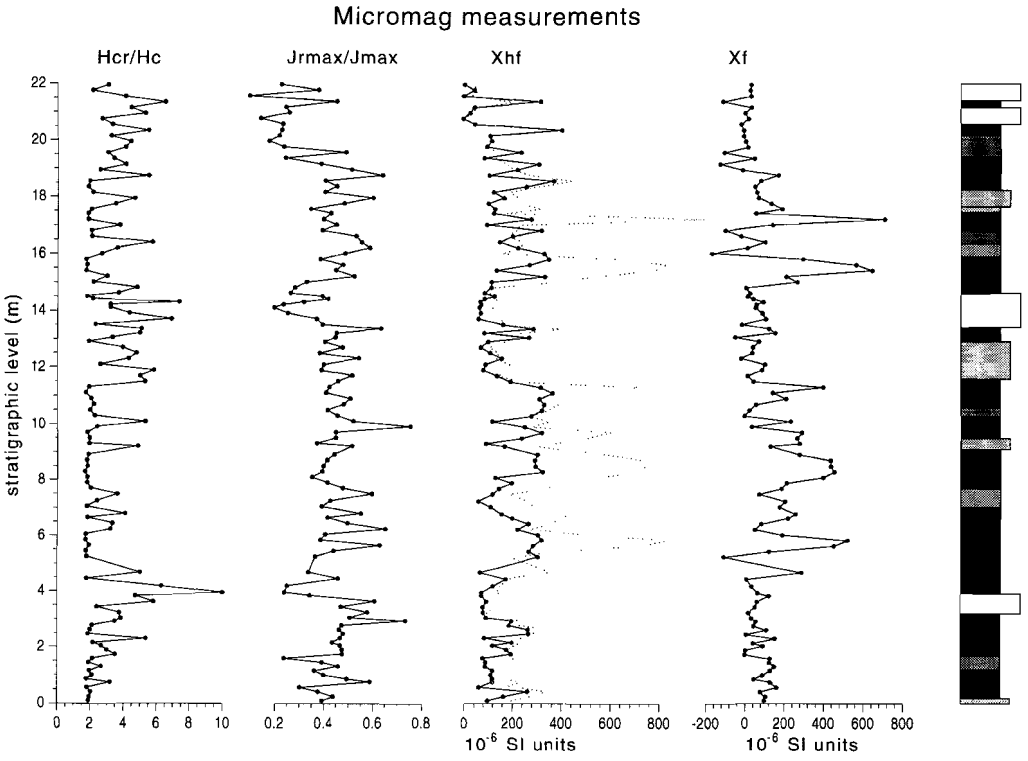

Figure 7 : Micromag measurements displaying the coercive force ratio H_{cr}/H_c, the magnetisation ratio J_{rmax}/J_{max}, the paramagnetic susceptibility χ_{hf} and the ferrimagnetic susceptibility χ_f (= χ_{in}- χ_{hf}) versus stratigraphic level. H_{cr}/H_c is relatively high, while in the limestones J_{rmax}/J_{max}, χ_{hf} and χ_f are relatively low. Dotted line denotes the initial susceptibility χ_{in}.

Coercive forces

The hysteresis loops display the contribution of the paramagnetic clay minerals to the total magnetisation. After correcting for the paramagnetic part, usually two different types of loops can be observed (Fig. 6). Both hysteresis loops show that the sample consists of magnetite, characterised by the strong increase at low magnetic fields, and of hematite, considering the fact that the hysteresis loops are not saturated at high magnetic fields. However, the shape of both hysteresis loops is very different. The "wasp waisted" shape of the corrected silt-bed hysteresis loop may have been caused by the presence of viscous (or superparamagnetic) magnetic minerals. It is more likely, however, that the

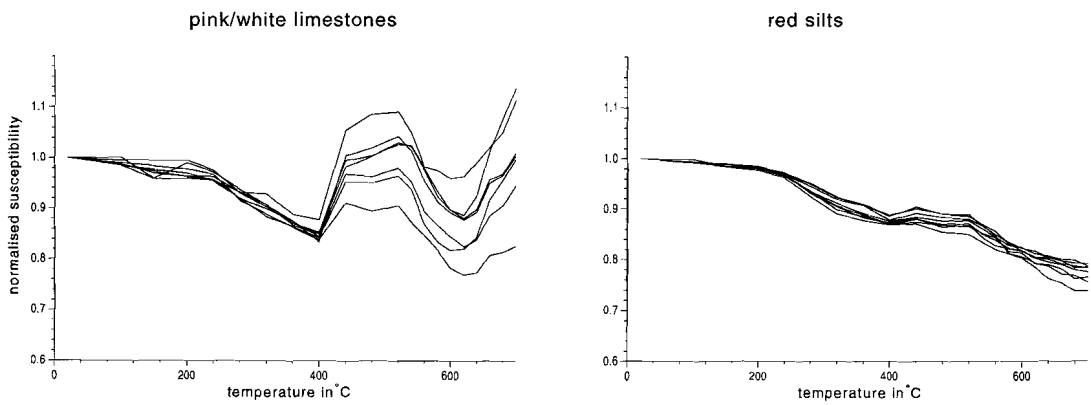

Figure 8 : Bulk susceptibility during thermal demagnetisation of the IRM. (A) examples from the limestone interval between 13.5-14.5 m (B) examples from the silty interval between 7.0-9.0 m. The increase in susceptibility between temperatures of 400-500 °C might be caused by a production of more magnetic impurity in small hematite grains. The increase in susceptibility at temperatures higher than 600 °C is possibly related to the presence of goethite or a Fe-bearing clay mineral.

"wasp-waisting" in this case is caused by a mixture of high and low coercivity minerals (Tauxe et al., 1995).

The H_c and H_{cr} values clearly display the presence of both magnetite and hematite. For samples containing relatively much magnetite, the H_{cr} values are approximately 30 mT, while for the samples containing mostly hematite, the H_{cr} ranges between 100 mT and 300 mT. The coercive force ratio (H_{cr}/H_c) shows a strong relation with the lithology (Fig. 7). H_{cr}/H_c displays high values for the thick limestone beds and lower values for the silts. These observations imply that hematite is dominantly present in the limestones. Also higher ratios are observed around the smaller indurated beds suggesting that these beds contain also a higher concentration of hematite. The ratio between the maximum remanent magnetisation (J_{rmax}) and the maximum magnetisation (J_{max}) displays the inverse correlation with the lithology (Fig. 7). Low magnetisation ratios (J_{rmax}/J_{max}) in the limestones indicate the presence of relatively large concentrations of hematite. J_{rmax}/J_{max} shows also a strong relation with the presence of viscous magnetite minerals; in the silt samples, which contain viscous magnetic minerals, J_{rmax}/J_{max} is generally higher.

Susceptibility

The initial susceptibility (χ_{in}) consists of a ferrimagnetic part (χ_f), caused by magnetic minerals, a paramagnetic part, the so-called high-field susceptibility (χ_{hf}), caused by paramagnetic clay minerals, and a diamagnetic part χ_{dia}, caused by

carbonates and quartz. The χ_{hf} was determined from the slope of the hysteresis loops at the highest available fields of 1.4 Tesla. Hence, the χ_f was determined by substracting the χ_{hf} from the χ_{in} (Fig. 7). Some samples, however, show a negative χ_f, which is physically impossible. These negative values result from the fact that the determined χ_{hf} is too high, which must be caused by a very high concentration of hematite and the fact that hematite is often not saturated at the highest fields (Fig. 5). Inhomogeneity in the sediment and the very small sample size for the Micromag may also result in too high χ_{hf} values.

During thermal demagnetisation of the IRM we also measured the bulk susceptibility after each temperature increment. The limestones and silts both show a decrease of χ_{in} above 200 °C (Fig. 8). An increase in χ_{in} is observed at temperatures above 400 °C, reaching its peak value at 510 °C, while a subsequent decrease follows till 600 °C. Dekkers and Linssen (1989) suggest that the increasing susceptibility in fine-grained hematite above 400 °C can be caused by production of more ferrimagnetic impurity, which was also noted by Dunlop (1971). This impurity in hematite can be maghemite which would disappear by inversion to hematite at temperatures of approximately 600 °C. When natural goethite is converted into hematite, also trace amounts of magnetite can be produced (Dekkers, 1988). The relative increase in χ_{in} during thermal demagnetisation is generally higher in the limestones than in the silts, probably because the relative contribution of hematite is larger in the limestones. Furthermore, it might have been emphasised by the normalisation of χ_{in} on the basis of its initial value, which is much smaller for the limestones. The high-carbonate samples show again an increase of χ_{in} above 600 °C (Fig. 8). This increase in χ_{in} is not well-understood.

NRM demagnetisation

The determination of reliable directions from the thermal demagnetisation diagrams was strongly hampered by a large disturbing magnetisation component, probably caused by a small residual field in the furnace (Fig. 9a,b). As a standard procedure, the samples are placed in an opposite position in the furnace at every subsequent temperature step. To obtain more reliable directions we averaged the direction and intensity afterwards by calculating a two-point running average. The thermal demagnetisation diagrams of these averaged directions clearly show that the NRM consists of several components (Fig. 9c-j). A small component is usually removed at temperatures of 100 °C; it is randomly directed, and thus has a viscous origin rather than being due to goethite. A secondary component is removed at temperatures of 240 °C. This component has an approximately present-day field direction and is of subrecent origin. After these components were removed, two other components could be observed. One relatively low temperature (LT) component is generally removed at temperatures below 600 °C, suggesting magnetite, and another high temperature (HT)

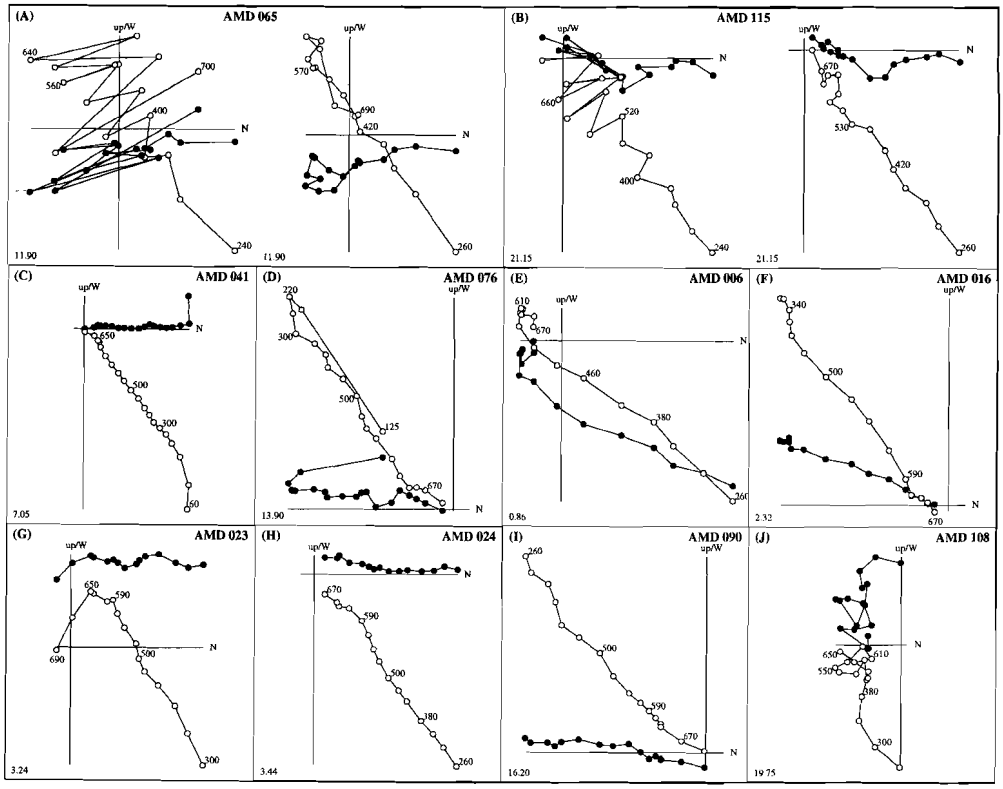

Figure 9. Thermal demagnetisation diagrams of selected samples from the Armantes section. Closed (open) circles denote the projection on the horizontal (vertical) plane; values are temperature steps in °C; stratigraphic levels are in the lower left corner. (A) and (B) are examples showing the effects of applying a two-point running average on the original data which are suffering from a viscous component that is related to a small residual field in the furnace. (C) shows the randomly oriented laboratory component at room temperature. (D) shows the secondary present-day field component which is generally removed at 240 °C. (E)-(I) are characteristic samples showing both a LT (magnetite) and a HT (hematite) component. Note that these two components do not always have the same polarity. An example from the upper part of the section in which the intensities for both the MT as HT component are relatively low is shown in (J).

component at temperatures of 680 °C, indicating hematite. For some samples, the total remanence is not entirely removed at the highest temperatures. Apparantly, the two-step averaging procedure does not entirely remove the disturbing magnetisation component induced by the very low magnetic residual field in the furnace.

Discussion

Lithological cycles

Calcretes and caliche are commonly interpreted to have formed in semiarid to arid, warm seasonally dry climates (Blodgett, 1988). Of course, the prerequisite for the formation of calcrete (caliche) is an adequate supply of (dissolved) calcium carbonate. The absence of channel and current structures in the studied part of the succession suggests that carbonate was supplied along with the ground water, which was fed from adjacent topographic highs through marginal alluvial fan deposits to the lower parts of the basin. Precipitation of the carbonate, as caliche nodules, calcretes and dispersedly through the sediment must have occurred during evaporation of the ground water in the topographically lower parts of the basin. Supply of carbonate as eolian dust may have played a role as well, but also in that case, (ground)water must have been present to allow vegetation (as observed from local root traces), and redistribution and concentration of carbonates. It is inferred that, during deposition of the studied interval, the basin, or the part of the basin in which the studied sequence was deposited, had an internal drainage most of the time. Only when water supply exceeds evaporation, external drainage will occur, and dissolved carbonates may be exported from the basin, either dissolved in ground water or as part of the surface runoff. The cyclic occurrence of carbonate-rich beds thus is interpreted to be the result of regular changes in the humidity.

NRM acquisition

A good paleomagnetic record in which polarity reversals can be accurately determined, is essential for the construction of an APTS. The rock magnetic results of the Armantes section clearly indicate that at least two components contribute to the NRM of these sediments and that the importance of each component depends on the type of lithology. IRM acquisition curves and hysteresis loops indicate that both a low-coercivity and a high-coercivity mineral are dominantly present in all samples. Relatively high blocking temperatures - between 680-700 °C - of both the NRM and IRM, corresponding to levels with high H_{cr} values, indicate that hematite is the high-coercivity mineral. Blocking temperatures between 580-600 °C, corresponding to levels with low H_{cr} values, suggest that magnetite or/and maghemite (partially oxidised magnetite) is the low-coercivity mineral. The existence of maghemite as ferrimagnetic impurity can explain the increases in χ_{in} at temperatures between 400-500 °C during thermal demagnetisation.

Due to the difference in blocking temperature, the hematite component can be separated from the magnetite component after thermal demagnetisation. In the

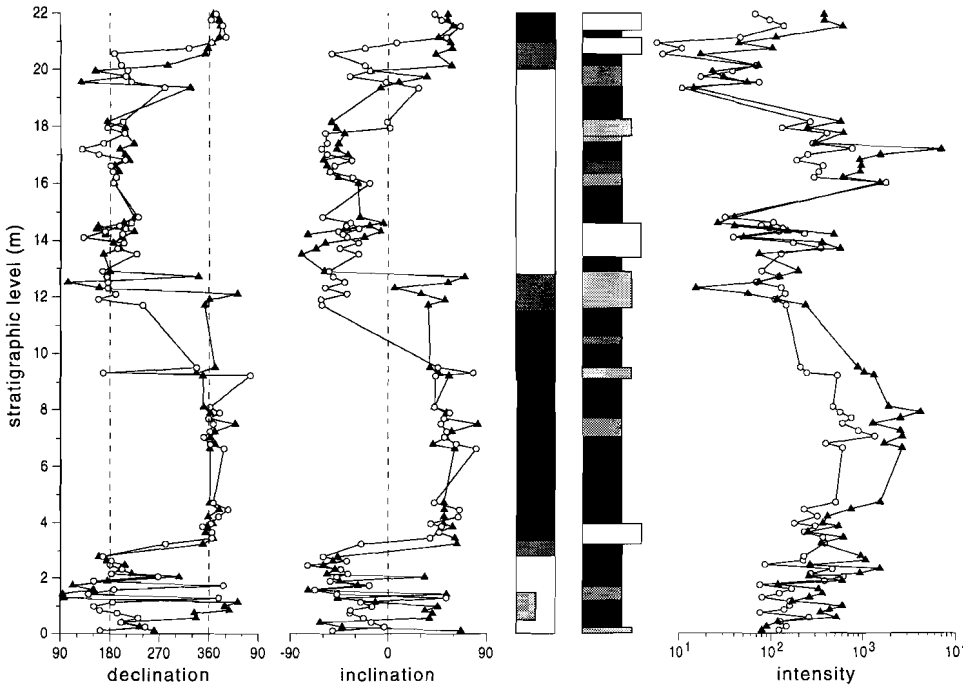

Figure 10. : Magnetostratigraphy, lithology and the intensities for the three components of the detailed studied part of the Armantes section. Triangles represent directions of the LT (400-600 °C) component, related to magnetite and/or maghemite. Solid dots represent directions of the HT (600-700 °C) component, which is related to hematite. See also caption to figure 2.

interpretation of the demagnetisation diagrams we distinguished two components; a LT component determined in the temperature range 400-600 °C, characteristic for magnetite, and a HT component (600-700 °C) characteristic for hematite. The LT and HT components both show reversed and normal polarities, suggesting a near primary origin, but they sometimes show opposite polarities at the same level or interval (Fig. 10). In the lowermost part (0-3 m) of the section, the HT component is predominantly reversed while the LT component shows normal polarities between 0.5-1.5 m (Fig. 10, 9e,f). These normal magnetic directions may be related to a cryptochron, although this was never recorded before at the corresponding age.

The lowermost polarity transition (3-3.5 m), from reversed to normal, appears to occur slightly "earlier" (i.e. lower in the stratigraphy) in the LT component than in the HT component (Fig. 9f-h). This lower transition in the LT component is also observed at the uppermost polarity transition (19-21 m), although the directions are less well determined because of a relatively lower intensity of both components (Fig. 10, 9j). However, the polarity transition from normal to reversed in the middle part of the section (12-13 m) suggests that there the

reversal of the HT component is "earlier" than the LT component. Since all three polarity reversals occur near the thick (dominant hematite) limestone beds, the LT intensities are generally very low at the polarity transitions.

The results of this study show that a clear difference in magnetic composition exists between the white limestones and the red silts. In the limestones χ_{in} and J_{rmax}/J_{max} are low, H_{cr}/H_c is high relative to that in the silts. IRM acquisition curves show that the relative contribution of hematite is 60-80 % in the limestones and only 20-40 % in the red silts. Hence, it is concluded that hematite is the dominant magnetic mineral in the limestones, whereas magnetite/maghemite is of major importance in the silts. Nevertheless, the absolute contribution of hematite to the IRM is higher in the silts, and thus the dominance of hematite in the limestones is controlled by a very low concentration of magnetite. The absolute concentration of hematite in the limestones is lower than in the silts.

The hematite, which gives these rocks their red colour, is probably authigenic, having grown from a precursor during early diagenesis. One argument that the hematite is authigenic rather than detrital comes from the limestones where spotty distributions of red colouration is such that hematite cannot be detrital in origin. A partial detrital origin for the hematite in the red silts can, however, not be excluded. Hematite pigment in red beds may be caused by a variety of diagenetic processes such as alteration of iron-magnesium silicates (Walker et al., 1981), the breakdown of iron-bearing clays (Walker and Honea, 1969) or dehydration of goethite (Channell et al., 1982). The hematite of the Armantes section probably also originates from oxidation of Fe-bearing precursors and/or precipitation upon oxidation of ground-water-dissolved reduced iron species, and thus carries a CRM. Precipitation of hematite from oxidising ground water was low in the silts due to a low evaporation rate. Consequently, also more magnetite grains are preserved which most likely generate the observed disturbing magnetic response in the silts. The process which controls the diagenetic growth of hematite thus seems to be related to the lithology and to the paleoclimate.

A possible mechanism for hematite growth in limestones, occurring during some time after deposition, was proposed by Channell et al. (1982). The CRM direction of the hematite grains depends on the ambient field at the time of growth through a critical volume and this direction does not change anymore during further growth. Channel et al. (1982) showed that the reversal of the largest hematite grains occurs earlier than the reversal of the detrital magnetite component, which indicates that some hematite grains may grow through their critical volume before the detrital magnetite component is fixed into the sediments. This mechanism may explain the "earlier" reversals of the magnetite component with respect to the hematite component in the lower and upper reversal.

Correlation to the astronomical curves

The earlier magnetostratigraphic and cyclostratigraphic study on the Armantes section showed that the distinct cyclic middle part of the Armantes section (54-235 m) covers approximately 3 Myr (Krijgsman et al, 1994b). In this part we counted 27 (large scale) cycles which results in an average periodicity of 111 kyr (Fig. 2), suggesting a relation with the eccentricity cycle of the Earth's orbit. To determine wether the cyclicity observed in the Armantes section is indeed related to the astronomical cycles, we applied spectral analysis on the astronomical solutions of La90 (Laskar, 1990) to determine which dominant frequencies are expected in the corresponding time interval. The frequency spectrum for the La90 eccentricity curve - using the CLEAN spectral analysis (Roberts et al., 1987) - shows that the corresponding interval (14.5-15.5 Ma) is determined by two equally strong peaks at 125 and 95 kyr, resulting in an average periodicity of 110 kyr (Fig. 11). This is in excellent agreement with the magnetostratigraphically estimated average periodicity of 111 kyr and confirms the suggestion that the generation of the thick limestone beds is related to the orbital eccentricity cycle. The smaller scale bedding (2-3 m) than is related to the precession cycle with main quasi-periodicities of 19, 23 and 25 kyr, according to La90. Indeed the carbonate, gamma-ray and susceptibility record show four smaller-scale peaks in between the thick limestone beds.

An important question is how to correlate the limestone beds to the eccentricity record. From a paleoclimatological point of view it is most logical to correlate the limestones to eccentricity maxima. During periods of maximum eccentricity the Earth is in perihelion during the northern hemisphere summer, summer temperatures are above average and winter temperatures below

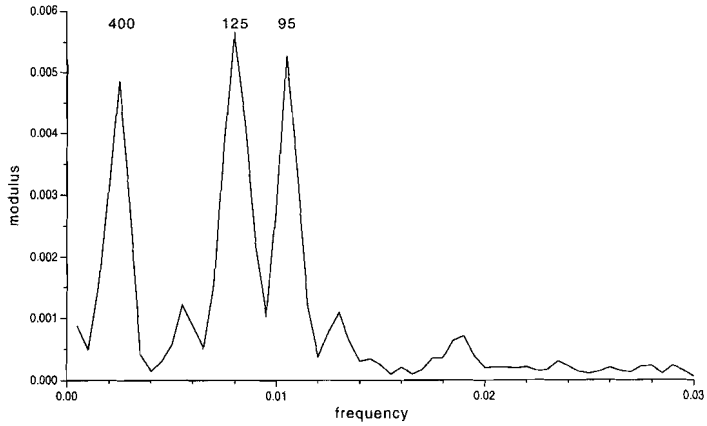

Figure 11. : Frequency spectrum of the La90 solution for eccentricity. The amplitude of the spectral peaks corresponding to the 125 and 95 kyr periods are of similar magnitude. This corresponds to a mean period of approximately 110 kyr, as found in the Armantes record.

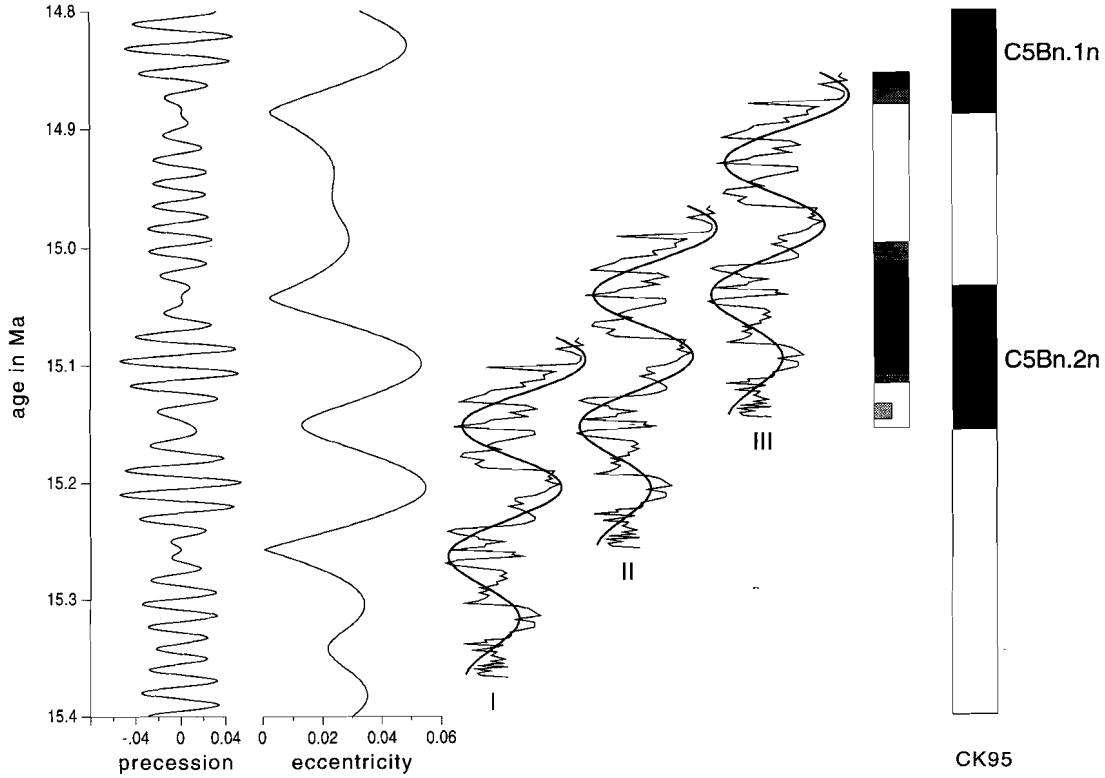

Figure 12. : Precession and eccentricity according to La90. The carbonate record (this line) has been filtered (thick line) using a low-pass filter in the frequency domain. Magnetostratigraphy is correlated to CK95. The three most appropriate correlations of the carbonate record to La90 are shown (see text); our preferred correlation is option I.

average. The orbital eccentricity defines the maximum possible insolation perturbations and precession defines the time of occurrence, i.e., when mid-winter and mid-summer solstices coincide with perihelion and aphelion (cf. Park and Oglesby, 1994). Increasing latitudinal temperature gradients during high eccentricity likely induce a greater depression activity, and hence an increased rainfall (cf. Valdes et al., 1995). A rise of the ground-water level resulting from the increased humidity thus would have allowed evaporation and the precipitation of carbonates as caliche nodules and carbonate crusts under marginal lacustrine conditions. From marine Pliocene sequences is has become clear that periods of increased humidity are connected with, among others, the monsoonal system which in turn results from orbitally forced variations in low latitude summer insolation, and correlate with periods of precession minimum (Rossignol-Strick,

1983; Rohling and Hilgen, 1991). Future research is needed to confirm the suggested relations between limestones and eccentricity.

To make a correlation to the astronomical curves, an independent age constraint is needed. In this study this is provided by the ages of the polarity reversals. The three reversals recorded in the section correspond to the chron boundaries C5Bn.2n(o) at 15.155 Ma, C5Bn.2n(y) at 15.034 Ma and C5Bn.1n(o) at 14.888 Ma (Krijgsman et al., 1994b). According to these ages of CK95, the interval between the youngest and oldest recorded reversal has a duration of 267 kyr. The same interval covers two large-scale eccentricity cycles which suggests only approximately 220 kyr (18% shorter). An explanation for this difference is an error in the ages of the calibration points in CK95. A magnetostratigraphic and cyclostratigraphic study on late Miocene sections on Crete (Krijgsman et al., 1994a) indeed showed that astronomically defined time spans are approximately 10 % shorter than expected in GPTS of CK92 (Cande and Kent, 1992).

The ages of the recorded reversals in our detailed studied part of the Armantes section are largely determined by the calibration point of 14.8 Ma in CK95, assigned to the younger end of chron C5Bn.1n(y). This is an average age based on radioisotopic age constraints on the correlative N9/N10 planktonic foraminifera zone boundary (Miller et al. 1985; Berggren et al., 1985), as estimated in Japan at 14.6 ± 0.04 Ma (Tsuchi et al., 1981) and in Martinique at 15.0 ± 0.3 Ma (Andreieff et al., 1976). However, Baksi (1993) presented a time scale, based on ages derived from $^{40}Ar/^{39}Ar$ incremental-heating of whole rock basalts, which suggests that chron C5Bn.1n is approximately 1 Myr older than indicated by CK95. Berggren et al. (1995) conclude that the Baksi (1993) time scale suffers from ambiguous correlations of isolated magnetic reversals to the GPTS. Astronomical ages for polarity reversals up to 9.5 Ma (Hilgen et al., 1995) are only slightly (50 kyr) older than in CK95 suggesting that the average age of 14.8 Ma of CK95 is probably a better estimate than the ages of Baksi (1993) but that a slightly older age can not be totally excluded.

If we assume that a maximum in the carbonate record corresponds to a maximum in eccentricity, then different correlations can be made to the astronomical solutions of La90 (Fig. 12). The best fit is given by the oldest correlation, the younger correlations are less likely because the maxima in carbonate record do not fit well to the eccentricity curve. The older correlation suggests that the age of 14.8 Ma of C5Bn.1n(y) in CK95 is probably too young, but it would be in good agreement with the radiometric dating of Andreieff et al. (1976). If our correlation is correct we find ages of 15.33 Ma for C5Bn.2n(o), 15.23 Ma for C5Bn.2n(y) and 15.10 Ma for C5Bn.1n(o). Obviously, longer detailed carbonate records are needed to confirm these suggestions.

Conclusions

The paleomagnetic signal of the Armantes red-bed section is generally of good quality. The ChRM is determined by hematite as well as magnetite and/or maghemite. Even though these components do not always show the same polarity at the same level, it is possible to determine the polarity reversals with an accuracy of approximately 1 m which corresponds to ± 10 kyr. The relative contribution of hematite is strongly dependent on the lithology. In the limestones, hematite is the dominant carrier of the magnetisation, whereas the contribution of magnetite/maghimite is of major importance in the silts. The absolute contribution of hematite is higher in the silts than in the limestones.

The distinct cyclic alternation of pink/white limestones and red silts is magnetostratigraphically dated to have a periodicity of on average 111 kyr (Krijgsman et al., 1994). Spectral analysis of the astronomical solutions of La90 for the correlative time interval (14.5-15.5 Ma) shows two equal intensity peaks at 125 and 95 kyr, resulting in an average periodicity of 110 kyr for eccentricity. This is in excellent agreement with our magnetostratigraphic results and confirms the suggestion that the large-scale cyclicity in the Armantes section is related to the eccentricity cycle of the Earth's orbit. From a paleoclimatological point of view it is most likely that the large-scale maxima in carbonate content correspond to maxima in eccentricy, and both the large-scale as small-scale maxima in carbonate content to minima in precession.

The magnetostratigraphic results from this detailed study show that the interval between the three reversals covers two large-scale cycles, suggesting a duration of approximately 220 kyr whereas the corresponding duration according to CK95 is 267 kyr. Tentative correlations of the carbonate record to the eccentricity curve of La90 shows a best fit, which suggests that ages in CK95 are slightly (175 kyr) too young. Such difference between astronomical duration and the duration according to the GPTS has been observed before, and mainly depends on errors in the ages of the calibration points in the GPTS. Our best fit correlation is in good agreement with the radiometric dating of 15.0 ± 0.3 Ma (Andreieff et al., 1976).

Altogether, this study indicates that the conditions for constructing an APTS in the continental deposits of the Calatayud-Daroca basin are favourable. On the basis of this study, our future research will be directed to much longer and more detailed sections, which will provide the necessary information about the effects of both long-term variations (~400 and ~100 kyr eccentricity cycle) and short-term variations (precession cycle).

Acknowledgements

We thank Mark Dekkers and Frits Hilgen for useful discussions. Luc Lourens is greatfully acknowledged for providing the astronomical solutions of La90. Ton Zalm and Marjan Reith assisted with the carbonate measurements and the TGA and X-ray experiments. This study was supported by the Netherlands Geosciences Foundation (GOA/NWO).

Chapter 9

Magnetic polarity stratigraphy of late Oligocene to middle Miocene mammal-bearing continental deposits in Central Anatolia (Turkey)

Abstract

The magnetostratigraphic results of six late Oligocene to middle Miocene mammal-bearing sections in central Anatolia are presented and - where possible - correlated to the geomagnetic polarity time scale (GPTS). Time stratigraphic constraints for the biostratigraphic zones recognised in the lower and middle Neogene are established. The *Eucricetodon* dominated assemblage (Yeniköy section) appear to be of early late Oligocene Age. The Yeniköy fossil locality is correlated to chron C10r (29.2 Ma). The *Meteamys* and *Muhsinia* dominated assemblages (Inkonak, Kargi sections) are of latest Oligocene to earliest Miocene Age; the age of the Inkonak locality is determined between 25.3-23.2 Ma. The Kargi section, which is estimated on biostratigraphic criteria to be somewhat younger than the Inkonak section, provided no reliable magnetostratigraphic results. The *Eumyarion* and *Spano/Democricetodon* dominated assemblages of the Harami 1 and 3 localities are correlated to chrons C6Bn.2n (22.9 Ma) and C6Bn.1r (22.8 Ma), respectively, and are of early Miocene Age. The similar, but biostratigraphically younger assemblage from the Keseköy section has an age of 20.1 ±2.2 Ma, based on fission track dating of zircons occurring in several intercalated tuff layers. The correlation to the GPTS of the polarity sequence of the Gemerek section remains uncertain.

This chapter has been accepted for publication as: W. Krijgsman, C.E. Duermeijer, C.G. Langereis, H. de Bruijn, G. Saraç, P.A.M. Andriessen, Magnetic polarity stratigraphy of late Oligocene to middle Miocene mammal-bearing continental deposits in Central Anatolia (Turkey). *Newslett. Stratigr.*, 1996.

Introduction

The biostratigraphic subdivision of the European continental Oligocene and Miocene is primarily based on rodents. Recent studies of late Oligocene to early/middle Miocene continental mammal-bearing sections in Anatolia (Ünay & de Bruijn, 1987; Sümengen et al., 1990; Langereis et al., 1990; de Bruijn et al., 1991, 1993) aimed at the development of a biostratigraphic zonation for the continental Neogene of Turkey. Although a local biostratigraphic scheme for Anatolia is now emerging, the fundamental differences between the succession and content of rodent faunas in Anatolia and Europe during the late Oligocene and early Miocene precludes biostratigraphic correlation to the standard zonations. This correlation is of vital interest to understand what geologic or climatic events have triggered the migration of mammals from Anatolia to Europe during the middle and late Miocene. To acquire knowledge of the rodent succession of Anatolia and to establish its correlation to the European standard schemes is a necessary step for understanding the complex context between the faunas of Central Asia and of Europe.

In Europe, last occurrences of characteristic Oligocene genera - *Issiodoromys*, *Archaeomys* (Theridomyidae), *Plesiosminthus* (Zapodidae) and *Adelomyarion* (Pseudocricetodontinae) - in combination with specific evolutionary stages in genera that straddle the Oligo/Miocene boundary interval - *Eucricetodon* (Eucricetodontinae) and *Eomys*, *Rhodanomys*, *Ritteneria*, *Pseudotheridomys* (Eomyidae) - allow biostratigraphic correlations for the MP 29 to MN 2 interval. The European MN 3 assemblages are characterised by the absence of Muroidae other than *Melissiodon* (the so-called cricetid-vacuum) in combination with the presence of *Ligerimys* (Eomyidae). These assemblages usually contain a very diverse association of dormice. The boundary with the next (MN 4) zone is usually drawn on the basis of the presence of Democricetodon. The zonal scheme for Europe as briefly outlined above, although it allows intra-European correlations, is not so straightforward as it may seem because of different usage by different authors (Hugueney & Ringeade, 1990; Agusti & Moya-Sola, 1991; Burbank et al., 1992; de Bruijn et al., 1992; Alvarez Sierra & Daams, 1994) and because of differences in the succession of faunistic events in different areas.

The succession of rodent faunas in Anatolia from deposits that have been considered to be of late Oligocene to early Miocene Age, on the basis of a combination of regional geological setting and fauna content, is very different from that in Europe. The Theridomyidae and *Adelomyarion* are not known from Anatolia, while the Zapodidae, although represented by a few specimens in many faunas, seem to be different from the European *Plesiosminthus*. *Eucricetodon* is only known from the middle Oligocene of the Yeniköy section, and the first of the eomyids to arrive in Anatolia seems to have been *Keramidomys* in the assemblage of Candir (MN 6 = middle Miocene).

The aim of this paper is to establish a time-stratigraphic framework for the continental Oligo-Miocene fauna assemblages of smaller mammals of Turkey.

Figure 1. Location of the Central Anatolian sections

Magnetostratigraphic studies enable the correlation of sedimentary sequences independently of their fossil content and may therefore be used to correlate local zonations from different regions. Magnetic polarity sequences of mammal-bearing sections will eventually result in the calibration of fossil localities to the geomagnetic polarity time scale (GPTS) and thus in assigning absolute ages to characteristic fauna assemblages (e.g. Barbera et al., 1994; Krijgsman et al., 1994; Garcés, 1995). To make a direct correlation of the Turkish fauna assemblages to the GPTS, we sampled six fossil bearing sections in Central Anatolia that play a key role in the late Oligocene-middle Miocene mammal sequence of Turkey. For three sections, additional radiometric datings provide independent age constraints. In this paper we present the magnetostratigraphic results of our sections and the most likely correlation of their fossil localities to the GPTS.

Sections and sampling

Six mammal-bearing sections of Central Anatolia with tentative ages ranging from late Oligocene to middle Miocene, have been sampled for magnetostratigraphic purposes. Three sections (Yeniköy, Inkonak and Gemerek) are located in the Kayseri-Sivas basin, SE of Ankara; the other sections (Kargi, Harami and Keseköy) are outcrops in coal quarries in small isolated basins (Fig. 1). Each section was sampled over the longest stratigraphic range possible, depending on the lithology, outcrop and tectonics, to establish a maximum number of polarity zones. Care was taken to sample fresh sediment by removing the weathered surface. Cores were drilled electrically with a generator as power

supply and water as a coolant. Oriented handsamples were taken when drilling was impossible because water dissolved to much of the core. Cores were drilled from these handsamples with compressed air after embedding them in plaster of Paris at the paleomagnetic laboratory Fort Hoofdddijk.

Fluviatile/lacustrine deposits of the Kayseri-Sivas basin

The Yeniköy, Inkonak and Gemerek sections are located in the Kayseri-Sivas basin. This NE-SW trending basin is delimited by metamorphic rocks in the north and south (Sümengen et al., 1990). Sediments are predominantly fluviatile/lacustrine deposits which overlie prominent gypsum deposits representing the regressive phase of marine Eocene-Oligocene deposits (Ünay & de Bruijn, 1987; Sümengen et al., 1990). Faunal analysis showed that these continental deposits range in age from late Oligocene to early Pliocene. They mainly consist of clays, silts and limestones which are often intercalated with thick sandy deposits.

The Yeniköy section is biostratigraphically the oldest continental section and contains *Eucricetodon* dominated assemblages. It consists of a rhythmic alternation of silty clays and sandstones and has a thickness of 800 metres. The dip of the bedding plane is not consistent because of folding. In the upper part of the section a non-exposed interval (river, valley) results in a stratigraphic gap of 80 metres. Handsamples were taken at 78 levels, mainly from the silty clay layers.

The Inkonak section is a road cut situated at approximately 50 km south of Sivas along the main road to Kangal (Fig. 1). The *Meteamys* and *Muhsinia* dominated assemblages from this section are tentatively considered to be of latest Oligocene/earliest Miocene age (De Bruijn et al., 1991). The Inkonak section is 313 metres thick and consists of a regular alternation of clays, limestones and sandy deposits. Oriented handsamples were taken at 197 levels.

The Gemerek section is situated in the southern limb of a complex anticline in the lower part of the Yenienbuk Formation (Sümengen et al., 1990). In this section only one poor assemblage of rodents has been collected. This assemblege contains *Cricetodon* sp., *Deperetomys* sp., *Democricetodon* cf. *gaillardi, Megacricetodon* cf. *collongensis, Vasseuremys* sp. and *Microdyromys* sp. and clearly belongs in the category of assemblages that are dominated by *Cricetodon* and *Megacricetodon,* but it could not be correlated unambiguously to the MN zonation (Sümengen et al., 1990; de Bruijn et al., 1992). Following the decision reached in Salzburg (March 1995) to extend unit MN 5 downwards to include former sub-unit MN 4b we agree with Steininger et al. (1990) that the Gemerek assemblage is best attributed to MN 5.

Preliminary magnetostratigraphic results of this section resulted in four possible correlations with ages for the Gemerek locality varying from 14.9 to 16.5 Ma (Langereis et al., 1990). Those correlations were largely based on the radiometric dating of an overlying basalt. The Gemerek section consists of an irregular alternation of clays, silts, sands and limestones. We extended the section

downward by approximately 30 metres and furthermore sampled the overlying basalt. Oriented cores at 11 additional levels resulted in a total of 73 sampled levels over a stratigraphic range of 200 metres.

Lake deposits of Central Anatolia

The sediments of the Kargi, Harami and Keseköy sections (Fig. 1) are deposited in small intramontane basins bordered by mainly volcanic and metamorphic rocks. The predominantly fine grained sediments suggest a low-energy depositional environment.

The Kargi section is situated in a coal quarry located near the village of Dodurga. The *Meteamys* and *Muhsinia* dominated assemblages are presumably somewhat younger than those from Inkonak (de Bruijn et al., in prep.). The deposits show a rhythmic alternation of white limestones and dark green clays. The area is strongly tectonised which resulted in folding and faulting. Samples were taken at 76 levels over a stratigraphic range of 53 metres. Cores could be drilled from the limestones but it was necessary to take handsamples from the often deformed clays.

The Harami section constitutes the sedimentary overburden of the main coal level of the Harami mine near the town of Ilgin (Fig. 1). It contains *Eumyarion* and *Spano/Democricetodon* dominated assemblages attributed to zone MN 1 or 2 (De Bruijn et al., 1992). Green-brown laminated or homogeneous clays comprise the main part of the section. At several levels small coal layers (1-10 cm) are present. The upper part of the Harami section shows a gradual transition to more calcareous sediments; marls and marly limestones. Cores were drilled at 127 levels from the 59 metres thick section. In the upper part two biotite-rich volcanic layers were sampled for radiometric dating.

The Keseköy section is a coal quarry near the town of Kizilcahamam (Fig. 1). It contains an *Eumyarion* and *Democricetodon* dominated assemblage that is attributed to MN 3 (De Bruijn et al., 1992). The Keseköy section predominantly consists of green-brown, partly laminated, clays showing a gradual transition to marly deposits towards the top. Several organic rich (coal) layers are intercalated. We drilled 27 levels over a stratigraphic range of 13.5 metres. Thin tuff layers are found in the lower part of the section and were sampled for radiometric datings.

Paleomagnetic results

The natural remanent magnetisation (NRM) was measured on a 2G Enterprises cryogenic magnetometer. At least one specimen from each sampling level was progressively demagnetised by applying stepwise thermal demagnetisation with small temperature increments (30°-50°C) up to a maximum of approximately 700°C. Further, some rock magnetic experiments were

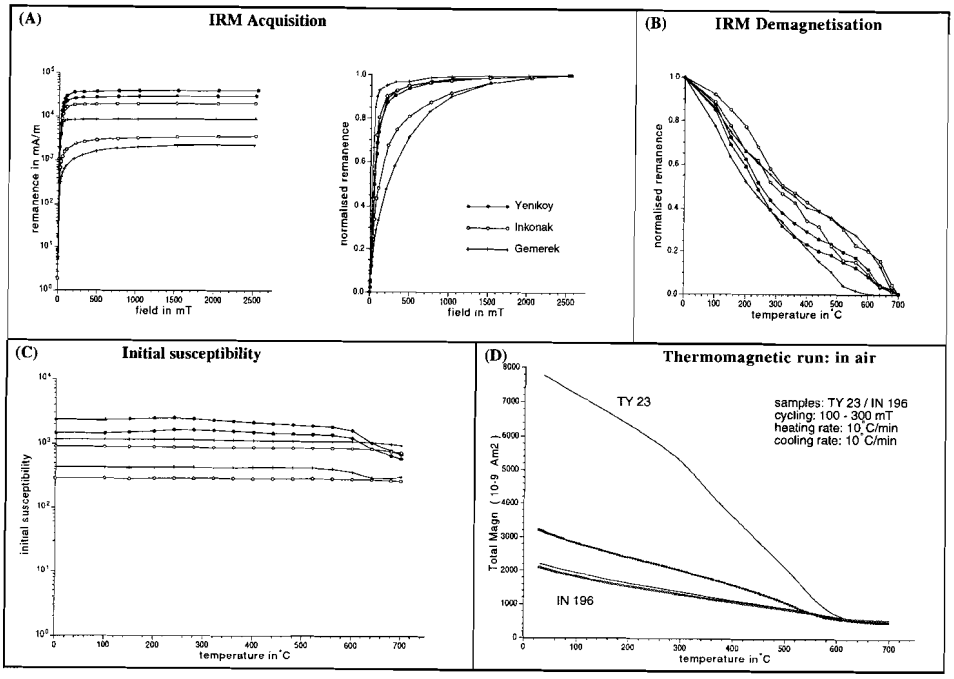

Figure 2. (A) IRM acquisition of selected samples of the Yeniköy, Inkonak and Gemerek sections. Left curves with absolute intensities; right curves with normalised remanence; (B) stepwise demagnetisation of the IRM of the same samples with temperature increments of 40 °C; (C) initial susceptibility of the IRM during thermal demagnetisation; (D) Thermomagnetic runs in air for specimens of Yeniköy and Inkonak.

performed and include the acquisition of isothermal remanent magnetisation (IRM) and subsequent thermal demagnetisation. IRM acquistion was achieved using a PM 4 pulse magnetiser (manifactured by H.N. Böhnel) and measured on a digitised spinner magnetometer based on a Jelinek JR-3 drive unit. The low field magnetic susceptibility from the same samples was measured after each temperature increment on a Kappabridge KLY-2. Finally, some thermomagnetic runs were recorded with a modified horizontal translation Curie balans making use of a cycling field (Mullender et al., 1993).

The Yeniköy, the Inkonak and the Gemerek section

The aquisition of the IRM generally shows an initial steep rise at low (300 mT) fields indicating the presence of a low coercivity mineral like magnetite, followed by a more gradual increase to 2500 mT (Fig. 2a). Saturation is not always reached in the highest fields which indicates the presence of a high-coercivity mineral like hematite. The high unblocking temperatures (700 °C) after demagnetisation of the

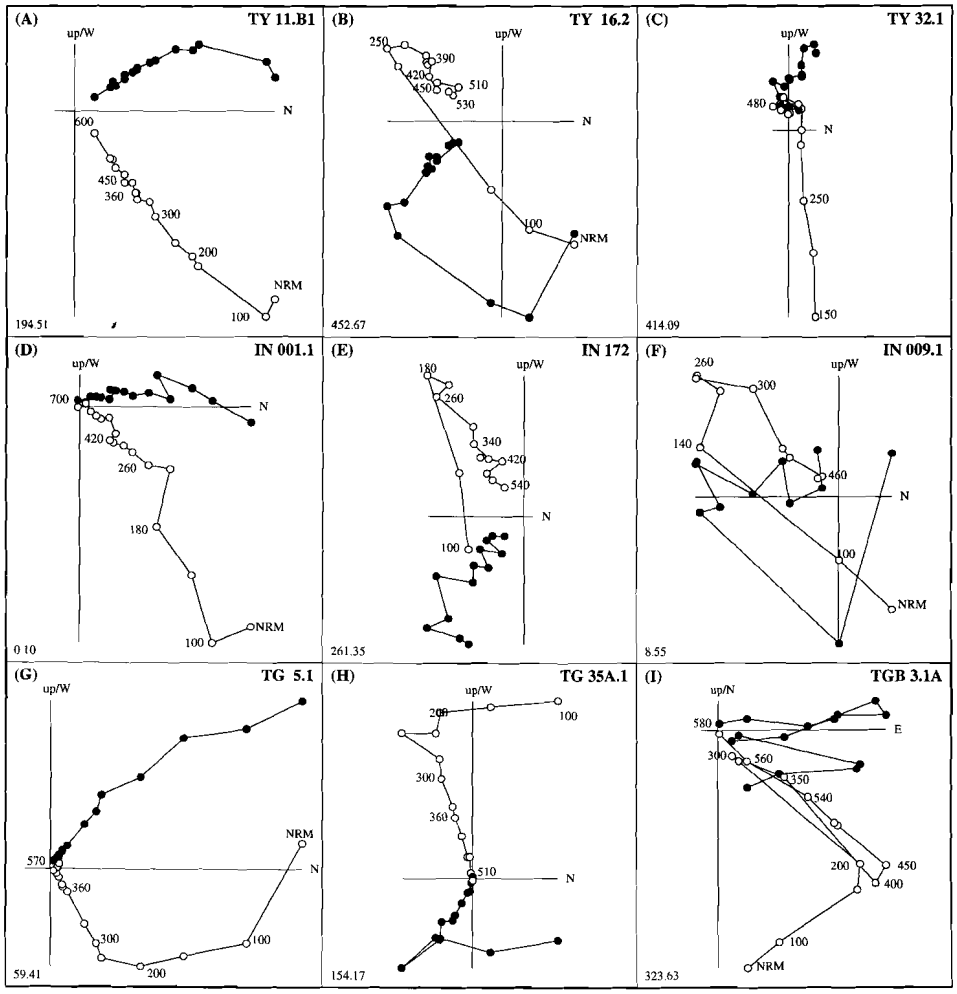

Figure 3. Orthogonal projections of stepwise thermal demagnetisation of selected samples from the Yeniköy (TY), Inkonak (IN) and Gemerek (TG) section. TGB shows sample of the Gemerek basalt. Closed (open) circles represent the projection of the ChRM vector end-point on the horizontal (vertical) plane. Values represent temperatures in °C; stratigraphic levels are in the lower left corners.

IRM suggest that hematite is an important carrier of the magnetisation (Fig.2b). The initial susceptibility does not show major changes when heated up to 600 °C. Between 600-700 °C a decrease in susceptibility is observed - in some cases - which may be the result of oxidation of magnetite into hematite (Fig. 2c). The thermomagnetic runs show unblocking temperatures higher than 600 °C but do not clearly show the Curie point for hematite (Fig. 2d).

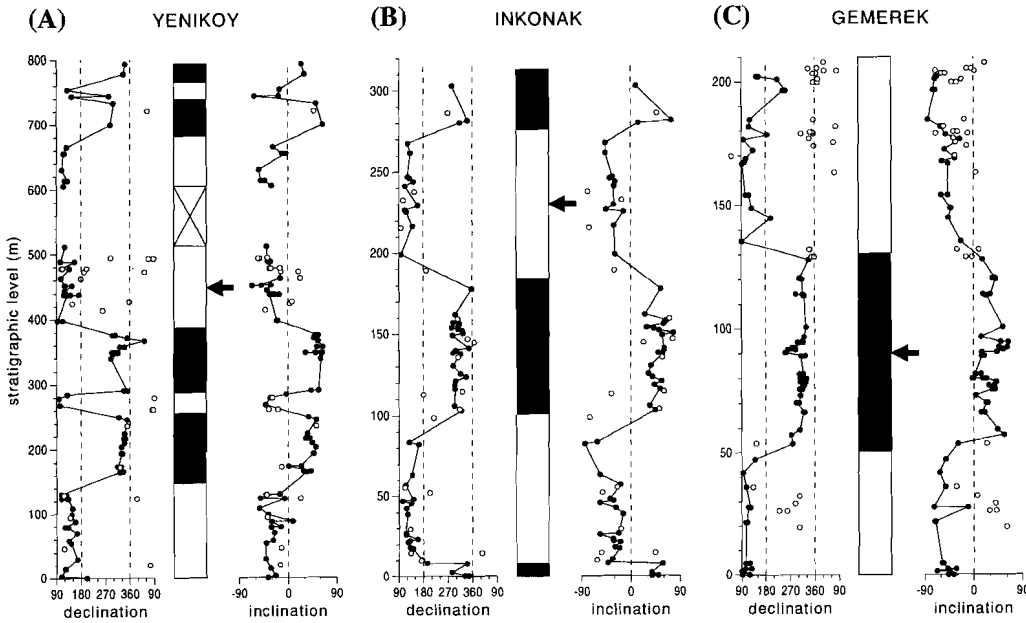

Figure 4. Magnetostratigraphy of the (A) Yeniköy, (B) Inkonak and (C) Gemerek sections. Closed circles represent reliable directions, open circles represent low intensity samples which are difficult to interpret. In the polarity column, black denotes normal polarity and white denotes reversed polarity zones. Crossed area in the Yeniköy polarity column denotes a non-exposed interval. Arrows point to position of the fossil localities.

The NRM of the fluviatile/lacustrine sections of the Kayseri-Sivas basin show relatively high intensities ranging from 0.5-2 (Inkonak), 1-2 (Gemerek) and 4-20 mA/m (Yeniköy). The NRM of almost all samples is composed of two components (Fig. 3), apart from a small viscous and randomly oriented laboratory induced component removed at 100° C. The first component is generally removed between 100° and 240° C, has a present-day direction before bedding tilt correction and is therefore of recent origin and most probably caused by weathering of the sediment. The second component, removed at higher temperatures (up to 700° C) is the characteristic remanent magnetisation (ChRM) component and is used for determining the polarity zones. The thermal demagnetisation diagrams of the basalt from the Gemerek section reveal a more complex behaviour. It shows a normal component at low (200-300 °C) and high (450-580 °C) temperatures and a reversed component at medium (300-450 °C) temperatures (Fig. 3i).

From most samples, thermal demagnetisation reveals a stable and reliable ChRM component and these directions are plotted with a solid dot (Fig. 4). Because we sampled widely varying lithologies not all levels give reliable results. When NRM intensities were too low or remagnetisation (weathering) processes disturb the primary signal too much, characteristic directions cannot reliably be

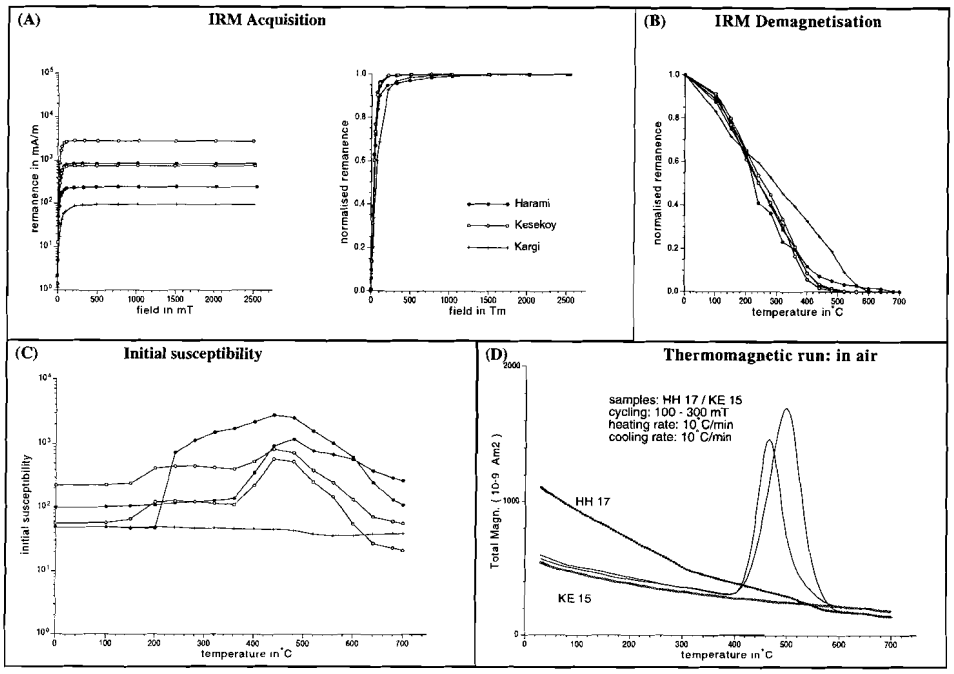

Figure 5. (A) IRM acquisition of selected samples of the Kargi, Harami and Keseköy sections. (B) stepwise demagnetisation of the normalised IRM and (C) initial susceptibility of the same samples with temperature increments of 40 °C. (D) Thermomagnetic runs in air for two specimens of Harami and Keseköy (see also caption to figure 2).

determined. The interpreted results of these samples are plotted with an open circle (Fig. 4).

The ChRM directions and polarity zones of the Yeniköy section (Fig. 4a) show that seven polarity reversals are recorded. The magnetostratigraphic record of the Inkonak section reveals four polarity reversals (Fig. 4b), only two reversals are recorded in the Gemerek section (Fig. 4c). The downward extension of this section only resulted in additional reversed polarities.

The Kargi, the Harami and the Keseköy section

The initial steep rise in IRM acquisition of the samples from the Kargi, Harami and Keseköy sections at low (100-200 mT) fields indicates a rapid saturation and suggests the presence of a low coercivity mineral like magnetite (Fig. 5a). The demagnetisation curve of the IRM for the Kargi sample shows an unblocking temperature of approximately 600 °C. The observed maximum unblocking temperatures (480-520 °C) for the samples from Harami and Keseköy are lower than the Curie point of magnetite (580 °C), suggesting that titanomagnetite is the

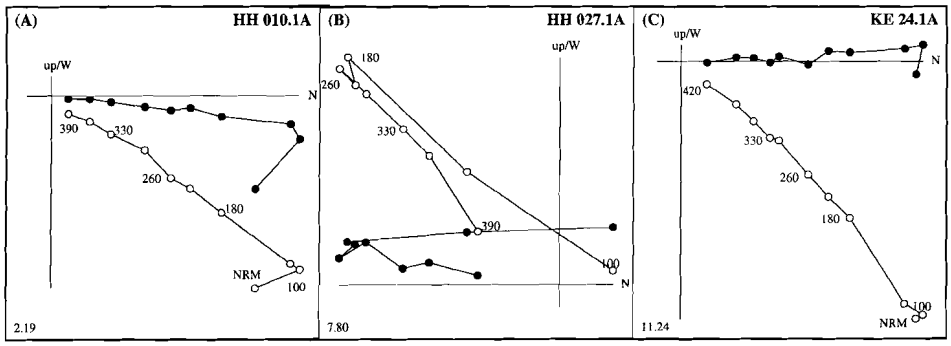

Figure 6. Orthogonal projections of stepwise thermal demagnetisation of selected samples from the Harami (HH) and Keseköy (KE) sections (see also caption to figure 3).

main carrier of the remanence (Fig. 5b). Both the thermomagnetic runs and the initial susceptibility records show that important chemical reactions occur between 400-600 °C, which suggest a significant increase in magnetic material (probably magnetite) when heated to temperatures above 400 °C (Fig. 5c,d). This may be the result of oxidation of an iron sulfide (pyrite). Further heating above 500 °C probably leads to oxidation of magnetite to hematite and consequently a decrease in susceptibility.

The NRM intensities of the Kargi section are too low to obtain any reliable magnetostratigraphic results. This is regrettable because this section is considered on biostratigraphic grounds to straddle the Oligo/Miocene boundary.

At Harami the NRM is composed of two components; a secondary present-day field component removed between 100 and 240 °C, and a probably primary component, showing both normal and reversed polarities, removed at higher (240-420 °C) temperatures (Fig. 6a,b). At temperatures higher than 420 °C the ChRM component is overprinted by a viscous and randomly oriented component, probably the result of the new magnetic material that is formed during heating.

The Keseköy section only shows normal polarities. Thermal demagnetisation can be applied up to temperatures of 420 °C (Fig. 6c). Rock magnetic studies as well as thermal demagnetisation show the same characteristics as in Harami. Therefore, we may assume that we are dealing with a primary component at Keseköy.

Magnetostratigraphic results show that nine polarity reversals are recorded in the Harami section. The Keseköy section only comprises one (normal) polarity (Fig. 7).

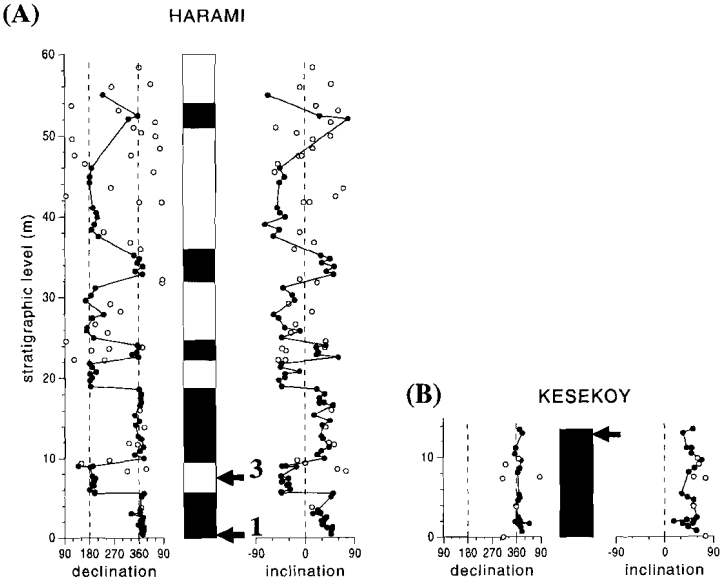

Figure 7. Magnetostratigraphy of the Harami (A) and Keseköy sections (see also caption to figure 4). Arrows point to the positions of the fossil localities (1=Harami 1; 3=Harami 3).

Radiometric datings

In the Gemerek section, an intercalated basalt flow has been dated by K/Ar techniques, resulting in a mean age of 14.9 ± 0.7 Ma. This mean age was used by Langereis et al (1990) as an age constraint for their magnetostratigraphic correlations. However, this mean value appeared to be composed of four separate datings of 10.4 ± 1.8, 12.4 ± 0.8, 13.0 ± 2.2 and 16.2 ± 1.8 Ma. The large spreading of these datings shows that a calculated mean age of 14.9 ± 0.7 is not meaningful and it can therefore not be used as an age constraint for magnetostratigraphic correlations.

Dating of the Harami ash layers was attempted by $^{40}Ar/^{39}Ar$ incremental heating of biotites. Biotite separated from both ash layers HAR-1 and HAR-2 yielded staircase patterns which are indicative for substantial loss of radiogenic argon; no plateaus were observed, but in the case of HAR-1 a maximum age of 28.3 ± 0.3 Ma and in the case of HAR-2 a maximum age of 30.5 ± 0.7 Ma suggests that crystallisation occurred in the Oligocene or older (J.R. Wijbrans, pers. comm.).

Fission track dating of zircons from volcanic tuff layers has proven to provide reliable time-markers in stratigraphic sections and for biostratigraphic correlations (Andriessen et al., 1993). Zircons from intercalated tuff layers from

sample	mineral	No. of grains	ρ_s (N_s) (10^6 cm^{-2})	ρ_i (N_i) (10^6 cm^{-2})	ρ_d (N_d) (10^6 cm^{-2})	P (χ^2) (%)	age ± 1σ (Ma)	D (%)
Tur 25	zircon	10	3.59 (344)	9.73 (502)	1.97 (4349)	50	21.1 ± 2.2	9
Tur 26	zircon	9	3.82 (337)	11.2 (492)	1.97 (4349)	5	20.3 ± 2.3	8
Tur 27	zircon	8	5.62 (253)	14.4 (323)	1.97 (4349)	98	24.9 ± 2.9	5
Tur 29	zircon	9	4.07 (359)	13.1 (578)	1.97 (4349)	50	18.6 ± 2.0	11
Tur 30	zircon	9	5.94 (621)	17.9 (934)	1.97 (4349)	10	20.5 ± 1.9	12

Table 1. Zircon fission track age determinations from the Keseköy section. Zircons were etched in an eutectic KOH-NaOH melt at 220 °C for 10 hours; mica's external detectors covering the zircons were etched with 48% HF at room temperature for 16 minutes and mica's covering the glass were etched for 60 minutes. NBS glass 962; ζ=315.15 ± 17.27, based on analyses of several international zircon age standards. ρ_S=spontaneous track density; ρ_i=induced track density (includes 0.5 geometry factor); ρ_d=density of tracks in the glass dosimeter; N_S, N_i, N_d=number of tracks actually counted to determine the reported track densities. All ages are reported as central ages (Galbraith & Laslett, 1993). P(χ^2)=Chi-squared probability that the single grain ages represent one population; D=age dispersion.

the Keseköy section were dated by the fission track method (Table 1). The obtained age range from 18.6 ± 2.0 Ma to 24.4 ± 2.9 Ma, with four age determinations overlapping eachother (18.6 ± 2.0 to 21.1 ± 2.2 Ma). The calculated mean age of these four age determinations is 20.1 ± 2.2 Ma.

Correlation to the GPTS

Correlation of the magnetic polarity sequences of the Anatolian sections to the GPTS has been made by reference to the most recent version CK95 (Cande & Kent; 1995). Because biostratigraphic control is poor, it is essential that several polarity reversals are recorded in each section. In the field, there was no evidence for major hiatuses and furthermore for each section a constant average sedimentation rate is assumed. From the six sampled sections only the Yeniköy and Harami sections can be directly correlated to the GPTS based on their polarity pattern alone. For Inkonak, Gemerek and Keseköy additional biostratigraphic and/or radiometric data are required to obtain a tentative correlation. Unfortunately, the samples from Kargi do not provide any magnetostratigraphic information because the NRM intensity was below the sensitivity of the cryogenic magnetometer.

The characteristic polarity pattern of the Yeniköy section results in only one correlation with CK95 if we assume that the stratigraphic gap of 80 metres

contains only reversed polarities (Fig. 8). The Yeniköy fossil locality is determined in chron C10r with a corresponding age of 29.2 Ma, which results in a correlation of the *Eucricetodon* dominated assemblage with the early late Oligocene. The total section comprises 2 Myr and has an average sedimentation rate of 42 cm/kyr, which is in agreement with the thick sandy intercalations.

The polarity sequence of the Harami section also gives only one significant correlation to CK95 (Fig. 8). The fossil localities Harami 1 and 3 are correlated with chrons C6Bn.2n and C6Bn.1r, with ages of 22.9 and 22.8 Ma, respectively. This corroborates the early Miocene age for the *Eumyarion* and *Spano/Democricetodon* dominated assemblages supposed by De Bruijn & Saraç (1991). The $^{40}Ar/^{39}Ar$ datings on the Harami ash layers, suggesting Oligocene ages, are in contradiction with the magnetostratigraphic and biostratigraphic results. We suggest that the older argon dates for the biotites points to redeposition of the ash layers after original eruptive emplacement in the Oligocene or older. Following the correlation table of Steininger et al. (1990) Harami 1 and 3 are correlative with MN 2. The lake deposits of the Harami section have a sedimentation rate of 5 cm/kyr which is much lower than the fluviatile deposits of Yeniköy. In the continental biostratigraphic record the MP 30/ MN 1 boundary has recently been magnetostratigraphically dated at 23.8 Ma (chron C6Cn.2n; CK95) in an alluvial lacustrine succession in NE Spain (Barbera et al., 1994). An early Miocene age for the Harami section is in agreement with these results from the spanish sections.

The Inkonak section reveals only four polarity reversals and no unambiguous correlation can be made with CK95 based on the polarity pattern alone. However, Inkonak is biostratigraphically positioned between Yeniköy and Harami and this constraint leads to possible correlations to either chrons C6Br, C6Cn.1r or C8r (Fig. 8) with ages varying from 23.2 to 25.3 Ma. The late Oligocene-early Miocene Muroidea assemblages from Anatolia show an important change from *Meteamys* and *Muhsinia* dominated (Inkonak, Kargi) to *Eumyarion* and *Spano/Democricetodon* dominated assemblages (Harami 1 and 3). We expect that this transition may take considerable time. Therefore, the correlations of the Inkonak section to either C6Br or C6Cn.1r (23.2 or 23.6 Ma) are less likely from a biostratigraphic point of view. Hence, the most probable correlation of the Inkonak locality is to chron C8r (25.3 Ma), which is correlative to the late Chattian and MN 1 according to Steininger et al. (1990). The inferred sedimentation rate from this correlation is 43 cm/kyr; almost the same as in Yeniköy. The earlier tentative age of latest Oligocene/earliest Miocene of de Bruijn et al. (1991) for the Inkonak locality agrees well with these results. Depending on which correlation is preferred the Inkonak section is of latest Oligocene (C8r; 25.3 Ma) or earliest Miocene (C6Br, 23.2 Ma; C6Cn.1r, 23.6 Ma) age.

The Gemerek section consists of the same type of fluviatile/lacustrine sediments as Yeniköy and Inkonak. The previously published magneto-stratigraphic results of Langereis et al. (1990) suggested four possible correlations to the GPTS, with ages ranging from 14.9-16.5 Ma. However, these correlations were largely based on a mean radiometric date of 14.9 ± 0.7 Ma for an overlying

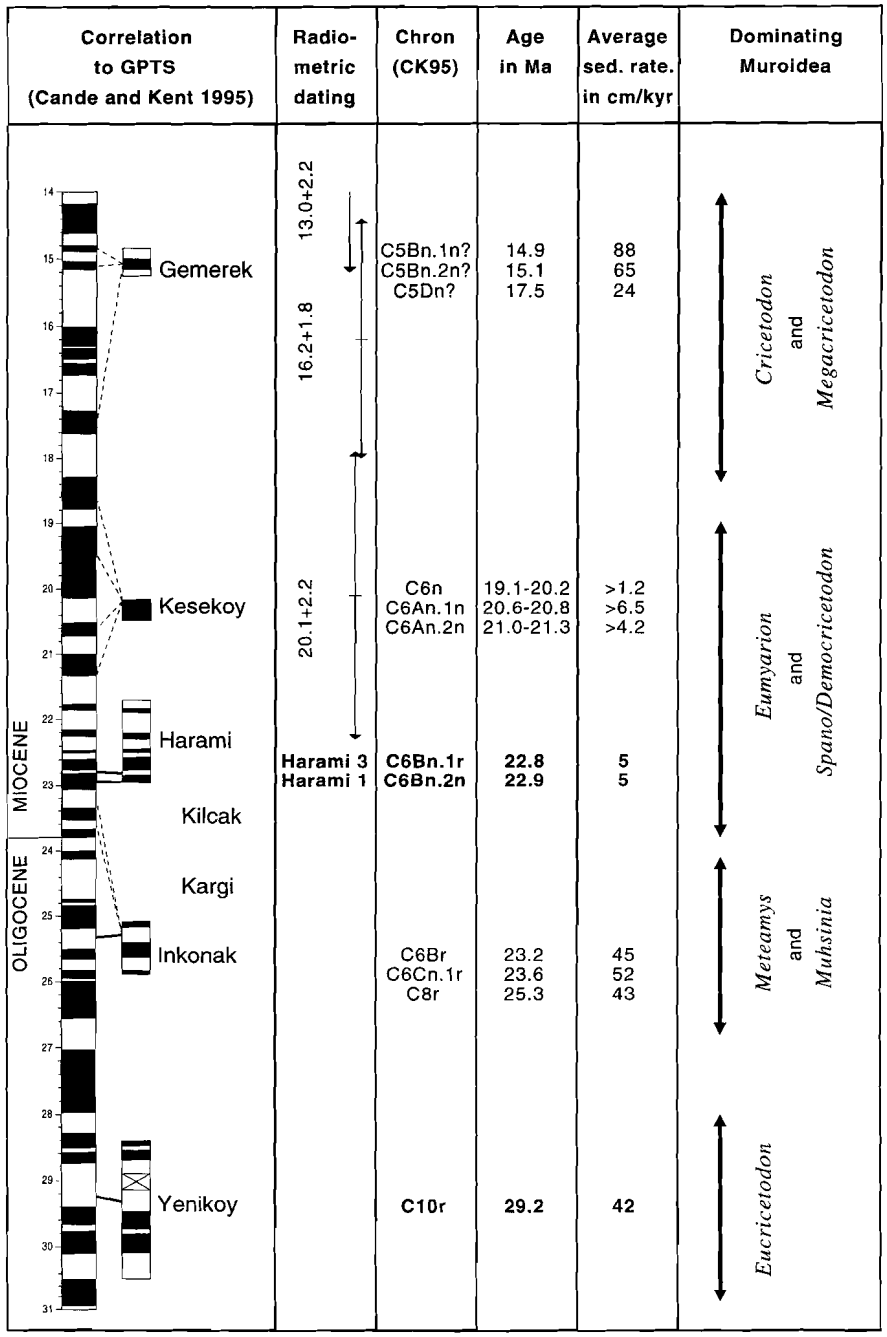
Correlation to GPTS (Cande and Kent 1995)
Radio-metric dating
Chron (CK95)
Age in Ma
Average sed. rate. in cm/kyr
Dominating Muroidea
MIOCENE
OLIGOCENE
Gemerek
Kesekoy
Harami
Kilcak
Kargi
Inkonak
Yenikoy
13.0+2.2
16.2+1.8
20.1+2.2
C5Bn.1n? 14.9 88
C5Bn.2n? 15.1 65
C5Dn? 17.5 24
C6n 19.1-20.2 >1.2
C6An.1n 20.6-20.8 >6.5
C6An.2n 21.0-21.3 >4.2
Harami 3 C6Bn.1r 22.8 5
Harami 1 C6Bn.2n 22.9 5
C6Br 23.2 45
C6Cn.1r 23.6 52
C8r 25.3 43
C10r 29.2 42
Cricetodon and Megacricetodon
Eumyarion and Spano/Democricetodon
Meteamys and Muhsinia
Eucricetodon

basalt flow. The non-exposed stratigraphic interval between the uppermost sample and the basalt is 80 m and may contain hiatuses, faults, etcetera. Furthermore, the large spreading of the four separate datings render this mean age unreliable.

The downward extension of the section did not reveal additional polarity reversals, but only extended the lower reversed interval. The length of this reversed interval suggests that two of the four possible correlations as proposed by Langereis et al. (1990) can be excluded, and make a correlation to chron C5Bn.1n (14.8 Ma) or to chron C5Bn.2n (15.1 Ma) more likely. This suggests sedimentation rates of 88 and 65 cm/kyr, respectively, which is higher than at Yeniköy and Inkonak and less likely considering the type of sediment. Regarding the separate radiometric datings, the maximum age limit of 16.2 ± 1.8 Ma from the oldest of these datings provides another correlation; to chron C5Dn, with an age of 17.5 Ma and a more likely sedimentation rate of 24 cm/kyr (Fig. 8). The minimum age constraint (8.6 Ma) would result in numerous other correlations. It is clear that no reliable correlation to the GPTS can be made for the Gemerek section.

The Gemerek locality is considered to be at the base of MN 5 according to Steininger et al. (1990). Furthermore, these authors use the Gemerek locality (choosing arbitrarily an age of 16.5 Ma) as one of their major tie points for the age of the MN 4/MN 5 boundary (Steininger et al. 1990). It is obvious, however, that no reliable age can be assigned to this boundary based on the data from Gemerek.

The sediments of Keseköy resemble those of Harami and show the same response during thermal demagnetisation. The rock magnetic results suggest that the NRM is carried by the same magnetic carriers. Based on these data we may assume that we are dealing with primary components and we think that a sedimentation rate, close to the 5 cm/kyr for Harami, is a reasonable assumption, because the lithology of Keseköy is similar to that of Harami. The Keseköy section shows only one (normal) polarity and can therefore be correlated with every normal zone of the GPTS. Additional fission track age determinations on zircons provided an age constraint of 20.1 ± 2.2 Ma. This date, together with the assumed sedimentation rate results in correlations to either chron C5En, C6n, C6An.1n or C6An.2n with ages ranging from 18.3-21.3 Ma, very well corresponding to the FT age range of 18.6 to 21.1 Ma. These ages are in agreement with the allocation of the assemblage from the Keseköy fossil locality to MN 3 (De Bruijn et al., 1993).

Figure 8. Correlation of the Anatolian polarity sequences with the GPTS of Cande & Kent (CK95) (1995). Solid lines connect fossil localities to GPTS. Kargi and Kilçak are fossil localities without polarity sequence but displayed at relative position based on biostratigraphic analysis (de Bruijn et al., in prep.). Middle columns show the corresponding chrons of CK95, radiometric datings, the resulting age and average sedimentation rate. Right column shows dominating Muroidea assemblages.

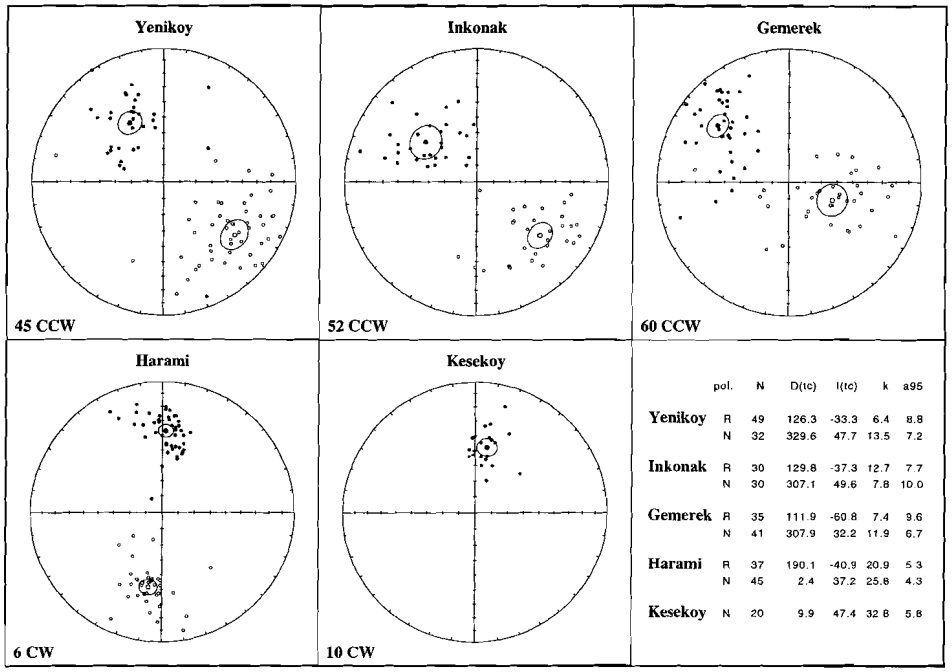

	pol.	N	D(tc)	I(tc)	k	a95
Yenikoy	R	49	126.3	-33.3	6.4	8.8
	N	32	329.6	47.7	13.5	7.2
Inkonak	R	30	129.8	-37.3	12.7	7.7
	N	30	307.1	49.6	7.8	10.0
Gemerek	R	35	111.9	-60.8	7.4	9.6
	N	41	307.9	32.2	11.9	6.7
Harami	R	37	190.1	-40.9	20.9	5.3
	N	45	2.4	37.2	25.8	4.3
Kesekoy	N	20	9.9	47.4	32.8	5.8

Figure 9. Equal area projections of the ChRM components of the Yeniköy, Inkonak, Gemerek, Harami and Keseköy sections. Circles give Fisher's (1953) α95 for the section means. Mean rotations are in the lower left corners; CW = clockwise, CCW = counterclockwise. In table: pol = polarity, N = number of samples used for calculation of mean direction, D(tc), I(tc) = Declination, Inclination after bedding tilt correction, k = precision parameter, α95 cone of confidence at the 95% level.

ChRM directions and rotations

The "reliable" ChRM directions which we used to determine the polarity sequences of the magnetostratigraphically studied sections can also be used to determine the tectonic rotation of the different parts of Central Anatolia since the Oligo-Miocene. For each section the ChRM directions were combined using Fisher (1953) statistics to calculate mean directions. The results show that Yeniköy, Inkonak and Gemerek, the three sections in the Kayseri-Sivas basin, reveal a counterclockwise rotation of 45-60° (Fig. 9). The Harami and Keseköy sections, however, show a small clockwise rotation of 10°. Although Turkey plays an important role in the tectonic evolution of the Mediterranean, paleomagnetic studies are few. The first work was carried out on Permian red sandstones from the Black Sea region where a 85° counterclockwise rotation was observed (Gregor & Zijderveld, 1964). Later, it was concluded that the Turkish plate has been rotated 50° counterclockwise since the Cretaceous (Van der Voo, 1968; Orbay & Bayburdi, 1979). For the Neogene, paleomagnetic measurements in western

Turkey have identified a counterclockwise rotation up to 45°, although some blocks show a clockwise rotation (Kissel, 1986; Kissel et al., 1987). Paleomagnetic and structural data suggest that several distinct domains exist which are bounded by major faults and have rotated around vertical axis, at different rates and in different senses, over the past 7 Myr or more (Kissel et al., 1987; Westaway, 1990). Kissel et al. (1987) suggested that in addition to local rotation of individual domains the actively extending region of West Turkey has rotated clockwise by 6° since late Miocene times. Our results from Central Anatolia are generally in good agreement with the observations and conclusions of Kissel et al. (1987) from western Turkey and suggest a major fragmentation between the Kayseri-Sivas basin and the area west of Ankara.

Conclusions

Of the six sections sampled for magnetostratigraphy, only two (Yeniköy and Harami) reveal a polarity sequence that can reliably be correlated to the GPTS on the basis of their polarity pattern alone. The *Eucricetodon* dominated Muroidea assemblage of the Yeniköy fossil locality is correlated to chron C10r, resulting in an age of 29.2 Ma. The *Eumyarion* and *Demo/Spanocricetodon* dominated assemblages from the Harami 1 and 3 localities, are determined in chron C6Bn.2n and C6Bn.1r, with ages of 22.9 and 22.8 Ma, respectively. According to Steininger et al. (1990) this means that they correlate with MN 2. The other sections are tentatively correlated to the GPTS based on biostratigraphical arguments, sedimentation rates and radiometric datings. The *Meteamys* and *Muhsinia* dominated assemblages of the Inkonak locality are of latest Oligocene-earliest Miocene age (23.2-25.3 Ma) and can be correlated to chron C6Br, or to C6Cn.1r, or to C8r. The Keseköy locality is correlated to chron C5En, C6n, C6An.1n or C6An.2n with ages ranging from 18.3-21.3 Ma, based on radiometric datings (20.1 ± 2.2 Ma) from fission tracks on zircons. This means that the Keseköy assemblage could be assigned to MN 3. The correlations of the Gemerek fossil locality are ambiguous.

Acknowledgements

We thank P.-J. Verplak, S. Sen, E. Ünay, P.J.J. Scheepers and J.D.A. Zijderveld for their help in the field. P.-J. Verplak and H.J. Meijer measured many of the samples. J.D.A. Zijderveld read an earlier version of this manuscript and made useful comments. We thank J.R. Wijbrans and M. Pringle of the Institute of Isotope Geology (VU Amsterdam) for the $^{40}Ar/^{39}Ar$ datings on the Harami ash layers. This study was supported by the Netherlands Foundation for earth Science Research (AWON/GOA) of the Netherlands Science Foundation (NWO) and by the N.A.T.O. Scientific Affairs Division (grant no. C.R.G. 910750).

References

Agustí, J. and Moyà-Solà S., Mammal extinctions in the Vallesian (Upper Miocene). In: *Extinction Events in Earth History*, p. 425-432, 1990.

Agustí, J. and Moyà-Solà, S., Spanish Neogene Mammal succession and its bearing on continental biochronology. *Newsl. Stratigr.*, **25(2)**, 91-114, 1991.

Alvarez Sierra, M.A., et al., Un estratotipo del límite Aragoniense-Vallesiense (Mioceno medio-Mioceno superior) en la sección de Torremormojón (Cuenca Duero, Provincia de Palencia). *Acta Salmant.* Univ Salamanca, **68**, 57-64, 1990.

Alvarez Sierra, M.A., Paleontología y Biostratigrafía del Mioceno superior del sector central de la Cuenca del Duero. Estudio de los Micromammiferos de la Serie de Torremormojón (Palencia). *Tesis de Licenciatura*, Univ. Complutense Madrid, 1983.

Alvarez Sierra, M.A. and Daams, R., Synthesis of Late Oligocene/Early Miocene micromammal faunas of the western part of the Ebro Basin (La Rioja, Spain). *Com. X Jornadas Paleont.* 15-18, 1994.

Anadón, P., Cabrera, L. and Roca, E., Contexto estructural y paleogeográfico de los sistemas lacustres cenozoicos en España. *Acta Geologica Hispanica*, **24**, 167-184, 1989.

Andreieff, P., Bellon, H. and Westercamp, D., Chronométrie et stratigraphie comparée des édifices volcaniques et formations sédimentaires de la Martiniques (Antilles francaises). *Bull. B.R.G.M. 2e ser.*, **4**, 335-346, 1976.

Andriessen, P.A.M., Helmens, K.F., Hooghiemstra, H., Riezebos, P.A. and Van der Hammen, T., Absolute chronology of the Pliocene-Quarternary sediment sequence of the Bogota area, Colombia. *Quarternary Sci. Rev.*, **12**, 483-501, 1993.

Baadsgaard, H., Lerbekmo, J.F., Wijbrans, J.R., Swisher III, C.C. and Fanning, M., Multi-method radiometric age for a bentonite near the top of the Baculites reesidei Zone of southwestern Saskatchewan (Campanian-Maastrichtian stage boundary?), *Can. Journ. Earth Sci.*, **30**, 769-775, 1992.

Baksi, A.K., A geomagnetic polarity time scale for the period 0-17 Ma, based on $^{40}Ar/^{39}Ar$ plateau ages for selected field reversals. *Geof. Res. Lett.*, **20**, No 15, 1607-1610, 1993.

Baksi, A.K., Hoffman, K.A. and Farrar, E., A new calibration point for the late Miocene section of the geomagnetic polarity time scale: $^{40}Ar/^{39}Ar$ dating of lava flows from Akaroa volcano, New Zealand. *Geophys, Res. Lett.*, **20**, 667-670, 1993.

Baranyi, I., Lippolt, H.J. and Todt,W., Kalium-Argon Altersbestimmungen an tertiären Vulkaniten des Oberrheingraben-Gebietes: II Der Alterstraverse vom Hegau nach Lothringen. *Oberrhein. geol. Abh.*, **25**, 41-62, 1976.

Barbera, X., Pares, J.M., Cabrera, L. and Anadon, P.: High-resolution magnetic stratigraphy across the Oligocene-Miocene boundary in an alluvial-lacustrine succession (Ebro Basin, NE Spain). *Phys. Earth Planet. Int.*, **85**, 181-193, 1994.

Barron, J., Keller, G. and Duncan, D.A., A multiple biochronology for the Miocene. In: J.P. Kennett (Ed.) The Miocene Ocean: Paleoceanography and Biogeography, *Mem. Geol. Soc. Am.*, **163**, 21-36, 1985.

Barton, C.E., Paleomagnetism of sediments collected during leg 90, southwest Pacific, edited by J.P. Kennett and C.C. von der Borch, *Initial Rep. Deep Sea Drill. Proj.*, **90**, 1273-1316, 1985.

Becker-Platen, J.D., Sickenberg, O and Tobien, H., Vertebraten-Vertebraten Lokalfaunaen der Türkei und ihre Altersstellung, in Sickenberg et al. (Eds), Die Gliederung des höheren

Jungtertiärs und Altquartärs in der Türkei nach Vertebraten und ihre Bedeutung für die internationale Neogen-Stratigraphie, *Geol. Jb., B.*, **15**, p. 9, 1975.

Benson, R.H., Rakic-El Bied, K. and Bonaduce, G., An important current reversal (influx) in the Rifian corridor (Morocco) at the Tortonian-Messinian boundary: the end of Tethys Ocean, *Paleoceanography*, **6**, 164-192, 1991.

Benson, R.H., Rakic-El Bied, K. and 10 others, The Bou Regreg section, Morocco: Proposed Global Boundary Stratotype Section and Point of the Pliocene, *Notes et memoires du service geol. Maroc*, **383**, 1-93, 1995.

Berger, A., Accuracy and frequency stability of the Earth's orbital elements during the Quarternary. In: *Milankovitch and Climate* (ed. by Berger, A.L., Imbrie J., Hays j., Kukla G. and Salzman B.), Riedel, Dordrecht, *NATO ASI Ser. C*, **126**, 3-39, 1984.

Berger, A., Support for the astronomical theory of climatic change, *Nature*, **269**, 44-45, 1977.

Berger, A. and Loutre, M.F., Insolation values for the climate of the last 10 m.y., *Quat. Sci. Rev.*, **10**, 297-317, 1991.

Berggren, W.A., Neogene planktonic foraminiferal biostratigraphy and biogeography: Atlantic, Mediterranean and Indo-pacific regions. In: (N. Ikebe and R. Tsuchi, eds), *Pacific Neogene Datum Planes (contributions to biostratigraphy and chronology) Univ. Tokyo Press*, 111-161, 1984.

Berggren, W.A. and Van Couvering, J.A., The late Neogene: Biostratigraphy, geochronology and paleoclimatology of the last 15 million years in marine and continental sequences. *Paleogeogr., Paleoclimato., Paleoecol.*, **16**, 1-216, 1974.

Berggren, W.A. and Van Couvering, J.A., Biochronology, In: Cohee, G.V., M.F. Glaessner and H.D. Hedberg (eds.), *Contributions to the Geologic Time Scale. Studies in Geology*, **6**, 39-55, 1978.

Berggren, W.A., Kent, D.V., Flynn, J.J. and Van Couvering, J.A., Cenozoic geochronology., *Geol. Soc. Am. Bull.*, **96**, 1407-1418, 1985.

Berggren, W.A, Kent, D.V. and Van Couvering, J.A., The Neogene: part 2 Neogene geochronology and chronostratigraphy. In: N.J. Snelling (Ed.), *The chronology of the Geological Record. Geol. Soc. London*, **10**, 211-260, 1985.

Berggren, W.A., Kent, D.V., Swisher III, C.C. and Aubry, M.P., A revised Cenozoic geochronology and chronostratigraphy, *SEPM Spec. Publ.*, **54**, Geochronology Time Scale and global stratigraphic correlation, 1996 (in press).

Blodgett, R.H., Calcareous paleosols in the Triassic Dolores Formation, southwestern Colorado. *Geol. Soc. Am. Spec. Pap.*, **216**, 103-121, 1988.

Bommarito, S. and Catalano, R., Facies analysis of an evaporitic Messinian sequence near Ciminna (Palermo, Sicily). In: Drooger, C.W. (ed.), *Messinian events in the Mediterranean. Geodyn. Sc. Rep.*, **7**, North Holland Publ. Co., Amsterdm, 172-177, 1973.

Bradley, W.H., The varves and climate of the Green river epoch, *U.S. Geol. Surv. Prof. Pap.*, **158E**, 87-110, 1929.

Brunhes, B., Recherches sur la direction d'aimantation des roches volcaniques. *J. Phys.*, **5**, 705-724, 1906.

Bulot, C., Nouvelle étude des rongeurs et des lagomorphes du Miocéne de Suèvres (Loir-et-Cher). *Bull. Mus. Natl. Hist. Nat., Paris, 4th ser.*, **10**, 385-404, 1988.

Burbank, D.W., Engesser, B., Matter, A. and Weidmann, M., Magnetostratigraphic chronology, mammalian faunas, and stratigraphic evolution of the Lower Freshwater Molasse, Haute-Savoie, France. *Eclogae Geol. Helv.*, **85**, 399-431, 1992.

Butler, R.W.H., Lickorish, W.H., Grasso, M., Pedley, H.M. and Ramberti, L., Tectonics and sequence stratigraphy in Messinian basins, Sicily: constraints on the initiation and termination of the Mediterranean 'salinity crisis'. *Geol. Soc. Am. Bull*, **107**, 425-439, 1995.

Calieri, R., Stratigrafia, analisi paleoclimatica e radiometria del Tortoniano superiore Messiniano preevaporitico in Appennino Romagnolo (M. del Casino-M. Tondo). *Thesis (unpubl.)*, Univ. Bologna, 79 pp., 1992.

Calvo, J.P., et al., Up-to-date Spanish continental Neogene synthesis and paleoclimatic interpretation. *Rev. Soc. Geol. España*, **6**, 29-40, 1993.

Cande, S.C. and Kent, D.V., A New Geomagnetic Polarity Time Scale for the Late Cretaceous and Cenozoic. *J. Geoph. Res.*, **97**, 13917-13951, 1992.

Cande, S.C. and Kent, D.V., Revised calibration of the Geomagnetic Polarity Time Scale for the Late Cretaceous and Cenozoic. *J. Geoph. Res.*, **100**, 6093-6095, 1995.

Chabbar-Ameur, R., Jaeger, J.J. and Michaux, J., Radiometric age of early *Hipparion* fauna in North-West Africa. *Nature*, **261**, 38-39, 1976

Channell, J.E.T., Freeman, R., Heller, F. and Lowrie, W., Timing of diagenetic hematite growth in red pelagic limestones from Gubbio (Italy), *Earth Planet. Sci. Lett.*, **58**, 189-201, 1982.

Channell, J.E.T., Torii, M. and Hawthorne, T., Magnetostratigraphy of sediments recovered at Sites 650, 651, 652, and 654 (Leg 107, Thyrrhenian Sea). In: Kastens, K.A., Mascle, J. et al., *Proc. ODP, Sci. Results*, **107**, 335-346, 1990.

Channell, J.E.T., Rio, D. and Thunell, R.C., Miocene/Pliocene boundary magnetostratigraphy at Capo Spartivento, Calabria, Italy, *Geology*, **16**, 1096-1099, 1988.

Chamley, M., Meulenkamp, J.E., Zachariasse, W.J. and van der Zwaan, G.J., Middle to late Miocene marine ecostratigraphy: clay minerals, planktonic foraminifera and stable isotopes from Sicily. *Oceanol. Acta*, **9**, 227-238, 1986.

Colalongo M.L., di Grande A., d'Onofrio S., Gianelli L., Iaccarino S., Mazzei R., Poppi Brigatti M.F., Romeo M., Rossi A. and Salvatorini G., A proposal for the Tortonian-Messinian boundary. *Ann. Géol. Pays Hellén., Tome hors série 1979*, fasc. I, 285-294, 1979.

Cowie, J.W., Ziegler, W., Boucot, A.J., Basset, M.G. and Remane, J., Guidelines and Statutes of the International Commission on Stratigraphy (ICS): *Courier Forschungsinst. Senckenberg*, **83**, 1-14, 1986.

Cox, A.V., Doell, R.R. and Dalrymple, G.B., Geomagnetic polarity epochs and Pleistocene geochronometry, *Nature*, **198**, 1049-1051, 1963.

Crusafont Pairo, M., Observations à un travail de M. Freudenthal et P.Y. Sondaar sur les nouveaux gisements à *Hipparion* d'Espagne. *Proc. Kon. Ned. Akad. Wetensch.*, **68**, 121-126,1965.

Crusafont Pairo, M., El sistema Miocénico en la depressión Española del Vallés-Penedés. *Inter. Geol. Congr. Report of XVIII Session*, Great Britain, 1948, part XI, 33-43, 1951.

Daams, R., Freudenthal, M. and Van de Weerd, A., Aragonian, a new stage for continental deposits of Miocene age. *Newsl. Stratigr.*, **6**, 42-55, 1977.

Daams, R., Freudenthal, M. and Alvarez, M.A., Ramblian: a new stage for continental deposits of Early Miocene age. *Geol. Mijnbouw*, **65**, 297-308, 1987.

Daams, R., and Freudenthal, M., Synopsis of the Dutch-Spanish collaboration program in the Aragonian type area, 1975-1986. In: M. Freudenthal (Ed.), *Biostratigraphy and Paleoecology of the Neogene Micromammalian faunas from the Calatayud-Teruel basin. Scr. Geol. Spec. Issue*, **1**, 3-18, 1988.

Dalrymple, G.B. and Duffield, W.A., High precision $^{40}Ar/^{39}Ar$ dating of Oligocene from Mogollon-Datil volcanic field using continuous laser systems, *Geophys. Res. Lett.*, **15**, 463-466, 1988.

Dalrymple, G.B., Izett, G.A., Snee, L.W. and Obradovich, J.D., $^{40}Ar/^{39}Ar$ age spectra and total-fusion ages of tektites from Cretaceous-Tertiary boundary sedimentary rocks in the Beloc Formation, Haïti, *U.S. Geol. Surv. Bull.*, **2065**, 20 pp., 1993.

De Boer, P.L. and Smith, D.G., Orbital forcing and cyclic sequences, *Spec. Publs Int. Ass. Sediment.*, **19**, 1-14, 1994.

De Bruijn, H., Miocene Gliridae, Sciuridae and Eomydae (Rodentia, Mammalia from the Calatayud area, prov. Zaragoza, Spain) and their bearing on the biostratigraphy. *PhD Thesis*, Univ. Utrecht. 1965.

De Bruijn, H., Ünay, E., Van de Hoek Ostende, L., and Saraç, G., A new association of small mammals from the lowermost lower miocene of central Anatolia., *Geobios*, **25**, 651-670, 1991.

De Bruijn, H., and Saraç, G., Early Miocene rodent faunas from the eastern Mediterranean area. Part 1 The genus *Eumyarion*. *Kon. Ned. Akad. Wetensch., Proc.*, **94**, 1-36, 1991.

De Bruijn, H., Fahlbusch, V., Saraç, G., and Ünay E., Early Miocene rodent faunas from the eastern Mediterranean area. Part III. The genera Deperetomys and Cricetodon with a discussion of the evolutionary history of the Cricetodontini. *Proc. Kon. Ned. Akad. v. Wetensch.* **96** , 151-216, 1993.

De Bruijn, H., Daams, R., Daxner-Höck, G., Fahlbusch, V., Ginsburg, L.,Mein, P. and Morales, J., Report of the RCMNS working group on fossil mammals, Reisenburg 1990. *Newsl. Stratigr.*, **26**, 65-118, 1992.

De Bruijn, H., et al. (in prep.): The Oligo-Miocene continental sediments of Anatolia, a multi-disciplinary review.

Decima, A. and Wezel, F.C., Late Miocene evaporites of the central Sicilian Basin, In: Ryan, W.B.F., K.J. Hsü et al. (eds.), *Init. Rep. DSDP, Leg. 13, Washington, D.C., U.S. Govern. Printing Office*, 1234-1240, 1973.

Decima, A., McKenzie, J.A. and Schreiber B.C., The origin of "evaporative" limestones: an example from the Messinian of Sicily (Italy). *J. Sediment. Petrol.*, **58**, 256-272, 1988.

Dekkers, M.J., Some rockmagnetic parameters for natural goethite, pyrrhotite and fine-grained hematite, *Geologica Ultraiectina*, **51**, *PhD thesis*, University of Utrecht, 1988.

Dekkers, M.J., Magnetic properties of natural pyrrhotite. II. High- and low-temperature behaviour of Jrs and TRM as function of grain size, *Phys. Earth Planet. Inter.*, **57**, 266-283, 1989.

Dekkers, M.J. and Linssen, J.H., Rockmagnetic properties of fine-grained natural low-temperature haematite with reference to remanence acquisition mechanisms in red beds. *Geophys. J. Int.*, **99**, 1-18, 1989.

Dijksman, A.A., Geomagnetic reversals as recorded in the Miocene Red Beds of the Calatayud-Teruel Basin (Central Spain). *PhD Thesis*, Univ. Utrecht. 1977.

Dodd, B. and Anderson, V.B., Design, construction, commissioning, and use of a new Cd lined incore irradiation tube for the Oregon State University TRIGA Reactor, *Internal report OSU Reactor Centre*, 1994.

Drooger, C.W., et al., Problems of detailed biostratigraphic and magnetostratigraphic correlations in the Potamidha and Apostoli sections of the Cretan Miocene., *Utrecht Micropaleontol. Bull.*, **21**, 1-222, 1979.

Dunlop, D.J., Magnetic properties of fine particle hematite, *Ann. Géophys.*, **27**, 269-293., 1971

Edwards, L.E., Miocene dinocysts from Deep Sea Drilling Project Leg 81, Rockall Plateau, eastern North Atlantic Ocean. In: Roberts, D.G., Schnitker, D., et al. (eds.), *Init. Repts. DSDP*, **81**, Washington (U.S. Govt. Printing Office), 581-594, 1984.

Edwards, A.R., Significant climatic vents in the Late Neogene marine strata of New Zealand. In: Barron, J.A. and Blueford, J.R. (eds.), *Fourth International Congress on Pacific Neogene Stratigraphy*, 26-27, 1987.

Emiliani, C., Pleistocene temperatures, *J. Geol.*, **63**, 538-578, 1955.

Emiliani, C., Paleotemperature analysis of the Caribbean cores P6304-8 and P6304-9 and a generalized temperature curve for the last 425,000 years. *J. Geol.*, **63**, 538-578, 1966.

Fahlbusch, V., Report on the international symposium on mammalian stratigraphy of the European Tertiary., *Newsl. Stratigr.*, **5**(2/3), 160-167, 1976.

Fisher, R.A., Dispersion on a sphere. *Proc. R. Soc. London.* A **217**, 295-305, 1953.

Flower, B.P. and Kennett, J.P., Middle Miocene ocean-climate transition: High-resolution oxygen and carbon isotopic records from Deep Sea Drilling Project site 588A, southwest Pacific, *Paleoceanography*, **8**, 811-843, 1993.

Füchtbauer, H. (Ed.), Sedimente und Sedimentgesteine. Sediment-Petrologie teil II. *E. Schweizbart'sche Verl. Stuttgart*, 1141 pp., 1988.

Galbraith, R.F. and Laslett, G.M., Statistical models for mixed fission track ages. *Nucl. Tracks Radiat. Meas.*, **21**, 459-470, 1993.

Garcés, M., Magnetostratigrafía de las sucesiones del Mioceno medio y superior del Vallès occidental (depresión del Vallès-Penedès, N.E. de España): implicationes biocronológicas y cronoestratigráficas. *Tesis del Univ. de Barcelona*, 1995.

Garcés, M., Agustí, J., Cabrera, L. and Parés, J.M., Magnetostratigraphy of the Vallesian type area (Late Miocene, Vallès-Penedès basin, NE Spain. *Earth Planet Sci. Lett.* (submitted).

Garcia Moreno, E., Roedores y lagomorfos del Mioceno de la zona central de la Cuenca del Duero, Sistemática, Biostratigrafía y Paleoecología. *Tesis Doctoral, Univ. Complutense Madrid*, 1987.

Garcia Moreno, E., Paleontología y Biostratigrafía de la zona central de la Cuenca del Duero. Estudio de los Micromamíferos del Mioceno medio de la Serie de Torremormojón (Palencia). *Tesis de Licenciatura Univ. Complutense*, 1-200, 1983.

Gilbert, G.K., Sedimentary measurement of geologic time, *J. Geol.*, **3**, 121-127, 1895.

Glacon, G., Vergnaud Grazzini, C., Iaccarino, S., Rehault, J.-P., Randrianasolo, A., Sierro, J.F., Weaver, P., Channell, J.E.T., Torii, M. and Hawthorne, T., Planktonic foraminiferal events and stable isotope records in the upper Miocene, Site 654, *Proc. Ocean Drill. Prog., Sci. results*, **107**, 415-428, 1990.

González Delgado, A., Civis, J., Valle, M., Sierro, J.F. and Flores, J.A., Distribución de los Foraminíferos, Moluscos y Ostracodos en el Neógeno de la Cuenca del Duero. Aspectos más significativos. *Studia Geol. Salmant.*, **22**, 277-292, 1986.

Gregor, C.B. and Zijderveld, J.D.A., Paleomagnetism and the alpine tectonics of Eurasia 1. The magnetism of some Permian red sandstone from northwestern Turkey. *Tectonophysics*, **1**, 289-306, 1964.

Hay, R.L., and Wiggins, B., Pellets, ooid, sepiolite and silica in three calcretes of the southwestern United States. *Sedimentology*, **27**, 559-576, 1980.

Hays, J.D., Imbrie, J. and Shackleton, N.J., Variations in the Earth's orbit: Pacemaker of the ice ages, *Science*, **194**, 1121-1132, 1976.

Head, M.J., Norris, G., and Mudie, P.J., Palynology and dinocysts stratigraphy of the Upper Miocene and lowermost Pliocene, ODP Leg 105, Site 646, Labrador Sea. In: Srivastava, S.P., Arthur, M., Clement., B., et al., *Proc. ODP, Sci. Results*, **105**, 423-451, 1989a.

Head, M.J., Norris, G., and Mudie, P.J., New species of dinocysts and a new species of acritarch from the Upper Miocene and lowermost Pliocene, ODP Leg 105, Site 646, Labrador Sea. In: Srivastava, S.P., Arthur, M., Clement., B., et al., *Proc. ODP, Sci. Results*, **105**, 453-466, 1989b.

Head, M.J., Norris, G., and Mudie, P.J., Palynology and dinocysts stratigraphy of the Miocene in ODP Leg 105, Hole 645E, Baffin Bay. In: Srivastava, S.P., Arthur, M., Clement., B., et al., *Proc. ODP, Sci. Results*, **105**, 467-514, 1989c.

Heider, F. and Dunlop, D.J., Two types of chemical remanent magnetization during oxidation of magnetite. *Phys. Earth Planet. Inter.*, **46**, 24-45, 1986.

Heirtzler, J.R., Dickson, G.O., Herron, E.M., Pitman III, W.C. and Le Pichon, X., Marine magnetic anomalies, geomagnetic field reversals, and motions of the ocean floor and continents. *J. geophys. Res.*, **73**, 2119-2136, 1968.

Hess, H.H., History of ocean basins, In: Engell, A.E.J., H.L. James and B.F. Leonard (eds), Petrologic studies: A Volume in Honour of A.F. Buddington. *Geological Society of Amerika*, New York, 599-620, 1962.

Hilgen, F.J., Sedimentary cycles and high-resolution chronostratigraphic correlations in the mediterranean Pliocene. *Newslett. Stratigr.*, **17**, 109-127, 1987.

Hilgen, F.J., Closing the gap in the Plio-Pleistocene boundary stratotype sequence at Crotone (southern Italy), *Newslett. Stratigr.*, **22**, 43-51, 1990.

Hilgen, F.J., Astronomical calibration of Gauss to Matayama sapropels in the Mediterranean and implication for the Geomagnetic Polarity Time Scale. *Earth Planet. Sci. Lett.*, **104**, 226-244, 1991a.

Hilgen, F.J., Extension of the astronomically calibrated (polarity) time scale to the Miocene/Pliocene boundary. *Earth Planet. Sci. Lett.*, **107**, 349-368, 1991b.

Hilgen, F.J., Astronomical forcing and geochronological application of sedimentary cycles in the Mediterranean Pliocene-Pleistocene, *Geologica Ultraiectina*, **93**, pp. 139, 1991c.

Hilgen, F.J. and Langereis, C.G., The age of the Miocene-Pliocene boundary in the Capo Rossello area (Sicily), *Earth Planet. Sci. Lett.*, **91**, 214-222, 1988.

Hilgen, F.J. and Langereis, C.G., Periodicities of $CaCO_3$ cycles in the Pliocene of Sicily: Discrepancies with the quasi-periods of the Earth's orbital cycles?, *Terra Nova*, **1**, 409-415, 1989.

Hilgen, F.J., and Langereis, C.G., A critical re-evaluation of the Miocene/Pliocene boundary as defined in the Mediterranean. *Earth Planet. Sci. Lett.*, **118**, 167-179, 1993.

Hilgen, F.J., Krijgsman, W., Langereis, C.G., Lourens, L.J., Santarelli, A. and Zachariasse, W.J., Extending the astronomical (polarity) time scale into the Miocene, *Earth Planet Sci. Lett.*, **136**, 495-510, 1995.

Hodell, D.A. and Kennett, J.P., Late Miocene - Early Pliocene stratigraphy and paleoceanography of the South Atlantic and Southwest Pacific: a synthesis. *Paleoceanography*, **1**, 285-311, 1986.

Hodell, D.A., Benson, R.H., Kent, D.V., Boersma, A. and Rakic-El Bied, K., Magnetostratigraphic, biostratigraphic, and stable isotope stratigraphy of an Upper Miocene drill core from the Salé Briqueterie (northwest Morocco): A high-resolution chronology for the Messinian stage. *Paleoceanography*, **9**, 835-855, 1994

Hugueney, M. and Ringeade, M., Synthesis on the "Aquitanian" lagomorph and rodent faunas of the Aquitaine basin (France). In: *European Neogene Mammal Chronology* (Ed. Lindsay et al.) Plenum Press, New York, 139-156, 1990.

Fischer, A.G., Gilbert-bedding rhythms and geochronology, In: E.L Yochelson (ed) The scientific ideas of G.K. Gilbert, *Spec. Pap. Geol. Soc. Am.*, **183**, 93-104, 1980.

Iaccarino, S., Mediterranean Miocene and pliocene planktic foraminifera In: Bolli, H.M., Saunders, J.B. and Perch-Nielsen, K. (eds), *Plankton Stratigraphy*: Cambridge (Cambridge Univ. Press), 283-314, 1985.

Imbrie, J., Hays, J.D., Martinson, D.G., McIntyre, A., Mix, A.C., Morley, J.J., Pisias, N.G., Prell, W.L. and Shackleton, N.J., The orbital theory of Pleistocene climate: Support from a revised chronology of the marine $\delta^{18}O$ record. In: *Milankovitch and Climate*, A. Berger et al. (Ed), 269-305, D. Reidel, Norwell, Mass., 1984.

Izett, G.A., Dalrymple, G.B. and Snee, L.W., $^{40}Ar/^{39}Ar$ age of the Cretaceous-Tertiary boundary tektites from Haïti. *Science*, **252**, 1539-1542, 1991.

Johnson, N.M., Opdyke, N.D., Johnson, G.D., Lindsay, E.H. and Tahirkheli, R.A.K., Magnetic polarity stratigraphy and ages of Siwalik group rocks of the Potwar plateau, Pakistan, *Paleogeogr. Paleoclimatol., Paleoecol.*, **37**, 17-42, 1982.

Kastens, K., Did a glacio-eaustatic sealevel drop trigger the Messinian salinity crisis? New evidence from ODP SIte 654 in the Tyrhhenian Sea., *Paleoceonography*, **7**, 333-356, 1992.

Kissel, C., Barrier, E., Laj, C. and Lee, T.Q., Magnetic fabric in undeformed marine clays from compressional zones. *Tectonics*, **5**, 769-781, 1986.

Kissel, C. Apport du paléomagnétisme à la compréhension de l'evolution géodynamique Tertiaire du domaine Égéen de l''Epire à L'Anatolie occidentale, *Ph.D. thesis, Univ. de Paris-sud Cent. d'Orsay*, Paris, France, 1986.

Kissel, C., Laj, C., Sengör, A.M.C. and Poisson, A., Paleomagnetic evidence for rotation in opposite senses of adjacent blocks in northeastern Aegea and western Anatolia. *Geophys. Res. Lett.*, **14**, 907-910, 1987.

Krijgsman, W., Hilgen, F.J., Langereis, C.G. and Zachariasse, W.J., The age of the Tortonian/ Messinian boundary, *Earth Planet. Sci. Lett.*, **121**, 533-547, 1994a.

Krijgsman, W., Langereis, C.G., Daams, R. and Van der Meulen, A.J., Magnetostratigraphic dating of the middle Miocene climate change in the continental deposits of the Aragonian type area in the Calatayud-Teruel basin (Central Spain). *Earth Planet. Sci. Lett.*, **128**, 513-526, 1994b.

Krijgsman, W., Hilgen, F.J., Langereis, C.G., Santarelli, A. and Zachariasse, W.J., Late Miocene magnetostratigraphy, biostratigraphy and cyclostratigraphy from the Mediterranean. *Earth Planet. Sci. Lett.*, **136**, 475-494, 1995.

Krijgsman, W., Hilgen, F.J, Negri, A., Wijbrans, J.R. and Zachariasse, W.J., The Monte del Casino section (Northern Apennines, Italy): a potential Tortonian-Messinian boundary stratotype, *Palaeogeogr. Palaeoclimatol. Palaeoecol.*, (submitted) 1996 .

Krijgsman, W., Garcés, M., Langereis, C.G., Daams, R., Van Dam, J., Van der Meulen, A.J., Agustí J., and Cabrera, L., A new chronology for the middle to late Miocene continental record in Spain. *Earth Planet. Sci. Lett.*, (submitted), 1996.

Kunk, M., Dalrymple, B. and Snee, L.W., Progress on the preparation of the proposed $^{40}Ar/^{39}Ar$ standard Mmhb-2, plans for its calibration, and interlaboratory calibration of argon facilities. *U.S.G.S., circular 1107*, **183**, 1994.

Kurihara, K. and Kennett, J.P., Paleoceanographic significance of Neogene benthic foraminiferal changes in a southwest Pacific bathyal depth transect, *Mar. Micropaleotol.*, **19**, 181-199, 1992.

Labreque, J.L., Kent, D.V. and Cande, S.V., Revised magnetic polarity time scale for Late Cretaceous and Cenozoic time. *Geology*, **5**, 330-335, 1977.

Langereis, C.G., Late Miocene magnetostratigraphy in the Mediterranean. *Ph.D. Thesis, University of Utrecht. Geologica Ultraiectina*, **34**, 180 pp, 1984.

Langereis, C.G., Zachariasse, W.J. and Zijderveld, J.D.A., Late Miocene magnetobiostratigraphy of Crete. *Mar. Micropaleontol.*, **8**, 261-281, 1984.

Langereis, C.G., Sen, S., Sümengen, M. and Ünay, E., Preliminary magnetostratigraphic results of some neogene mammal localties from Anatolia (Turkey). In: *European Neogene Mammal Chronology, Plenum. Press*, New York, 515-525, 1990.

Langereis, C.G., and Hilgen, F.J., The Rossello composite: A Mediterranean and global reference section for the Early to early Late Pliocene. *Earth Planet. Sci. Lett.*, **104**, 211-225, 1991.

Langereis, C.G., and Dekkers, M.J., Paleomagnetism and rock magnetism of the Tortonian-Messinian boundary stratotype at Falconara, Sicily. *Phys. Earth Plan. Int.*, **71**, 100-111, 1992.

Langereis, C.G., Van Hoof, A.A.M. and Hilgen, F.J., Steadying the rates. *Nature*, **369**, pp. 615, 1994.

Lanphere, M.A., Sawyer, D.A. and Fleck, R.J., High-resolution 40Ar/39Ar geochronology of Tertiary volcanic rocks, Western U.S.A., *Geol. Soc. Australia Abs.*, **27**, p. 57, 1990.

Laskar, J., The chaotic motion of the solar system: anumerical estimate of the size of the chaotic zones, *Icarus*, **88**, 266-291, 1990.

Laskar, J., Joutel, F. and Boudin, F., Orbital, precessional, and insolation quantities for the Earth from -20 Myr to +10 Myr. *Astron. Astrophys.*, **270**, 522-533, 1993.

Laurenzi, M., Tateo, F., Villa, I.M. and Vai, G.B., New radiometric datings bracketing the Tortonian/Messinian boundary in the Romagna potential stratotype sections (Northern Apennines), In: A. Montanari, G.S. Odin and R. Coccioni (Eds): *Miocene Integrated Stratigraphy*. Elsevier Amsterdam; (in press), 1996.

Lippolt, H.J., Gentner, W. and Wimmenauer, W., Altersbestimmungen nach der Kalium-Argon-Methode an tertiären Eruptivgesteinen Südwestdeutschlands. *Jh. geol. L.-Amt Baden-Württemberg*, Freiburg, **6**, 507-538, 1963.

Linssen, J.H., Properties of Pliocene sedimentary geomagnetic reversal records from the Mediterranean, *Thesis Univ. Utrecht, Geologica Ultraiectina*, **80**, 1991.

López Martinez, N., Garcia Moreno, E. and Alvarez Sierra, M.A., Paleontología y Biostratigrafía (micromamíferos) del Miocenico medio y superior del sector central de la Cuenca del Duero. *Studia Geol. Salamant.*, **22**, 191-212, 1986.

López Martinez, N. and Borja Sanchiz, F.,. Los primeros microvertebrados de la Cuenca del Duero: listas faunísticas preliminares e implicaciones biostratigráficas y paleofisiográficas. *I Reun. Nac. Geol. Cuenca del Duero, Temas Geol. Min. (IGME)*, **6**, 339-353, Salamanca, 1982.

Lourens, L.J., Hilgen, F.J., Gudjonsson, L. and Zachariasse, W.J., Late Pliocene to early Pleistocene astronomically forced sea surface productivity and temperature variations in the Mediterranean. *Mar. Micropaleontol.*, **19**, 49-78, 1992.

Lourens, L.J., Astronomical forcing of Mediterranean climate during the last 5.3 Million years, *Thesis Utrecht University*, pp. 247, 1994.

Lourens, L.J., Hilgen, F.J., Zachariasse, W.J., Van Hoof, A.A.M., Antonarakou, A., and Vergnaud-Grazzini, C., Evaluation of the Pliocene to early Pleistocene astronomical time scale, *Paleoceanography*, (in press) 1996.

Loutit, T.S. and Kennett, J.P., Application of carbon isotope stratigraphy to Late Miocene shallow marine sediments, New Zealand. *Science*, **204**, 1196-1199, 1979.

Lowrie, W. and Alvarez, W., One hundred million years of geomagnetic polarity history. *Geology*, **9**, 392-397, 1981.

Marks, P., Turolian, *Giornale di Geologia*, **37**, 209-213, 1971.

Martini E., Standard Tertiary and Quaternary calcareous nannoplankton zonation, In: Farinacci A. (Ed) *Proceeding II Planktonic Conference, Roma 1970*, **2**, 739-785, 1971.

Matuyama, M., On the direction of magnetization of basalt in Japan, Tyosen and Manchuria, *Japon. Acad. Proc.*, **5**, 203-205, 1929.

McFadden, P.L. and McElhinny, M.W., The combined analysis of remagnetisation circles and direct observations in paleomagnetism, *Earth Planet. Sci. Lett.*, **87**, 161-172, 1988.

McDougall, I., Kristjansson, L., and Saemundsson, K., Magnetostratigraphy and geochronology of northwest Iceland. *J. Geophys. Res.*, **89**, 7029-7060, 1984.

McFadden, P.L. and McElhinny, M.W., The combined analysis of remanetisation circles and direct observations in paleomagnetism, *Earth Planet. Sci. Lett.*, **87**, 161-172, 1988.

Mein, P., Resultats du Groupe de travail des Vertebres, In: J. Senes (Ed.), *Report on Activity of R.C.M.N.S. Working Group*, 78-81, 1975.

Mein, P., Updating of MN zones. In: Lindsay et al. (Ed.), *European Neogene Mammal Chronology*, Plenum Press, New York, 73-90, 1990.

Mein, P., Moissenet, E. and Truc, G., Les formations continentales du Néogène supérieur des vallées du Jucar et du Cabriel au NE d'Albacete (Espagne), biostratigraphie et environment. *Doc. Lab. Geol. Fac. Sci. Lyon*, **72**, 99-147, 1978.

Milankovitch, M., Kanon der Erdbestrahlung uns seine Anwendung auf das Eiszeitenproblem, *Royal Serb. Acad., Spec. Publ.*, **133**, 1-633, 1941.

Miller, K.G., Aubry, M.P., Kahn, M.J., Melillo, A., Kent, D.V. and Berggren, W.A., Oligocene-Miocene biostratigraphy, magnetostratiography, and isotope stratigraphy of the western North Atlantic, *Geology*, **13**, 257-261, 1985.

Miller, K.G. and Katz, M.E., Oligocene to Miocene benthic foraminiferal and abyssal circulation changes in the North Atlantic, *Micropaleontology*, **33**, 97-149, 1987.

Miller, K.G., Feigenson, M.D., Wright, J.D. and Clement, B.M., Miocene isotope reference section, Deep Sea Drilling Project site 608: An evaluation of isotope and biostratigraphic resolution. *Paleoceanography*, **6**, 33-52, 1991a.

Miller, K.G., Wright, J.D. and Fairbanks, R.G., Unlocking the icehouse: Oligocene-Miocene oxygen isotopes, eustacy and margin erosion, *J. geophys. Res.*, 6829-6848, 1991b.

Moreau, M.G., Feinberg, H. and Pozzi, J.P., Magnetobiostratigraphy of a Late Miocene section from the Moroccan Atlantic margin. *Earth Planet. Sci. Lett.*, **76**, 167-175, 1985.

Mullender, T.A.T., Van Velzen, A.J. and Dekkers, M.J., Continuous drift correction and separate identification of ferrimagnetic and paramagnetic contributions in thermomagnetic runs, *Geophys. J. Int.*, **114**, 663-672, 1993.

Negri, A. and Vigliotti, L., Calcareous nannofossil biostratigraphy and paleomagnetism of the Monte Tondo and Monte del Casino sections (Romagna Appennine, Italy), In: A. Montanari, G.S. Odin and R. Coccioni (Eds): *Miocene Integrated Stratigraphy*. Elsevier Amsterdam, in press, 1996.

Nijenhuis, I.A. and Schenau, S.J., On the origin of some Miocene sapropelites of Faneromeni, Crete. A geo-chemical survey. *Internal Report, Dept. of Geochemistry, Inst. of Earth Sciences, Utrecht Univ.*, 1995.

Okada, H. and Bukry, D., Supplementary modifications and introduction of code numbers to the low-latitude coccolith biostratigraphic zonation, *Mar. Micropaleontol.*, **5**, 321-325, 1980.

d'Onofrio S., Gianelli L., Iaccarino S., Morlotti E., Romeo E., Salvatorini G., Sampo M. and Sprovieri R., Planktonic foraminifera of the Upper Miocene from some Italian sections and the problem of the lower boundary of the Messinian. *Boll. Soc. Paleont. Ital.*, **14**, 177-196, 1975.

Opdyke, N., Mein, P., Moissenet, E., Pérez-Gonzalez, A., Lindsay, E. and Petko, M., The magnetic stratigraphy of the Late Miocene sediments of the Cabriel Basin, Spain. In: Lindsay et al. (Ed.), *European Neogene Mammal Chronology*. Plenum. Press, New York, NY, 507-514, 1990.

Orbay, N. and Bayburdi, A., Paleomagnetism of dykes and tuffs from the Mesudiye region and rotation of Turkey. *Geophys. J. R. astr. Soc.*, **59**, 437-444, 1979.

Park, J., and Oglesby, R.J., The effect of orbital cycles on Late and Middle Cretaceous climate: a comparative general circulation model study. In: de Boer, P.L. and D.G. Smith (Eds), *Orbital forcing and cyclic sequences. Int. Assoc. Sedim. Spec. Publ.*, **19**, 509-529, 1994.

Pedley, H.M. and Grasso, M., Controls on faunal and sediment cyclicity within the Tripoli and Calcare di Base basins (Late Miocene) of central Sicily: *Palaeogeogr., Palaeoclimatol., Palaeoecol.*, **105**, 337-360, 1993.

Perch Nielsen, K., Cenozoic Calcareous Nannofossils. In Bolli H.B., Saunders, J.B. and Perch Nielsen, K. (Eds): *Plankton Stratigraphy*, Cambridge University Press, pp. 427-555, 1985.

Postma, G., Hilgen, F.J. and Zachariasse, W.J., Precession-punctuated growth of a late Miocene submarine-fan lobe on Gavdos (Greece), *Terra Nova*, **5**, 438-444, 1993.

Powell, A.J., The stratigraphic distribution of Late Miocene dinoflagellate cysts from the Castellanian superstage stratotype, northwest Italy. *Am. Assoc. Stratigr. Palynol. Contr. Ser.*, **17**, 129-150, 1986.

Pringle, M.S., Sarna-Wojcicki, A. and Wijbrans, J.R., Age of the Bishop Tuff (western USA) and the Brunhes-Matuyama magnetic polarity transition, *Terra Nova*, **5**, 79, (abstract) 1993.

Raffi, I., Rio, D., d'Atri, A., Fornaciari, E. and Rocchetti, S., Quantitative distribution patterns and biomagnetostratigraphy of middle and late Miocene calcareous nannofossils from equatorial Indian and Pacific Oceans (Legs 115, 130 and 138), *Proc. ODP, Sci. Results*, **138**, 479-503, 1995.

Renne, P., Walter, R., Verosub, K., Sweitzer, M. and Aronson, J., New data from Hadar (Ethiopia) support orbiatlly tuned time scale to 3.3 Ma, *Geophys. Res. Lett.*, **20**, 1067-1070, 1993.

Renne, P.R., Deino, A.L., Walter, R.C., Turrin, B.D., Swisher, C.C., Becker, T.A., Curtis, G.H., Sharp, W.D. and Jaouni, A.R., Intercalibration of astronomical and radioisotopic time. *Geology*, **22**, 783-786, 1994.

Rio D., Raffi I., and Villa G., Plio-Pleistocene calcareous nannofossil distribution patterns in the Western Mediterranean. In Kastens, K.A., Mascle, J. et al., *Proc. ODP, Sci. Results*, **107**, 513-553, 1990.

Rivas Carballo, R., and Valle, M.F., Nuevas aportaciones a la Palinología del Terciario de la Cuenca del Duero. Torremormojón (Palencia). *Studia Geol. Salamant.*, **22**, 133-143, 1986.

Roberts, A. P., Magnetic properties of sedimentary greigite (Fe_3S_4). *Earth Planet. Sci. Lett.*, **134**, 227-236, 1995.

Roberts, D.H., Lehar, J. and Dreher, J.W., Time series analysis with CLEAN. I. Derivation of a spectrum, *Astron. J.*, **93** (4), 968-989, 1987.

Rohling, E. and Hilgen, F.J., The eastern Mediterranean climate at times of sapropel formation: a review, *Geol. & Mijnb.*, **70**, 253-264, 1991.

Rossignol-Strick, M., Mediterranean Quaternary sapropels, an immediate climatic response to orbital insolation. *Nature*, **303**, 46-49, 1983.

Roy, J.L. and Park, J.K., Red beds: DRM od CRM?, *Earth Planet. Sci. Lett.*, **17**, 211-216, 1972.

Ryan, W.B.F., Stratigraphy of Late Quarternary sediments in the eastern Mediterranean, In: *The Mediterranean Sea: A natural sedimentation laboratorium*, D.J. Stanley (ed.), Dowden, Hutchinson and Ross, Pa., 146-169, 1972.

Savin, S.M., Douglas, R.G. and Stehli, F.G., Tertiary marine paleotemperatures, *Geol. Soc. Am. Bull.*, **86**, 1499-1510, 1975.

Scheepers, P.J.J., Tectonic rotations in the Tyrrhenian Arc system during the Quaternary and late Tertiary. *Geol. Ultraiectina*, **112**, pp. 350, 1994.

Scheepers, P.J.J. and Langereis, C.G., Analysis of NRM directions from the Rosello composite: implications for tectonic rotations of the Caltanissetta basin (Sicily), *Earth Planet. Sci. Lett.*, **119**, 243-258, 1993.

Schneider, D.A., Paleomagnetism of some leg 138 sediments: detailing Miocene magnetostratigraphy (ODP, in press), 1995.

Scott, G.H., Upper Miocene biostratigraphy: does *Globorotalia conomiozea* occur in the Messinian? *Rev. Esp. Micropal.*, **12**, 489- 506, 1980.

Sen, S., Hipparion datum and its chronologic evidence in the Mediterranean area. In: Lindsay et al. (Ed.), *European Neogene Mammal Chronology*. Plenum. Press, New York, NY, 495-514, 1990.

Sen, S., Valet, J.P. and Ioakim, C., Magnetostratigraphy and biostratigraphy of the Neogene deposits of Kastellios Hill (Central Crete, Greece). *Palaeogeogr., Palaeoclimatol., Palaeoecol.*, **53**, 321-334, 1986.

Shackleton, N.J. and Opdyke, N.D., Oxygen isotope and paleomagnetic stratigraphy of Pacific core V28-238: oxygen isotope temperatures and ice volumes on a 105 and 106 year scale., *Quat. Res.*, **3**, 39-55, 1973.

Shackleton, N.J. and Kennett, J.P., Paleotemperature history of the Cenozoic and initiation of Antarctic glaciation: Oxygen and carbon isotopic analyses in DSDP sites 277, 279, and 281, edited by J.P. Kennett and R.E. Houtz, *Initial Rep. Deep Sea Drill. Proj.*, **29**, 743-755, 1975.

Shackleton, N. J., Berger A. and Peltier W.R., An alternative astronomical calibration of the lower Pleistocene time scale based on ODP site 667, *Trans. R. Soc. Edinburgh E. S.*, **81**, 251-261, 1990.

Shackleton, N.J., Hall, M.A. and Pate, D., Pliocene stable isotope stratigraphy of ODP site 846. *Proc. ODP, Sci. Res.*, **138**, (in press) 1995.

Shackleton, N.J., Crowhurst, S., Hagelberg, T., Pisias, N.G., and Schneider, D.A., A new late Neogene time scale: Application to leg 138 sites, In: Pisias, N.G., Mayer, L.A., Janecek, T.R., Palmer-Julson, A. and Van Andel, T.H. (Eds.), *Proc. ODP, Sci. Res.*, **138**, 73-101, 1995.

Shackleton, N.J, Baldauf, J.G., Flores, J.A., Iwai, M., Moore Jr., T.C., Raffi, I. and Vincent, E., Biostratigraphic summary for Leg 138, *Proc. ODP, Sci. Results*, **138**, 517-533, 1995.

Sierro, F.J., The replacement of the *"Globorotalia menardii"* group by the *"Globorotalia miotumida"* group: An aid to recognizing the Tortonian/Messinian boundary in the Meditarrenean and adjacent Atlantic. *Mar. Micropaleontol.*, **9**, 525-535, 1985.

Sierro, F.J., Flores, J.A., Civis, J., González Delgado, J.A., and Francés, G., Late Miocene globorotaliid event-stratigraphy and biogeography in the NE-Atlantic and Mediterranean. *Mar. Micropaleontol.*, **21**,143-168, 1993.

Skinner, B.J., R.C. Erd and F.S. Grimaldi, Greigite, the thio-spinel of iron: A new mineral, *Am. Mineral.*, **50**, 1487-1489, 1964.

Spender, M.R., Coey, J.M.D., and Morrish, A.H., The magnetic properties and Mossbauer spectra of synthetic samples of Fe_3S_4, *Can. J. Phys.*, **50**, 2313-2326, 1972.

Spiegler, D., and Rögl, F., *Bolboforma* (Protophyta, incertae sedis) im Oligozän und Miozän de Mediterran und der Zentralen Paratethys. *Ann Naturhist. Mus. Wien*, **94**, 59-95, 1992.

Stigter, H. de, Neogene-Recent compressional tectonics in the southern Hellenic Arc. *Internal report of the Utrecht Univ.*, 1-34, 1989.

Sümengen, M., Ünay, E., Saraç, G., De Bruijn, H., Terlemez, I., and Gürbüz, M., New Neogene rodent assemblages from Anatolia (Turkey). In: *European Neogene Mammal Chronology.*, 1990

Swisher, C.C., Grajales-Nishimura, J.M., Montanari, A., Margolis, S.V., Claeys, P., Alvarez, W., Renne, P., Cedillo-Pardo, E., Maurrasse, F.J-M., Curtis, G.H., Smit, J. and McWilliams, M.O., Coeval $^{40}Ar/^{39}Ar$ ages of 65.0 million years ago from Chicxulub Crater melt rock and Cretaceous-Tertiary boundary tektites, *Science*, **257**, 954-958, 1992.

Tauxe, L. and Opdyke, N., A time framework based on magnetostratigraphy for the Siwalik sediments of the Khaur Area, northern Pakistan, *Paleogeogr., Paleoclimatol., Paleoecol.*, **37**, 43-61, 1982.

Tauxe, L., Mullender, T.A.T. and Pick, T., Potbellies, wasp-waists, and superparamagnetism in magnetic hysteresis, *J. Geoph. Res.*, 1995.

Tiedemann, R., Sarnthein, M. and Shackleton, N.J., Astronomic timescale for the Pliocene Atlantic d18O and dust flux records of Ocean Drilling Program site 659. *Paleoceanography*, 9, 619-638, 1994.

Tsuchi, R., (ed.) Neogene of Japan: its biostratigraphy and chronology. *IGCP-114 International workshop on Pacific Neogene Biostratigraphy (Osaka)*, 1-138, 1981.

Turner, G.M., Roberts, A.P., Laj, C., Kissel, C., Mazaud, A., Guitton, S. and Christoffel, D.A., New paleomagnetic results from Blind River: Revised magnetostratigraphy and tectonic rotation of the Marlborough region, South Island, New Zealand. *New Zealand J. Geol. Geophys.*, **32**, 191-196l, 1989.

Ünay, E. and De Bruijn, H. (1987): Middle Oligocene to Early Miocene rodent assemblages from Turkey, a priliminary report. *Münchner Geowiss. Abh.*, **10**, 203-210.

Vai, G.B., A field trip guide to the Romagna Apennine geology. The Lamone valley. In: De Giuli, C. and G.B. Vai (eds.), *Fossil vertebrates in the Lamone valley, Romagna Apennines. Field trip guidebook*, 7-37, 1989.

Vai, G.B., Cyclostratigraphic estimate of the Messinian Stage duration. MICOP vol., 1995 (submitted).

Vai, G.B. and Ricci Lucchi, F., The Vena del Gesso in northern Apennines: growth and mechanical breakdown of gypsified algal crusts. *Mem. Soc. Geol. It.*, **16**, 217-249, 1976.

Vai, G.B, Villa, I.M. and Colalongo, M.L., First direct radiometric dating of the Tortonian/Messinian boundary. *C. R. Acad. Sci. Paris*, **316**, Serie II, 1407-1414, 1993.

Vai, G.B. and Laurenzi, M., Radiometric dating of the Tortonian/Messinian boundary (N. Apennines, Italy). *8th Confer. Geochron., Cosmochron., Isotope Geol., Berkeley, USGS Circular*, **1107**, 133, 1994.

Valdes, P.J., Sellwood, B.W. and Price, G.D., Modelling Late Jurassic Milankovitch climate variations. In: House, M.R. and A.S. Gale (Eds) *Orbital forcing timescales and cyclostratigraphy. Geol. Soc. Spec. Publ.*, **85**, 115-132, 1995.

Van den Ende, C., Palaeomagnetism of Permian red beds of the Dôme de Barrot (S. France), *PhD thesis, University of Utrecht.*, 1977.

Van der Meulen, A.M. and Daams, R., Evolution of early-middle Miocene rodent faunas in relation to long-term paleoenvironmental changes, *Paleogeogr., Paleoclimatol., Paleoecol.*, 93, 227-253, 1992.

Van der Voo, R. (1968): Jurassic, Cretaceous and Eocene pole positions from northeastern Turkey. *Tectonophysics*, **6**, 251-269.

Van de Weerd, A., Rodent faunas of the Mio-Pliocene continental sediments of the Teruel-Alfambra region, Spain. *Utrecht Micropal. Bull. Spec. Publ.*, **2**, 1-217, 1976.

Van Gessel, S.F., The age and synchroneity of the Early Messinian "Starvation Event" on Crete, *Internal Report, Faculty of Earth Sciences, Utrecht University*, 30 pp., 1994.

Van Hoof, A.A.M., Geomagnetic polarity transitions of the Gilbert and Gauss chrons recorded in marine marls from Sicily, *Geologica Ultraiectina*, **100**, pp. 123, 1993.

Van Hoof, A.A.M., Van Os, B.J., Rademakers, J.G., Langereis, C.G. and De Lange, G.J., A paleomagnetic and geochemical record of the upper Cochiti reversal and two subsequent precessional cycles from southern Sicily (Italy), *Earth Planet. Sci. Lett.*, **117**, 235-250, 1993.

Van Os, B.J.H., Primary and diagenetic signals in Mediterranean sapropels and North Atlantic turbidites. Origin and fate of trace metals and paleo-proxies, *Geologica Ultraiectina*, **109**, pp. 127, 1993.

Van Velzen, A.J., Thermal alteration of magnetic sulphides in marine marls from the Vrica section and the influence on the demagnetization of the natural remanent magnetization. *Geologica Ultraiectina*, **122**, pp.154, 1993.

Versteegh, G.J.M, Palaeoenvironmental changes in the Mediterranean and North Atlantic in relation to the onset of northern hemisphere glaciations (2.5 Ma B.P.) a palynological approach, *Thesis Utrecht University*, pp. 133, 1995.

Vine, F.J. and Matthews, D.H., Magnetic anomalies over ocean ridges, *Nature*, **199**, 947-949, 1963.

Walker, T.R. and Honea, R.M., Iron content of modern deposits in the Sonoran Desert: a contribution to the origin of red beds, *Geol. Soc. Am Bul.*, **80**, 535-544, 1969.

Walker, T.R., Larson, E.E. and Hoblitt, R.P., Nature and origin of hematite in the Moenkopi Formation (Triassic), Colorado Plateau: a contribution to the origin of magnetism in red beds., *J. Geophys. Res. B*, **86**, 317-333, 1981.

Weidmann, M., Soulounias, N., Drake, R.E. and Curtis, G.H., Neogene stratigraphy of the eastern basin, Samos Island, Greece, *Geobios*, **17**(4), 477-490, 1984.

Westaway, R. (1990): Block rotation in western Turkey. 1. Observational evidence. *J. Geoph. Res.*, **95**, 19857-19884.

Wilson, D.S., Confirmation of the astronomical calibration of the magnetic polarity timescale from sea-floor spreading rate. *Nature*, **364**, 788-790, 1993.

Wijbrans, J.R., Pringle, M.S., Koppers, A.A.P. and Scheveers, R., Argon geochronology of small samples using the Vulkaan argon laserprobe, *Proc. Kon. Ned. Akad. v. Wetensch.*, **98**(2), 185-218, 1995.

Woodruff, F. and Savin, S.M., Mid-Miocene isotope stratigraphy in the deep sea: High-resolution correlations, paleoclimatic cycles and sediment preservation, *Paleoceanography*, **6**, 755-806, 1991.

Wright, J.D., Miller, K.G. and Fairbanks, R.G., Early and middle Miocene stable isotopes: Implications for deepwater circulation and climate, *Paleoceonography*, **7**, 357-389, 1992.

Zachariasse, W.J., Planktonic foraminiferal biostratigraphy of the Late Neogene of Crete (Greece). *Utrecht Micropal. Bull.*, **11**, 1975.

Zachariasse, W.J., The origin of *Globorotalia conomiozean* in the Mediterranean and the value of its entry level in biostratigraphic correlations. *Ann. Geol. Pays. Hellen., Tome hors serie, fasc. III, VIIth international Congress on Mediterranean Neogene, Athens*, 1281-1292, 1979.

Zachariasse, W.J. and Spaak, P., Middle Miocene to Pliocene paleoenvironmental reconstruction of the Mediterranean and adjacent Atlantic Ocean: planktonic foraminiferal record of southern Italy. In: Meulenkamp, J.E., (ed.), *Reconstruction of marine paleoenvironments., Utrecht Microp. Bull.*, **30**, 91-110, 1983.

Zachariasse, W.J., Gudjonsson, L., Hilgen, F.J., Langereis, C.G., Lourens, L.J., Verhallen P.J.J.M. and Zijderveld, J.D.A., Late Gauss to early Matuyama invasions of Neogloboquadrina atlantica in the Mediterranean and associated record of climatic change, *Paleoceanography*, **5**, 239-252, 1990.

Zijderveld, J.D.A., Hilgen, F.J., Langereis, C.G., Verhallen, P.J.J.M. and Zachariasse, W.J., Integrated magnetostratigraphy and biostratigraphy of the upper Pliocene-lower Pleistocene from the Monte Singa and Crotone areas in Calabria, Italy, *Earth Planet. Sci. Lett.*, **107**, 697-714, 1991.

Zijderveld, J.D.A., Zachariasse, W.J., Verhallen, P.J.J.M. and Hilgen, F.J., The age of the Miocene-Pliocene boundary, *Newslett. Stratigr.*, **16**, 169-181, 1986.

Epilogue

About time

Earth Sciences, inevitably, must deal with time. First of all with time in its simplest form: that of superposition, or relative time. But also with time in the sense of age, or absolute time. The concept of absolute age is crucial to modern Earth Sciences since it enables to determine differences in age, and thus duration. And once we know duration - be it a second, a century or a million years - we are able to determine any earthscientific process: rate of change, movement and velocity.

In principle, astronomical dating in Earth Sciences, combines the best of both worlds: absolute age and duration. Absolute dating is achieved by directly correlating observed geological but clearly astronomically induced cycles - or complex patterns of cycles - to the computed astronomical solutions which are derived from strictly physical laws (Newton and Kepler). Once we have recognised the concept of astronomical forcing and its geological expression, we can also determine duration without knowing the age: accepting that particular geological cycles represent, for instance, precession, we may derive duration by simple counting of cycles.

Time - in the sense of duration - is important in Earth Sciences, because it enables us to determine and hence understand the underlying process in much greater detail. As an example, we may refer to plate tectonics or to sea-floor spreading. Averaged over a long period of time this may seem a smooth process, but using astronomical time constraints it appears that there are rapid and important changes at shorter time scales. Since such changes must be somewhere accommodated on a spherical Earth, we may expect to find a wide-spread tectonic event, like the 'Circum-Pacific tectonic event', as a result of spreading-rate changes and plate reorganisation.

Perhaps the most important developments in Earth Sciences today are (numerical) modelling of the Earth's geodynamical processes and their confrontation with observations which entail (preferably) long, continuous and high-resolution geological records, be they paleoclimatic and pertaining to the outermost Earth, or geomagnetic and pertaining to the innermost Earth. The mastery of time is clearly essential for the construction of geological time series which, in turn, lead to a better understanding of the processes and thus, ultimately, to our understanding of the dynamical "system Earth".

The subject of this thesis involves only a small - but essential - step in our efforts to get a grip on geochronology. The true value of constructing a high-resolution and accurate (polarity) time scale has still to come: its application in constructing time series and time constraints. This has become very apparent from earlier results: the construction of Hilgen's Plio/Pleistocene time scale has caused an avalanche of spin-off, in the form of many theses and numerous articles, and this avalanche is still continuing today. And already in the framework of the EU-funded network MIOMAR, many international specialists of various disciplines are working on the records from this thesis.

The future

A thesis can never be complete. We have established a new astronomical time scale, from 6.7 to 9.7 Ma. This leaves us, however, with a gap between 5.3 and 6.7 Ma, the so-called "Messinian Gap". The importance of closing this gap has been recognised by our international collegues who reviewed a proposal to this end, and the Netherlands Geosciences Foundation (GOA) has gracefully granted financial support for the next two years. Similarly, our new magnetostratigraphy and chronology of the continental realm (8-18 Ma) enables a first-order and straightforward correlation to the astronomically calibrated marine record. Our reconnaissance (in chapter 8) shows that also the continental record is subject to astronomical forcing, and our future efforts will therefore be directed to constructing (and extending to ~18 Ma) an astronomical time scale based on these continental sequences. Also this research has just received full support by GOA and will be the subject of a new PhD study for the next four years. A new programme illustrating our confidence in correlating the Pliocene marine and continental record, "bed-to-bed", with a resolution < 5 kyr, is the just started "Ptolemais project". This project, again being supported by GOA, aims at high-resolution continental-marine correlations and reconstruction of Mediterranean late Neogene climatic and environmental history and involves the disciplines of paleomagnetism, stratigraphy, sedimentology, (organic) geochemistry and palynology, to begin with. At the slightly longer term, future research will be directed to extension both in space and in time. For instance, pilotstudies are now being planned to determine the correlation of (paleoclimatic and tectonic) events between Tethys and Paratethys realms.

The results of this thesis has, naturally, required diverse efforts. Almost one year (53 weeks) has in total been spent on fieldwork. This has proved to be a necessary - though not always unpleasant - effort: reconnaissance and pilot studies are needed to determine suitable sections that are the most appropriate to our goals. Optimum suitability requires, among others, a decipherable cyclic pattern and good paleomagnetic properties. Determining the primary properties necessitates fresh sediments and this means digging. The next step in data-acquisition is in the laboratory. The throughput of large amounts of samples (>8000 cores) can only be achieved by using modern technological facilities, but still then the human effort is needed in the form of many hours of measuring, either behind the cryogenic magnetometer or behind the microscope. A more serious and scientific limitation lies in the inevitable deterioration and increasing complexity of the geological signal with age, due to weathering, tectonics, erosion etc. This involves new challenges and, once met, yields new experience and the expertise necessary to continue. For instance, the "Messinian gap" could not be closed just because the necessary expertise lacked. Only now, we can start feeling confident to approach this problem, having learned from this work.

A minimum criterion for good paleomagnetic results involves the routine application of rock magnetic methods to asses the reliability of the paleomagnetic signal. This enables us to accept or discard results from which it is not a priori clear that they represent the geomagnetic signal at the time of deposition. Routine IRM acquisition and demagnetisation, for instance, has allowed to define "reliability classes" in the Metochia section (chapter 2) thus contributing to the fidelity of the recorded polarities. It has become clear that delayed NRM acquisition may cause apparent asynchrony of reversals. Since reversals of the geomagnetic field may be taken as essentially synchronous, we must conclude that the delay of NRM acquisition is a function of sedimentary environment which is determined by numerous parameters that depend on both common (climate) and different (e.g. organic matter supply) variables. Inherent to some of the environments encountered in this thesis is the presence of Fe-sulphides. Their occurrence is a clear proof of important diagenetic processes that may have disturbed the reliability of the paleomagnetic signal, if not on a larger time-scale, then certainly on the time-scale (kyrs) involved in this thesis. A fundamental study of diagenesis and the properties of magnetic sulphides is needed to separate the geomagnetic and diagenetic magnetic signal. Fundamental research on these processes could never have been the subject of this thesis. Indeed, such studies must be the subject of considerable research efforts in the near future, as described in a PIONIER proposal which is currently in review. Nevertheless, a fundamental understanding of the magnetic effects of early diagenetic processes requires accurate time-control. This, at least, can be provided by astronomical dating.

" KNOWLEDGE AND TIME ABIDE IN THE SAME PLACE"

Curriculum Vitae

Toegevoegd op verzoek van het College van Decanen van de Universiteit Utrecht

Wout Krijgsman werd geboren op 25 december 1966 te Rotterdam. In 1985 behaalde hij het diploma Gymnasium aan het Gymnasium Camphusianum te Gorinchem en begon in hetzelfde jaar met de studie Geologie aan de Universiteit Utrecht. In 1991 legde hij het doctoraal examen af, met hoofdvak Geologie/Geofysica en bijvak Environmental Modelling, aan de Universiteit Utrecht. Vanaf maart 1992 tot maart 1996 was hij werkzaam voor NWO/GOA als OIO op het paleomagnetisch laboratorium "Fort Hoofddijk". Aansluitend is de auteur werkzaam op hetzelfde laboratorium, als postdoctoraal onderzoeker op het project "Closing the Messinian Gap in the astronomical polarity time scale", gefinancierd door de Nederlandse Organisatie voor Wetenschappelijk Onderzoek (NWO/GOA).

Acknowledgements

I would like to thank all my collegues, friends and family; without their help and support this thesis could not have been established.

Special thanks to Cor Langereis, who was always there for me when I needed him. His constant enthousiasm and interest for me and my research were enlightening and very important. Our good and close cooperation formed a firm basis for this successful thesis. During these years, Cor changed from being a friendly supervisor to a supervising friend.

The co-working with Frits Hilgen was of major importance; his amazing expertise in the field opened my doors to the magic world of cyclostratigraphy. His guiding and our frequent and fruitful discussions were highly enjoyable and unforgettable. It is really precious to have a colleague like Frits with whom I can work, talk, and laugh at the same time.

I like to thank Hans Zijderveld and Johan Meulenkamp for giving me the opportunity to do this research and for having confidence in me. Likewise, I will always remember the enthousiastic support of Jan-Willem Zachariasse.

Furthermore, I would like to thank all the people at Fort Hoofddijk for the nice time during the last four years. Mark Dekkers and Lisa Tauxe, for various discussions. Tom Mullender, for his help with all the instruments and his endless conversations (to which I sometimes even listened). Piet-Jan, for his pleasant company on Gavdos and in Holland. Henk Meijer, for his measurements, especially during the last part of my thesis. I would not easily forget the help of Ton van Hoof, both in the field and in the laboratory. Finally, I like to express my gratitude to our coach Willy van Beek for the numerous small but important favours.

For additional data and support I am indebted to my collegues (and co-authors):
Jordi Agustí, Paul Andriessen, Poppe de Boer, Hans de Bruijn, Luiz Cabrera, Remmert Daams, Jan van Dam, Wilbert Delahaije, Miguel Garcés, Albert van der Meulen, Alessandra Negri, Andrea Santarelli, Gerçek Saraç, and Jan Wijbrans.

For the numerous fieldtrips the support was enormous. For help and lots of fun I thank: Assimina (café d'Assi) Antonarakou, Poppe de Boer, Hans (Karate Kid) and Yes de Bruijn, Remmert (lonely at Vargas) Daams, Jan van Dam, Mark Dekkers, Frits (Frizzitelli) Hilgen, Ton van Hoof, Cor (this wine is good) Langereis, François Lévèque, Luc (dreaming is for losers) Lourens, Albert en Joke van der Meulen, Johan Meulenkamp, Andrea (Il Capo) Santarelli, Gerçek (the worldfamous mosquito-hunter) Saraç, Peter (PetruSanctus) Scheepers, Piet-Jan Verplak, Friso (and his dolphins) van Welderen Rengers, Jan-Willem (afraid to spend the night on the beach of Koufonisi) Zachariasse, Hans (dancing on raki) Zijderveld.

I appreciate the friendship and fun I had with Cor de Boer, my room-, house-, and Fort-mate.

Finally, I thank Charon for her love and understanding.